Pattern Recognition of the HIV-1 Capsid by the Innate Immune Receptor TRIM5

Dissertation

zur

Erlangung der naturwissenschaftlichen Doktorwürde

(Dr. sc. nat.)

vorgelegt der

Mathematisch-naturwissenschaftlichen Fakultät

der

Universität Zürich

von

Damien Morger

von

Eschenbach SG

Promotionskomitee

Prof. Dr. Markus G. Grütter (Vorsitz)
Prof. Dr. Jeremy Luban
Prof. Dr. Ohad Medalia

Zürich 2014

Table of Contents

Summary

TRIM5 proteins are intracellular host restriction factors that constitute a species-specific barrier to the infection by a broad spectrum of retroviruses. TRIM5 interferes with the retroviral life-cycle at an early post-entry stage by binding to incoming capsid (CA) cores. In certain primate species, including rhesus macaques, African green monkeys and owl monkeys, TRIM5 potently blocks the infection by HIV-1. By contrast, human TRIM5 has only weak activity against HIV-1, but efficiently restricts N-MLV instead.

TRIM5 is an innate immune sensor for the retrovirus capsid lattice
We established a protocol for the purification of owl monkey (*aotus*) TRIMCyp that yielded protein amounts amenable to biochemical assays and crystallization trials. This protocol could also be adapted for the production of human and African green monkey TRIM5α.
In a collaboration with Pertel *et al.* we demonstrate that TRIM5 mediates innate immune signaling in a fashion that can be either uncoupled or coupled from retroviral capsid recognition. This novel activity of TRIM5 was abolished by mutation or deletion of the RING E3 ubiquitin-ligase domain. Using the recombinant owl monkey TRIMCyp and assembled HIV-1 CA cylinders in *in-vitro* ubiquitin assays alongside with cell-based infectivity assays we uncovered that TRIM5 cooperates with the E2 enzyme Ubc13-Uev1a to catalyze the formation of free K63-linked ubiquitin chains, which activate the TAK1 kinase complex and stimulate AP-1 and NF-κB signaling. Interaction with the HIV-1 capsid lattice greatly enhances the Ubc13-Uev1a dependent E3 activity of TRIM5 and challenge with TRIM5 sensitive retroviruses induces the transcription of AP-1 and NF-κB-dependent factors.

Dissecting the HIV-1 Capsid Lattice into Distinct TRIM5 Binding Units
To understand how TRIM5α senses the retroviral CA lattice on a molecular basis we characterized the direct interaction between TRIM5α and a collection of cross-linked CA oligomers that are engineered to mimic individual interfaces of the HIV-1 CA lattice. This selection of CA oligomers includes a known hexameric HIV-1 CA alongside with novel trimeric CAs cross-linked at the three-fold symmetric lattice interfaces. By measuring the binding affinities of these CA oligomers for the isolated *rhesus* TRIM5α B30.2 domain and comparing with the K_Ds for monomeric or *wild-type* dimeric CAs we show that TRIM5α has an increased affinity for CA constructs mimicking the three-fold and six-fold symmetric interfaces. Hence we conclude that TRIM5α binds to multiple CA subunits that may map to an overlapping lattice epitope located at the threefold axis including two neighboring hexamers.

Overall architecture and mode of dimerization of TRIM proteins revealed by the TRIM20 structure
The crystal structure of a fragment encompassing the CC-L2 and B30.2 domains of the TRIM5α homolog TRIM20/pyrin shows for the first time that TRIM proteins dimerize in an antiparallel fashion forming an elongated structure with the N-termini of the two monomers placed 167 Å apart. This reveals the overall domain organization in TRIM proteins and based on this structure a full-length stereotype TRIM was modelled taking available TRIM5 structures as templates.

To prove that the TRIM20 structure also applies to TRIM5, we determined the low-resolution shape of a homologous human TRIM5α construct by SAXS. A preliminary SAXS envelope of the human TRIM5 CC-L2 and B30.2 domains is shown in the discussion of this thesis.
In addition, a crystal contact between two neighboring TRIM20/pyrin dimers suggests the existence of TRIM tetramers which reveals a new mechanism how TRIM5 may self-assemble into hexagonal arrays upon recognition of a retroviral CA lattice.

Zusammenfassung

TRIM5 Proteine sind intrazelluläre Restriktions-Faktoren, welche einen Spezies-spezifischen Schutz gegen ein breites Spektrum von Retroviren bieten. TRIM5 wehrt Infektionen bereits in einer frühen Phase des retroviralen Lebenszyklus ab, indem es unmittelbar nach dem Virus-Eintritt in die Wirtszelle an die virale Kapsid (CA) hülle bindet. Bei gewissen Primaten Arten, wie zum Beispiel Rhesus Makaken, Afrikanischen Grünmeerkatzen und Nachtaffen verhindert TRIM5 die Infektion mit HIV-1. Beim Menschen jedoch wirkt TRIM5 nur schwach gegen HIV-1. Stattdessen bewirkt das menschliche TRIM5 eine Abwehr gegen das N-tropische Maus Leukämievirus (N-MLV).

TRIM5 ist ein Sensor des angeborenen Immunsystems für das retrovirale Kapsid Gitter.
Wir etablierten ein Protokoll zur Reinigung von TRIMCyp aus Nachtaffen, welches ausreichende Mengen an Protein zur Durchführung von biochemischen Experimenten und Kristallisations Versuchen lieferte. Dieses Protokoll konnte auch zur Produktion von TRIM5α aus Afrikanischen Grünmeerkatzen oder dem Menschen angewendet werden.
In Zusammenarbeit mit Pertel *et al*. weisen wir auf, dass TRIM5 angeborene Immun Signale auslöst. TRIM5 vermittelt diese Signale sowohl gekoppelt an der Erkennung retroviraler Kapside, als auch unabhängig davon. Diese neu entdeckte Aktivität von TRIM5 wurde aufgehoben wenn man die RING E3 Ubiquitin-Ligase Domäne mutierte oder entfernte. Anhand von zell-basierten Infektivitäts Versuchen und *in-vitro* Analysen mit Ubiquitin, rekombinantem TRIMCyp aus Nachtaffen und assemblierten CA Partikeln konnte aufgedeckt werden, dass TRIM5 zusammen mit dem E2 Enzym Ubc13-Uev1a die Bildung freier Ubiquitin-Ketten katalysiert, welche wiederum den TAK1 Kinasen Komplex aktivieren und dadurch AP-1 und NF-κB Signalwege stimulieren. Durch Interaktion mit dem HIV-1 Kapsid Gitter wird die Ubc13-Uev1a abhängige E3 Aktivität von TRIM5 massgeblich stimuliert und die Infektion mit TRIM5 sensitiven Retroviren löst die Transkription AP-1 und NF-κB-abhängiger Faktoren aus.

Zerlegung des HIV-1 Kapsid Gitters in unterscheidbare TRIM5 bindende Einheiten.
Um auf molekularer Ebene zu verstehen wie TRIM5 das retrovirale Kapsid Gitter erkennt haben wir die direkte Interaktion zwischen TRIM5 und einer Sammlung künstlich verbrückter HIV-1 Kapsid Oligomere charakterisiert. Diese Kapsid Oligomere wurden so konzipiert, dass sie individuelle Nahtstellen zwischen Kapsiden im assemblierten Gitter nachahmen. Die Sammlung verbrückter Kapside beinhaltet ein publiziertes HIV-1 Kapsid Hexamer sowie neuartige HIV-1 Kapsid Trimere, welche unterschiedlich an der dreifach-symmetrischen Schnittstelle des Kapsid Gitters verbrückt wurden. Indem wir die Bindungs-Affinitäten dieser Kapsid Oligomere für die isolierte B30.2 Domäne von *Rhesus* TRIM5α gemessen und mit den K_Ds für monomeres oder *Wild-Typ* dimeres Kapisid verglichen haben zeigen wir, dass *Rhesus* TRIM5α eine erhöhte Affinität für Kapsid Konstrukte vorweist, welche die dreifach- und sechsfach-symetrischen Nahtstellen des Kapsid Gitters imitieren. Daraus folgern wir, dass TRIM5α an multiple Kapside bindet, welche am wahrscheinlichsten ein überlappendes Epitop bilden, das die dreifach-symmetrische Achse und zwei benachbarte Hexamere beinhaltet.

Gesamtarchitektur und Art der Dimerisierung von TRIM Proteinen aufgedeckt durch die Struktur von TRIM20.

Die Kristall Struktur eines Fragmentes, welches die CC-L2 und B30.2 Domänen des zu TRIM5α homologen TRIM20/pyrin beinhaltet zeigt zum ersten Mal, dass TRIM protein antiparallel dimerisieren und eine elongierte Struktur bilden in welcher die N-Termini der Beiden Monomere an entgegengesetzten Enden, 167 Å voneinander entfernt, zu liegen kommen. Dadurch wird die relative Domänen Anordnung in TRIM Proteinen aufgedeckt und basierend auf dieser Struktur haben wir ein Stereotyp Modell für voll-längen TRIM Proteine erstellt, indem bekannte TRIM5 Strukturen als Vorlage genommen wurden. Um zu beweisen dass die TRIM20 Struktur auch für TRIM5α zutrifft, haben wir die nieder-auflösende Kontur eines homologen TRIM5 Konstrukts mittels Kleinwinkel-Röntgenstreuungs Experimenten SAXS bestimmt. Eine vorläufig berechnete SAXS Hülle der CC-L2 und B30.2 Domänen des humanen TRIM5 ist in der Diskussion dieser Doktorarbeit aufgeführt.

Zusätzlich, weist ein Kristall Kontakt zwischen zwei benachbarten TRIM20/pyrin Dimeren auf die Existenz von TRIM Tetrameren hin, was auf einen neuen Mechanismus für die Selbst-Assemblierung von TRIM5 in ein hexagonales Gitter hinweist.

Abbreviations

AIDS	Acquired Immune Deficiency Syndrome
CA	Capsid
CA-NC	Capsid nucleocapsid fusion
CC	Coiled-coil domain
CCR5	C-C motif chemokine receptor 5
CD4	Cluster of differentiation 4
cDNA	Complementary DNA
CsA	Cyclosporine A
CTD	C-terminal domain
CXCR4	CXC motif chemokine receptor 4
CypA	CyclophilinA
dscDNA	Double-stranded cDNA
EIAV	Equine infectious anemia virus
Env	Envelope Glycoprotein
FIV	Feline immunodeficiency virus
HAART	Highly active antiretroviral therapy
HIV-1	Human immunodeficiency virus type 1
HIV-2	Human immunodeficiency virus type 2
IN	Integrase
LEDGF	Lens epithelium-derived growth factor
LINE1	Long interspersed element 1
LTR	Long terminal repeat
MA	Matrix protein
MHC complex	Major histocompatibility
NC	Nucleocapsid
Nef	Negative Regulatory Factor
N-MLV	N-tropic murine leukemia virus
NMR	Nuclear Magnetic Resonance
NOE	Nuclear Overhauser effect
nsSNP	Non-synonymous single nucleotide polymorphism
NTD	N-terminal domain
PIC	Pre-integration complex
RING	Really interesting new gene
RNAi	RNA interference
RT	Reverse transcriptase
RTC	Reverse transcription complex
shRNA	Short hairpin RNA
SIV	Simian immunodeficiency virus
SIVagm	SIV from African green monkeys
SIVcpz	SIV from chimpanzees
SIVmac	SIV from rhesus macaques
SIVrcm	SIV from red-capped mangabeys
SIVtan	SIV from tantalus monkeys
TAR	Trans-acting response element
TRIM	Tripartite motif protein
Vpu	Viral Protein Unique

1 Introduction

1.1 The AIDS Pandemic and Discovery of the Restriction Factor TRIM5

The Acquired Immune Deficiency Syndrome (AIDS) was first recognized as a new disease in 1981 [1] and the causative retrovirus, now called human immunodeficiency virus type 1 (HIV-1), was identified only a few years later [2,3]. Since then more than 75 million people have been infected by HIV worldwide and more than 36 millions have died from AIDS related diseases [4,5]. Meanwhile AIDS is known to be caused by either of two distantly related lentiviruses: HIV-1 or HIV-2, with HIV-1 being the pandemic virus. Although advances in the development of antiretroviral drugs have lowered death tolls, morbidity and mortality has remained high in developing countries due to limited access to preventive measurements and antiretroviral treatment.

The reasons for the worldwide AIDS pandemic have been intensively studied and it's only since a few years that an overall picture of its origins can be drawn. First clues came from the discovery of HIV-2 in patients from western Africa and its close relationship to a simian virus that caused immunodeficiency in captive macaques [6,7]. The subsequent finding of additional viruses in various different primates that were collectively termed simian immunodeficiency viruses (SIVs) laid the basis for tracing back the source of HIV. HIV-1 and HIV-2 were found to be close relatives to SIVs from chimpanzees and sooty mangabeys, respectively [8,9]. This indicated that AIDS had emerged as a consequence of cross-species infections with SIVs from primates (Figure 1). While SIVs appeared to be mostly nonpathogenic for their natural hosts, SIVmac caused AIDS in rhesus macaques. Later studies revealed that SIVmac too was generated accidently by zoonotic transfers of a simian virus after captive macaques had contacted blood or tissue samples from sooty mangabeys in an US primate center [10,11].

Studies on SIVcpz, the genetically closest relative to HIV-1, had for a long time been hampered by the endangered status of chimpanzees. Finally, the development of noninvasive diagnostic methods had allowed investigations on wild-living animals identifying the common chimpanzee as a natural reservoir for SIVcpz [12-15]. Infected animals showed many properties common to human HIV infections, including increased mortality, CD4+ T-cell depletion and similar routes of transmission [15,16]. Phylogenetic analysis of isolated viruses revealed that SIVcpz was generated by recombination of two SIVs, one resembling to SIVrcm in red-capped mangabeys and the other to a SIV lineage that infects several African green monkeys [17] (Figure 1). This implies that multiple cross-species transmissions had to take place and is further supported by the known hunting behavior of chimpanzees that includes killing of other monkeys, suggesting that they acquired SIV in the context of predation.

Humans must have acquired the precursors of HIV-1 through mucosal exposure to infected ape blood or body fluids, which most commonly occurs with the consumption of raw meat [18]. HIV-1 is subdivided into four distinct lineages, termed groups M, N, O and P, with group M representing the pandemic form. Genetic analysis showed that each of these groups arose from an independent cross-species transmission event (Figure 1). All four groups cluster with

SIVcpzPtt that infects the P.t. troglodytes subspecies of chimpanzees in central Africa and the ape precursors of groups M and N could even be traced back to particular P.t. troglodytes communities [13,14].

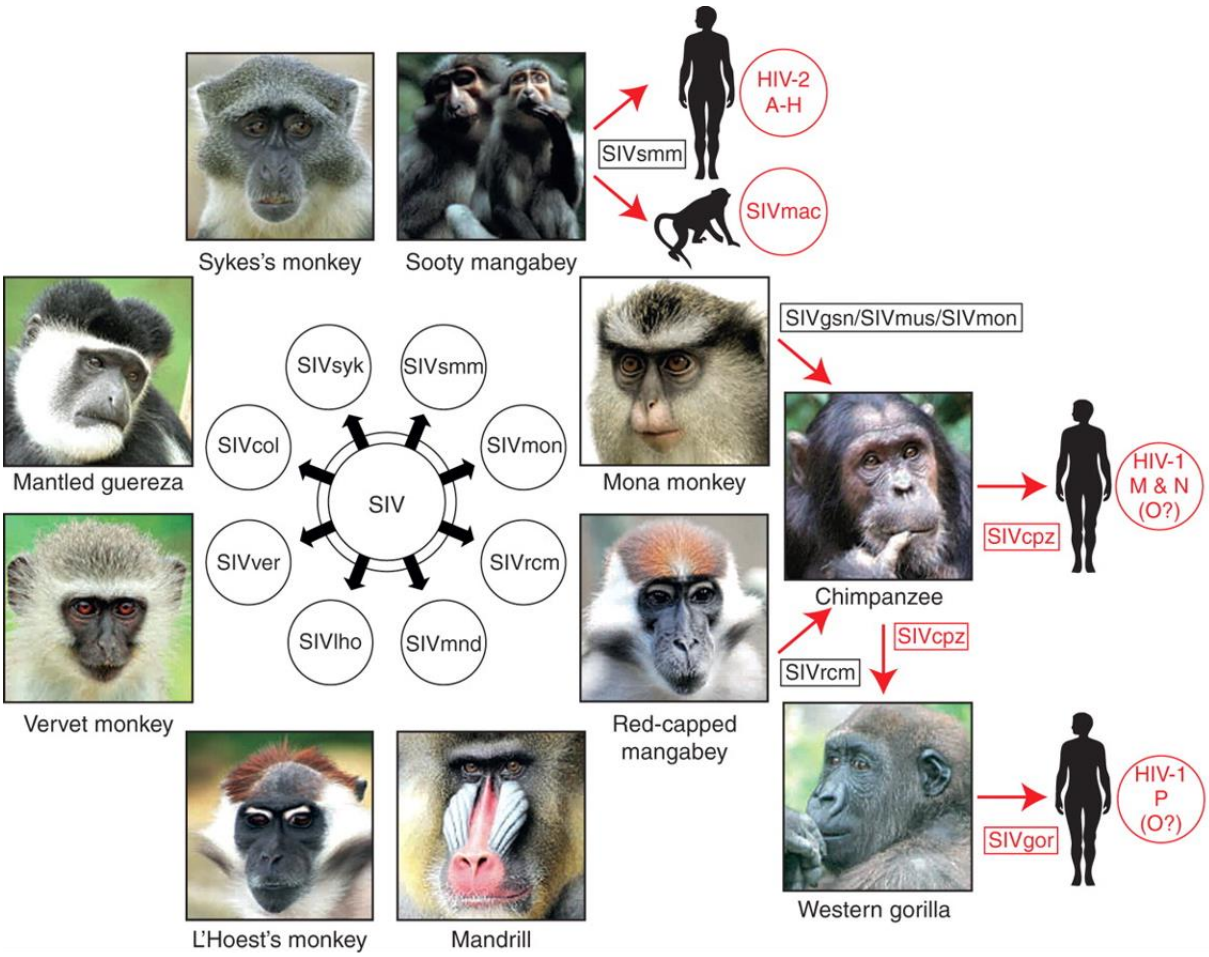

Figure 1: Origins of human AIDS viruses. Old World monkeys are naturally infected with more than 40 different lentiviruses, termed simian immunodeficiency viruses (SIVs) with a suffix to denote their primate species of origin (e.g., SIVsmm from sooty mangabeys). Several of these SIVs have crossed the species barrier to great apes and humans, generating new pathogens. Known examples of cross-species transmissions, as well as the resulting viruses, are highlighted in red (Figure & Legend taken from [19]).

SIVcpzPtt had to counteract different host restriction factors in order to cross the species barrier to humans and become a productively infectious virus. Of the restriction factors that constitute a barrier to SIV cross-species transmissions, tetherin probably had the greatest impact on the precursors of HIV-1 and HIV-2. Tetherin is a transmembrane protein, which inhibits budding and release of virions from infected cells by "tethering" the released virions at the cell surface. SIVs inactivate tetherin either by using their Nef protein to remove it from the cell surface, or by using their Vpu protein to degrade it. Some viruses use their envelope glycoprotein to bind and inhibit tetherin. The human tetherin gene differs from its ape orthologs by a five codon deletion in the cytoplasmic domain rendering the SIVcpz Nef protein inactive on transmissions

to humans [20]. In the case of HIV-1 group M, this adaptive hurdle was overcome by alterations in the Vpu gene rendering the gene product potently active against tetherin [21].
While SIVs that coevolved with their natural hosts appear to be mostly nonpathogenic, multiple examples have shown that successful zoonosis can lead to the emergence of new SIVs that are pathogenic to their new hosts, causing immunodeficiency-like symptoms. This emphasizes the important role of host restriction factors in maintaining a barrier to cross-species transmissions of pathogens.
HIV-1 is potently blocked in many Old World monkey species [22-28]. This is not the case in New World monkeys with the exception of owl monkeys: They restrict HIV-1, but are susceptible to SIV [26,29].
The finding that the block to HIV-1 was saturable at high virus titers and that restriction was dominant in cell-fusion experiments already suggested existence of a specific antiviral factor [23,24,28]. Finally, two independent approaches uncovered TRIM5 as the HIV-1 specific antiviral factor in old world monkeys and owl monkeys, respectively. The first approach screened a cDNA library from rhesus macaque cells for the ability to confer resistance to otherwise permissive human cells [30] identifying the α isoform of the TRIM5 gene products as the responsible restriction factor. The second approach was based on the observation that disruption of the CA-CypA interaction in owl monkey cells, either by cyclosporine, mutations or shRNAs targeting CypA, lead to suppression of anti-HIV-1 restriction activity. Surprisingly, reintroduction of CypA protein into shRNA expressing cells did not restore resistance to HIV-1. A search for additional potential RNAi targets amongst owl monkey cDNAs uncovered a TRIM5-CypA fusion protein that was sufficient to transfer HIV-1 restriction activity to human cells [31,32].

1.2 The HIV Life Cycle and the Early Block to Retroviral Infection by TRIM5

HIV-1 can persistently infect humans by evading the innate and adaptive immune systems, despite encoding only 15 mature proteins. HIV-1 compensates for this apparent simplicity by exploiting a myriad of cellular factors to replicate and conquers several host restriction factors that fight to suppress its replication [33]. The HIV-1 life cycle can be divided into an early phase that occurs between viral entry into the host cell and integration into its genome, and a late phase that comprises the transition from the state of integrated provirus to full viral replication [34].

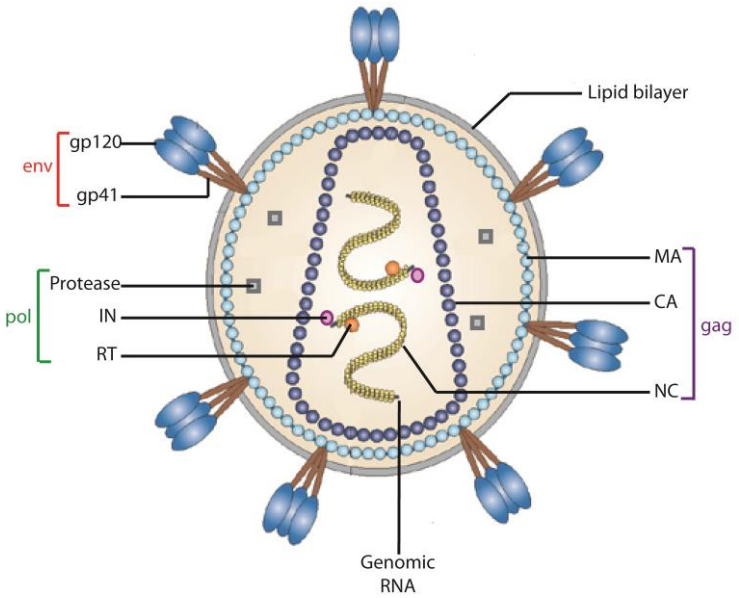

Figure 2: Schematic depiction of a mature HIV-1 virion. The infective mature HIV-1 virus contains two positive-sense genomic RNAs that are stabilized by bound nucleocapsid (NC) proteins and encapsulated inside a conical capsid (CA) shell together with the reverse transcriptase (RT) and integrase (IN). The CA core is surrounded by a layer of matrix (MA) proteins associated to the lipid bilayer that contains the trimeric spikes composed of the envelope glycoproteins gp120 and gp41. These are essential for the attachment to the host and subsequent fusion with the cell membrane. The virus contains also the viral protease, which is essential for processing of the Gag, Gag-Pol and Env polyproteins and virus maturation. The respective processed viral proteins encoded by the gag, pol and env genes are indicated in purple, green and red brackets, respectively (Figure adapted from [35]).

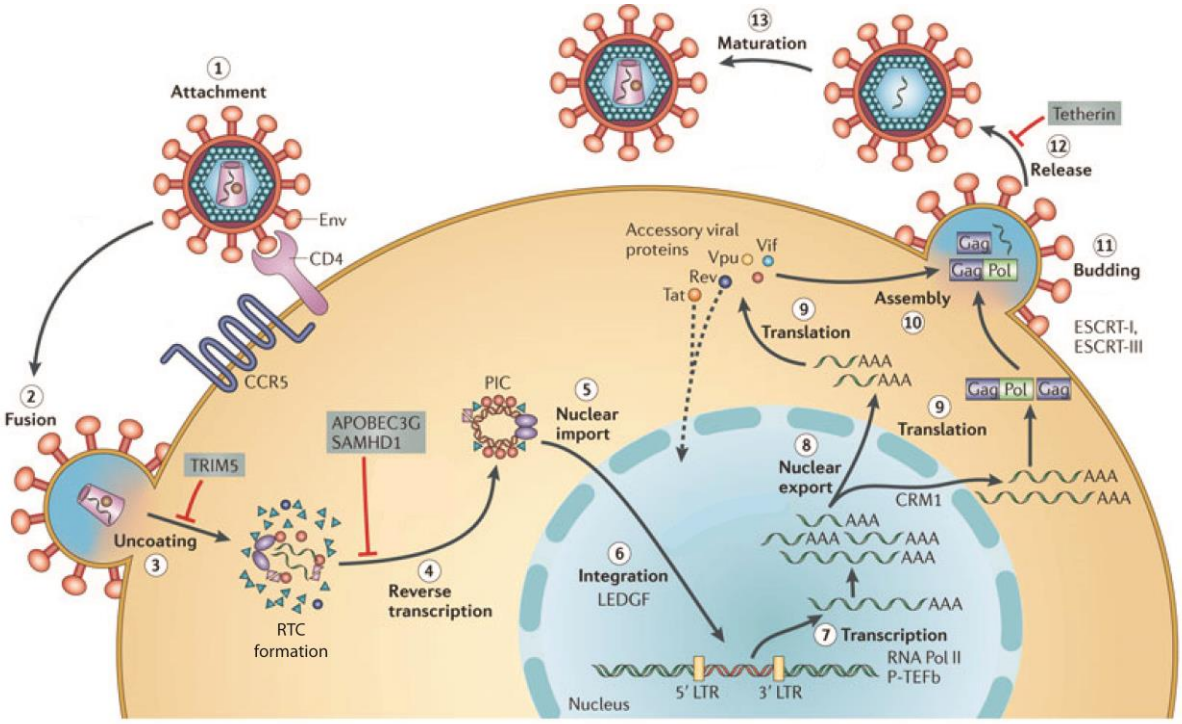

Figure 3: Overview of the HIV-1 replication cycle. The infection begins when the envelope (Env) glycoprotein spikes engage the receptor CD4 and the membrane-spanning co-receptor CCR5 or CXCR4 (step 1), leading to fusion of the viral and cellular membranes and entry of the viral particle into the cell (step 2). Partial core shell uncoating (step 3) facilitates reverse transcription (step 4), which in turn yields the pre-integration complex (PIC). Following import into the cell nucleus (step 5), PIC-associated integrase orchestrates the formation of the integrated provirus, aided by the host chromatin-binding protein lens epithelium-derived growth factor (LEDGF) (step 6). Proviral transcription (step 7), mediated by host transcription factors, yields viral mRNAs of different sizes, the larger of which require energy-dependent export to leave the nucleus via host protein CRM1 (step 8). mRNAs serve as templates for protein production (step 9), and genome-length RNA is incorporated into viral particles with protein components (step 10). Viral-particle budding (step 11) and release (step 12) from the cell is mediated by ESCRT (endosomal sorting complex required for transport) complexes and is accompanied or soon followed by protease-mediated maturation (step 13) to create an infectious viral particle. Some of the cellular restriction factors (blue boxes) that limit HIV-1 infection are indicated: TRIM5α blocks HIV-1 infection in many old world monkeys by interfering at the step of viral uncoating prior to reverse transcription, APOBEC3G is a cytidine deaminase that inhibits reverse transcription, SAMHD1 is a phosphohydrolase that depletes the pool of nucleotides available for reverse transcription by converting nucleotide triphosphates into a nucleoside and a triphosphate and Tetherin is a transmembrane protein that prevents virus release by cross-linking budded virions at the cell surface (Figure & Legend adapted from [33]).

The viral envelope contains spikes that are composed of the glycoproteins gp120 and gp41, forming trimers of noncovalent heterodimers [36-38] (Figure 2). Gp120 binds to the cell-surface receptor CD4 of different CD4+ leukocytes, in particular CD4+ T cells and

macrophages, and engages with an additional chemokine co-receptor, that is either CXCR4 on CD+ T cells or CCR5 on macrophages [39,40]. This triggers a cascade of conformational changes in the spike glycoproteins leading to fusion of the viral and host membranes [41-43]. The HIV-1 core, which contains reverse transcriptase (RT), integrase (IN) and two nucleocapsid (NC) bound plus-sense RNA genomes encapsulated by a conical shell of the viral capsid (CA) protein, is released into the host cytoplasm upon fusion with the cell membrane (Figure 2Figure 3). Once inside the cell, the viral core is named reverse transcription complex (RTC) as exposure to cytosolic nucleotides initiates reverse transcription [34]. The RT reverse transcribes the single-stranded viral RNA into DNA while continuously digesting the RNA component of the RNA–DNA hybrids. The resulting single stranded DNA is then transformed into double-stranded cDNA (dscDNA) by the host DNA polymerase [33]. As the RTC migrates towards the nucleus by dynein driven retrograde transport along microtubules, it progressively disassembles and reorganizes with various host proteins to form the pre-integration complex (PIC) [44-46] (Figure 3). The PIC that is composed of linear dscDNA, integrase, matrix (MA) protein and host proteins is then imported into the nucleus and becomes competent for integration into the host cell chromosome. At some point between viral entry and nuclear import uncoating of the CA core has to take place. Not much is known about the exact time point and location of viral uncoating, but it is well established that interference with timing of this essential process, e.g. by stabilizing or destabilizing the CA shell, critically impairs reverse transcription and all following steps [47].

The dscDNA is flanked by so-called long terminal repeats (LTR) which serve as sites of integration and promoter/termination regions [48]. Once the viral DNA has entered the nucleus it can either integrate into the host chromosomes or circularize as one or two long terminal repeat (LTR)-containing circles [46]. Although non-integrated viral DNA cannot produce viable particles, it can contribute to HIV-1 replication by generating RNA transcripts that increase activation of T-cells and render them more permissive to HIV-1 infection, e.g. through production of Nef protein [49-52]. Integration of the viral dscDNA into the host genome is carried out by the viral integrase. It nucleolytically processes the dscDNA at both LTRs generating recessed 3’ ends and ligates them to the 5’ phosphates of a double stranded cut in the cell DNA. Host enzymes complete the integration process by repairing the single-strand gaps at the viral 5’ends resulting in establishment of a stable provirus [33]. To target preferable sites of integration, the PIC associates with the host protein lens epithelium-derived growth factor (LEDGF). The chromatin-binding protein LEDGF is a transcriptional co-activator that binds integrase and promotes viral integration within active genes [53].

Depending on the host cell, the integrated provirus can either remain quiescent as in the case of resting CD4+ T cells or generate a persistent infection like in macrophages [54]. Latent pools of HIV-1 as achieved in resting CD4+ T cells constitute a major obstacle to eradication of the virus even in the presence of highly active antiretroviral therapy (HAART) [55,56]. Unless they are activated, these cells do not progress to complete viral replication, allowing the virus to hide from the host immune system and remain unaffected by current antiretroviral drugs. Immune activation of latently infected CD4+ T cells induces binding of host transcription factors to enhancer elements in the 5’ LTR promoter region [57]. Initial transcription output is, however very low and just sufficient to produce tiny amounts of the viral transactivator protein Tat.

Binding of Tat to the stem-loop trans-acting response element (TAR) in the 5' region of viral transcripts is required for efficient elongation and synthesis of full-length HIV-1 mRNAs [58,59]. Viral mRNAs are produced as a variety of alternatively spliced species. The fully spliced (encoding Tat, Rev and Nef) and partially spliced (encoding Vif, Vpr and Env) mRNAs are readily exported from the nucleus, whereas the unspliced and singly spliced mRNAs (genomic RNA, also encoding Gag-Pol and Gag) require assistance by the viral Rev protein. Rev bridges the unspliced and partially spliced transcripts to the nuclear export machinery by binding both to Rev response element (RRE) of the viral mRNA and to the host nuclear export factor CRM1 [60,61] (Figure 3).

Once in the cytoplasm, the viral genomic-length mRNA is translated into the precursor polyproteins Gag and Gag-Pol. Both precursors multimerize and are targeted to the cell membrane by myristoylation of the N-terminal matrix domain [62-64]. Gag and Gag-Pol are thus concentrated at phosphatidylinositol-4,5-biphospate rich lipid rafts at the inner cell membrane and assemble into virus-like particles [65,66]. In parallel, the trimeric envelope glycoprotein (Env) is recruited to the membrane through interactions with the matrix domain and two genomic RNA strands are packed into each virus-like particle by interacting with the zinc fingers in the NC domain of Gag. The NC-RNA interactions further contribute to the tight assembly of Gag and Gag-Pol [67]. Retroviral budding is coordinated by interactions of the Pro-rich late domains with cellular components of the class E vacuolar protein sorting (VPS) pathway, which normally act in the budding of cellular vesicles into late endosomes [68,69]. HIV-1 thus hijacks those VPS proteins to complete viral budding and release newly formed immature particles, which have a spherical morphology. Shortly after release, the viral protease (PR) is auto-activated and converts the immature particles into infectious virions by cleaving the Gag and Gag-Pol precursors into the structural MA, CA and NC proteins and the enzymes PR, RT, and IN [70]. Virus maturation is completed upon structural reorganization of these proteins and assembly of a conical CA core shell surrounding the NC-RNA complexes [71] (Figure 2).

The antiretroviral restriction factor TRIM5 had been found to block infection in the early phase of the retroviral life cycle. More precisely, this block occurred after viral entry because HIV-1 variants carrying the envelope protein from an unrelated virus (VSV-G), that would bypass blocks related to cell-surface binding, fusion and entry, were still inhibited by TRIM5 [72]. Also it had to occur before reverse transcription, because little or no linear dscDNA could be detected in restrictive cells [73]. Infectivity experiments with chimeric viruses in which components from a restricted virus were swapped with those from an unrestricted virus identified the viral CA protein as the determinant for virus susceptibility [24,74-76]. Quantitative separation of intact cytoplasmic virion cores from soluble CAs of HIV-1 infected cells ("faith of the capsid assay") revealed a good correlation between TRIM5 restriction and loss of intact CA particles, suggesting that TRIM5 blocks retroviral infection through premature uncoating of the CA core prior to reverse transcription [77].

1.3 Domain Architecture of TRIM5

TRIM5 is part of the tripartite motif (TRIM) containing family of proteins that comprises nearly 100 human members [78]. The TRIM motif, also called RBCC, is characterized by the presence

of an N-terminal RING, followed by one or two B-Boxes and a CC domain which are conserved in relative order and spacing (Figure 4) [79]. The α splice isoform of TRIM5 has retroviral restriction activity and contains an additional C-terminal B30.2 domain harboring the determinants for virus specifity (Figure 4 A) [30]. In a few examples however, the B30.2 domain has been replaced by CypA, another CA binding domain, during evolution (Figure 4 B) [31].
None of the four TRIM5 domains is dispensable for full restriction activity and each of them adopts a different role in contributing to the proteins function.

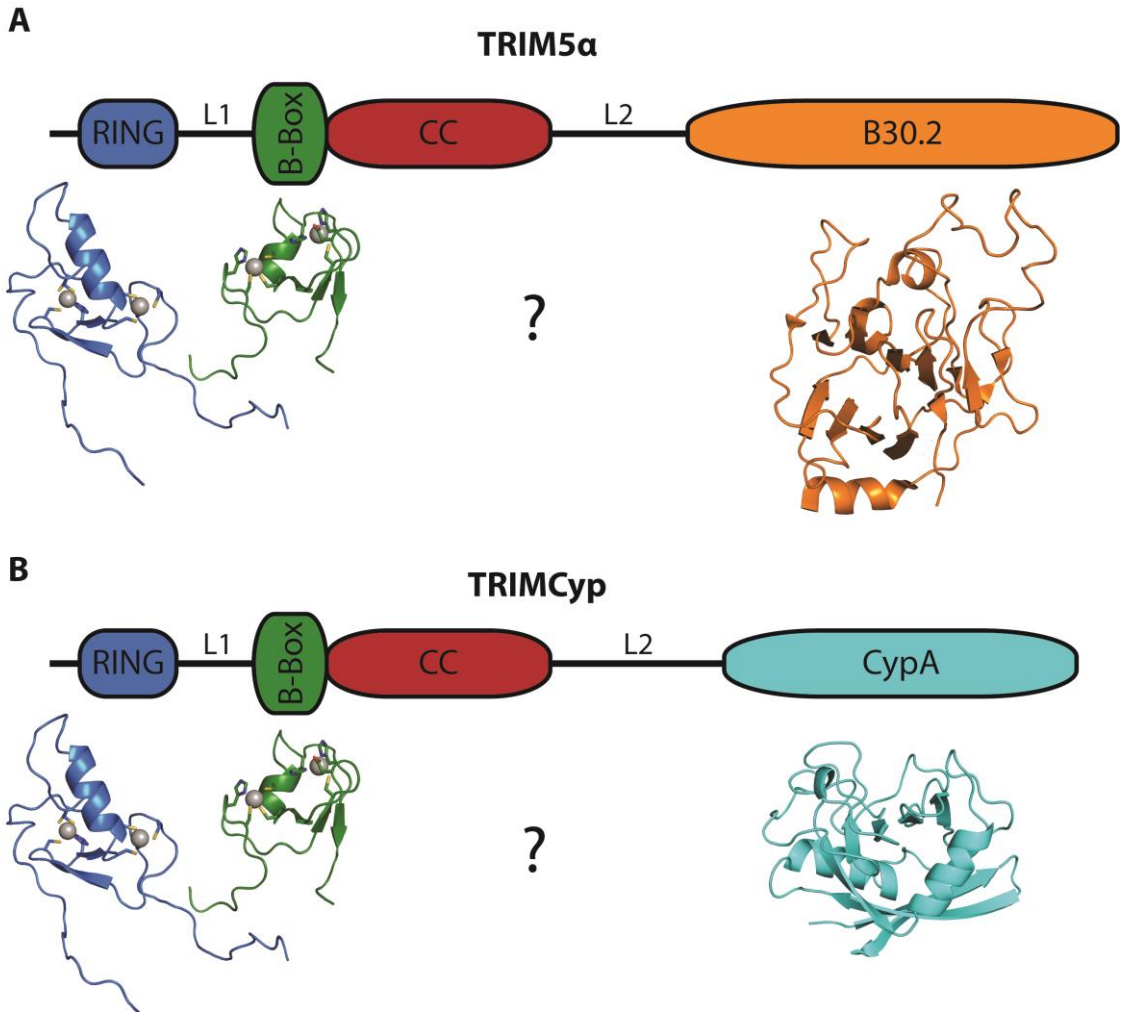

Figure 4. Domain architecture of TRIM5 proteins. Available atomic structures of corresponding TRIM5 domains are shown below a conceptual scheme illustrating the domain composition in TRIM5 proteins. RING, B-Box and coiled-coil (CC) domains, characteristic of the RBCC motif, are colored in blue, green and red, respectively. The lack of structural information on the CC-L2 part of TRIM5 proteins is symbolized by a question mark. **(A)** TRIM5α possesses a C-terminal B30.2 domain (orange). The atomic structures of the RING and B-Box from human TRIM5α (pdb entries: 2ECV and 2YRG) and the B30.2 from rhesus TRIM5α (pdb entry: 2LM3) are shown in cartoon representation. **(B)** In TRIMCyp proteins, the C-terminal B30.2 domain has been replaced by a Cyclophilin A (CypA) domain (cyan, pdb entry 1AK4) during evolution. Due to the high sequence conservation in the RING and B-Box, these domains can be expected to share the same structure as in human TRIM5α.

1.3.1 The RING E3-ligase domain

The N-terminal RING domain of TRIM5 has E3-ligase activity and thus confers the ability to catalyze the formation of polyubiquitin chains [80]. As the name implies, ubiquitin is ubiquitously expressed inside the cell and the attachment of mono- or polyubiquitin chains to proteins expands their functional repertoire or controls their lifespan [81]. The consequences of ubiquitination include the regulation of many cellular events, such as protein degradation, protein trafficking, transcription, DNA repair, cell-cycle progression and apoptosis. Such a diverse outcome of ubiquitination is achieved through selective attachment of ubiquitin to protein substrates and interaction of the ubiquitin signal with a vast array of ubiquitin receptors

and modulators. To distinguishably communicate with more than 150 known ubiquitin receptors, the ubiquitin signal itself needs to be diverse. Thus, ubiquitin chains are variable length and linkage type, thereby providing selectivity for ubiquitin receptors [81].
Ubiquitination is achieved through an enzymatic cascade involving ubiquitin-activating (E1), ubiquitin-conjugating (E2), and ubiquitin-ligating (E3) enzymes [82]. E1 charges ubiquitin via a thioester bond with its catalytic cysteine in an ATP-dependent manner. This induces structural changes in E1 that promote binding to an E2 conjugating enzyme, to which ubiquitin is transferred [83]. Typically, the ubiquitin loaded E2 subsequently binds to an E3 ligase which passes the activated ubiquitin to its protein substrate. This usually results in the covalent attachment of the ubiquitin C-terminal glycine to a lysine ε-amino group of the protein substrate. Furthermore, ubiquitins can be linked to each other via any of its seven lysines and its N-terminal methionine providing variability of the formed ubiquitin chains. Different linkage positions result in different ubiquitin chain conformations, defining the specifity for ubiquitin receptors and downstream events. For example, Lys48-linked chains adopt a “closed” conformation with tightly packed ubiquitin subunits and target the substrate protein for proteasomal degragation. By contrast, Lys63-linked chains are extended and frequently interact with ubiquitin receptors that are involved in cellular signaling events.
The human genome is estimated to encode two E1s, about 40 E2s and more than 600 E3 ligases [82]. In most cases it’s the pairing of E2 and E3 that determines both substrate specifity and the type of ubiquitin chain linkage, with the E2 having the major influence on the type of polyubiquitin chains formed and the E3 defining the ubiquitinated target substrate.
E3 ligases are sub-characterized by the presence of RING (Really Interesting New Gene), HECT (homologous to the E6-AP carboxyl terminus) or U-box domains. E3-ligases containing a HECT domain are by themselves catalytically active and transfer ubiquitin from the E2 to the protein substrate by forming a thioester bonded intermediate via a catalytic cysteine. By contrast, the structurally similar RING and U-box domains only serve a scaffolding role in linking an E2 enzyme to a specific protein substrate without forming a covalent intermediate [81].
The NMR structure of the human TRIM5α RING domain encompassing the first 78 N-terminal residues has recently been solved and features a characteristic ββα RING fold. However, the RING of TRIM5α contains shorter β-strands and a longer α-helix as compared to other typical RING domain structures (Figure 5 A) [84]. The domain coordinates two Zn2+ atoms tetrahedrally in a cross-brace conformation, with the first zinc finger being formed by four cysteines (CCCC finger) and the second zinc being coordinated by one histidine and three cysteines (CHCC finger) (Figure 5 B). By comparison to homologous RING domain structures, two functionally important surface regions were identified on the RING domain of rhesus TRIM5α. The first region defines a putative E2-binding patch that has a similar amino acid composition as in the E2-binding regions of Cbl, CHIP and cIAP2 RING domains [82]. The second identified region is located on the opposite side of the E2-binding patch and represents a putative RING-RING interaction surface that is similar to the interaction region in BCRA1 and BARD1 RING heterodimers [85]. In some non-TRIM proteins, RING domains play the role of molecular scaffolds for the formation of supramolecular complexes by self-association, which in a few cases improves E3-ligase activity [86-89].

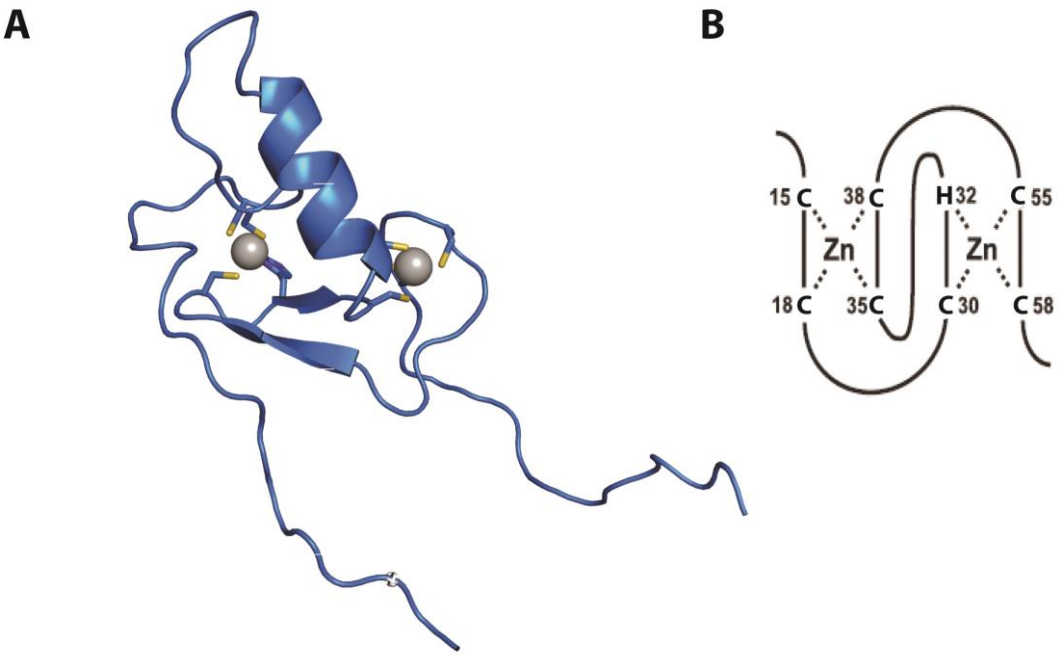

Figure 5. The RING domain of human TRIM5α. (A) The NMR structure of the human TRIM5α RING domain (pdb entry: 2ECV) is shown in cartoon representation with coordinated zinc atoms as grey spheres. **(B)** Schematic representation of the RING-finger showing the cross-brace coordination of the zinc atoms.

TRIM5α has been reported to mediate self-ubiquitination by cooperating with the E2 ubiquitin conjugating enzyme UbcH5b both in vitro and in vivo [80,84,90]. A role for the RING mediated self-ubiquitination was found in the rapid turnover rate of TRIM5α inside the cell that occurs in an ubiquitin and proteasome dependent manner [91]. Moreover, TRIM5α degrades at a higher rate when cells are challenged with viruses bearing restriction-sensitive capsids, suggesting a mechanism where proteasomes are recruited to auto-ubiquitinated TRIM5α bound virus particles [92]. Indeed, TRIM5α biochemically interacts with the proteasome component PSMC2 as well as the proteasomal adaptor protein p62 and colocalizes with proteasomes in infected cells [93,94]. Deletion of the RING domain or disruption of its zinc finger by the C15A/C18A mutation leads to a major loss of restriction activity and much prolonged half-lives of TRIM5α [30,95,96]. Although proteasome inhibitors simultaneously lengthen TRIM5α half-life and rescue viral reverse transcription as well, they do not eliminate restriction activity [97,98]. This apparent discrepancy might at least partially be explained by the fact that the RING domain is also required for the formation of higher-order self-assemblies and efficient CA binding [99]. However, a more detailed mutational study of the TRIM5α RING domain identified mutations in the putative E2 binding region that abrogated self-ubiquitination, but retained the ability of TRIM5α to self-associate and bind HIV-1 CA-NC tubes in vitro. These mutants did no longer block reverse transcription and showed a clear correlation between decreased ubiquitination activity and loss of restriction potency [84]. Interestingly, mutants of rhesus TRIM5α with substitutions at residue Tyr63 near the E2-binding cleft in the RING domain have lost the ability to block reverse transcription and fail to dismantle HIV-1 capsids in the faith of the capsid assay, but retain potent restriction of HIV-1 [100]. This phenotype

resembles more to the effect of proteasome inhibitors and suggests an additional redundant mechanism for TRIM5 mediated restriction that occurs after reverse transcription and prevents viral integration into the host genome.

1.3.2 The B-Box self-association domain

All TRIM proteins possess at least one, in some cases two B-Box domains. Based on differences in their zinc binding consensus motif and overall length, they are divided into B-Box type 1 (B-Box1) and B-Box type 2 (B-Box2) domains. While the B-Box1 is only found in a few TRIMs, the B-Box2 is present in all of its family members known to date and is regarded the determinant of the TRIM family of proteins [101]. In general, B-Box domains have been implicated in protein-protein interactions and in some cases like e.g. TRIM5 mediate higher-order self-association [102]. Atomic structures of B-Box1 and B-Box2 domains share a RING-like ββα fold and the similarity in tertiary structures suggests that these domains have evolved from a common ancestor gene [101-104]. In the crystal structure of TRIM63/MuRF1, the B-Box2 self-associates into homodimers with their α-helixes binding into the hydrophobic groove formed by β-sheets on the opposite protomer [101]. Insight into the relative domain arrangement in TRIMs containing two B-Boxes is given by the solution structure of TRIM18/MID1 B-Box1 B-Box2 tandem motif. Here, the two B-Boxes are forming a stable intramolecular interaction via an interface formed between the two domains, that is located on the opposite side of the B-Box2 homodimer interface [105].

TRIM5 possesses a B-Box2 domain and the NMR solution structure has been solved for residues 86-131 encompassing the B-Box2 of human TRIM5. It features the characteristic ββα RING-like fold that is maintained by two zinc ions in a CHCDC2H2-type coordination mode with an additional very short β-strand just before the helix (Figure 6). Interestingly, the majority of hydrophobic residues are solvent exposed and clustered, forming two hydrophobic patches on the domain surface, cluster1 and cluster2. Mutations near or within cluster1, which corresponds to the dimerization interface found in TRIM63/MuRF1, impaired the ability of TRIM5α to self-associate without affecting dimerization. Higher-order self-association of TRIM5α contributes to the efficiency of binding to CA-NC tubes in vitro and correlates with potency of retroviral restriction [102]. Thus the B-Box2 domain is required for TRIM5α restriction activity and plays an essential role in enhancing TRIM5 avidity to the retroviral capsid by mediating higher-order self-association.

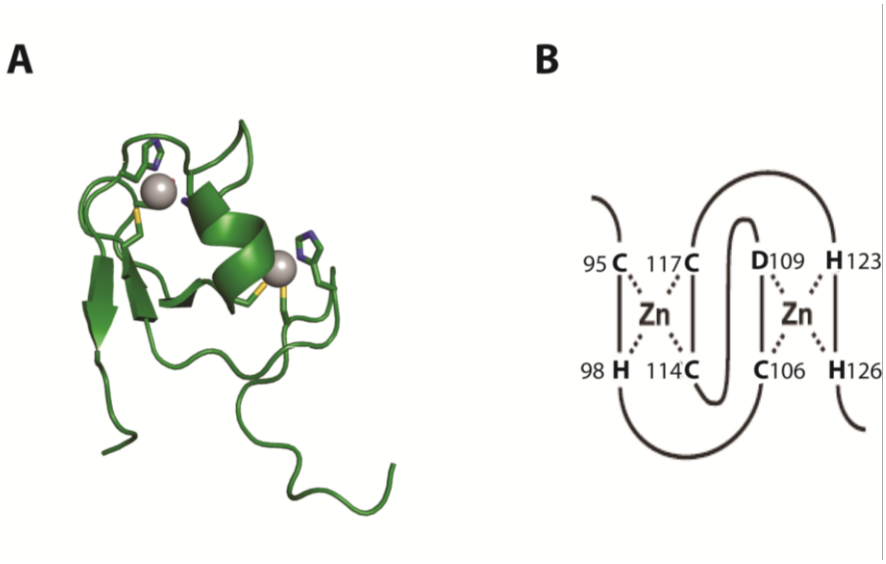

Figure 6. The B-Box2 domain of human TRIM5α. (A) The NMR structure of the human TRIM5α B-box2 domain (pdb entry: 2YRG) is shown in cartoon representation with coordinated zinc atoms as grey spheres. **(B)** Schematic representation of the zinc-fingers showing the coordination of the zinc atoms in a cross-brace manner.

1.3.3 The coiled-coil (CC) dimerization domain

TRIM proteins are predicted to contain a coiled-coil (CC) domain as part of their RBCC-motif (RING, B-Box and Coiled-Coil) [106]. CCs typically consist of two to five α-helixes that wrap around each other into a left-handed helix to form a supercoil [107]. Here each α-helix goes through 3.5 residues along the superhelical axis for each complete turn of the helix, whereas it is taking 3.6 residues per turn in regular α-helixes. This forces the helixes to intertwine against each other with a characteristic periodicity of seven residues (heptad repeat) occuring every two turns of the helix [108,109]. This repeat is usually denoted $(a\text{-}b\text{-}c\text{-}d\text{-}e\text{-}f\text{-}g)_n$ in one helix, $(a'\text{-}b'\text{-}c'\text{-}d'\text{-}e'\text{-}f'\text{-}g')_n$ in the next and so on, with positions a and d being hydrophobic core residues located in the interface between the bundled helices, e and g being exposed polar residues that give specifity between the helices through electrostatic interactions and the remaining three being hydrophilic solvent exposed residues [110] (Figure 7Figure 8). Due to this heptad pattern one nonpolar face is formed along each helix that facilitates oligomerization by packing of the hydrophobic side chains in a "knobs-into-hole" manner. This means that the hydrophobic side chains from one helix, such as the amino acid at position a (knob) binds into a hole formed by residues d', g', a' and d' + 1 heptad of the opposing helix [111]. The hydrophobic interactions are complemented by ionic interactions between charged residues at position e and g (Figure 7).

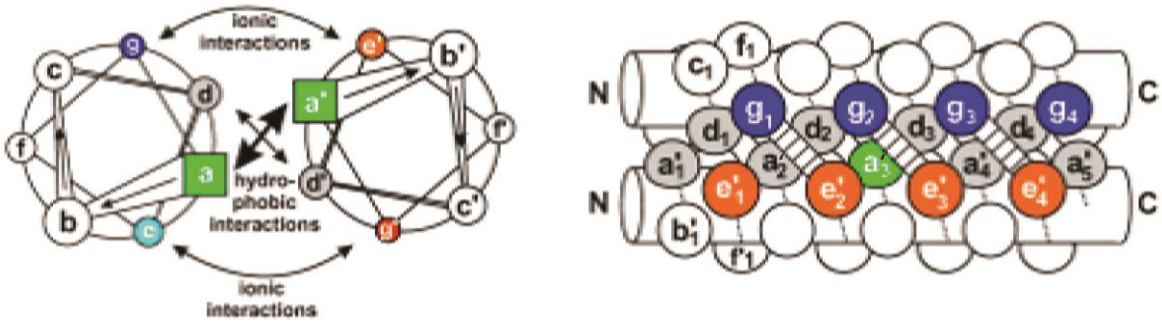

Figure 7: Schematic representation of a parallel dimeric CC. The helical wheel diagram on the left shows residues of the heptad repeat pattern with their contributions to the CC α-helical assembly. The knob-into-hole packing of hydrophobic residues as well as the ionic interactions are shown on the right (figure taken from [107]).

Subtle variations to the rules described above or changements in the type of hydrophobic and polar amino acids placed at position a, d or e, g, respectively determine the orientation, specifity and oligomerization state of the CC. Thus CCs can exist as parallel or anti-parallel homo- or hetero-oligomers and can vary in the extent of superhelical character due to shifts in the heptad pattern. A more dramatic shift in the repeat pattern is found in right-handed CCs: In these CCs the number of residues per turn is slightly increased to 3.67, thus giving a right-handed supercoil with eleven residues every three turns of the helix, forming a characteristic undecatad repeat pattern [112,113] (Figure 8).

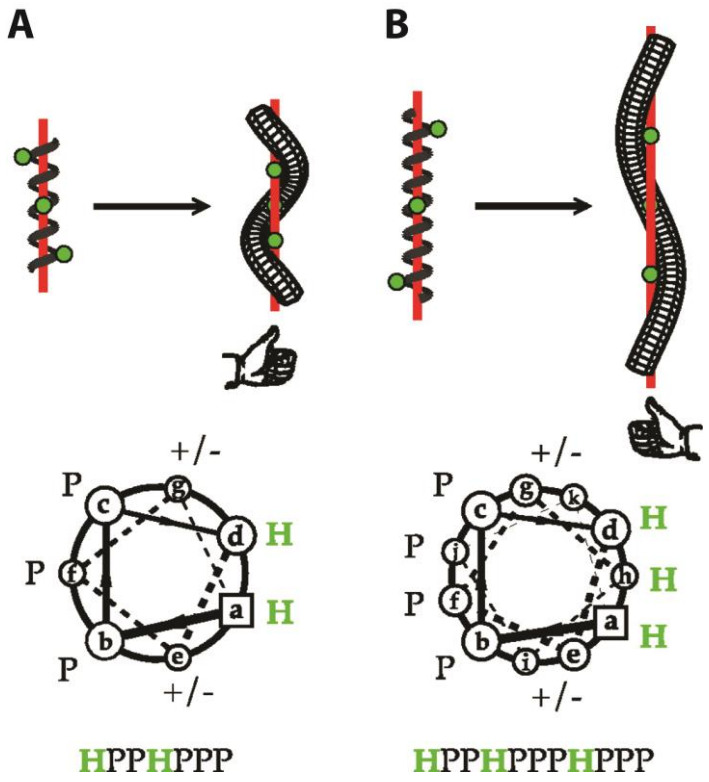

Figure 8: Schematic representation of left- and right-handed CCs. (A) A heptad repeat in a regular α helix produces a left-handed hydrophobic stripe and a left-handed supercoil. This arrangement is schematically illustrated alongside the standard sevenfold helical wheel projection for coiled coils. **(B)** An undecatad repeat in a regular α helix produces a right-handed hydrophobic stripe and a right-handed supercoil. The 11-fold helical wheel projection is illustrated. H, hydrophobic residue; P, polar residue; +/−, charged residue (figure and legend taken from [112]).

In TRIM5α, the predicted CC-domain is succeeded by a designated L2 linker region that connects to the C-terminal B30.2. Together, the CC and L2 confer low-order dimerization of the protein, which is indispensable for TRIM5α antiviral activity [114-119]. Alternative splice variants of TRIM5 that lack the B30.2 and sometimes other domains exert a dominant negative effect on retroviral restriction by higher-order associating with the alpha isoform, thereby down-regulating TRIM5 activity. Interestingly, splice variants or constructs that lack the CC domain fail to have any effect on TRIM5-mediated retroviral restriction [30,117,120,121]. From this point of view, the CC domain can be regarded the most crucial domain in TRIM5 proteins. Not only does it mediate dimerization, but together with the L2 it additionally contributes to the ability to form higher oligomers, through a mechanism that is not known [99,119,122]. Residues in the L2 region of TRIM5α have been identified that do not interfere with dimerization, but lead to a loss of restriction [122]. To date the CC is the only domain in TRIM proteins, for which no structural information is available.

1.3.4 The B30.2 capsid binding domain

The longest TRIM5 splice variant, isoform alpha, is the only one conferring retroviral restriction activity and it is unique in bearing a B30.2 (or PRYSPRY) domain at its C-terminus. This domain has its name from the exon it was first identified in, exon B30-2 in the human

major histocompatibility complex (MHC) class I region [123]. The alternative name PRYSPRY comes from the independent identification of a closely related domain named SPRY in the splA kinase from Dictyostelium discoideum and in mammalian ryanodine receptors (RyR) [124]. Sequence alignments revealed that the SPRY domain shares a consensus motif with the C-terminal part of the B30.2 domain. However, B30.2 domains have an additional N-terminal consensus motif that is not present in SPRY domains on a sequence level [125]. This extension is sometimes referred to as PRY (for SPRY associated domain), hence the name PRYSPRY that is synonymous with the B30.2 domain [126].

B30.2 domains are found in over 500 different proteins [127], including many that have later been identified as TRIM family members [123]. Indeed, the B30.2 domain is present in almost half of the TRIM proteins and the structures of several B30.2 domains have been solved. These include the structures from sRFPL1, TRIM5α, TRIM20/pyrin, TRIM21, TRIM25 and TRIM72/MG53 [126,128-133]. B30.2 structures share an identical fold composed of two layers of antiparallel β-sheets that stack together into a distorted β-sandwich with non-structured loops connecting the individual β-strands. TRIM5α differs slightly from other B30.2 domains due to the increased length and flexibility of its unstructured loops. This is in particular true for the longest loop v1, which was found to be highly dynamic and completely unhooked from the domains core structure as determined by a complementary structural study that combined NMR with X-ray crystallographic data [129] (Figure 9).

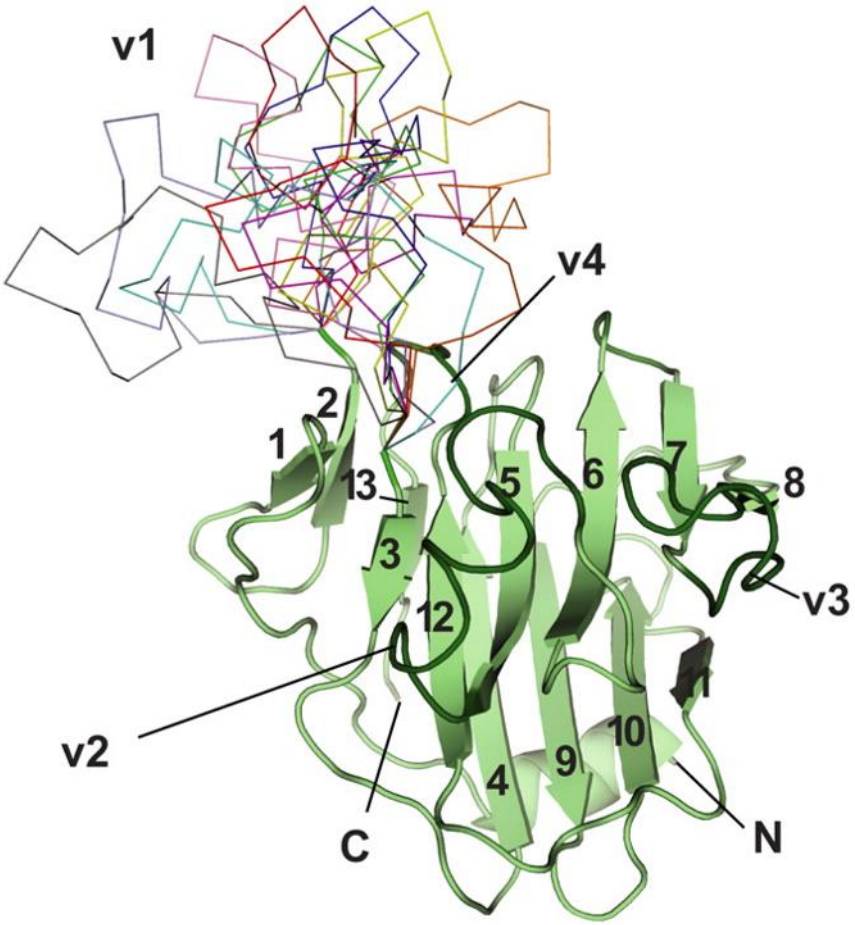

Figure 9: Structure of the rhTRIM5α B30.2 domain. The X-ray structure of the rhesus TRIM5α B30.2 domain with the most dynamic variable loop (v1) substituted by a two amino acid linker shown in cartoon representation and was supplemented with the NMR relaxation parameters of the variable v1 loop. The ten lowest-energy conformations of the v1 loop calculated using NOE restraints are shown as colored ribbons. The strands forming the beta sandwich B30.2 fold are numbered, and the variable loop regions (v1-v4) are labeled and highlighted in dark green (figure taken from [129]).

Deletion of the B30.2 domain in several proteins, including TRIM5, abolishes the interaction with their respective binding partners suggesting that the B30.2 acts as a protein-interaction module [134]. Direct binding of TRIM5α to retrovirion CA cores is required for restriction and is mediated by the B30.2 domain. This has been demonstrated by co-sedimentation of TRIM5α either with detergent-stripped virion cores or with in-vitro assembled core-like CA particles [77,114,115,135,136]. Association of TRIM5α orthologs with retroviral CA particles correlated with respective restriction specifities and was dependent on the presence of the B30.2 domain [77,135]. In the case of TRIM5α, the B30.2 domain constitutes the main determinant for virus specifity and hybrid TRIM5α proteins with swapped B30.2 domains originating from orthologs of a different restriction specifity regain the respective restriction phenotype. For example cells expressing a chimeric TRIM5α composed of human RBCC domains fused to the rhesus B30.2

domain obtain the restriction phenotype of rhesus TRIM5α, thus becoming restrictive against HIV-1 [121].
Overall, the B30.2 domain functions as a point of contact with the retroviral CA and manipulations that disrupt this interaction also disrupts TRIM5α restriction activity against that retrovirus [30,32,76,117,121,137-146].

1.3.5 Independent Evolution of a TRIMCyp fusion gene

As already mentioned, a TRIM-cyclophilin A (TRIMCyp) fusion gene that confers potent HIV-1 restriction activity was first discovered in new world owl monkeys, independent of the simultaneous discovery of TRIM5α in rhesus monkeys [31]. Cyclophilin A (CypA) in its free form is a ubiquitously expressed cytoplasmic protein that catalyzes cis/trans isomerization of peptidyl-prolyl bonds [147]. It acts as a co-factor for HIV-1 by binding to an exposed loop on the viral CA surface and promotes an early step of HIV-1 infection in human cells [147-156]. Knock-down or inhibition of CypA by cyclosporine A (CsA) in target cells delays HIV-1 replication [153,154]. CypA is incorporated into HIV-1 CA cores in a stoichiometric ratio of 1:10 and has a measured affinity of KD = 16 µM for the isolated CA protein [157]. The relatively high affinity of CypA for the HIV-1 CA likely explains the potent HIV-1 restriction activity found in TRIMCyp expressing owl monkey cells.
The TRIMCyp fusion gene in owl monkeys, carries all the hallmarks characteristic for LINE1-mediated retrotransposition events, giving a likely explanation for the mechanism behind the insertion of a complete CypA cDNA into the TRIM5 locus [31]. In the case of owl monkeys, TRIMCyp is the only TRIM5 allele found in all ten species from the genus *Aotus* (owl monkeys) and phylogenetic analysis of these genes suggest a single retrotransposition event having occurred in a common ancestor several million years ago [31,144,158,159]. Though not as ubiquitous as in the *Aotus* species, a similar TRIMCyp fusion gene arose in the genus Macaca by convergent evolution and is found in at least three Macaca species [160-163]. As in Aotus, the Macaca fusion gene was most likely generated by the enzymatic machinery of a LINE-1 element. However, they were clearly generated independently of the Aotus fusion gene, because the cDNAs encoding CypA are inserted at different positions into the TRIM5 locus: While in Aotus the CypA cDNA is inserted into TRIM5 intron 7 proceeding exon 8 encoding the B30.2 domain, the Macaca CypA was retrotransposed just 3’ of exon 8 requiring a different splicing pattern to yield a functional TRIMCyp protein. In Macaca the 3’ splice acceptor site before TRIM5 intron 7 is disrupted, thus bypassing exon 7 and 8 and linking exon 6 to CypA by splicing to generate mRNAs encoding TRIMCyp [161]. Compared to *Aotus*, the Macaca TRIMCyp gene product is slightly shorter because it lacks exon 7 coding for the N-terminal α-helix of the B30.2 domain.

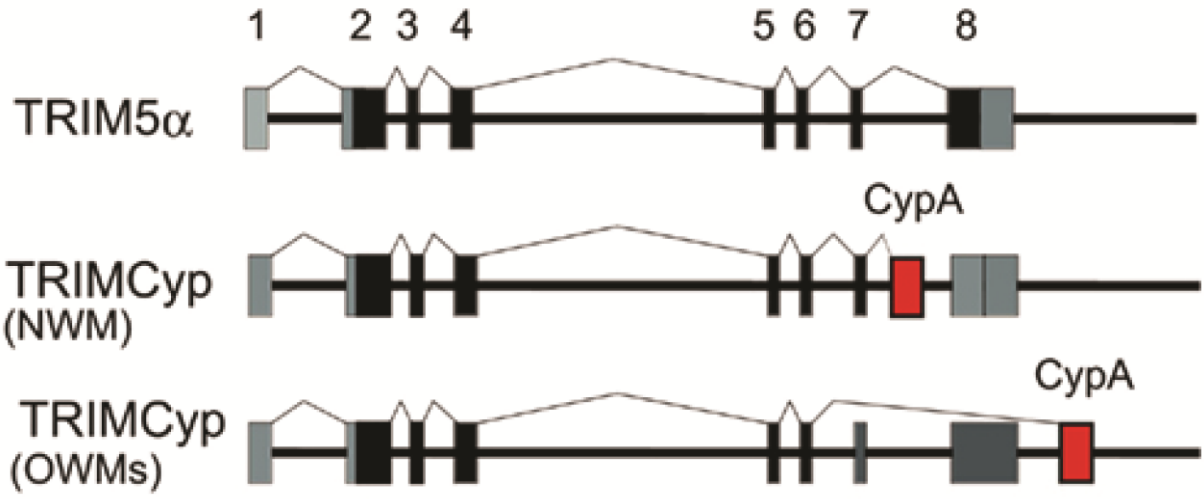

Figure 10: Structure of the *Aotus* and *Macaca* TRIMCyp genes compared to TRIM5α. Diagram illustrating the splicing pattern of TRIM5α or TRIMCyp in New World monkey (NWM) *Aotus* and Old World monkeys (OWMs) *Macaca*. Non-coding and coding exons and cyclophilin A (CypA) sequences are shown in gray, black, and red, respectively (figure taken from [164]).

Based on the Aotus TRIMCyp gene sequence, Neagu *et al.* have engineered a series of TRIMCyp fusions using human gene sequences, some of which potently restricted HIV-1. However, the exact positioning of the CypA insertion into the TRIM5 locus turned out to be very critical, as some of the engineered constructs failed to restrict HIV-1 [165]. Differences regarding the relative spatial arrangement of the CypA domains in the context of a TRIM5 dimer may account for the different restriction phenotypes observed with the engineered TRIMCyp constructs. Therefore, it will be very interesting to gain insight into the structure function relationship of these constructs, once structural information on TRIM CC-L2 dimerization domains is available.

1.4 The Broad Restriction Spectrum of TRIM5 and Determinants for Viral Tropism

Each TRIM5 ortholog ranging from human to various primate species recognizes and restricts a slightly different set of retroviruses in a species-specific manner. For example, TRIM5α from rhesus macaques inhibits HIV-1, EIAV, as well as FIV, while human TRIM5α only weakly inhibits HIV-1, but restricts infection by N-MLV and EIAV instead [32,137,138,141,166,167]. Remarkably, even TRIMCyp orthologs from Aotus or Macaca that harbor a C-terminal CypA as a CA binding domain instead of a B30.2 domain differ from each other in their respective restriction range for retroviruses: Whereas Aotus TRIMCyp recognizes HIV-1 and FIV, TRIMCyp bearing Macaca subspecies have evolved to restrict different subsets of retroviruses [162,163,168-170]. Macaca mulatta (rhesus macaque) TRIMCyp restricts HIV-2 and the O-groups of HIV-1. In contrast, Macaca fascicularis TRIMCyp restricts HIV-1, FIV and SIVtan but not HIV-2, similar to *Aotus*.

It is subtle differences in the amino acid sequence of the B30.2 or CypA domains, such as non-synonymous single nucleotide polymorphisms (nsSNPs) or small insertions that account for the inter-species differences in restriction specifities [142-144,171-174]. This is best illustrated by the fact that a single amino acid substitution, R332P, in the B30.2 domain of human TRIM5α is sufficient to confer potent anti HIV-1 restriction activity [145,146].
Altogether, TRIM5 orthologs have divergently evolved to restrict a broad range of retroviruses, spanning the families of spumaviruses, betaretroviruses, lentiviruses and gammaretroviruses [78]. The ability of a same TRIM5 ortholog to bind to various retroviral CAs and the minor changements required to switch restriction specifity towards different retroviruses transpires that different retroviral CAs share a common binding epitope recognized by TRIM5. While high-resolution structures are available both for retroviral CAs and the TRIM5 B30.2 domain, there is no direct structural information identifying the binding interface. However, by looking at residues under strong positive selection, determinants for restriction specifitiy or CA mutations that allow viruses to escape TRIM5 restriction, a glimpse into the putative binding epitopes can be gained.

1.4.1 Determinants of antiviral specifity on the B30.2 domain

As mentioned above, it is the C-terminal B30.2 domain that carries the determinants for virus specifity of TRIM5α. Sequence analysis comparing TRIM5α orthologs from different primate species has revealed four poorly conserved variable regions (v1 – v4) within the B30.2 domain that coincide with hot spots of positive selection through primate evolution [142,143]. Most of these sequence variations are clustered in a 13-amino-acid stretch comprising the longest variable loop v1 [142,143]. Experiments with chimeric rhesus-human TRIM5α proteins containing exchanged v1 regions have demonstrated that HIV-1 restriction specifity is largely determined by this variable hotspot [121,142,145]. These included the single amino acid substitution (R332P) in human TRIM5α that conferred potent HIV-1 restriction activity to this otherwise permissive ortholog. In contrast, spider monkeys have an expanded B30.2 v3 region in TRIM5α due to a tandem triplication that was found to be determinant for its broadened range of restricted viruses, including SIVmac, SIVagm, HIV-1 and N-MLV [144]. Mapping of specifity determinants for N-MLV restriction by human TRIM5α has also pointed out the importance of other variable regions besides the v1 (Figure 11 A) [175-177].

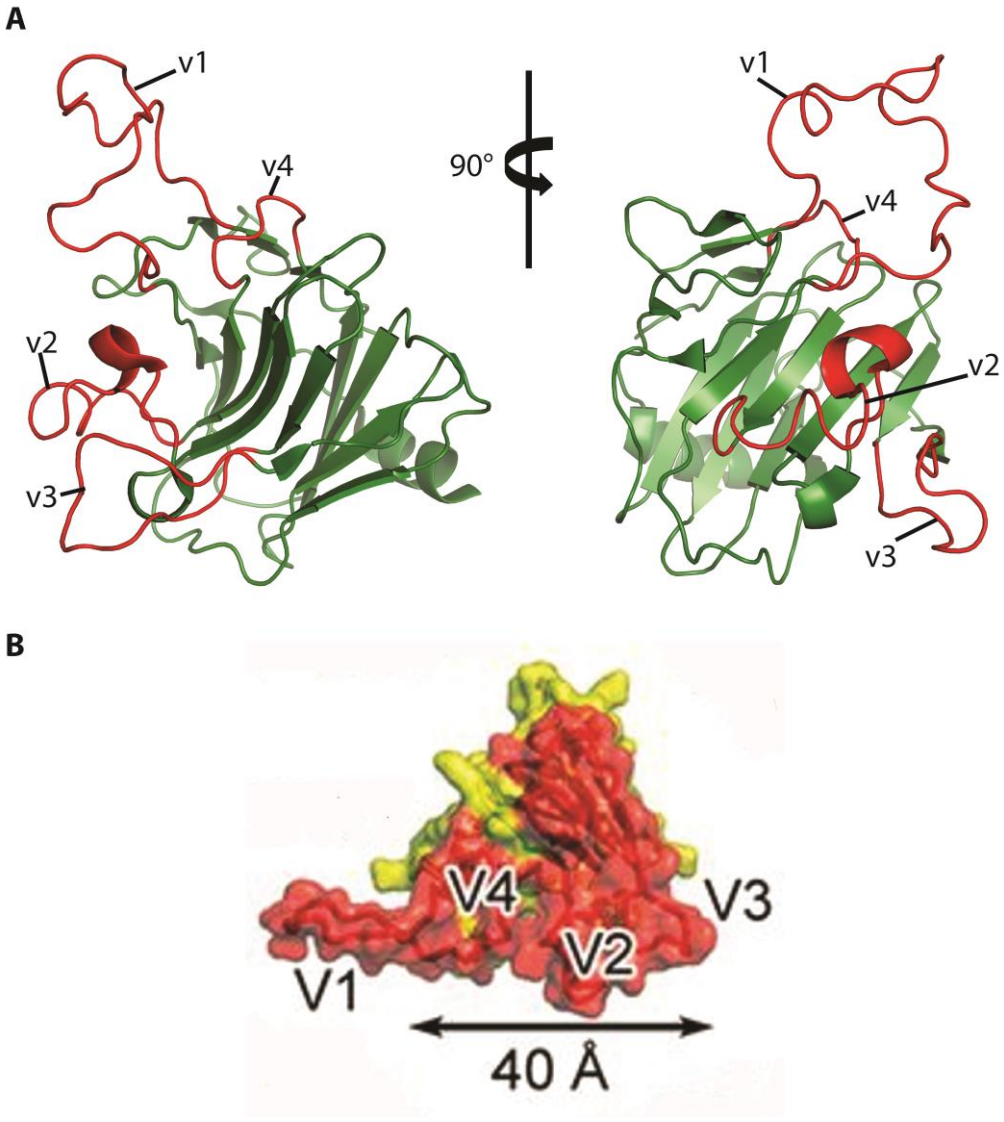

Figure 11: Putative binding surface on the rhesus TRIM5α B30.2 domain. (A) Two views of the atomic structure of the rhesus TRIM5α B30.2 domain in cartoon representation. The variable loops (v1 –v4) that are determinant for virus specificity are colored in red and the domains core structure colored in green. **(B)** Altogether, the determinant regions for virus specificity make up for a large binding surface on the B30.2 domain (colored in red). The dimension of this surface are indicated by the arrow on the bottom.

Inspection of the rhesus TRIM5 B30.2 structure reveals that the major differences between TRIM5α species of different virus specifities cluster on one surface of the B30.2 domain, comprising the longest variable loops [129,130]. These residues form a large surface predicted to span a distance of 45 Å up to 70 Å, likely covering more than just one molecule on the CA core [130]. This surface is formed by the variable loops and the β-sheet surface between them (Figure 11 B). Intriguingly, there is striking congruence between the positions of residues that influence capsid recognition in TRIM5α, antibody binding in TRIM21, and the occurance of a hereditary disease when mutated in TRIM20/pyrin and TRIM18/MID1 [78,178].

1.4.2 Determinants on the CypA domain of TRIMCyp fusion proteins

Human CypA and its interaction with the HIV-1 CA are well characterized and the crystal structure of CypA bound to the HIV-1 CA N-terminal domain has already been solved in the nineties [148,149,179]. CypA binds to residues G89 and P90 in a surface exposed loop on the HIV-1 CA surface, thereby promoting an early step in the infection of human cells [148-156]. This loop in the CA N-terminal domain is therefore termed as the CypA binding loop.

Whereas Aotus TRIMCyp recognizes HIV-1 and FIV, as does the parental CypA protein, the restriction profiles of Macaca TRIMCyp orthologs differ from the set of viral CAs recognized by their parental CypA [162,163,168,169,180]. Several non-synonymous amino acid changes are found when the CypA domain of the fusion gene is compared with the parental Macaca CypA [134]. These single amino acid substitutions cause a switch in restriction specifity in the respective TRIMCyp variants bearing them (Figure 12). In M. mulatta and M. nemestrina (pigtail macaque) two amino acid changes are found, D66N and R69H. Structural analysis of the CypA domain from M. mulatta TRIMCyp revealed that these substitutions alter the conformational space of the cyclophilin active site loop encompassing residues 66 and 69 [169,170,181]. The R69H mutation expands antiviral specifity by allowing an open binding site conformation and enabling binding to the CA of HIV-2, while maintaining the ability to hold the closed binding site conformation that allows binding and restriction of HIV-1. The second substitution D66N directs specifity away from M-group, while keeping the ability to restrict O-group HIV-1 and HIV-2 thus maintaining the conformational flexibility (Figure 12 A,B) [181]. The CA of HIV-2 differ from HIV-1 mainly by bearing a CypA binding loop that is shorter by one residue. The shift of restriction specifity towards O-group HIV-1 is associated with the occurance of methionine, valine or isoleucine at CA position 88 that is preferentially found in O-group HIV-1 isolates [169]. Interestingly, like Aotus TRIMCyp, the M. fasicularis (cynomolgus macaque) TRIMCyp restricts HIV-1, FIV and SIVtan but not HIV-2 despites bearing the specifity enhancing R69H substitution. Here the substitution E143K that is located distant from the CypA active site has been found to cause a conformational change that is propagated to the active site loop and alters CA recognition towards M-group HIV-1 (Figure 12 C) [78,170]. Remarkably, the occurrence of these specifity determining substitutions does not follow the macaque phylogenetic history, hinting that suggestive waves of infections with an unknown ancestral lenivirus has differentially affected the selection of TRIMCyp variants in the macaque subspecies (Figure 12 B).

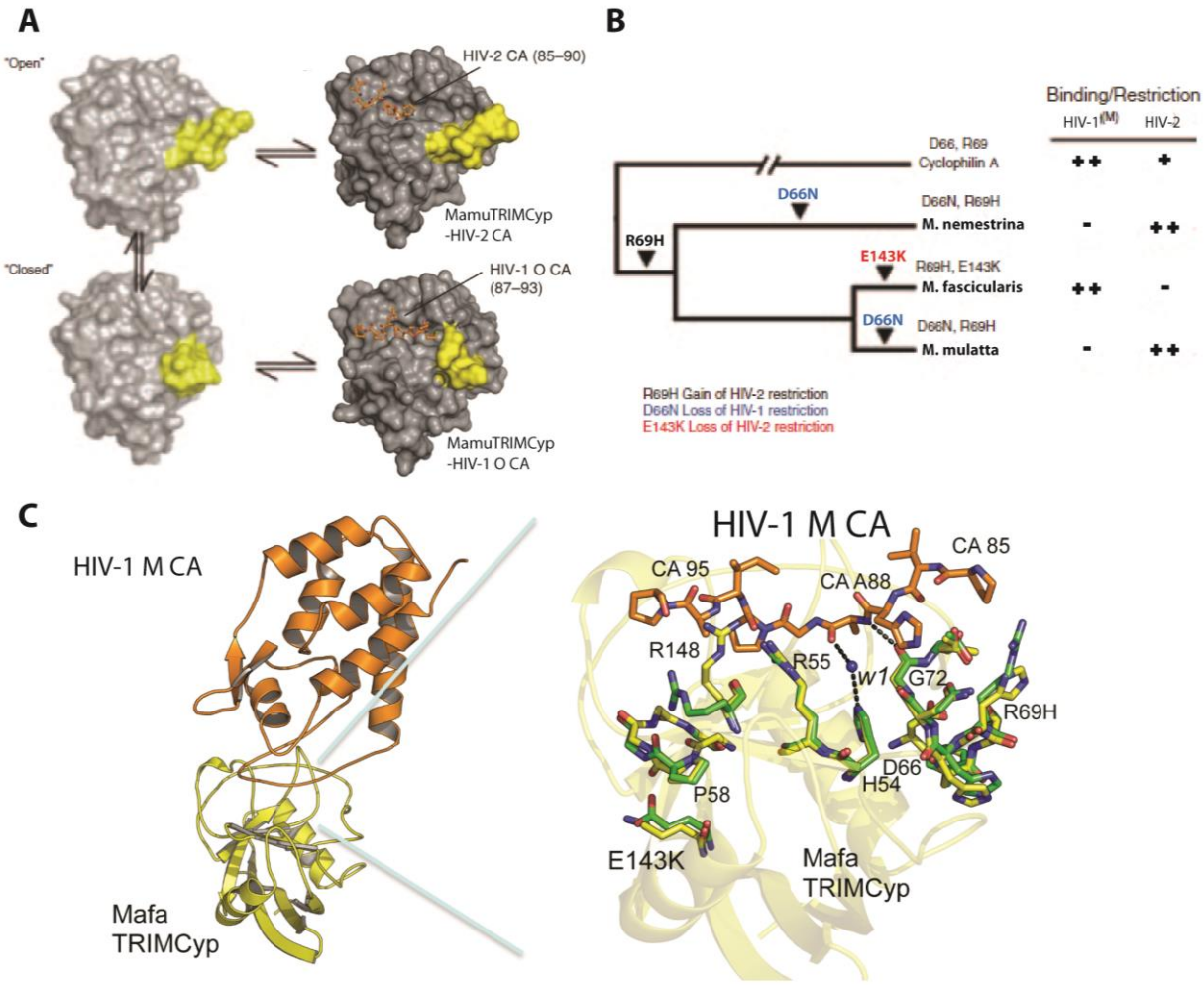

Figure 12. Evolution of TRIMCyp in Asian macaques. (A) Conformational diversity conveyed by the mutations D66N and R69H in the TRIMCyp cyclophilin domain from Asian monkeys. This diversity enables TRIMCyp to simultaneously restrict HIV-2 and O-group HIV-1 by switching between an "open" and a "closed" conformation. The CypA domain of *M.mulatta* TRIMCyp is shown in a gray surface representation. Bound HIV-2 and HIV-1 O-group derived CA peptides are shown in orange. **(B)** Dentogram illustrating the macaque phylogeny with the amino acid changes that have occurred. The restriction specificity of the TRIMCyp species variants is shown on the right. **(C)** X-ray crystal structure of the HIV-1 CA NTD (orange) in complex with *M. fascicularis* (Mafa) CypA (yellow) next to a detailed view of the active site. The detailed view shows a superposition of side chains from the M-type HIV-1 CA:human CypA complex (pdb entry: 1AK4) colored in green and the Cyp side chains from *M. fascicularis* CypA TRIMCyp colored in yellow with interacting residues from the HIV-1 CA CypA-binding loop colored in orange (Figure adapted from [78,170,181]).

1.4.3 Determinants for TRIM5α sensitivity on the Retroviral Capsid

Collectively, TRIM5α proteins restrict a surprising diversity of retroviruses, bearing capsids that are only distantly related, at least on the level of primary sequence [78]. For example human TRIM5α restricts both the murine lentivirus N-MLV and the equine gammaretrovirus EIAV [32,137,138,141]. The rhesus TRIM5α protein inhibits HIV-1, N-MLV, EIAV, as well as FIV with HIV-1 and EIAV CAs sharing as little as 25% sequence identity [137,138,166,182]. Thus, retroviral CAs must share common binding epitopes recognized by TRIM5α despite the

sometimes low sequence identity. Another conserved structural feature shared amongst retroviruses is the organization of CA molecules into a hexagonal lattice in the context of an assembled mature CA core [183]. The fact that TRIM5α requires an assembled CA for efficient binding supports the hypothesis that TRIM5 recognizes a lattice associated pattern on the CA surface [77,135]. A model whereupon the interaction between TRIM5α and the CAs is based on multiple low-affinity interactions at multiple points of contact in the CA lattice is supported by the existence of two similar clefts in the N-terminal domains of MLV and HIV-1 CA [136,184]. Residues that influence sensitivity to TRIM5α map into those two clefts (Figure 13). One cleft is formed by CA α-helices 4-6 in MLV and 4-7 in HIV-1 and contains determinants for viral tropism such as residue 110 that is determinant for N- or B-tropism, or residues 82 and 117 that when mutated allowed B-MLV to escape restriction by the B-MLV tropic human TRIM5α(Y336A) v1-loop mutant [73,140,175,182,185,186]. Recently, efforts to construct a macaque-tropic HIV-1 have led to the identification of three amino acid substitutions in HIV-1 Gag-CA (M96L/R100S/G116) that map into the same cleft [187]. HIV-1 clones bearing these mutations escaped restriction by rhesus TRIM5α suggesting that these amino-acids interact with rhesus TRIM5α. The second cleft is formed by the N-terminal β-strands and α-helix 6 in both MLV and HIV-1 CAs. This region is critical for N-MLV restriction by rhesus TRIM5α, as the L10W mutation that obscures the cleft prevents rhesus TRIM5α binding and allows the virus to escape restriction [182].

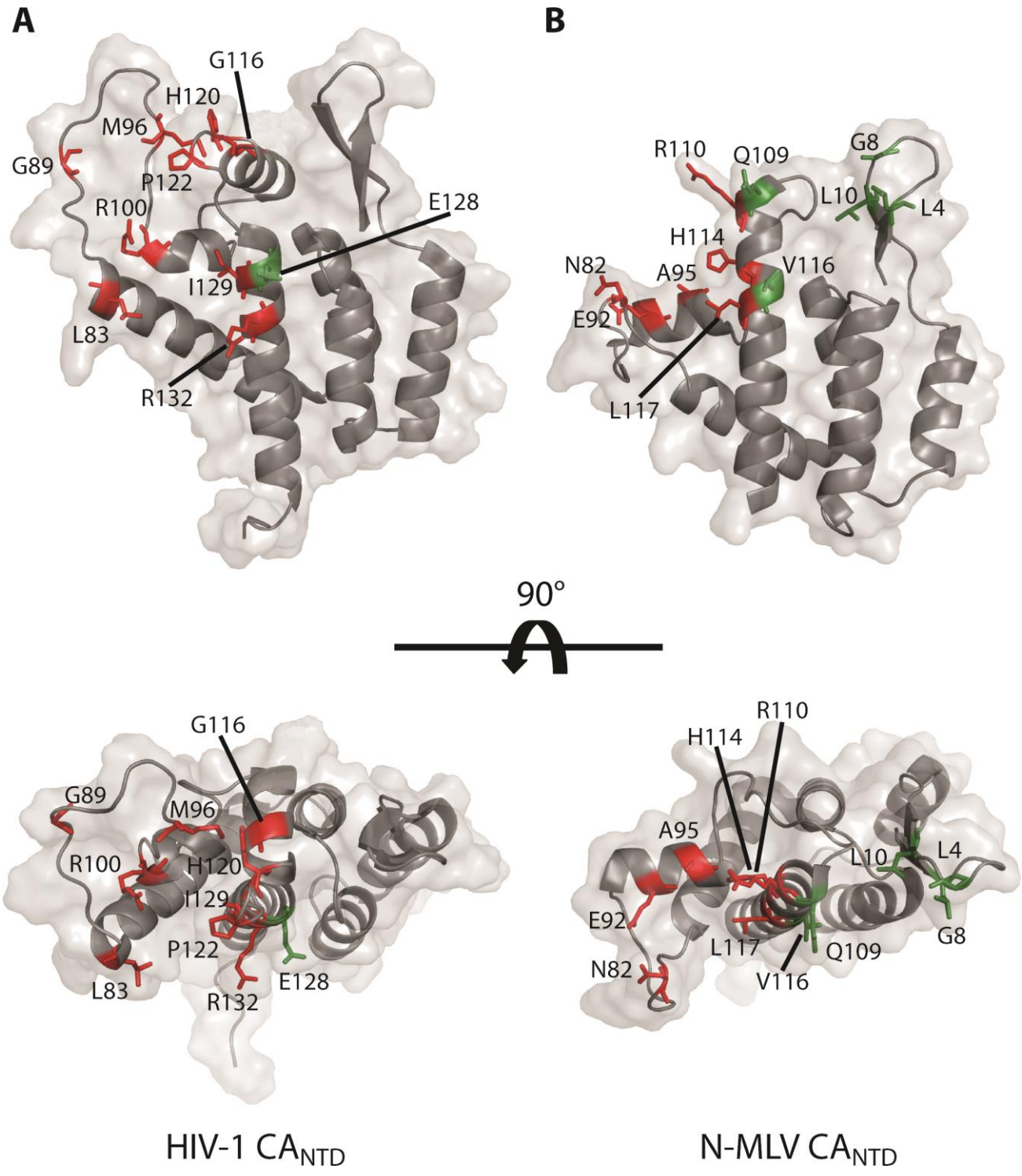

Figure 13: Determinants for TRIM5α sensitivity on the N-termimal CA domains of HIV-1 and MLV. The atomic structures of the HIV-1 and MLV CA NTDs are shown in cartoon representation inside the surface envelope. Residues in the NTDs of HIV-1 and MLV CA proteins that influence sensitivity to TRIM5α occupy two surface-exposed clefts. Residues mapping to the outer edge near the CypA binding loop are colored in red and residues in the cleft near the β-hairpin are colored in green.

Nevertheless, it is very difficult to predict the CA regions bound by TRIM5α, because residues influencing TRIM5 restriction cover virtually the whole accessible surface on the CA N-terminal domain. Further insight into the mode of ligand binding by B30.2 domains can be gained by the B30.2 domain structures of sRFPL1, TRIM21 and the SPRY of GUSTAVUS that were crystallized with a bound ligand [128,178,188]. Although the B30.2 domains all use a similar epitope for ligand binding, the mode of interaction with their ligands differs considerably from each other: While sRFPL1 and GUSTAVUS both bind to a linear peptide, TRIM21 binds to the Fc-region of IgG via a complex interface including both the constant region 2 and 3 of the antibody's heavy chain. Therefore it is well possible that the TRIM5 B30.2 recognizes retroviral CAs by binding both to linear epitopes, such as the CypA binding loop, and to complex surfaces of the CA N-terminal domain.

1.5 The Quaternary Lattice Structure of the mature HIV-1 Capsid

Retroviral CA proteins share a conserved tertiary structure and arrange into hexagonal lattices to form a retroviral core surrounding the viral genome [183]. However, retroviral CAs assemble into cores of different morphologies. The preferred shapes adopted by retroviral CAs include cones (e.g. HIV), cylinders (e.g. Mason-Pfizer monkey virus (MPMV)), or spheres (e.g. MLV) [183]. The HIV-1 capsid is best described by a fullerene cone model, where CA molecules assemble into a curved hexagonal surface lattice that forms a closed shell by the incorporation of 12 pentamers [184,189-194]. Molecular dynamics simulations based on cryo-electron microscopic (cryo-EM) data of assembled HIV-1 CA particles and preexisting atomic-resolution structures suggest that the fullerene cone is composed of 186 – 216 CA hexamers with five CA pentamers placed at the narrow end and seven CA pentamers at the wide end [191]. To understand how the drastically different curvatures required to achieve a conical shape are accommodated in the hexagonal CA lattice, the intermolecular interactions at all four interfaces critical for assembly need to be considered: the inter-hexamer CTD interfaces at the pseudo-two-fold and pseudo-three-fold axes, and the hexamer forming NTD-NTD and NTD-CTD interfaces [191].

HIV-1 CA molecules primarily exist as stable dimers in solution and therefore constitute the starting unit for mature CA assembly, which is thought to occur de-novo during virus maturation. Semi-three-dimensional Monte Carlo simulations of the initial stages of HIV-1 CA self-assembly suggest that CA dimers first condense into trimers of dimers initiating the formation of disordered clusters, which nucleate lattice formation upon appearance of the hexamer unit within a cluster (Figure 14) [191,195].

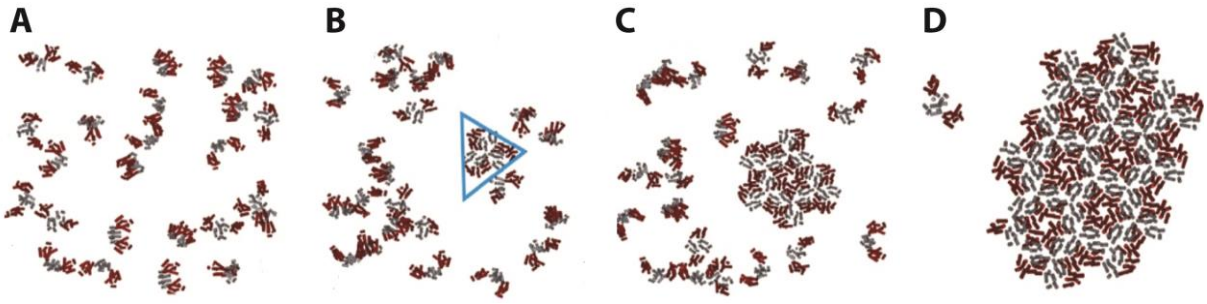

Figure 14. Monte Carlo simulation of HIV-1 CA assembly. The Monte Carlo simulation with CA interaction parameters as described in [191] reveals the initial steps of CA assembly. HIV-1 CA molecules are depicted with the NTDs colored in red and the CTDs colored in grey. Snapshots of assembly during the simulation process are shown. **(A)** Prior to assembly, the HIV-1 CA molecules are present as dimers in solution. A trimer of three CA dimers is initially formed (highlighted by the blue triangle) **(B)** and following the appearance of a first hexamer **(C)** quickly grows into a full hexagonal lattice **(D)**. (Figures are adapted from [191]).

Molecular dymanics flexible fitting (MDFF) of atomic CA structures into the 8.6 Å resolution cryo-EM map of tubular HIV-1 CA assemblies revealed an almost invariant NTD hexamer that closely resembles to the crystal structure of a cross-linked CA hexamer (Figure 15). This structure shows that the NTD-NTD contacts are dominated by complex hydrogen networks involving coordinated water molecules and the CA hexamer is further stabilized by interlocking NTD-CTD interactions between neighboring protomers. The NTD hexamer is surrounded by a more variable girdle of CTDs, which connect adjacent NTD hexamers via CTD-CTD interactions. CA dimerization is mediated by CTD α-helix 9 forming homotypic interactions between CTDs. Three distinct CTD dimer conformations are observed in the MDFF model of helical CA tubes, with dimerization helix 9 crossing angles of 36°, 44° or 54°, possibly adapting to the relative orientation of hexamers along the three helical directions of tubular CA assemblies (Figure 15 A). Another important feature is the CTD trimer interface formed at the pseudo-three-fold axis between adjacent hexamers. This interface is formed by a patch of hydrophobic residues situated on one face of CTD α-helix 10 and is specific to the mature capsid, as these residues do not contact each other in maturation defective virions in which cleavage of the nucleocapsid is prohibited [191,196].

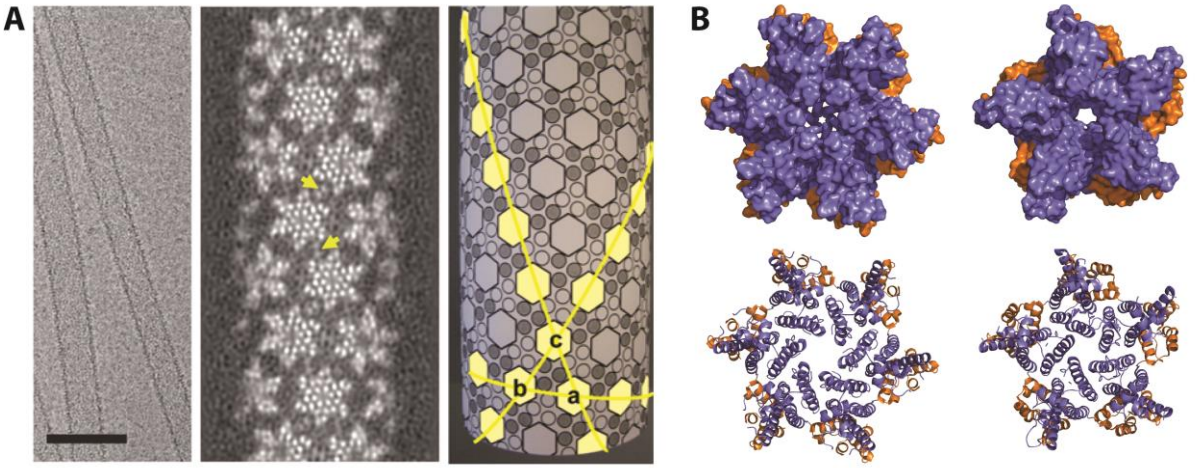

Figure 15. HIV-1 CA tubular assemblies and building blocks of the HIV-1 CA cone. (A) A cryo-EM image of recombinant A92E CA tubular assembly (scale bar, 100 nm) is shown on the left, with the electron density map of the A92E CA tube showing helical symmetry depicted in the middle. Yellow arrows indicate CA helix 9 located at the CTD dimer interfaces adjacent hexamers. On the right side is a schematic representation of the CA tubular assembly. The three helical directions of tubular CA assemblies (a-b, b-c and a-c) are highlighted in yellow. **(B)** X-ray structures of a disulfide linked A14C/E45C/W184A/M185A CA hexamer (pdb entry: 3H47) as present in HIV-1 CA tubular assemblies and a disulfide linked N21C/A22C/W184A/M185A CA pentamer (pdb entry: 3PO5) as required to close the HIV-1 CA cone. The structures are shown in surface representation on the top and in cartoon representation below. The NTDs are colored in blue and the CTDs are colored in orange. (Figures are adapted from [191], [114], [189], [190]).

Formation of a HIV-1 CA fullerene cone requires the insertion of 12 CA pentamers to close the shell (Figure 16 A). The crystal structure of a pentameric HIV-1 CA mutant reveals subtle rearrangements of the NTD-NTD interactions compared to the quasi-equivalent hexameric CA structure (Figure 15 B) [189,190]. These minor differences are adopted by coordinated water molecules in the hydrogen-bonding network between the NTDs, as direct hydrophilic contacts are absent in either of the two structures [189,190]. The molecular dynamics simulation of a CA pentamer surrounded by five hexamers (pentamer-of-hexamers / POH) and comparison to the hexamer-of-hexamers (HOH) extracted from the helical CA tube model, illustratively demonstrates how CA pentamers induce a sharp increase in CA curvature at the point of insertion: POHs form a highly curved dome-like structure, while HOHs are just slightly bent (Figure 16 B) [191]. Differences in CA curvature are accommodated at the trimeric CTD interface, which is more closely packed in the POH compared with the HOH (Figure 16 C) and even absent in the planar two-dimensional crystal of the assembled HIV-1 CA [191,197].

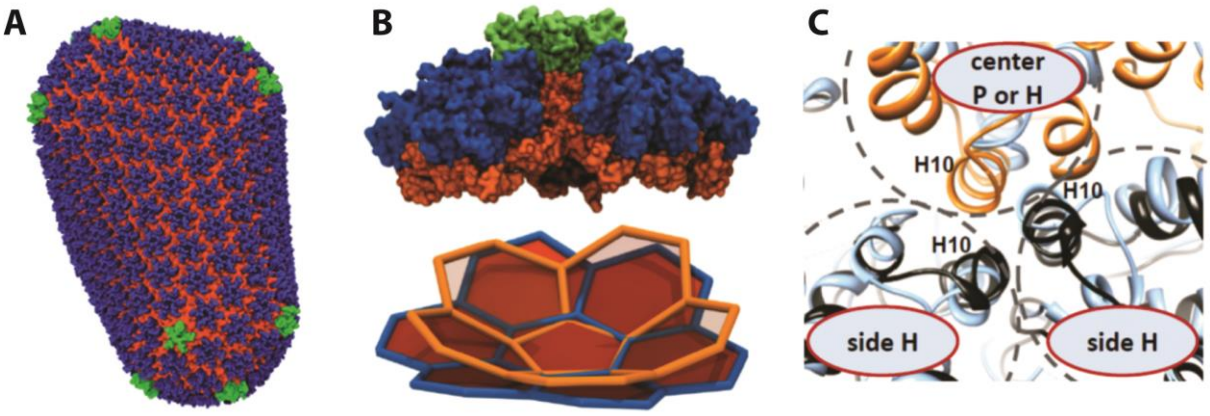

Figure 16. Incorporation of curvature enhancing pentamers into the HIV-1 CA cone. (A) Molecular dynamics equilibrated all-atom model of the HIV-1 CA cone (pdb entry: 3J3Q) comprising 216 CA hexamers (blue, NTD; orange, CTD) and 12 CA pentamers (green). **(B)** All-atom MD simulation of a CA pentamer surrounded by CA hexamers (POH). On the top is a surface representation of the POH viewed along the tube axis (NTD in green for the pentamer and blue for the hexamers with CTDs all in orange). Below is a comparison of curvatures between POH (orange) and HOH (blue). **(C)** Comparison of CTD trimer interfaces arising in HOH (light blue) and POH (orange and black). The three CTDs at the trimer interface are within the dashed circles. (Figures taken from [191]).

Zhao *et al.* have shown that HIV-1 CA tubes cross-linked via introduced cysteines at the CTD trimer interface resist structural damage exerted by a truncated rhesus TRIM5α construct comprising the CC and B30.2 domains. By contrast, cysteine cross-linking at the hexamer interfaces did not prevent TRIM5 mediated CA damage, which results in the release of CA strings. Based on these findings, the authors conclude that TRIM5α engages at the inter-hexamer interfaces, connecting adjacent hexamers while destabilizing the CTD trimer interface [114]. This goes in line with the observation that most residues that influence TRIM5α sensitivity map to the outer edges of the CA hexamer [73,140,175,182,185-187].

1.6 TRIM5 Avidity for the Retroviral Capsid Lattice

TRIM5α does not appreciably interact with monomeric or dimeric CAs, but readily engages with assembled virus-like CA particles [77,115,135]. While the rhesus TRIM5 B30.2 domain is sufficient for detectable co-sedimentation with assembled HIV-1 CA tubes, this interaction is greatly enhanced in the presence of the CC-L2 dimerization domain (CC-B30.2) and full avidity to the CA lattice is only achieved in the presence of all four domains of TRIM5α, with B-box and RING mediating higher-order oligomerization [84,99,102,114,115,130,136,198]. This relationship between TRIM5 domain composition and avidity for the CA lattice becomes obvious when comparing the concentrations of respective TRIM5 construct needed for efficient co-sedimentation with assembled CA tubes: It takes about 30–50 µM B30.2 domain, 1-10 µM CC-B30.2 dimer and only 0.15-0.5 µM TRIM5-21R chimera for significant co-sedimentation with comparable amounts of CA-NC (5–10 µM) or wild-type CA (60-70 µM) tubes [114,115,130]. These results demonstrate that CA recognition by TRIM5 not only requires an oligomerized retroviral CA, but also relies on oligomerization of TRIM5 itself. Nevertheless,

the real dimension of how TRIM5 oligomerization and self-association contributes to CA binding was only unveiled when Ganser-Pornillos *et al.* reported that recombinant rhesus TRIM5-21R spontaneously self-assembles into paracrystalline two-dimensional hexagonal arrays (Figure 17 A) [136]. TRIM5-21R assembly is further promoted upon binding to planar HIV-1 CA lattices resulting in the formation of a complementary TRIM5-21R lattice matching on top of the hexagonal HIV-1 CA array. Although both TRIM5-21R and HIV-1 CA form hexagonal lattices, their lattice dimensions differ considerably in size with inter-hexamer spacings of 315-355 Å and 90 Å for TRIM5-21R and HIV-1 CA, respectively (Figure 17 B). The projection density map generated from Fourier-filtered Cryo-EM images of TRIM5-21R 2D-crystals displays regions of high density at the threefold and twofold symmetry axes connected by thinner regions of weaker density (Figure 17 A) [136].

TRIM5-21R lattice formation is dependent on CC mediated dimerization and B-Box mediated higher-order oligomerization, as kinetically trapped TRIM5-21R monomer and the R121E B-Box cluster 1 mutant both fail to self-assemble into hexagonal arrays [136]. Other studies have also identified the L2 region and the RING domain as important determinants for higher-order self-assembly [84,99]. Modifications that interfere with TRIM5 self-assembly correlate in each case with decreased avidity for retroviral CA particles. By contrast, truncation of the B30.2 domain in TRIM5 does not prohibit hexagonal lattice formation, although the efficiency of assembly is lowered resulting in the formation of smaller and less well ordered 2D-crystals [136]. Based on these findings, Ganser-Pornillos and colleagues have proposed a model of how individual TRIM5 molecules may arrange in the hexagonal lattice (Figure 17 C). In this model, the CC domains are located within the narrowest electron density regions linking the L2/B30.2 and RING/B-Box domains that occupy regions of high density at the midpoint and the ends of each hexamer edge. Thereby, two parallel TRIM5 dimers that contact each other via L2/L2 interactions are placed along each hexagon side forming tetramers that span the length of 180-205 Å [136].

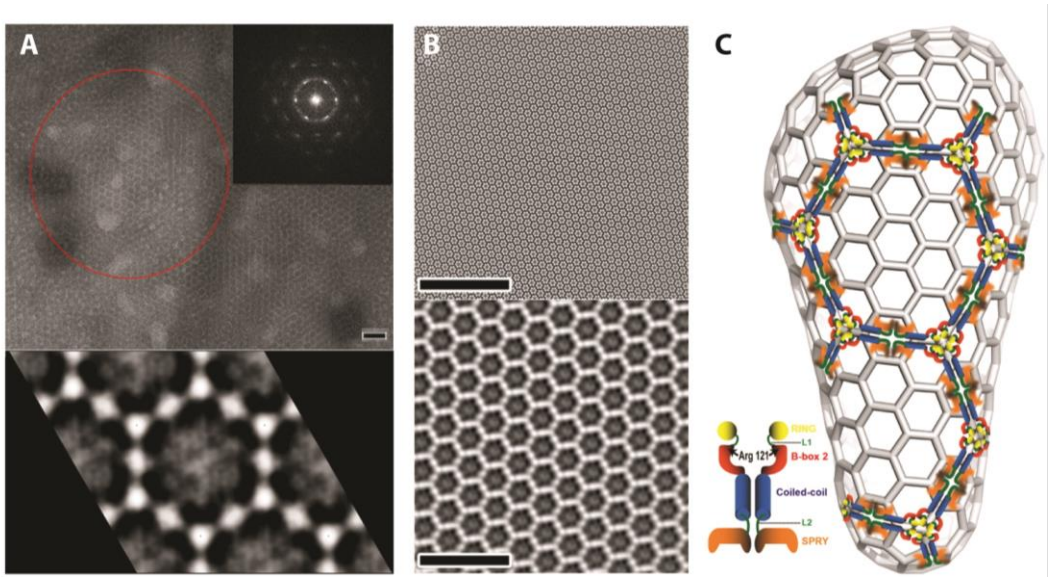

Figure 17. Higher-order self-assembly of TRIM5-21R into a hexagonal lattice. (A) On top is a negative-stained EM image of a spontaneously formed TRIM5-21R lattice (scale bar, 100 nm). The computed Fourier transform (inset) of the area inside the red circle shows a clear hexagonal order. Below is a projection density map generated from TRIM5-21R lattices in vitreous ice. **(B)** Fourier-filtered images of A14C/E45C/W184A CA-NC crystals alone (top) and TRIM5-21R crystals alone (bottom) illustrate the dramatic difference in unit cell size of the two lattices. **(C)** Schematic model of the HIV-1 fullerene cone surrounded by a putative TRIM5 lattice. A possible arrangement of the TRIM5 domains in the hexagonal lattice is proposed based on the assumption that TRIM5 forms parallel dimers. (Figure adapted from [136]).

The mechanism of template induced complementary lattice formation upon recognition of an assembled retroviral CA suggests that TRIM5 multimerization may align multiple B30.2 domains over repeating binding sites on the hexagonal CA lattice, thus synergistically combining multiple low affinity interactions to achieve a high avidity towards restrictive virion cores. This indicates that TRIM5 likely employs “pattern recognition” to bind to hexagonal CA arrays, which are common to all retroviral CAs.

1.7 Scope of the Thesis

The discovery of TRIM5 as the factor responsible for the HIV-1 resistance in rhesus macaques has unleashed a fury of publications, unveiling many aspects of TRIM5 function in retroviral restriction. Only a few years after discovery, it became well established that TRIM5 blocks retroviral infection at an early post-entry stage prior to reverse transcription by binding to invading CA cores and accelerating CA uncoating. It turned out that full restriction activity of TRIM5 requires all of its four domains, with the individual domains contributing differently to the proteins function: the B30.2 domain is required for CA binding, the CC domain mediates multimerization and the RING domain confers E3 ubiquitin ligase activity. However, at the beginning of this thesis the function of the B-Box domain was still unknown as well as the mechanism of how the TRIM5 domains cooperate to mediate retroviral restriction. At this point of time, existing knowledge on TRIM5 was almost exclusively founded on cell-based assays and the scarcity of insight into the molecular mechanisms of TRIM5 function was largely due to the lack of structural and *in-vitro* biochemical data on TRIM5 proteins.

The first aim of this thesis was therefore to establish protocols for the production of recombinant TRIM5 proteins and their functional characterization using *in-vitro* biochemical assays. By screening of full-length TRIM5 orthologs fused to different N-terminal solubility tags we aimed to identify a construct that is solubly expressed in insect cells and allows the purification to sufficient amounts for *in-vitro* biochemical assays and crystallization trials. As described in the first publication "TRIM5 is an innate immune sensor for the retrovirus capsid lattice", we established a protocol for the purification of full-length owl monkey TRIMCyp, which allowed the detailed characterization of its E3-ligase activity using *in-vitro* biochemical assays in a collaboration. The TRIMCyp purification protocol could also be adapted for the production of TRIM5α orthologs.

The second aim was to characterize the interaction of rhesus TRIM5α with the HIV-1 CA and to identify the binding epitope on the HIV-1 CA lattice. This required the identification of new truncated TRIM5α constructs that are amenable to standard biochemical binding assays, as full-length TRIM5 proteins are notoriously prone to aggregation. Furthermore we had to make the HIV-1 CA amenable to these binding assays, because TRIM5α binding is specific to assembled CA particles, which are present as large aggregates. Therefore we aimed to generate soluble oligomeric HIV-1 CAs that recapitulate individual interfaces of the assembled CA. The binding studies performed with the B30.2 domain of TRIM5α and interface mimics of the HIV-1 CA lattice are described in the second manuscript "Dissecting the HIV-1 capsid lattice into distinct TRIM5 binding units".

The final aim of the thesis was to gain structural information on the relative domain organization of TRIM5 proteins. The structure of a homologous TRIM20 fragment encompassing the CC-L2-B30.2 domains is described in the third manuscript "Overall architecture and mode of dimerization of TRIM proteins revealed by the TRIM20 structure". Based on the atomic model of TRIM20 and available structures of individual TRIM5 domains we provide a model for the structure of full-length TRIM proteins.

2 Articles

2.1 Publication: TRIM5 is an innate immune sensor for the retrovirus capsid lattice

LETTER

doi:10.1038/nature09976

TRIM5 is an innate immune sensor for the retrovirus capsid lattice

Thomas Pertel[1], Stéphane Hausmann[1], Damien Morger[2], Sara Züger[2], Jessica Guerra[1], Josefina Lascano[1], Christian Reinhard[1], Federico A. Santoni[1], Pradeep D. Uchil[3], Laurence Chatel[4], Aurélie Bisiaux[5], Matthew L. Albert[5], Caterina Strambio-De-Castillia[1], Walther Mothes[3], Massimo Pizzato[1], Markus G. Grütter[2] & Jeremy Luban[1]

TRIM5 is a RING domain-E3 ubiquitin ligase that restricts infection by human immunodeficiency virus (HIV)-1 and other retroviruses immediately following virus invasion of the target cell cytoplasm[1,2]. Antiviral potency correlates with TRIM5 avidity for the retrovirion capsid lattice[3,4] and several reports indicate that TRIM5 has a role in signal transduction[5–7], but the precise mechanism of restriction is unknown[8]. Here we demonstrate that TRIM5 promotes innate immune signalling and that this activity is amplified by retroviral infection and interaction with the capsid lattice. Acting with the heterodimeric, ubiquitin-conjugating enzyme UBC13–UEV1A (also known as UBE2N–UBE2V1), TRIM5 catalyses the synthesis of unattached K63-linked ubiquitin chains that activate the TAK1 (also known as MAP3K7) kinase complex and stimulate AP-1 and NFκB signalling. Interaction with the HIV-1 capsid lattice greatly enhances the UBC13–UEV1A-dependent E3 activity of TRIM5 and challenge with retroviruses induces the transcription of AP-1 and NF-κB-dependent factors with a magnitude that tracks with TRIM5 avidity for the invading capsid. Finally, TAK1 and UBC13–UEV1A contribute to capsid-specific restriction by TRIM5. Thus, the retroviral restriction factor TRIM5 has two additional activities that are linked to restriction: it constitutively promotes innate immune signalling and it acts as a pattern recognition receptor specific for the retrovirus capsid lattice.

To determine if TRIM5 contributes to signal transduction, the effect of ectopic human TRIM5α expression on transcriptional reporters in HEK-293 cells was examined. TRIM5 stimulated either of two luciferase reporters for AP-1 with a magnitude comparable to that of MAVS or the AP-1 transcription factor c-Jun (Fig. 1a and Supplementary Fig. 1a). TRIM5 also stimulated NF-κB (Fig. 1b) but minimally activated *IFNB1*-, or IRF3-dependent, luciferase reporters (Fig. 1c and Supplementary Fig. 1b and c). The TRIM5–cyclophilin A fusion protein from owl monkey[1] activated AP-1 and NF-κB to similar levels as human TRIM5α (Supplementary Fig. 1d, e). Although TRIM5 was not sufficient to activate *IFNB1*, induction of *IFNB1* by IRF3 was greatly enhanced by TRIM5 (Fig. 1c), consistent with the fact that *IFNB1* transcription requires NF-κB and AP-1, as well as IRF3 (Supplementary Fig. 1f)[9].

To determine if endogenous TRIM5 regulates AP-1 and NF-κB signalling pathways, the effect of *TRIM5* knockdown was assessed in myeloid cells. THP-1 cells were transduced with lentiviral vectors engineered to confer puromycin-resistance and to express RNA polymerase II (Pol II)-driven, microRNA-based short hairpin RNAs (shRNAs) targeting either *TRIM5* or control RNAs (Supplementary Fig. 2a–c). Pools of puromycin-resistant cells were generated with each knockdown vector and global expression profiles were assessed. The effect of *TRIM5* knockdown was extraordinarily specific in that, of 25,000 genes probed, only 33 were significantly decreased (Fig. 1d). The majority of these were NF-κB- and AP-1-responsive inflammatory mediators, 70% being inflammatory chemokines and cytokines (Supplementary Table 1).

Lipopolysaccharide (LPS), a pathogen-associated molecular pattern (PAMP) recognized by the pattern recognition receptor (PRR) TLR4-MD-2, activates AP-1 and NF-κB-signalling and this culminates in the expression of inflammatory genes like those perturbed by *TRIM5* knockdown[10,11]. Monocyte-derived dendritic cells (MDDC), macrophages (MDM) and THP-1 cells were challenged with LPS and induction of the AP-1- and NF-κB-dependent genes *CXCL9*, *CXCL10*, *CCL8*, *IL6*, *IL8* and *PTGS2* (also known as *COX2*), was found to be attenuated by *TRIM5* knockdown (Fig. 1e and f and Supplementary Fig. 2d and e). These results demonstrate that TRIM5 activates MAPK- and NF-κB-dependent genes and makes a major contribution to LPS signalling and gene induction (Supplementary Fig. 1f).

Given the contribution of TRIM5 to the production of inflammatory mediators by LPS, the effect of TRIM5 on the previously reported anti-HIV-1 activity of LPS[12] was examined. Transduction of MDDC, MDM or THP-1 macrophages by vesicular stomatitis virus (VSV) G-pseudotyped HIV-1 was blocked by LPS, by other PAMPs, and by type 1 IFN (Supplementary Fig. 3a–c). *TRIM5* mRNA increased tenfold in response to these factors (Supplementary Fig. 3d, e), but this increase was not sufficient for the anti-HIV-1 state (Supplementary Fig. 3f, g). Nonetheless, *TRIM5* knockdown rescued HIV-1 from LPS, although not from type 1 IFN, and the magnitude rescue correlated with the efficiency of *TRIM5* knockdown (Fig. 1g and Supplementary Fig. 4a and b). These phenotypes were indistinguishable from those observed with knockdown of *IRF3*, a critical transcription factor that acts proximal to *IFNB1* (ref. 10; Fig. 1h and Supplementary Fig. 4c). In contrast, knockdown of *STAT2*, a factor that acts downstream of the type I IFN receptor, blocked the anti-HIV-1 activity of either LPS or type 1 IFN (Fig. 1i and Supplementary Fig. 4d).

Rescue from LPS seems to be independent of capsid-recognition by TRIM5 in that *TRIM5* knockdown rescued a molecular clone of simian immunodeficiency virus (SIV_{MAC}), a retrovirus that differs greatly from HIV-1 in terms of its sensitivity to TRIM5-mediated restriction[1,2], as well as two non-retroviruses, the rhabdovirus vesicular stomatitis virus and the paramyxovirus Newcastle disease virus (Fig. 1j and Supplementary Fig. 4e–i). Although TRIM5 is not sufficient to activate IFNB1 (Fig. 1c), it promotes the first wave of innate immune signalling upstream of IFNB1 and thereby contributes to the antiviral state established by LPS (Supplementary Fig. 1f).

To understand how TRIM5 activates AP-1 and NF-κB, 20 candidate proteins, selected on the basis of signalling activity above the MAPK/NF-κB bifurcation in the LPS signalling pathway, were tested for the ability to immunoprecipitate with TRIM5. Strong signal was observed with TAK1, TAB2, and TAB3 (Fig. 2a and Supplementary Fig. 5a), all components of the TAK1 kinase complex that phosphorylates proximal MAPK and NF-κB kinases in response to LPS[11]. Like TRIM5, TAK1 potently activated AP-1 and modestly activated NF-κB (Fig. 2b). 5Z-7-oxozeaenol, a TAK1-inhibitor, blocked AP-1 induction by TRIM5 or

[1]Department of Microbiology and Molecular Medicine, University of Geneva, Geneva CH-1211, Switzerland. [2]Department of Biochemistry, University of Zurich, Zurich CH-8057, Switzerland. [3]Section of Microbial Pathogenesis, Yale University School of Medicine, New Haven, Connecticut 06536, USA. [4]Novimmune SA, Geneva CH-1228, Switzerland. [5]Institut Pasteur, Inserm U818, Paris 75724, France.

RESEARCH LETTER

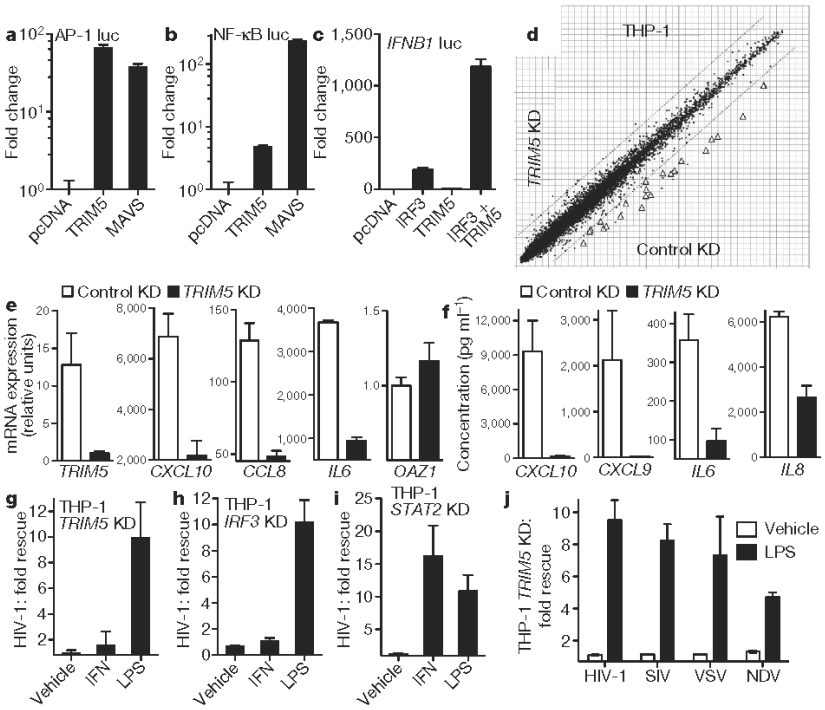

Figure 1 | TRIM5 promotes innate immune signalling. **a**–**c**, HEK-293 cells transfected with the indicated pcDNA-based expression plasmids and luciferase reporters for AP-1 (**a**), NF-κB (**b**) or *IFNB1* (**c**). Bars show mean luciferase activity ± s.d. ($n = 6$). **d**, Global expression profile comparing *TRIM5* knockdown (KD) to control KD THP-1 macrophages. Triangles indicate inflammatory genes significantly downregulated in *TRIM5* KD. **e**, qRT–PCR for the indicated mRNAs collected from MDDCs 2 to 8 h after LPS treatment, depending on the peak values for that gene. Shown are the means ± s.e.m ($n = 3$) relative to untreated cells. **f**, Concentration of the indicated proteins in the culture supernatant, 24 h after LPS treatment (mean ± s.d., $n = 3$). RNA and protein data are representative of at least three separate donors. **g**–**j**, THP-1 macrophages transduced with miR30-based lentivirus KD vectors targeting either *TRIM5* (**g** and **j**), *IRF3* (**h**), or *STAT2* (**i**), were treated for 24 h with the indicated compounds and challenged with VSV-G pseudotyped HIV-1 luciferase reporter virus (**g**–**i**) or with the indicated green fluorescent protein (GFP) reporter viruses (**j**). Data are expressed as fold-change compared to control KD cells, with s.e.m ($n = 4$). All data are representative of at least three independent experiments.

TAK-1 without effect on AP-1 induction by the downstream effector c-Jun (Fig. 2b). *TAK1* knockdown blocked AP-1 activation by TRIM5 (Fig. 2c), but not by c-Jun (Fig. 2c and Supplementary Fig. 5c). *TRIM5* knockdown blocked LPS-induced TAK1 autophosphorylation on threonine 187 (Fig. 2d), a post-translational modification required for TAK1 activation[11]. Like *TRIM5* knockdown, *TAK1* knockdown rescued HIV-1 from the LPS-induced antiviral state (Fig. 2e and Supplementary Fig. 5d), and either TAB2 or TAB3 acted synergistically with TRIM5 to activate AP-1 (Fig. 2f). These results indicate that TRIM5 and the TAK1 kinase complex cooperate to promote signal transduction, and given that TAK1 phosphorylates both IκB kinases (IKKs) and mitogen-activated protein kinase kinases (MKKs)[11], explains how TRIM5 activates both MAPK and NF-κB signalling pathways.

The well-characterized restriction of HIV-1 by owl monkey TRIMCyp[1,13] (a TRIM5–CypA fusion protein) was exploited to determine if TAK1 contributes to TRIM5-mediated, capsid-specific restriction. Pools of THP-1 cells were selected for puromycin-resistance after transduction with a bicistronic lentiviral vector encoding owl monkey TRIM5Cyp[13]. As shown previously, these cells were resistant to infection with wild-type HIV-1, but not to the HIV-1 G89V capsid mutant, and the infectivity of wild-type HIV-1 was rescued by cyclosporine[13] (Supplementary Fig. 5e). Control cells transduced with a vector bearing TRIM5Cyp(H436Q), a mutant that does not bind HIV-1 capsid and does not restrict HIV-1 (ref. 13), were infected with efficiency equal to that of cells transduced with the empty vector. THP-1 cells transduced with either wild-type or H436Q mutant TRIM5Cyp were then subjected to a second round of selection after transduction with miR30-based knockdown vectors targeting *TAK1* or luciferase control and expressing hygromycin-resistance. The pools of puromycin/hygromycin double-resistant THP-1 cells were then challenged with HIV-1. *TAK1* knockdown rescued HIV-1 transduction and nascent HIV-1 cDNA synthesis (Fig. 2g, h). This effect was specific to the cells with TRIM5Cyp-mediated restriction activity because *TAK1* knockdown had no effect on HIV-1 transduction in the non-restrictive, H436Q control cells (Fig. 2g).

The contribution of TAK1 to restriction of N-tropic murine leukemia virus (MLV) by human TRIM5α was examined using miR30-based knockdown vectors in THP-1, HeLa and HT1080 cells. Inhibition of both N-tropic and B-tropic MLV infection by the *TAK1* knockdown was observed, perhaps because, unlike HIV-1, infection with MLV is cell-cycle dependent[14], and these viruses were sensitive to growth inhibitory effects of the knockdown. This precluded assessment of capsid-specific effects on reporter gene transduction, although nascent viral cDNA synthesized after infection of THP-1 cells was rescued by the *TAK1* knockdown in an N-tropic MLV-specific manner (Supplementary Fig. 5g). Similar non-specific effects on MLV were observed after transfection of double stranded RNA (dsRNA) oligonucleotides targeting *TAK1*. Like HIV-1, equine infectious anaemia virus (EIAV) is a lentivirus that infects non-dividing cells, but it differs from HIV-1 in that it is relatively sensitive to human TRIM5α-mediated restriction[15]. Transfection of dsRNAs targeting *TAK1* rescued EIAV transduction almost to the same level as the *TRIM5* knockdown (Fig. 2i). These results indicate that TAK1 contributes to capsid-specific restriction mediated by TRIM5.

AP-1 induction by TRIM5 was impaired by mutants of the RING E3 ubiquitin (Ub)-ligase domain (Fig. 3a). This raised the question which

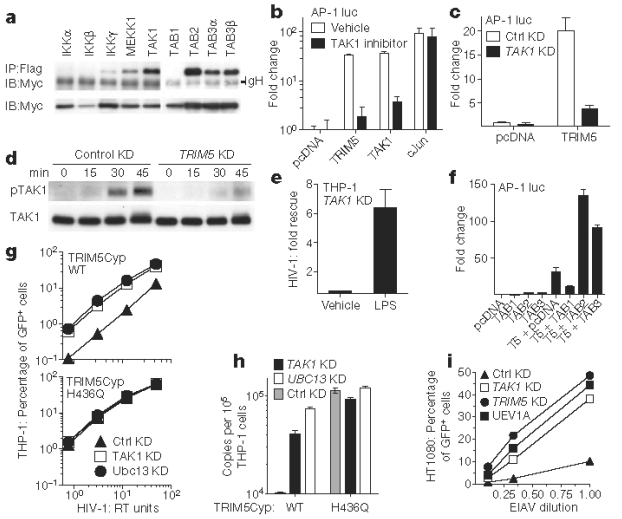

Figure 2 | The TAK1 kinase complex interacts biochemically and functionally with TRIM5. **a**, HEK-293T cells were co-transfected with Myc-tagged human TRIM5α and the indicated Flag-tagged constructs. Shown are immunoblots (IB) with anti-Myc antibody after immunoprecipitation with anti-Flag (upper panel), or of total cell lysate (bottom panel). **b**, **c**, and **f**, HEK-293 cells were transfected with the indicated pcDNA-based expression plasmids and an AP-1 luciferase reporter and show the effect of TAK1 inhibitor 5Z-7-oxozeaenol (**b**) or *TAK1* KD (**c**). *TAK1* KD and control KD THP-1 macrophages were treated with LPS for the indicated times and immunoblotted with anti-TAK1 antibody (lower panel) or anti-phospho-TAK1 antibody (upper panel) (**d**), or, cells were treated 24 h with LPS or vehicle and challenged with an HIV-1 luciferase reporter virus (**e**). The results in (**e**) are reported as fold rescue due to *TAK1* KD, with respect to control KD. **g** and **h**, THP-1 cells were transduced with lentiviral vectors encoding owl monkey TRIM5Cyp, either wild-type (WT) or the H436Q mutant. Pools of each were then transduced with lentiviral KD vectors targeting either *TAK1*, *UBC13* or control, and challenged with an HIV-1-GFP reporter vector. Infectivity was monitored by FACS (**g**) or by PCR for synthesis of full-length viral cDNA (**h**). **i**, HT1080 cells were transfected with dsRNA oligonucleotides targeting *TRIM5*, *TAK1* or *UEV1A* and challenged with EIAV-GFP reporter vector.

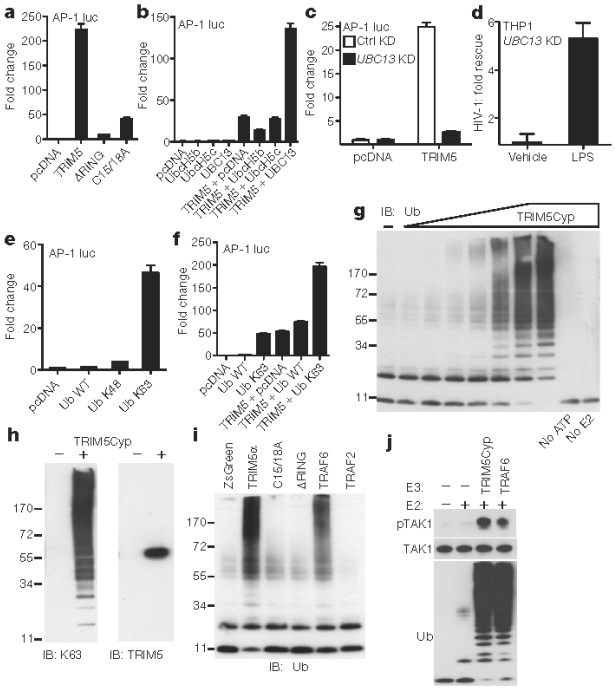

Figure 3 | TRIM5 acts with UBC13–UEV1A to synthesize free K63-linked Ub chains that activate TAK1. **a**–**c**, **e** and **f**, HEK-293 cells were transfected with an AP-1 luciferase reporter and the indicated pcDNA-based expression plasmids. Bars show mean ± s.d. ($n = 6$). In **c**, HEK-293 cells had stable *UBC13* KD or control KD. **d**, *UBC13* KD or control KD THP-1 macrophages were treated for 24 h with LPS or vehicle and challenged with an HIV-1 luciferase reporter virus. Shown is the fold rescue due to *UBC13* KD, with respect to the control KD. **g**–**j**, Products of *in vitro* reactions with ATP, Ub, UBE1, UBC13–UEV1A, and the indicated E3 Ub ligases were revealed by immunoblot for total Ub (**g**, **i**, and **j**), K63-linked Ub chains (left panel of **h**), or TRIM5 (right panel of **h**). E3 ubiquitin ligases included purified owl monkey TRIM5Cyp (**g**, **h**, and **j**), or the indicated Flag-tagged proteins immunoprecipitated from HEK-293T cells (**i**). **j**, *In vitro* Ub reactions like those in (**i**) were incubated with purified TAK1 kinase complex. Products were probed in immunoblot with the indicated antibodies.

of the many E2 Ub-conjugating enzymes might be relevant for TRIM5-mediated effects on signal transduction. Among candidate E2s, UBC13 synergized with TRIM5 to activate AP-1 (Fig. 3b). Interestingly, the TAK1 kinase complex is activated by the heterodimeric E2 UBC13–UEV1A[11]. Knockdown of *UBC13* or *UEV1A* severely blocked AP-1 activation by TRIM5 (Fig. 3c and Supplementary Fig. 6a–c), rescued HIV-1 from the LPS-induced antiviral state in THP-1 macrophages (Fig. 3d and Supplementary Fig. 6d), and rescued HIV-1 and EIAV from TRIM5-mediated restriction (Fig. 2g–i).

The UBC13–UEV1A E2 heterodimer is notable in that it generates K63-linked Ub chains that are unlinked to substrates; these free Ub chains multimerize and activate the TAK1 kinase complex via the Ub binding components, TAB2 and TAB3 (ref. 11). Ub in which all lysines except K63 are mutated to arginine (Ub K63) activated AP-1 and NF-κB (Fig. 3e and Supplementary Fig. 6e, f), and enhanced the ability of TRIM5 to activate AP-1 (Fig. 3f). K48-only Ub did not have these activities (Fig. 3e, f), nor did wild-type Ub, perhaps because of the dominance of competing Ub metabolic pathways and the tight regulation of K63 chains within cells[16]. These experiments indicate that the heterodimeric E2 UBC13–UEV1A and the K63-linked Ub chains that it produces have a role in TRIM5-mediated signalling.

Because TRIM5 interacted biochemically and functionally with TAK1, TAB2, TAB3, UBC13, UEV1A and K63-Ub, the ability of TRIM5 to synthesize K63-linked Ub chains was assessed. A purification protocol was established that yielded 0.5 mg of soluble, full-length, owl monkey TRIM5Cyp from 1 l of Sf9 cell culture (Supplementary Fig. 7). No procedure has been reported to date for the production of purified, full-length, recombinant TRIM5 protein[17]. Purified TRIM5Cyp was incubated with purified Ub, E1 and the E2 Ub-conjugases UBC13 and UEV1A, and reaction products were separated by SDS–polyacrylamide gel electrophoresis (SDS–PAGE). With increasing TRIM5Cyp concentration, monomeric Ub was progressively depleted and the yield of Ub chains increased (Fig. 3g and Supplementary Fig. 8a). Synthesis of Ub chains was ATP-dependent and required both UBC13 and UEV1A.

The Ub chains generated by TRIM5Cyp were detected with antibody specific for K63-linked Ub and immunoblot showed TRIM5Cyp to be a monomer with no detectable incorporation into the Ub chains (Fig. 3h). To obtain an independent assessment of their identity, reaction products were isolated by PAGE and analysed by matrix-assisted laser desorption/ionization and tandem mass spectrometry (Supplementary Figs 8a and 9a–c). These methods identified peptides corresponding to K63-linked Ub and failed to detect conjugates with other Ub lysines or peptides corresponding to TRIM5Cyp, confirming that reaction products were free, unattached K63 Ub chains. Additionally, synthesis of Ub chains was undetectable with a Ub mutant in which K63 was mutated to arginine (Supplementary Fig. 8b). Conversely, Ub was efficiently incorporated into chains when all lysines except K63 were mutated to arginine (Supplementary Fig. 8b), indicating that K63 was necessary and sufficient to form the Ub chains.

RESEARCH LETTER

Human TRIM5α, produced by transfection of 293T cells and enriched by immunoprecipitation, catalysed the synthesis of free K63 Ub chains like those of TRIM5Cyp, in a RING domain-dependent manner (Fig. 3i and Supplementary Fig. 8c, d). It had at least as much activity as TRAF6 (Fig. 3i), an E3 Ub ligase previously reported to synthesize unattached K63 chains that activate TAK1 (ref. 11). TRAF2, a close paralogue of TRAF6 that does not interact with UBC13 (ref. 18), lacked activity (Fig. 3i).

Free K63-linked Ub chains generated by TRAF6 result in TAK1 autophosphorylation on threonine 187 (ref. 11), a modification required for TAK1 activation. To test the effect of K63-linked Ub chains generated by TRIM5 on TAK1 activation, the essential components of a TAK1 kinase complex, TAK1, TAB1 and TAB2 (ref. 11), were purified and combined (Supplementary Fig. 10). This complex was then incubated with Ub, UBC13–UEV1A, and either TRAF6 or purified owl monkey TRIM5Cyp. TAK1 phosphorylation was observed in response to the K63-linked Ub chains synthesized by either TRAF6 or by TRIM5Cyp (Fig. 3j). Kinase activity required the TAK1-associated TAB1, the Ub receptor TAB2, and UBC13–UEV1A (Fig. 3j). These experiments show that, like TRAF6 (ref. 11), TRIM5 synthesizes free K63-linked Ub chains that activate TAK1 autophosphorylation.

If TRIM5 were a PRR specific for the retroviral capsid lattice, infection with retroviruses would activate signalling, the magnitude of which would correlate with TRIM5 avidity for the capsid of the challenge virus. To determine if this is the case, myeloid cells were challenged with pairs of retroviruses that differ with respect to TRIM5 avidity for the capsid[3,4] and the subsequent induction of NF-κB- and MAPK-dependent genes was assessed. VSV G-pseudotyped N-tropic and B-tropic MLV vectors, normalized for exogenous reverse transcriptase activity and for titre on non-restrictive MDTF cells[19], were used to challenge THP-1 macrophages. The multiplicity of infection of the non-restricted B-tropic MLV on cycling THP-1 cells was 0.1. mRNA was harvested from the THP-1 cells and processed by reverse transcription and quantitative PCR (qRT–PCR). Greater induction of *PTGS2*, *CXCL10*, *CCL8* and *IL6* mRNA was observed after challenge with N-MLV than with B-MLV (Fig. 4a, b), in correlation with the higher avidity of human TRIM5α for the capsid of N-tropic MLV than for the capsid of B-tropic MLV[3]. *TRIM5* knockdown suppressed the higher inflammatory gene induction by N-MLV, indicating its dependence upon endogenous TRIM5 (Fig. 4b). Similar differential induction of *PTGS2*, *CXCL10*, *CCL8* and *IL6* mRNAs by N-tropic and B-tropic MLV was observed after challenge of MDDCs or MDMs (Supplementary Fig. 11).

Retroviral cDNA activates innate immune signalling under some conditions[20]. Restriction by human TRIM5α results in N-MLV cDNA levels that are an order of magnitude lower than for B-MLV cDNA[21] so the experiments described above might underestimate the effect of N-MLV capsid on TRIM5-mediated signalling. Therefore, MDDCs were challenged with matched pairs of virus-like particles (VLPs) devoid of the viral genome that serves as the reverse transcription template. VLPs bearing N-MLV capsid activated *CXCL9*, *CXCL10*, *IFIT1* and *IFIT2* mRNAs from 5- to 55-fold over the levels in untreated MDDCs (Fig. 4c). Inflammatory gene induction was not detected with VLPs bearing the unrestricted NB-MLV capsid[22] (Fig. 4c). As with the mRNA, soluble IL8, CCL5, CXCL9 and CXCL10 protein was differentially induced by N-MLV (Fig. 4d).

To determine if differential gene induction after retrovirus challenge was peculiar to N-tropic MLV, a similar experiment was performed with OMK, a kidney cell line from the owl monkey, *Aotus trivirgatus*. The TRIM5 orthologue in this species restricts HIV-1 but not SIV[1]. VSV G-pseudotyped HIV-1 and SIV vectors, normalized for exogenous reverse transcriptase activity and for titre on HeLa cells, were used to challenge OMK cells. The multiplicity of infection of the unrestricted SIV on OMK cells was 0.3. Among the MAPK- and NF-κB-dependent gene products that were detectable in this species using human probes, transcriptional activation of *PTGS2*, *IFIT1* and *IFIT2* mRNAs, and

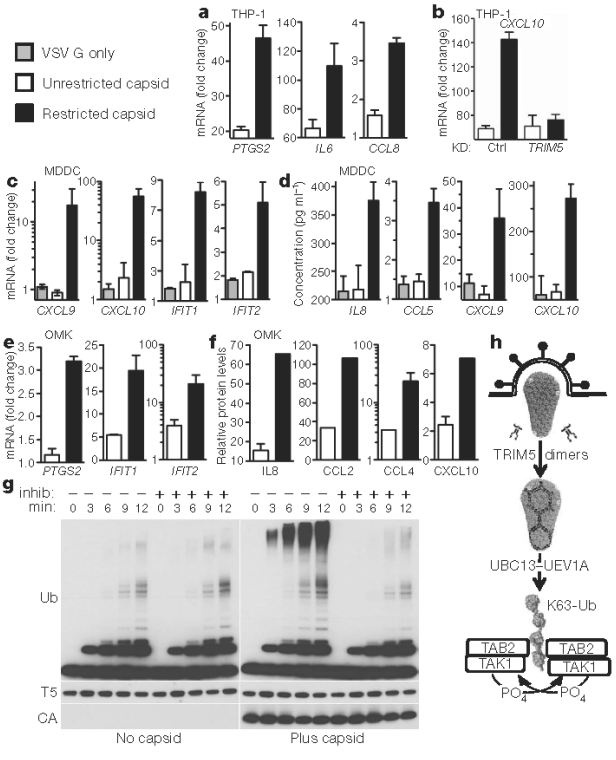

Figure 4 | Retrovirus capsid sensing by TRIM5. THP-1 cells (**a** and **b**), MDDCs (**c** and **d**), or owl monkey kidney cells (OMK; **e** and **f**), were challenged with matched pairs of VSV G-pseudotyped particles bearing retrovirion capsids that are restricted by the TRIM5 orthologue endogenous to that cell type (black bars), or unrestricted (white bars), or VSV G-derived particles that are devoid of capsid (grey bars). Restricted capsids were from N-tropic MLV (**a**–**d**) or HIV-1 (**e** and **f**). Unrestricted capsids were B-tropic MLV (**a** and **b**), N/B-tropic MLV (**c** and **d**) or SIV_{MAC239} (**e** and **f**). Particles bore viral genomes in **a**, **b**, **e** and **f**, but not in **c** and **d**. mRNA was harvested for qRT–PCR (**a**–**c** and **e**) and reported as fold change versus media control. Protein in the supernatant was quantified (**d** and **f**). Bars show means ± s.d. ($n = 3$), and are representative of at least three independent experiments. **g**, Immunoblots with the indicated antibodies of products from *in vitro* time-course with ATP, Ub, UBE1 (E1), UBC13–UEV1A (E2) and purified owl monkey TRIM5Cyp, with or without assembled HIV-1 capsid-A14C/E45C, and with or without competitive inhibitor MeIle4CsA. (**h**) Schematic showing entry of an HIV-1 virion core[27] (courtesy of Pornillos and Yeager) into the target cell cytoplasm where it induces dimeric TRIM5 to form a hexameric lattice[25] with increased E3 Ub ligase activity. With UBC13–UEV1A, TRIM5 synthesizes free K63 Ub chains that are recognized by TAB2, which multimerizes and activates the TAK1 kinase complex.

secretion of IL8, CCL2, CCL4 and CXCL10 proteins, was higher after challenge with the restricted virus (Fig. 4e, f).

TRIM5 senses retrovirus capsids in the target cell cytoplasm (Fig. 4a–f) and activates MAPK- and NF-κB-dependent transcription via the synthesis of TAK1-activating, K63-linked Ub chains (Fig. 3g–j). If these observations were linked functionally, interaction with capsid would be expected to stimulate the synthesis of Ub chains by TRIM5Cyp. Soluble, recombinant HIV-1 capsid or capsid hexamers generated by the oxidation of recombinant capsid bearing strategically-placed cysteine substitutions (A14C/E45C/W184A/M185A)[23] had no effect on the synthesis of K63-linked Ub chains (data not shown). Current models of the HIV-1 capsid lattice are based on cylinders generated under high salt with either capsid or capsid-nucleocapsid fusion protein[17,24]; both preparations were generated but the high salt necessary to maintain capsid cylinders blocked E3 Ub ligase activity. Capsid cylinders were then assembled with A14C/E45C-substituted

capsid protein in 1 M NaCl and the cysteines were oxidized. These oxidized cylinders were stable in the absence of salt (Supplementary Fig. 12a) and greatly stimulated the production of K63-linked Ub chains by TRIM5Cyp (Fig. 4g). No Ub-linked products were detected with anti-capsid (p24) or anti-TRIM5 antibodies, indicating that the reaction products were unattached Ub chains (Fig. 4g).

Finally, two factors that disrupt the HIV-1 capsid-TRIM5Cyp interaction and block restriction activity—a non-immunosuppressive cyclosporine analogue[1] or the TRIM5Cyp(H436Q) mutant protein[13]—each eliminated the enhancement of E3 Ub ligase activity by the A14C/E45C capsid cylinders, without effect on the baseline activity in the absence of capsid (Fig. 4g and Supplementary Figs 7d and 12b–d).

The experiments presented here demonstrate that TRIM5 is a multifunctional component of the innate immune system. In addition to functioning as a retroviral capsid-specific restriction factor, TRIM5 synthesizes K63 Ub chains that activate TAK1 and inflammatory transcription, most probably via multimerization of the TAK1-associated Ub-binding protein TAB2 (ref. 11; Fig. 4h). This activity was greatly increased by the hexameric capsid lattice, a molecular signature of HIV-1 and other retroviruses. TRIM5, then, satisfies criteria for a bona fide PRR[10]. Interestingly, TRIM5 spontaneously forms an hexagonal lattice that is complementary to the capsid lattice[25], but the efficiency of TRIM5 lattice formation is greatly stimulated by the capsid hexameric lattice[25] (Fig. 4h). Little is known about how the innate immune system detects retroviruses[26] and the discovery that TRIM5 acts as a PRR is an important step towards filling this critical gap. The cellular factors required for TRIM5 E3 activity and inflammatory gene induction, UBC13, UEV1A and TAK1, also promoted capsid-specific restriction activity, indicating that the multiple functions of TRIM5 are mechanistically linked. Identification of relevant TAK1 substrates will inform future attempts to pinpoint the mechanism of restriction.

METHODS SUMMARY

Plasmids, cells and viruses. These methods were described previously[1,13,19] or are detailed in the Supplementary Information.

Recombinant protein. Production of full-length, soluble, TRIM5Cyp is described in the supplement. CA A14C E45C was produced and assembled into tubes as described[23,24].

Microarray. Illumina HumanHT-12 V3.0 expression bead chips were probed with RNA from *TRIM5* knockdown THP-1 cells. Data set and methods are available at the Gene Expression Omnibus (www.ncbi.nlm.nih.gov/geo) under accession number GSE25041.

Received 31 July 2010; accepted 3 March 2011.

1. Sayah, D. M., Sokolskaja, E., Berthoux, L. & Luban, J. Cyclophilin A retrotransposition into TRIM5 explains owl monkey resistance to HIV-1. *Nature* **430,** 569–573 (2004).
2. Stremlau, M. *et al.* The cytoplasmic body component TRIM5α restricts HIV-1 infection in Old World monkeys. *Nature* **427,** 848–853 (2004).
3. Sebastian, S. & Luban, J. TRIM5α selectively binds a restriction-sensitive retroviral capsid. *Retrovirology* **2,** 40 (2005).
4. Stremlau, M. *et al.* Specific recognition and accelerated uncoating of retroviral capsids by the TRIM5α restriction factor. *Proc. Natl Acad. Sci. USA* **103,** 5514–5519 (2006).
5. Berthoux, L. *et al.* As_2O_3 enhances retroviral reverse transcription and counteracts Ref1 antiviral activity. *J. Virol.* **77,** 3167–3180 (2003).
6. Shi, M. *et al.* TRIM30α negatively regulates TLR-mediated NF-κB activation by targeting TAB2 and TAB3 for degradation. *Nature Immunol.* **9,** 369–377 (2008).
7. Tareen, S. U. & Emerman, M. Human Trim5α has additional activities that are uncoupled from retroviral capsid recognition. *Virology* **409,** 113–120 (2011).
8. Luban, J. & Cyclophilin, A. TRIM5, and resistance to human immunodeficiency virus type 1 infection. *J. Virol.* **81,** 1054–1061 (2007).
9. Panne, D., Maniatis, T. & Harrison, S. C. An atomic model of the interferon-β enhanceosome. *Cell* **129,** 1111–1123 (2007).
10. Ishii, K. J., Koyama, S., Nakagawa, A., Coban, C. & Akira, S. Host innate immune receptors and beyond: making sense of microbial infections. *Cell Host Microbe* **3,** 352–363 (2008).
11. Xia, Z. P. *et al.* Direct activation of protein kinases by unanchored polyubiquitin chains. *Nature* **461,** 114–119 (2009).
12. Kornbluth, R. S., Oh, P. S., Munis, J. R., Cleveland, P. H. & Richman, D. D. Interferons and bacterial lipopolysaccharide protect macrophages from productive infection by human immunodeficiency virus *in vitro*. *J. Exp. Med.* **169,** 1137–1151 (1989).
13. Neagu, M. R. *et al.* Potent inhibition of HIV-1 by TRIM5-cyclophilin fusion proteins engineered from human components. *J. Clin. Invest.* **119,** 3035–3047 (2009).
14. Roe, T., Reynolds, T. C., Yu, G. & Brown, P. O. Integration of murine leukemia virus DNA depends on mitosis. *EMBO J.* **12,** 2099–2108 (1993).
15. Berthoux, L., Sebastian, S., Sokolskaja, E. & Luban, J. Cyclophilin A is required for TRIM5α-mediated resistance to HIV-1 in Old World monkey cells. *Proc. Natl Acad. Sci. USA* **102,** 14849–14853 (2005).
16. Zeng, W. *et al.* Reconstitution of the RIG-I pathway reveals a signaling role of unanchored polyubiquitin chains in innate immunity. *Cell* **141,** 315–330 (2010).
17. Langelier, C. R. *et al.* Biochemical characterization of a recombinant TRIM5α protein that restricts human immunodeficiency virus type 1 replication. *J. Virol.* **82,** 11682–11694 (2008).
18. Yin, Q., Lamothe, B., Darnay, B. G. & Wu, H. Structural basis for the lack of E2 interaction in the RING domain of TRAF2. *Biochemistry* **48,** 10558–10567 (2009).
19. Sokolskaja, E., Berthoux, L. & Luban, J. Cyclophilin A and TRIM5α independently regulate human immunodeficiency virus type 1 infectivity in human cells. *J. Virol.* **80,** 2855–2862 (2006).
20. Yan, N., Regalado-Magdos, A. D., Stiggelbout, B., Lee-Kirsch, M. A. & Lieberman, J. The cytosolic exonuclease TREX1 inhibits the innate immune response to human immunodeficiency virus type 1. *Nature Immunol.* **11,** 1005–1013 (2010).
21. Perron, M. J. *et al.* TRIM5α mediates the postentry block to N-tropic murine leukemia viruses in human cells. *Proc. Natl Acad. Sci. USA* **101,** 11827–11832 (2004).
22. Ulm, J. W., Perron, M., Sodroski, J. & Mulligan, R. C. Complex determinants within the Moloney murine leukemia virus capsid modulate susceptibility of the virus to Fv1 and Ref1-mediated restriction. *Virology* **363,** 245–255 (2007).
23. Pornillos, O. *et al.* X-ray structures of the hexameric building block of the HIV capsid. *Cell* **137,** 1282–1292 (2009).
24. Ganser, B. K., Li, S., Klishko, V. Y., Finch, J. T. & Sundquist, W. I. Assembly and analysis of conical models for the HIV-1 core. *Science* **283,** 80–83 (1999).
25. Ganser-Pornillos, B. K. *et al.* Hexagonal assembly of a restricting TRIM5α protein. *Proc. Natl Acad. Sci. USA* **108,** 534–539 (2011).
26. Medzhitov, R. & Littman, D. HIV immunology needs a new direction. *Nature* **455,** 591 (2008).
27. Pornillos, O., Ganser-Pornillos, B. K. & Yeager, M. Atomic-level modelling of the HIV capsid. *Nature* **469,** 424–427 (2011).

Supplementary Information is linked to the online version of the paper at www.nature.com/nature.

Acknowledgements We thank D. Baltimore, M. J. Birrer, J. Brojatsch, A. Cimarelli, A. Delaco, S. Elledge, M. Emerman, W. Ferlin, D. Garcin, S. Ghosh, O. Haller, T. Hatziioannou, J. Hiscott, A. Iwasaki, D. Kolakofsky, M. Kosco-Vilbois, H. Malik, R. Medzhitov, M. R. Neagu, G. Napolitani, P. Palese, D. Pinschewer, O. Pornillos, L. Roux, O. Schwartz, M. Strubin, V. Studer, W. Sundquist, G. Towers, D. Trono, J. Tschopp, M. Yeager, M. Zufferey, and the Functional Genomics Center (Zürich), for ideas, technical assistance, and reagents. This work was supported by NIH grant RO1AI59159 to J.L., NIH grant R21AI087467 to W.M., Swiss National Science Foundation grant 3100A0-128655 to J.L. and 3100A0-122342 to M.G. and UZH Forschungskredit 54041402 to S.Z.

Author Contributions T.P., S.H., J.G., C.R., C.S., M.P., W.M., M.G.G. and J.L. designed the experiments; T.P., S.H., D.M., S.Z., J.G., J.La., C.R., F.A.S., M.P., A.B., P.D.U. and L.C. performed the experiments. All authors contributed to the assembly and writing of the manuscript.

Author Information Reprints and permissions information is available at www.nature.com/reprints. The authors declare no competing financial interests. Readers are welcome to comment on the online version of this article at www.nature.com/nature. Correspondence and requests for materials should be addressed to J.L. (jeremy.luban@unige.ch).

SUPPLEMENTARY INFORMATION

doi:10.1038/nature09976

Supplementary Methods

Chemicals and drugs. The following compounds were used at the given final concentrations: Ultrapure LPS from *E. coli* K12 (100 ng/mL), poly(I:C) (25 μg/mL, or 2 μg/mL when complexed with Lipofectamine 2000 (Invitrogen)), and poly(dA:dT) (2 μg/mL) were obtained from Invivogen. Cyclosporine was from Bedford, and nonimmunosuppressive MeIle4-cyclosporine was from Sandoz. Recombinant, human IFN-β (10 ng/mL) and recombinant, human IFN-α2a (10 ng/mL) were obtained from PBL InterferonSource. U0126 (a selective MEK1/MEK2 inhibitor) (20 μmol/L), SP600125 (a selective JNK inhibitor) (20 μmol/L), SB 203580 (a selective p38 inhibitor) (20 μmol/L), 5Z-7-Oxozeaenol (a TAK1 inhibitor)(300 nmol/L), and Hybri-Max-grade dimethyl sulfoxide (DMSO) (1:500 v/v) were from Sigma-Aldrich.

Cell lines and primary cell cultures. THP-1 cells, an acute monocytic leukemia cell line, were obtained from ATCC and maintained in RPMI-1640 (Invitrogen) supplemented with 10 % fetal bovine serum (FBS) (Hyclone), 20 mmol/L HEPES (Invitrogen), 1 × MEM Non-Essential Amino Acids Solution (Invitrogen), and 1 × GlutaMAX-I (Invitrogen). In order to differentiate THP-1 monocytes into macrophage-like cells, THP-1 cells were counted, centrifuged at 200 × *g* for 10 min, and resuspended at a concentration of 1×10^6 cells/mL in fresh cell culture medium containing 100 ng/mL tetradecanoylphorbol acetate (TPA) (Sigma-Aldrich). Cells were plated into each well of a sterile tissue culture plate (2 mL culture/well of a 6-well plate or 200 μL culture/well of a 96-well flat-bottom plate) and allowed to differentiate for 24 h, at which point the TPA-containing medium was removed and fresh cell culture medium (without TPA) was added. The cells were rested for an additional 48 h before use. TPA-differentiated THP-1 cells were placed in culture medium containing 0.5 % FBS 24 h prior to lipopolysaccharide (LPS) stimulation for western blot analysis of protein phosphorylation. CD4-CCR5-THP-1, THP-1 cells that overexpress both human

doi:10.1038/nature09976

CD4 and human CCR5, were generated by sequential transduction with pAIB-CD4 and pAIH-CCR5 (see below). CD4-CCR5-THP-1 cells were maintained in cell culture medium containing 400 μg/mL hygromycin B (Sigma-Aldrich) and (15 μg/mL) blasticidin S hydrochloride (Sigma-Aldrich), and high-level surface expression of CD4 and CCR5 was routinely confirmed by fluorescence activated cell sorting (FACS) after staining with allophycocyanin (APC) anti-human CD4 and phycoerythrin (PE) anti-human CCR5 (BD Biosciences). Human TRIM5α-THP-1 cells, and empty pAIB vector control cells, were generated by transduction with pAIB-TRIM5α or empty pAIB vectors, and selected with 15 μg/mL blasticidin S hydrochloride. AtTRIM5Cyp-THP-1, AtTRIM5Cyp H436Q-THP-1, and empty pFUPI vector control cells were generated by transduction with AtTRIM5Cyp-pFUPI, AtTRIM5Cyp H436Q-pFUPI, or empty pFUPI vectors (see below), and selected with 2 μg/mL puromycin dihydrochloride (Sigma-Aldrich).

HEK-293 cells, a human fetal kidney epithelial cell line, 293T cells, a human fetal kidney epithelial cell line transformed with the SV40 large T antigen, OMK cells, an Owl monkey kidney epithelial cell line, HT-1080 cells, a human fibrosarcom cell line, and the human embryonal rhabdomyosarcoma cell line TE671 were obtained from ATCC. HEK-293, 293T, OMK, HT-1080, and TE671 cells were grown in Dulbecco's modified Eagle medium (D-MEM) (high glucose) (Invitrogen) with 10 % FBS, 1 × MEM NEAA, and 1 × GlutaMAX-I. 293T cells were periodically grown in cell culture medium containing 500 μg/mL Geneticin (Invitrogen) to maintain expression of the SV40 large T antigen.

Peripheral blood mononuclear cells (PBMCs) were isolated from buffy coats prepared from healthy, anonymous donors using Ficoll-Paque Plus (GE Healthcare) following the protocol supplied by Miltenyi Biotec. $CD14^+$ cells (monocytes) were enriched from PBMCs by positive selection using CD14 MicroBeads (Miltenyi Biotec)

doi:10.1038/nature09976

with purity routinely greater than 95 %, as determined by FACS after staining with PE anti-human CD14 (BD Biosciences). Enriched $CD14^+$ cells were counted, centrifuged at 200 × *g* for 10 min, and resuspended in RPMI-1640 supplemented with 10 % FBS, 20 mmol⁄L HEPES, 1 × MEM NEAA, and 1 × GlutaMAX-I, at a concentration of 1×10^6 cells⁄mL. In order to generate monocyte-derived macrophages (MDM), recombinant, human GM-CSF (R&D Systems) was added to the cell suspension to a final concentration of 50 ng⁄mL, and in order to generate monocyte-derived dendritic cells (MDDC), recombinant, human IL-4 (R&D Systems) was added to a final concentration of 25 ng⁄mL along with 50 ng⁄mL GM-CSF. $CD14^+$ cells were allowed to either differentiate into MDDCs in the presence of GM-CSF and IL-4 for 4 d, or into MDMs in the presence of GM-CSF alone for 10 d, before use.

All primary cells and cultured cell lines were maintained in cell culture media without penicillin or streptomycin, and were cultured at 37 °C in a humidified incubator containing 5 % carbon dioxide.

Plasmids, Vectors, and Viruses. The cDNAs listed in Supplementary Table 2 were amplified using the AccuPrime Pfx SuperMix (Invitrogen), following the manufacturer's protocol, from the templates described and using the given primer pairs. The resultant PCR products were gel purified using the QIAquick Gel Extraction Kit (Qiagen), digested with the given restriction endonucleases (New England Biolabs), column purified using the QIAquick PCR Purification Kit (Qiagen), and ligated into the noted plasmids using T4 DNA Ligase (New England Biolabs), following standard molecular biological techniques. MneTRIM5Cyp-pLNCX2 was a gift from Dr. Theodora Hatziioannou (Aaron Diamond AIDS Research Center). The c-Jun expression plasmid was provided by Dr. Michael J. Birrer (National Cancer Institute). The MEKK1 (MAP3K1) expression plasmid was a gift from Dr. Sankar Ghosh (Columbia University). The N-terminal Xpress and HA tags in the MEKK1 plasmid were replaced

doi:10.1038/nature09976

with a 3 × FLAG tag. pRK5-HA-Ubiquitin-WT, pRK5-HA-Ubiquitin-KO, pRK5-HA-Ubiquitin-K48, and pRK5-HA-Ubiquitin-K63 plasmids[1] were obtained through Addgene.

The following viruses and vectors were used in this study: pFSGW is an HIV-1-based transfer vector with EGFP expression under the control of the spleen focus-forming virus (SFFV) long terminal repeat (LTR). pFSGW was generated by replacing the Ubiquitin promoter in pFUGW[2], provided by Dr. David Baltimore (California Institute of Technology), with the U3 region of the SFFV LTR, which was amplified by PCR from the pCSGW[3] plasmid and inserted into the PacI and XbaI sites of pFUGW. psPAX2 (an HIV-1 packaging plasmid) and pMD2.G (a Vesicular stomatitis virus glycoprotein (VSV-G) expression plasmid) were generous gifts from Dr. Didier Trono (Ecole Polytechnique Fédérale de Lausanne). pNL4-3.GFP.E^{-}[4] and pNL4-3.Luc.E^{-}[5] are pNL4-3 with an env-inactivating mutation and EGFP or luciferase cloned in place of Nef. SIV_{MAC239} env^{-} GFP[6] is similar for this virus. pCNCG is an MLV-based transfer vector with EGFP expression driven by the CMV promoter (Oxford Biomedica). pCIG3N and pCIG3B[7] are MLV packaging vectors expressing N- or B-tropic gag-pol, and were gifts of Dr. Greg Towers (University College London). The Equine Infectious Anemia Virus (EIAV) gag-pol expression plasmid pONY3.1 and the EGFP transfer vector pONY8.0 have been previously described.[8] pSVIIIenv JR-FL[9] is a CCR5-tropic env expression plasmid. pshRLP-TRIM5 and pshRLP-Luc, standard shRNA lentiviral transfer vectors based on pSUPER.retro.puro (Oligoengine), were described previously[10]. pFUPI, a lentiviral transfer vector where the AtTRIM5Cyp wild type or H436Q mutant cDNA were cloned downstream of a puromycin N-acetyltransferase - Encephalomyocarditis virus (EMCV) internal ribosome entry site (IRES) cassette, is described elsewhere.[11] The vesicular stomatitis virus (VSV)-GFP was a generous gift from Dr. John Hiscott (McGill University) and the Newcastle disease virus (NDV)-GFP was a generous gift from Dr. Peter Palese (Mount Sinai School of Medicine).

doi:10.1038/nature09976

pALPS was generated as follows: The single NotI site in pFSGW, described above, was eliminated by digest with NotI and subsequent treatment with DNA Polymerase I, Large (Klenow) Fragment (New England BioLabs) to create blunt ends, which were ligated together using T4 DNA Ligase (New England BioLabs). The fragment PmeI to PciI was removed, ends blunted, and re-ligated. The MluI site was removed by digest with MluI, blunting with Klenow, and blunt-end cloning of the SV40 origin of replication (amplified from pcDNA3.1(−) (Invitrogen)) into the blunted MluI site. The XhoI-XhoI fragment, containing the posttranscriptional regulatory element (PRE) of the Woodchuck hepatitis virus (WHV) (WPRE), was removed and replaced with the WPRE from pLVTHM[12] (a gift from Dr. Didier Trono (Ecole Polytechnique Fédérale de Lausanne)). The WPRE from pLVTHM was amplified with a 5′ XhoI site and a 3′ SalI site, eliminating the 3′ XhoI site and preserving the 5′ XhoI site in the vector. A new multiple cloning site (MCS) was generating by complimentary annealing of synthesized oligonucleotides and cloned into the XbaI-XhoI sites using XbaI and SalI, removing the second XhoI site and removing the original MCS and EGFP. The resultant plasmid was named pALPS. pAIP (pALPS-IRES-Puromycin N-acetyltransferase), pAIH (pALPS-IRES-Hygromycin B phosphotransferase), and pAIB (pALPS-IRES-Blasticidin S deaminase) were created by subcloning the EcoRI-PacI fragment, containing the EMCV IRES-drug-resistance gene cassette, from pMIP, pMIH, and pMIB[13], respectively, and ligating into the EcoRI-AsiSI sites of pALPS.

pAPM (pALPS-Puro-miR-30) was created by subcloning the NotI-MluI miR-30 cassette from pPRIME[14], a generous gift from Dr. Stephen J. Elledge (Harvard University), into the NotI-MluI sites in the MCS of pALPS. The puromycin N-acetyltransferase gene was amplified by PCR from pLPCX (Clontech) and cloned into the XbaI-NotI sites of pALPS to generate pAPM, and ZsGreen1 was amplified by PCR from pIRES2-ZsGreen1 (Clontech) and cloned in the XbaI-NotI sites of pALPS to create pAGM. Using the RNAi Central web-based shRNA design program

doi:10.1038/nature09976

(http://cancan.cshl.edu/RNAi_central/RNAi.cgi?type=shRNA - lab of Dr. Gregory Hannon, Cold Spring Harbor Laboratory), a microRNA-based shRNA targeting sequence was designed against firefly luciferase from pGL4 (Promega) (5′-TACAAACGCTCTCATCGACAAG-3′ "L1221"). A 97-mer oligonucleotide, which encodes the shRNA targeting firefly luciferase, 5′-TGCTGTTGACAGTGAGCGCACAAACGCTCTCATCGACAAGTAGTGAAGCCACAGATGTACTTGTCGATGAGAGCGTTTGTATGCCTACTGCCTCGGA-3′, was synthesized, PAGE purified, and amplified by PCR using the following primers: miR-30 XhoI 5′: 5′-AAGGCTCGAGAAGGTATATTGCTGTTGACAGTGAG-3′ and miR-30 EcoRI 3′: 5′-AGCCCCTTGAATTCCGAGGCAGTAGGCA-3′. The PCR reaction was carried out in a 50 μL volume with AccuPrime Pfx SuperMix, 1 mol/L Betaine (Sigma-Aldrich), 0.4 μmol/L each primer, and 100 ng 97-mer oligonucleotide template. After an initial incubation at 95 °C for 5 min, 30 cycles of 95 °C for 15 s, 55 °C for 30 s, 75 °C for 30 s were performed, followed by a 5 min extension at 75 °C. The PCR product was column purified, digested with XhoI and EcoRI, and ligated in pAPM to create pAPM-Luc (L1221). Knockdown of firefly luciferase was confirmed by generating stable, puromycin-selected THP-1 cells with pAPM-Luc and challenging with a pALPS reporter vector that expresses firefly luciferase from pGL4 (pALPS-Luc) (data not shown). pAPM-Luc does not target luciferase from pGL2 or pGL3 (Promega) (data not shown).

Production of virus, lentiviral vectors, and virus-like particles (VLPs). Viruses, minimal vectors, and VLPs were produced by transfection of 293T cells using Lipofectamine 2000 (Invitrogen), according to the manufacturer's instructions. For three-part vector systems, the following DNA ratio was used: 4 parts transfer vector : 3 parts packaging plasmid : 1 part envelope. For two-part virus systems a 7:1 ratio was used (7 parts env^- virus : 1 part envelope). For VLPs, a 7:1 ratio was used (7 parts gag-pol expression plasmid : 1 part envelope). 16 h after transfection the transfection

doi:10.1038/nature09976

medium was replaced with fresh target-cell medium. 48 h after transfection the viral supernatant was collected, centrifuged at 200 × *g* for 5 min, filtered through a sterile 0.45 μm syringe filter (Millipore), and stored in 1 mL aliquots at −80 °C. Viral stocks and VLPs were screened for endotoxin using the chromogenic Limulus Amoebocyte Lysate assay (Cambrex) and discarded if >0.05 EU/ml. The frozen stocks were then titered on HEK-293 cells by serial 1:4 dilutions of the viral supernatant and analyzed by FACS or luciferase assay 72 h after transduction. When comparing viruses, vectors, or VLPs, samples were normalized by single-cycle infectivity assays on HEK-293 cells and/or the reverse transcriptase (RT) activity present in the viral supernatant by qRT-PCR. Data from single-cycle infectivity assays, acquired by FACS or luciferase assay, are represented as either curves of serial dilutions of virus, under various experimental or control conditions, or as the fold-change (experimental/control) of at least three different dilutions of virus (+/− the standard deviation).

SIV_{MAC251} VLPs were produced by cotransfecting pSIV3+, a SIV_{MAC251} gag-pol expression plasmid containing Vpx[3], (a gift from Dr. Andrea Cimarelli, École Normale Supérieure de Lyon) and pMD2.G, at a 7:1 ratio into 293T cells using Lipofectamine 2000.

Generation of stable microRNA-based shRNA knockdown cell lines and transient siRNA gene silencing. Stable microRNA-based shRNA knockdown lines were generated by transfecting 293T cells with the experimental pAPM knockdown vector or pAPM-Luc as a control, along with the HIV-1 packaging plasmid psPAX2 and the VSV-G expression plasmid pMD2.G as described above. Freshly harvested viral supernatant was added to the target cells at a 1:2 final dilution. 24 h after the first transduction, a second transduction was performed using a 1:3 final dilution of fresh viral supernatant. 48 h after the second transduction, the cells were placed in cell culture medium containing 10 μg/mL puromycin dihydrochloride (Sigma-Aldrich). After one

doi:10.1038/nature09976

week of selection, cells were analyzed for knockdown efficiency by SDS-PAGE/western blot, qRT-PCR, and/or functional assay.

To generate stable microRNA-based shRNA knockdowns in primary human MDM or MDDC, human $CD14^+$ cells, freshly isolated from PBMC as described above, were treated with SIV_{MAC251} virus-like particles (VLPs) for 3 h, and then transduced with either a control or experimental pAPM vectors. The $CD14^+$ cells were then allowed to differentiate into MDM in the presence of 50 ng/mL GM-CSF (R&D Systems) for 10 d, or into MDDC in the presence of 50 ng/mL GM-CSF and 25 ng/mL IL-4 (R&D Systems) for 4 d. After differentiation, the MDM or MDDC were selected with 10 μg/mL puromycin dihydrochloride (Sigma-Aldrich) for 2 d and assayed for knockdown by SDS-PAGE/western blot analysis or qRT-PCR. Using this technique we routinely observed greater than 90 % transduced MDM or MDDC.

All shRNA target sequences are listed in Supplementary Table 3.

For transient gene silencing experiments using siRNA, 3×10^5 cells were plated per well of a 6-well culture plate. Once the cells had adhered to the plate, they were transfected the same day with 30 pmol of siRNA pools complexed to 4 μL RNAiMAX (Invitrogen). A second transfection was performed the following day. 48 h after the first transfection, the cells were harvested and plated at a concentration of 1×10^4 cells per well of a 96-well flat bottom culture plate. 72 h after the first transfection, the cells were challenged with serial dilutions of virus or reporter vectors as described above. The following siRNA pools were used: the FlexiTube GeneSolution siRNA pools targeting TAK1 (*MAP3K7*), UBC13 (*UBE2N*), and UEV1A (*UBE2V1*) were from Qiagen, and the ON-TARGET*plus* SMARTpool targeting TRIM5 and the ON-TARGET*plus* Non-targeting Pool were from Thermo Fisher Scientific.

doi:10.1038/nature09976

Quantitative reverse transcription polymerase chain reaction (qRT-PCR). Total RNA was extracted from 2×10^6 cells using the RNeasy Plus Mini Kit (Qiagen), following the manufacturer's instructions. First-strand cDNA was generated using the SuperScript III First-Strand Synthesis System (Invitrogen) using 2 μg total RNA and random hexamers, according to the manufacturer's protocol. The qPCR reaction was performed in triplicate in a 20 μL volume using 1 × TaqMan Gene Expression Master Mix (Applied Biosystems), 1 μL of undiluted cDNA, and 1 μL of the specified TaqMan Gene Expression Assay (Applied Biosystems) on either the 7900HT Fast Real-Time PCR System (Applied Biosystems) or the CFX96 Real Time System/C1000 Thermal Cycler (Bio-Rad) using the following program: 95 °C for 10 min and 45 cycles of 95 °C for 15 s and 60 °C for 1 min. The following TaqMan Gene Expression Assays were used: *CCL2* (Hs00234140_m1), *CCL8* (Hs00271615_m1), *CXCL9* (Hs00171065_m1), *CXCL10* (Hs00171042_m1), *IFIT1* (Hs00356631_g1), *IFIT2* (Hs00533665_m1), *IFNB1* (Hs01077958_s1), *IL6* (Hs00985639_m1), *PTGS2* (Hs00153133_m1), and *TRIM5* (Hs01552558_m1 or Hs01552552_g1). *OAZ1* (Hs00427923_m1) was used as an endogenous control. Data were analyzed using the SDS software v2.2.2 (Applied Biosystems) or the CFX Manager software v1.6 (Bio-Rad), which calculate relative mRNA expression levels using the standard comparative Ct method ($2^{-\Delta\Delta Ct}$) with error bars representing +/− the standard error.

Sodium dodecyl sulfate polyacrylamide gel electrophoresis (SDS-PAGE)/western blot analysis. 2×10^6 cells were lysed in 200 μL 1 × Laemmli sample buffer (62.5 mmol/L Tris, pH 6.8, 2 % SDS, 10 % glycerol, 357.5 mmol/L 2-mercaptoethanol (2-ME), 0.0025 % bromophenol blue (Bio-Rad)), supplemented with 1 × Halt Protease and Phosphatase Inhibitor Cocktail, EDTA-free (Thermo Fisher Scientific) and 5 mmol/L EDTA, pH 8.0. Whole-cell lysates were heated at 100 °C for 5 min, centrifuged at 14, 000 × *g* for 2 min, and 50 μL were loaded onto a 10 % ProSieve 50 gel (Lonza) for SDS-PAGE. Relative protein concentration was normalized after staining gel with

doi:10.1038/nature09976

SimplyBlue SafeStain (Invitrogen). After SDS-PAGE, proteins were transferred onto an Immun-Blot polyvinylidene fluoride (PVDF) membrane (Bio-Rad) for 16 h at 30 V (constant voltage) at 4 °C. After the protein transfer, the membrane was washed 3 × 5 min with deionized water and blocked 1 h at 4 °C with 5 % non-fat dry milk dissolved in TBST (Tris-buffered saline (50 mmol/L Tris, pH 7.4, 150 mmol/L sodium chloride (NaCl)) with 0.1 % Polysorbate 20 (Tween 20)). The membrane was then washed 3 × 5 min with TBST. The primary antibody was diluted to 1 μg/mL in either 5 % bovine serum albumin (BSA) or 5 % non-fat dry milk dissolved in TBST and added to the membrane and incubated 16 h at 4 °C with gentle rocking. After the 16 h incubation with the primary antibody the membrane was washed 3 × 5 min with TBST. The secondary antibody was diluted 1:10,000 in 5% non-fat dry milk dissolved in TBST and added to the washed membrane and incubated at room temperature for 1 h with gentle rocking. The membrane was washed 3 × 10 min and developed using either the ECL or ECL Plus Western Blotting Detection Reagents (GE Healthcare Life Sciences) and exposed to Hyperfilm ECL film (GE Healthcare Life Sciences).

The following antibodies were used in this study: rabbit anti-ATF2 (20F1), rabbit anti-phospho-ATF2 (Thr71), rabbit anti-c-Jun (60A8), rabbit anti-phospho-c-Jun (Ser63), rabbit anti-SAPK/JNK (56G8), rabbit anti-phospho-SAPK/JNK (Thr183/Tyr185), rabbit anti-TAK1, rabbit anti-phospho-TAK1 (Thr184/187), rabbit anti-IKKα, rabbit anti-phospho-IKKα (Ser176)/IKKβ (Ser177) (C84E11), rabbit anti-IκBα, rabbit anti-STAT2, rabbit anti-UBC13, rabbit anit-TAB1, rabbit anti-TAB2, rabbit anti-TRAF2 (C192), and rabbit anti-Ubiquitin were from Cell Signaling Technology; mouse anti-FLAG (M2), rabbit anti-FLAG, mouse anti c-Myc (9E10), rabbit anti-c-Myc, mouse anti-HA (HA-7), rabbit anti-HA, and mouse anti-β-Actin (AC-74) were from Sigma-Aldrich; anti-Ubiquitin, Lys48-specific (Apu2) and anti-Ubiquitin, Lys63-specific (Apu3) were from Millipore; mouse anti-Ubiquitin (P4D1) and rabbit anti-IRF3 (FL-425) were from Santa Cruz Biotechnology; rabbit anti-

doi:10.1038/nature09976

Cyclophilin A and rabbit anti-ubiquitin-protein conjugates were from Enzo Life Sciences; rabbit anti-UEV1A and rabbit anti-TRIM5α (C-terminus) were from ProSci; goat anti-TRIM5 (N-terminus) was from Abcam. Secondary antibodies used: HRP-linked donkey anti-rabbit IgG and HRP-linked sheep anti-mouse IgG were from GE Healthcare Life Sciences and donkey anti-goat IgG-HRP was from Santa Cruz Biotechnology.

Immunoprecipitation (IP). Sub-confluent 293T cells grown on T-75 tissue culture flasks were transfected with 16 μg total plasmid DNA using TransIT-LT1 Transfection Reagent (Mirus Bio), following the manufacturer's protocol. 40 h post-transfection, cells were washed with 30 mL ice-cold phosphate buffered saline (PBS) (Invitrogen) and lysed with 1 mL ice-cold lysis buffer (50 mmol/L Tris, pH 7.4, 150 mmol/L NaCl, 0.5 % CHAPSO (Affymetrix)) supplemented with 1 × Halt Protease and Phosphatase Inhibitor Cocktail, EDTA-free (Thermo Fisher Scientific). Crude cell lysates were scraped off the surface of the flask, transferred to pre-chilled 2 mL microcentrifuge tubes, and rotated at 4 °C for 20 min. The crude cell lysates were then centrifuged at 14,000 × *g* for 10 min and 900 μL of the clarified lysate was transferred to pre-chilled microcentrifuge tubes, and the remaining 100 μL of the clarified lysate was diluted equally in 2 × Laemmli sample buffer, incubated at 100 °C for 5 min, and stored at −80 °C. 2 μg antibody was conjugated to 50 μL of Protein G Dynabeads (Invitrogen) following the manufacturer's protocol. The beads were washed 3 times with 1 mL ice-cold lysis buffer, resuspended in 100 μL lysis buffer, and added to the clarified cell lysates. After 2 h rotating at 4 °C, the Protein G magnetic bead immune complexes were washed 5 times with 1 mL ice-cold lysis buffer, resuspended in 100 μL of 1 × Laemmli sample buffer, incubated at 100 °C for 5 min, and stored at −80 °C until ready for SDS-PAGE.

doi:10.1038/nature09976

Luciferase assays. HEK-293 cells were plated on white, opaque 96-well CulturPlate-96 microplates (PerkinElmer) at a concentration of 2×10^4 cells per 100 μL tissue culture medium per well, 24 h prior to transfection. Cells were transfected with Lipofectamine 2000 (Invitrogen), using 0.5 μL Lipofectamine 2000 per well, with 1 ng of the *Renilla* luciferase internal control reporter plasmid pRL-TK (Promega), 5 ng firefly luciferase experimental reporter plasmid, and 15 to 50 ng of pcDNA3.1(−) containing the experimental cDNA or empty pcDNA3.1 as a control, following the manufacturer's instructions. Each experimental condition was performed in sextuplicate. 48 h after transfection, the plate was assayed using the Dual-Glo Luciferase Assay System (Promega) and read using a Veritas Microplate Luminometer (Turner Biosystems). Firefly luciferase readings were normalized to *Renilla* luciferase readings in each well, and the data are represented as fold-change compared to empty pcDNA (+/− the standard deviation). The following firefly luciferase plasmids were used: the minimal 6 × AP-1 binding site reporter pHTS-AP1 was from Biomyx, *IFNB1*-luc was a gift from Dr. Jürg Tschopp (University of Lausanne); ISRE-luc was from Dr. Akiko Iwasaki (Yale School of Medicine), the *Prl* promoter AP-1-luc construct was from Dr. Ruslan Medzhitov (Yale School of Medicine), and NF-κB-luc was from Dr. Jurgen Brojatsch (Albert Einstein College of Medicine).

For single-cycle infectivity assays using the HIV-1 luciferase reporter virus described above, THP-1 cells were plated on white, opaque 96-well CulturPlate-96 microplates (PerkinElmer) at 2×10^5 cells per well in 200 μL tissue culture medium containing 100 ng/mL TPA. After 24 h, the medium was replaced with fresh tissue culture medium, and after another 48 hours the TPA-differentiated THP-1 cells were challenged with HIV-1 luciferase reporter virus. 72 h after transduction the plate was assayed using the Bright-Glo Luciferase Assay System (Promega) and read using a Veritas Microplate Luminometer (Turner Biosystems). Data are expressed either as

doi:10.1038/nature09976

relative light units (RLU) or as the fold-change (experimental/control) of at least three different dilutions of virus (+/− the standard deviation).

Illumina. Raw microarray data were processed and analyzed using the Bioconductor R package, lumi, with default values for background correction, variance stabilization and quantile normalization. For further analysis, all Illumina probe IDs were converted to unique Entrez IDs. Gene ontology terms and pathways that were enriched in the downregulated and upregulated gene sets were measured using DAVID[15] with the total set of genes mapped on the microarray as the background. Significance was evaluated by a modified Fisher's exact test and p-values were Bonferroni corrected for multiple testing.

Luminex. Human chemokines and cytokines from cell culture supernatants (stored at −80 °C prior to analysis) were measured by Luminex (32 plex kits, Millipore) following the manufacturer's instructions. For data mining purposes, values below the lower assay limit were changed to ½ the lowest value in the given dataset. Coefficient of Variance for all assays reported was < 10 %. Averages of biologic replicates are shown and data are representative of three independent experiments.

PCR for viral cDNA. Lentiviral vectors based on pWPT (a gift from Dr. Didier Trono (Ecole Polytechnique Fédérale de Lausanne) were produced in 293T cells as described above. Gag-pol plasmids used: pCMV8.9 WT and the RT double mutant D185K/D186L.[16] 1.5×10^6 cells were transduced by mixing 2 mL of cell culture with 1 mL of undiluted virus. Transductions were performed in triplicate in 6-well plates. Viruses were left on the cell cultures for 18 h, at which point the transduced cells were harvested and washed 3 times in PBS + 2 % FBS and once in PBS. The cells were pelleted and extraction of non-chromosomal DNA was performed using the QIAprep Spin Miniprep Kit (QIAGEN), following the protocol isolation for plasmid from bacteria cells, including one wash of the columns with buffer PB. DNA was eluted in

doi:10.1038/nature09976

100 uL of elution buffer (EB). 6 μL of extracted DNA was used as template for the PCR reaction: SYBR Green Mix: 5 mmol/L $(NH_4)_2SO_4$, 20 mmol/L KCl, 20 mmol/L Tris pH 8.3, 5 mmol/L $MgCl_2$, 0.1 mg/mL BSA, 1/20,000 SYBR Green I, 200 μmol/L dNTPs, 320 nmol/L primers (forward primer (in loxP): 5′-GCATACATTATACGAAGTTATGCTGC-3′ and reverse primer: 5′-GCCGTGCGCGCTTCAGCAAGC-3′). Amplification conditions: 95 °C for 2 min, then 40 cycles of: 95 °C 5 s, 60 °C 5 s, 72 °C 30 s, acquisition: 80 °C 6 s, followed by a melting curve analysis. A standard curve was made by serial dilutions of a known copy amount of the gel-purified PCR product.

Purified, soluble, full-length TRIM5Cyp. Owl monkey TRIM5Cyp (residues 1-474; EMBL: AAT73777) was cloned into multiple cloning site 2 of the MultiBac vector pFBDM along with an N-terminal StrepII-MBP tag and 3C cleavage site using standard PCR methods. Recombinant bacmid DNA was produced by transforming the resulting construct into *E.coli* DH10α (Invitrogen). Bacmid DNA was used to transfect Sf9 cells and isolate recombinant virus expressing MBP-fused TRIM5Cyp. Sf9 insect cells were infected with 1:100 (v/v) recombinant baculovirus and incubated in serum-free SF-900 II media (Invitrogen) supplemented with 1:100 (v/v) penicillin-streptomycin solution (Invitrogen) for 45 h at 27 °C. Cells were harvested by centrifugation at 2,200 × *g* for 10 min, rinsed with PBS, and resuspended in lysis buffer (50 mmol/L Tris, pH 8, 150 mmol/L NaCl, 100 mmol/L 2-ME, 50 μmol/L zinc acetate, 10 % glycerol) in the presence of complete, EDTA-free protease-inhibitor cocktail (Roche). Infected cells were lysed with an EmulsiFlex-C3 homogenizer (Avestin) at 15,000 psi. Cell debris was removed by centrifugation at 47,500 × *g* for 20 min and the resulting supernatant was mixed with amylose resin (New England Biolabs). MBP-fused TRIM5Cyp was eluted from the resin with 15 mmol/L amylose and cleaved with 1:20 (m/m) 3C-protease overnight at 4 °C. StrepII-MBP was removed on a Strep-Tactin Superflow gravity column (IBA). For further purification the protein sample was concentrated and injected

doi:10.1038/nature09976

onto a Superdex 200 column (GE Healthcare) equilibrated with lysis buffer containing only 20 mmol/L 2-ME. Fractions containing pure TRIM5Cyp were pooled, concentrated, and stored at −80 °C.

Owl monkey TRIM5Cyp fused to $(His)_6$-MBP was soluble after immobilized metal ion affinity chromatography (Supplementary Fig. 7a). Wild-type protein was produced, as well as a mutant, H436Q, that disrupts TRIM5Cyp interaction with HIV-1 capsid. The identity of the two purified proteins was confirmed by electrospray ionization mass spectrometry (ESI-MS). For wild-type TRIM5Cyp, a molecular mass of 54,360.2 g/mol was obtained ($MW_{calculated}$ = 54,360.3 g/mol). The molecular mass of the H436Q mutant was 54,350.3 g/mol ($MW_{calculated}$ = 54,351.2 g/mol). Purified TRIM5Cyp eluted in gel filtration chromatography with an apparent molecular weight of 153 kDa (Supplementary Fig. 7b and c). Comparison of this finding with previous work suggests that TRIM5Cyp was a dimer with an extended Stokes radius. The oligomeric state was determined by size exclusion chromatography coupled to in-line, multi-angle light-scattering and refractive index detection (SEC-MALS). The molecular mass extracted from the light-scattering data was 95 ± 2 kDa for both the wild-type and the H436Q mutant protein (Supplementary Fig. 7d and e), indicating that owl-monkey TRIM5Cyp is indeed a dimer.

Gel filtration and multi-angle light scattering. Purified protein was applied to a Superdex 200 10/300 GL column (GE Healthcare) with 50 mmol/L Tris, pH 8.0, 150 mmol/L NaCl, 20 mmol/L 2-ME, 50 μmol/L zinc acetate as running buffer, followed by analysis of the fractions using standard SDS-PAGE. The apparent molecular weight was estimated by comparison to molecular weight markers Ferritin (440 kDa), Aldolase (158 kDa) and Ovalbumin (44 kDa). Oligomeric state was determined by multi-angle light scattering. Data were collected using a Superdex 200 10/300 GL column (GE Healthcare) with in-line multi-angle light scattering (miniDAWN) (Wyatt Technology),

doi:10.1038/nature09976

variable wavelength UV (ÄKTAexplorer) and refractive index (Optilab rEX) (Wyatt Technology) detection. The column was pre-equilibrated with 50 mmol/L Tris pH 8.0, 150 mmol/L NaCl, 20 mmol/L 2-ME, 50 μmol/L zinc acetate and approximately 100 μL of 1 mg/mL protein in lysis buffer was injected. The molecular mass was determined using the ASTRA program (Wyatt Technology).

***In vitro* ubiquitin assays.** Reaction mixtures (15 μL) containing 50 mmol/L Tris, pH 8.0, 2 mmol/L ATP, 5 mmol/L $MgCl_2$, 50 μmol/L Ub, 200 nmol/L E1, 1 μmol/L Ubc13/Uev1a, 0.25 μmol/L TRIM5Cyp and either 5 μmol/L capsid or the corresponding buffer were incubated for 60 min at 30 °C. For the capsid addition experiment in Fig. 4g, the reaction buffer contained 150 mM NaCl. The reaction was halted by adding SDS to 1% final concentration. Samples were analyzed by SDS-PAGE. For time-course reactions, 90 μL reaction mixtures containing 50 mmol/L Tris, pH 8.0, 2 mmol/L ATP, 5 mmol/L $MgCl_2$, 50 μmol/L Ub, 200 nmol/L E1, 0.5 μmol/L E2, and 0.25 μmol/L TRIM5Cyp were incubated at 30 °C. Aliquots (15 μL) were withdrawn at the times specified. If the recombinant proteins were expressed in HEK-293 cells, C-terminal 3 × FLAG-tagged proteins were purified by immunoprecipitation (see Supplementary methods). After the final wash, the beads were resuspended in 50 μL reaction mixtures containing 50 mmol/L Tris, pH 8.0, 2 mmol/L ATP, 5 mmol/L $MgCl_2$, 50 μmol/L Ub, 200 nmol/L E1, and 1 μmol/L Ubc13/Uev1a were incubated for 60 min at 30 °C. The reaction was halted by adding SDS to 1% final concentration. The samples were analyzed by SDS-PAGE. Human recombinant UBE1 (E1; E-305), human recombinant UbcH13/Uev1a (E2-664), human recombinant Ub (U-100H), human recombinant Ub K48R (UM-K48R), human recombinant Ub K63R (UM-K63R), human recombinant Ub K48 only (UM-K480), human recombinant Ub K63 only (UM-K630), and human recombinant Ub no lysines (UM-NOK) were from Boston Biochem.

doi:10.1038/nature09976

***In vitro* TAK1 activation assay.** The FLAG tag, in combination with the *Strep*-tag II from pSH-FS-DDB1 (a gift from Dr. Michel Strubin, University of Geneva), was PCR-amplified using primers designed to introduce a 5′ SpeI site and a 3′ XbaI site. The PCR product was digested with SpeI and XbaI and then inserted into pcDNA3.1(−) linearized with XbaI. The resulting expression plasmid pcDNA3.1(−)-FS encodes a double tag consisting of a FLAG tag followed by two *Strep*-tag II sequences spaced with linkers (GSAASWSHPQFEKGGGSGGGSGGGSWSHPQFEKGAS). The TAK1 coding sequence was excised from pcDNA3.1(−) 3×FLAG-TAK1 with XbaI and NotI and inserted between XbaI and NotI of pcDNA3.1(−)-FS. The resulting expression plasmid pcDNA3.1(−)-FS-TAK1 encodes TAK1 fused in-frame to an N-terminal FLAG-*Strep*-tag. pcDNA3.1(−)-FS-TAB1, pcDNA3.1(−)-FS-TAB2, and pcDNA3.1(−)-FS-TRAF6 were constructed similarly.

Sub-confluent HEK-293 cells grown on 10-cm plates were transfected with 12 μg plasmid DNA using TransIT-LT1 Transfection Reagent (Mirus Bio), following the manufacturer's instructions. 6 10-cm plates were transfected with pcDNA3.1(-)-FS-TAK1, 2 10-cm plates with pcDNA3.1(-)-FS-TAB1, and 4 10-cm plates with pcDNA3.1(-) FS-TAB2. 42 h post-transfection, cells from every dish were washed with 10 ml ice-cold PBS and lysed with 600 μL ice-cold lysis buffer (50 mmol/L Tris, pH 7.5, 150 mmol/L NaCl, 1 % NP-40, 1 mmol/L DTT, 10 % glycerol, and a protease inhibitor cocktail (Roche)). Crude cell lysates were scraped off the surface of the flask, transferred to pre-chilled 2 mL microcentrifuge tubes, and the crude cell lysates were centrifuged at 10,000 × *g* for 10 min. The clarified lysates of every transfection were pooled together into a pre-chilled 15 mL falcon tube and rotated at 4 °C for 15 min. This mixture was applied to a 300 μL column of *Strep*-Tactin (IBA) following the manufacturer's instructions. The column was washed 5 times with 1 mL ice-cold wash buffer (50 mmol/L Tris, pH 7.5, 150 mmol/L NaCl, 1 mmol/L DTT, 10 % glycerol), and eluted 5 times with 200 μL aliquots of buffer (50 mmol/L Tris, pH 7.5, 50 mmol/L

doi:10.1038/nature09976

NaCl, 1 mmol/L DTT, 5 % glycerol, 2.5 mmol/L desthiobiotin). The elution profiles were monitored by SDS-PAGE. The desthiobiotin eluates 2 and 3 containing the Flag-*Strep* fusion polypeptides were pooled and stored at −80 °C. The protein concentration was determined using the Bio-Rad dye reagent with BSA as the standard. FS-TRAF6 was purified as described above using 8 10-cm transfected plates.

Reaction mixtures (15 µL) containing 50 mmol/L Tris, pH 7.5, 2 mmol/L ATP, 5 mmol/L $MgCl_2$, 1 mmol/L DTT, 12.5 µmol/L ubiquitin, ~100 nmol/L TAK1 complex (composed of FS-TAK1, FS-TAB1, and FS-TAB2, respectively), 100 nmol/L E1, 500 nmol/L UBC13/UEV1A, and either 0.5 µmol/L recombinant TRIM5Cyp or 0.1 µmol/L FS-TRAF6 were incubated for 60 min at 30 °C. The reaction was halted by adding SDS to a 1 % final concentration, heated at 100 °C for 5 min, and subjected to SDS/PAGE and immunoblot analysis.

MS-analysis. Products of *in vitro* ubiquitin assays were separated by SDS-PAGE. Gel bands were washed twice with 100 µL 100 mmol/L NH_4HCO_3, 50 % acetonitrile, once with 50 µL acetonitrile, and digested overnight at 37 °C with 2.5 ng/µL trypsin in 10 mmol/L Tris pH 8.2, 2 mmol/L $CaCl_2$. After removal of the supernatant and extracting the gel pieces twice in 100 µL 0.1 % trifluoroacetic acid (TFA), 50 % acetonitrile, the supernatants from the digestion and extraction steps were combined, dried, and dissolved in 20 µL 0.1 % TFA. For MALDI-TOF-TOF measurements (Bruker Ultraflex II with Smartbeam upgrade) 10 µL samples were desalted by Ziptip C18 and mixed 1:1 with matrix solution (5 mg/mL HCCA in 0.1 % TFA, 50 % acetonitrile). The remaining 10 µL samples were desalted using Ziptip C18. Samples were dried and analysed by MALDI-MS-MS.

To obtain an independent assessment of their identity, reaction products of >170 kDa or between 40 and 70 kDa were isolated by PAGE (Supplementary Fig. 8c), digested with trypsin, and analyzed separately by matrix-assisted laser

doi:10.1038/nature09976

desorption/ionization (MALDI). Peaks of theoretical mass matching Ub peptides bearing an internal lysine modified with residues Gly-Gly or Leu-Arg-Gly-Gly were detected (Supplementary Fig. 9a). Subsequent tandem mass spectrometry (MS/MS) identified Ub peptide 55–72 in which K63 was covalently attached to the C-terminal Ub residues Gly-Gly or Leu-Arg-Gly-Gly (Supplementary Fig. 9b and c). K63-modified Ub peptides were not found in control reactions lacking ATP. Peptides corresponding to conjugates with other Ub lysines such as K48 were not detected. Additionally, no peptides corresponding to TRIM5Cyp, nor to Ub conjugates with TRIM5Cyp, were detected, consistent with the conclusion that reaction products were free K63 Ub chains.

Transmission electron microscopy (TEM). Capsid assemblies were verified by TEM (Philips CM-100) using Formvar-coated copper-grids. 7 μL of approximately 15 μmol/L assembled capsid (estimated from input before assembly) was incubated 30-60 s on the grid and negatively stained by immersion, 3 × 15s in 2% uranyl acetate.

doi:10.1038/nature09976

Supplementary References

1 Lim, K. L. *et al.* Parkin mediates nonclassical, proteasomal-independent ubiquitination of synphilin-1: implications for Lewy body formation. *J Neurosci* **25**, 2002-2009 (2005).

2 Lois, C., Hong, E. J., Pease, S., Brown, E. J. & Baltimore, D. Germline transmission and tissue-specific expression of transgenes delivered by lentiviral vectors. *Science* **295**, 868-872 (2002).

3 Demaison, C. *et al.* High-level transduction and gene expression in hematopoietic repopulating cells using a human immunodeficiency [correction of imunodeficiency] virus type 1-based lentiviral vector containing an internal spleen focus forming virus promoter. *Hum Gene Ther* **13**, 803-813 (2002).

4 He, J. *et al.* CCR3 and CCR5 are co-receptors for HIV-1 infection of microglia. *Nature* **385**, 645-649 (1997).

5 Chen, B. K., Saksela, K., Andino, R. & Baltimore, D. Distinct modes of human immunodeficiency virus type 1 proviral latency revealed by superinfection of nonproductively infected cell lines with recombinant luciferase-encoding viruses. *J Virol* **68**, 654-660 (1994).

6 Zhang, Y. J. *et al.* Envelope-dependent, cyclophilin-independent effects of glycosaminoglycans on human immunodeficiency virus type 1 attachment and infection. *J Virol* **76**, 6332-6343 (2002).

7 Bock, M., Bishop, K. N., Towers, G. & Stoye, J. P. Use of a transient assay for studying the genetic determinants of Fv1 restriction. *J Virol* **74**, 7422-7430 (2000).

8 Mitrophanous, K. *et al.* Stable gene transfer to the nervous system using a non-primate lentiviral vector. *Gene Ther* **6**, 1808-1818 (1999).

9 Bannert, N., Schenten, D., Craig, S. & Sodroski, J. The level of CD4 expression limits infection of primary rhesus monkey macrophages by a T-tropic simian immunodeficiency virus and macrophagetropic human immunodeficiency viruses. *J Virol* **74**, 10984-10993 (2000).

10 Sokolskaja, E., Berthoux, L. & Luban, J. Cyclophilin A and TRIM5alpha independently regulate human immunodeficiency virus type 1 infectivity in human cells. *J Virol* **80**, 2855-2862 (2006).

11 Neagu, M. R. *et al.* Potent inhibition of HIV-1 by TRIM5-cyclophilin fusion proteins engineered from human components. *J Clin Invest* **119**, 3035-3047 (2009).

12 Wiznerowicz, M. & Trono, D. Conditional suppression of cellular genes: lentivirus vector-mediated drug-inducible RNA interference. *J Virol* **77**, 8957-8961 (2003).

13 Sebastian, S., Sokolskaja, E. & Luban, J. Arsenic counteracts human immunodeficiency virus type 1 restriction by various TRIM5 orthologues in a cell type-dependent manner. *J Virol* **80**, 2051-2054 (2006).

14 Stegmeier, F., Hu, G., Rickles, R. J., Hannon, G. J. & Elledge, S. J. A lentiviral microRNA-based system for single-copy polymerase II-regulated RNA interference in mammalian cells. *Proc Natl Acad Sci U S A* **102**, 13212-13217 (2005).

doi:10.1038/nature09976

15 Huang da, W., Sherman, B. T. & Lempicki, R. A. Systematic and integrative analysis of large gene lists using DAVID bioinformatics resources. *Nat Protoc* **4**, 44-57 (2009).

16 Buckman, J. S., Bosche, W. J. & Gorelick, R. J. Human immunodeficiency virus type 1 nucleocapsid zn(2+) fingers are required for efficient reverse transcription, initial integration processes, and protection of newly synthesized viral DNA. *J Virol* **77**, 1469-1480 (2003).

doi:10.1038/nature09976

Supplementary Table 1. Genes downregulated in TRIM5 KD THP-1 macrophages.

Gene	Log-fold-change	p-value
CCL4L2	-1.9094665	1.137209e-12
LEPREL1	-1.8048689	8.446835e-18
ADAMDEC1	-1.7853244	1.504312e-19
SOD2	-1.7609531	4.509784e-19
CCL20	-1.6993661	5.106188e-18
CCL3L1	-1.6970908	7.226333e-18
CCI3L3	-1.6874491	9.692193e-18
IGFBP3	-1.6827103	6.340911e-18
TDO2	-1.6790243	1.132651e-18
COL22A1	-1.6348531	3.037757e-18
CCL3	-1.6038464	1.740055e-18
CCL4L1	-1.5576211	2.728843e-13
HSD17B12	-1.5550841	2.129582e-18
APOC1	-1.5331057	9.306874e-17
LYPLA1	-1.4905905	1.970047e-17
KYNU	-1.4498504	1.162455e-17
TFPI2	-1.3949242	1.179825e-16
TNF	-1.3616706	3.422493e-16
EBI3	-1.3457546	7.161719e-15

doi:10.1038/nature09976

IL8	-1.2870183	1.783836e-16
IL1B	-1.2840598	2.378150e-15
GIMAP8	-1.2784021	7.497927e-14
MMP8	-1.2410771	6.072772e-14
HS3ST3A1	-1.2222269	4.249029e-13
LRFN5	-1.1769765	1.780408e-12
CCL2	-1.1625656	4.968945e-11
STC1	-1.1146556	2.679298e-13
SLC39A14	-1.1143511	1.060465e-11
GNG11	-1.0983294	5.495883e-12
IER3	-1.0774993	1.878617e-12
TGFB3	-1.0754890	4.814354e-11
GEM	-1.0590824	4.018161e-11

doi:10.1038/nature09976

Supplementary Table 2. Oligonucleotides used in this study.

Primer name	Sequence	Template	Plasmid
AtTRIM5Cyp NotI 3′	5′-ACCAGCGGCCGCTTAAAGTTGT CCACAGTCAGCA-3′	AtTRIM5Cyp-pMIP	pcDNA3.1(−)
AtTRIM5Cyp XbaI 5′	5′-CAACTCTAGAGCCACCATGGCT TCCAGAATCCTGGT-3′		
CA A14C 3′	5′-CTAGGTGATATGCACTGATGTA CCATTTG-3′	psPAX2	pET-20b
CA A14C 5′	5′-CAAATGGTACATCAGTGCATAT CACCTAG-3′		
CA E45C 3′	5′-GTGGGGTGGCTCCGCATGATA ATGCTGAAAAC-3′	psPAX2	pET-20b
CA E45C 5′	5′-GTTTTCAGCATTATCATGCGGA GCCACCCCAC-3′		
CaTRIM5α NotI 3′	5′-ACCAGCGGCCGCTCAAGAGCT TGGTGAGCACA-3′	CaTRIM5α-pMIP	pcDNA3.1(−)
CaTRIM5α XbaI 5′	5′-CAACTCTAGAGCCACCATGGCT TCTGGAATCCTGCTT-3′		
CCR5 NotI 3′	5′-TTTGCGGCCGCTCACAAGCCCA CAGATATTTCC-3′	MDDC/MDM cDNA	pAIH
CCR5 XbaI 5′	5′-CCCTCTAGAGCCACCATGGATT ATCAAGTGTCAAGTCCAA-3′		

doi:10.1038/nature09976

CD4 NotI 3′	5′-TTTGCGGCCGCTCAAATGGGGC TACATGTCTTC-3′	MDDC/MDM cDNA	pAIB
CD4 XbaI 5′	5′-CCCTCTAGAGCCACCATGAACC GGGGAGTCCCTTTTA-3′		
IKKα NheI 5′	5′-CAACGCTAGCATGGAGCGGCC CCCGG-3′		
IKKα NotI 3′	5′-GAAGGCGGCCGCTCATTCTGTT AACCAACTCCAATC-3′	MDDC/MDM cDNA	pcDNA3.1(−) N-3×FLAG
IKKβ NotI 3′	5′-TTAAGCGGCCGCTCATGAGGC CTGCTCCAG-3′	MDDC/MDM cDNA	pcDNA3.1(−) N-3×FLAG
IKKβ XbaI 5′	5′-ACCATCTAGAATGAGCTGGTCA CCTTCCCT-3′		
IKKγ NotI 3′	5′-ACCAGCGGCCGCCTACTCAATG CACTCCATGACATG-3′	MDDC/MDM cDNA	pcDNA3.1(−) N-3×FLAG
IKKγ XbaI 5′	5′-CAACTCTAGAATGAATAGGCAC CTCTGGAAGA-3′		
IRF3 NotI 3′	5′-ACCAGCGGCCGCTCAGCTCTCC CCAGGGCC-3′	MDDC/MDM cDNA	pcDNA3.1(−)
IRF3 XbaI 5′	5′-CAACTCTAGAGCCACCATGGGA ACCCCAAAGCCA-3′		
Luciferase NotI 3′	5′-TAATGCGGCCGCTTACACGGCG ATCTTGCC-3′	pGL4.10 (Promega)	pALPS

doi:10.1038/nature09976

Luciferase XbaI 5′	5′-CAACTCTAGAGCCACCATGGAA GATGCCAAAAACATT-3′		
MAVS NotI 3′	5′-ACCAGCGGCCGCCTAGTGCAG ACGCCGCCGGTA-3′	MDDC/MDM cDNA	pcDNA3.1(−)
MAVS XbaI 5′	5′-CAACTCTAGAGCCACCATGCCG TTTGCTGAAGACAA-3′		
TAB1 NotI 3′	5′-ACCAGCGGCCGCCTACGGTGC TGTCACCACGCT-3′	MDDC/MDM cDNA	pcDNA3.1(−) N-3×FLAG
TAB1 XbaI 5′	5′-CAACTCTAGAATGGCGGCGCA GAGGAGGAG-3′		
TAB2 NotI 3′	5′-ACCAGCGGCCGCTCAGAAATG CCTTGGCATCT-3′	MDDC/MDM cDNA	pcDNA3.1(−) N-3×FLAG
TAB2 XbaI 5′	5′-CAACTCTAGAATGGCCCAAGGA AGCCACCAAATT-3′		
TAB3 NheI 5′	5′-CAACGCTAGCATGGCGCAAAG CAGCCCACAGCTT-3′		
TAB3 NotI 3′	5′-ACCAGCGGCCGCTCAGGTGTA CCGTGGCATCT-3′	MDDC/MDM cDNA	pcDNA3.1(−) N-3×FLAG
TAK1 NotI 3′	5′-ACCAGCGGCCGCTCATGAAGT GCCTTGTCGTTTC-3′	MDDC/MDM cDNA	pcDNA3.1(−) N-3×FLAG
TAK1 XbaI 5′	5′-CAACTCTAGAATGTCTACAGCC TCTGCCGCCT-3′		

doi:10.1038/nature09976

TRIM5α C15/18A 3′	5′-CAGGAGTTCCAGAGCGATGGG GGCGGTCACCTCCTC-3′	TRIM5α-pcDNA3.1(−)	pcDNA3.1(−)
TRIM5α C15/18A 5′	5′-GAGGAGGTGACCGCCCCCATC GCTCTGGAACTCCTG-3′		
TRIM5α NotI 3′	5′-ACCAGCGGCCGCTCAAGAGCT TGGTGAGCACA-3′	MDDC/MDM cDNA	pcDNA3.1(−)
TRIM5α XbaI 5′	5′-CAACTCTAGAGCCACCATGGCT TCTGGAATCCTGGTTA-3′		
TRIM5α XhoI 3′	5′-ACCACTCGAGAGAGCTTGGTG AGCACAGAGT-3′	TRIM5α-pcDNA3.1(−)	pcDNA3.1(−) C-Myc/6×His, C-3×FLAG,C-3×HA
TRIM5α Δ1-60 (ΔRING) XbaI 5′	5′-CAACTCTAGAGCCACCATGAGT TACCAGCCTGAGAACATA-3′	TRIM5α-pcDNA3.1(−)	pcDNA3.1(−)
TRIM6 NotI 3′	5′-ACCAGCGGCCGCTCAAGAGCT TGGACGACGCAG-3′	MDDC/MDM cDNA	pcDNA3.1(−)
UBC13 Not 3′	5′-ACCAGCGGCCGCTTAAATATTA TTCATGGCATATAGCCTAGT-3′	MDDC/MDM cDNA	pcDNA3.1(−)
UBC13 XbaI 5′	5′-CAACTCTAGAGCCACCATGGC CGGGCTGCCCCGC-3′		
UBCH5B NotI 3′	5′-ACCAGCGGCCGCTTACATCGCA TACTTCTGAGTCC-3′	MDDC/MDM cDNA	pcDNA3.1(−)
UBCH5B XbaI 5′	5′-CAACTCTAGAGCCACCATGGCT		

doi:10.1038/nature09976

	CTGAAGAGAATCCACA-3′		
UBCH5C NotI 3′	5′-ACCAGCGGCCGCTCACATGGC ATACTTCTGAGTCC-3′	MDDC/MDM cDNA	pcDNA3.1(−)
UBCH5C XbaI 5′	5′-CAACTCTAGAGCCACCATGGCG CTGAAACGGATTAA-3′		
ZsGreen1 NotI 3′	5′-TAATGCGGCCGCTCAGGGCAA GGCGGAG-3′	pIRES2-ZsGreen1 (Clontech)	pcDNA3.1(−) N-3×FLAG
ZsGreen1 XbaI 5′	5′-CAACTCTAGAATGGCCCAGTCC AAGCACGGCCTG-3′		
ZsGreen1 XhoI 3′	5′-ACCACTCGAGGGGCAAGGCGG AGCC-3′	pIRES2-ZsGreen1 (Clontech)	pcDNA3.1(−) C-3×FLAG

doi:10.1038/nature09976

Supplementary Table 3. shRNA target sequences used in this study.

Target	shRNA Target Sequence
IRF3 TS1-1213 (pAPM)	5′-GGCCCTTCATTGTAGATCTGAT-3′
Luciferase (pGL4) TS1-1221 (pAPM)	5′-TACAAACGCTCTCATCGACAAG-3′
STAT2 TS1-4172 (pAPM)	5′-GTCCAAGTCTGTGGAACTTAAA-3′
Non-targeting control	5′-CTTACTCTCGCCCAAGCGAGAG-3′
TAK1 TS1-1123 (pAPM)	5′-AGCGCCCTTCAATGGAGGAAAT-3′
TAK1 TS2-440 (pAPM)	5′-AGCCTTTGGAGTTGTTTGCAAA-3′
TRAF2 TS1-1,112	5′-GGGTCTTCATCTGGAAGATCTC-3′
TRAF2 TS2-1,634	5′-GGGCCAGGGTCTCACTGTACAA-3′
TRAF2 TS3-1,770	5′-TTGGCAGACGGTCTTAGCCAAG-3′
TRAF2 TS4-870	5′-GTGCGAGAGCCTGGAGAAGAAG-3′
TRAF6 TS1-1,380	5′-AGCAGTGCAATGGAATTTATAT-3′
TRAF6 TS2-1,620	5′-AGGGTACAATACGCCTTACAAT-3′
TRAF6 TS3-1,375	5′-AGCACAGCAGTGCAATGGAATT-3′
TRIM5 TS1-259 (pAPM)	5′-TGGCTTCTGGAATCCTGGTTAA-3′
TRIM5 TS2-360 (pAPM)	5′-TGCCAAGCATGCCTCACTGCAA-3′
TRIM5 TS3-420 (pAPM)	5′-TGCCCTGTGTGCCGGATCAGTT-3′
TRIM5 TS4-545 (pAPM)	5′-ACGCCATGGAGAGAAACTTCTA-3′
TRIM5 TS8-2102 (pAPM)	5′-TCGTGTGATAATTGTTCACCAA-3′
TRIM5 TS1-540 (pshRLP)	5′-GCTCAGGGAGGTCAAGTTG-3′
UBC13 TS1-1267 (pAPM)	5′-AGCTAACCAGGTCTTTAGAATA-3′
UBC13 TS3-1966 (pAPM)	5′-ACCTTTCATGTGTGTTAAGAAA-3′
UEV1A TS3-1409 (pAPM)	5′-CCCTGGTTTCTTTAAGTCTTAA-3′

SUPPLEMENTARY INFORMATION

doi:10.1038/nature09976

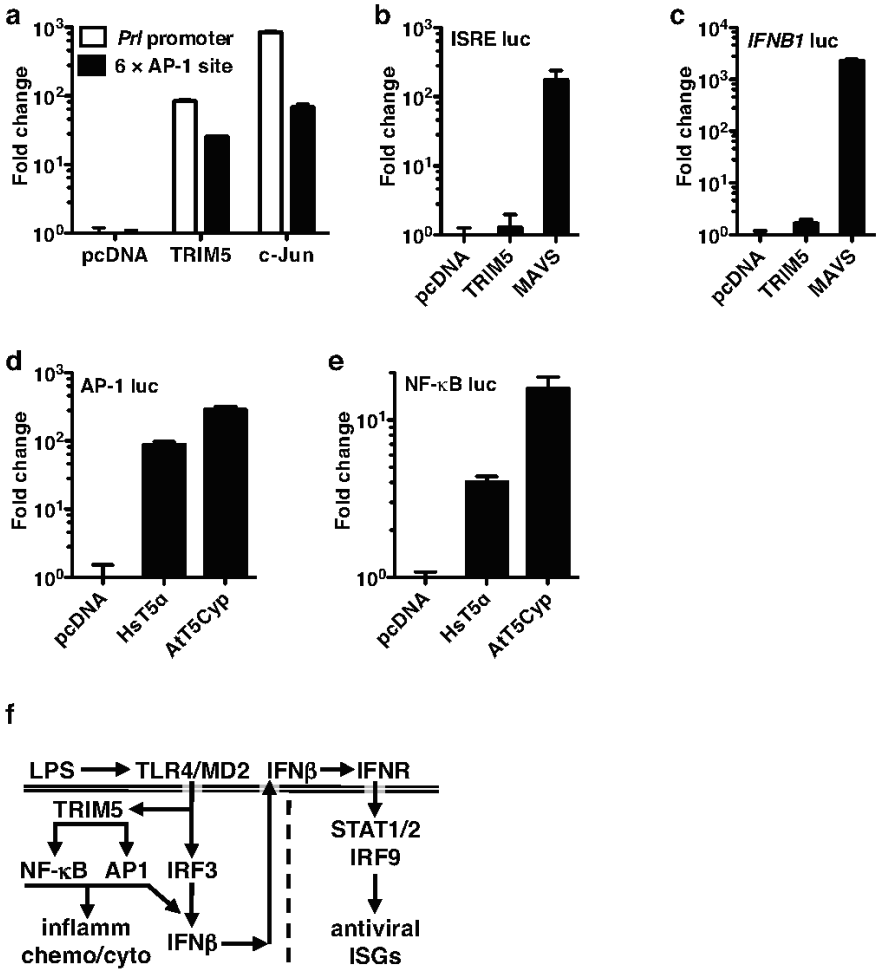

Supplementary Figure 1. a-e Luciferase assays of HEK-293 cells transfected with the indicated luciferase reporter plasmids and pcDNA3.1 expression plasmids for the indicated genes. **f**, The role of TRIM5 in signaling. Horizontal double line, cytoplasmic membrane; vertical dashed line separates the two waves of innate signaling.

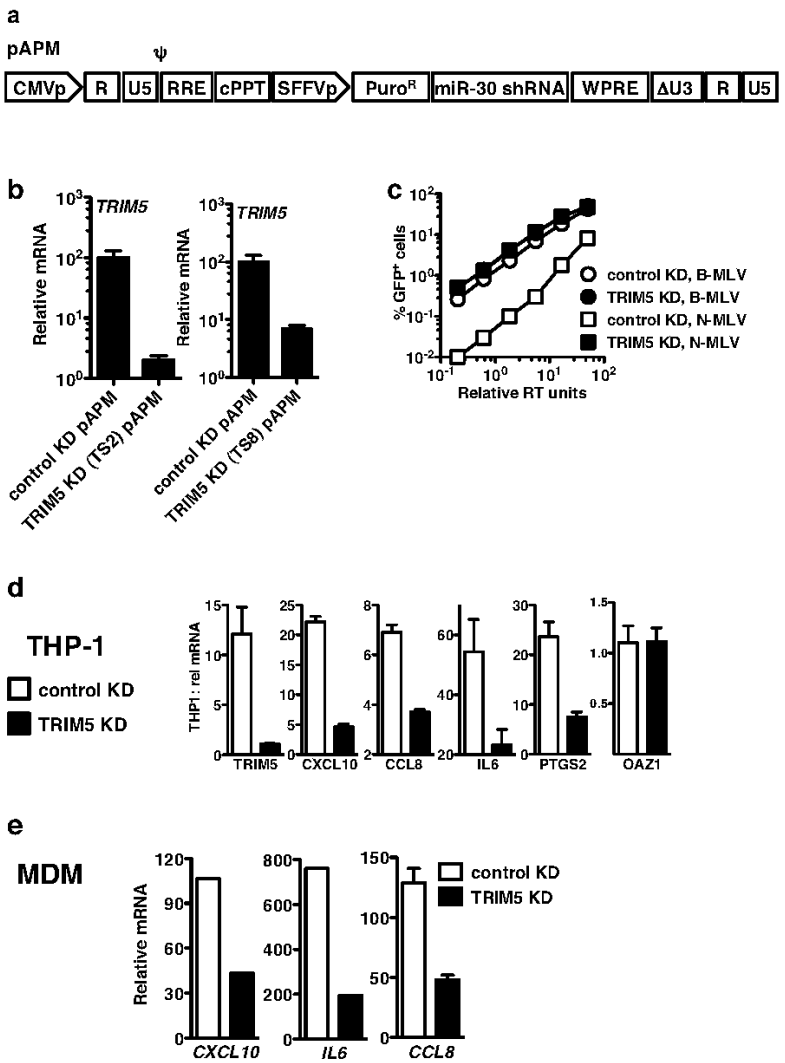

Supplementary Figure 2. a, Schematic of the lentiviral vector pAPM where both puromycin N-acetyltransferase and microRNA-based shRNA expression are driven by the spleen focus forming virus (SFFV) pol II promoter. **b,** TE671 cells, transduced with pAPM stably expressing the indicated shRNAs, were assayed for *TRIM5* knockdown by qRT-PCR. **c,** cycling THP-1 monocytes, stably expressing pAPM shRNA targeting TRIM5 or control shRNA, were challenged with VSV-G-pseudotyped N- or B-MLV GFP reporter vectors and assayed by FACS 72 h post-transduction. **d,** qRT-PCR for the indicated mRNAs harvested 2 to 8 hrs after LPS-treatment of THP-1 macrophages, depending on the peak values for that gene. **e,** qRT-PCR for the indicated mRNAs harvested 2 to 8 hrs after LPS-treatment of MDM, depending on the peak values for that gene.

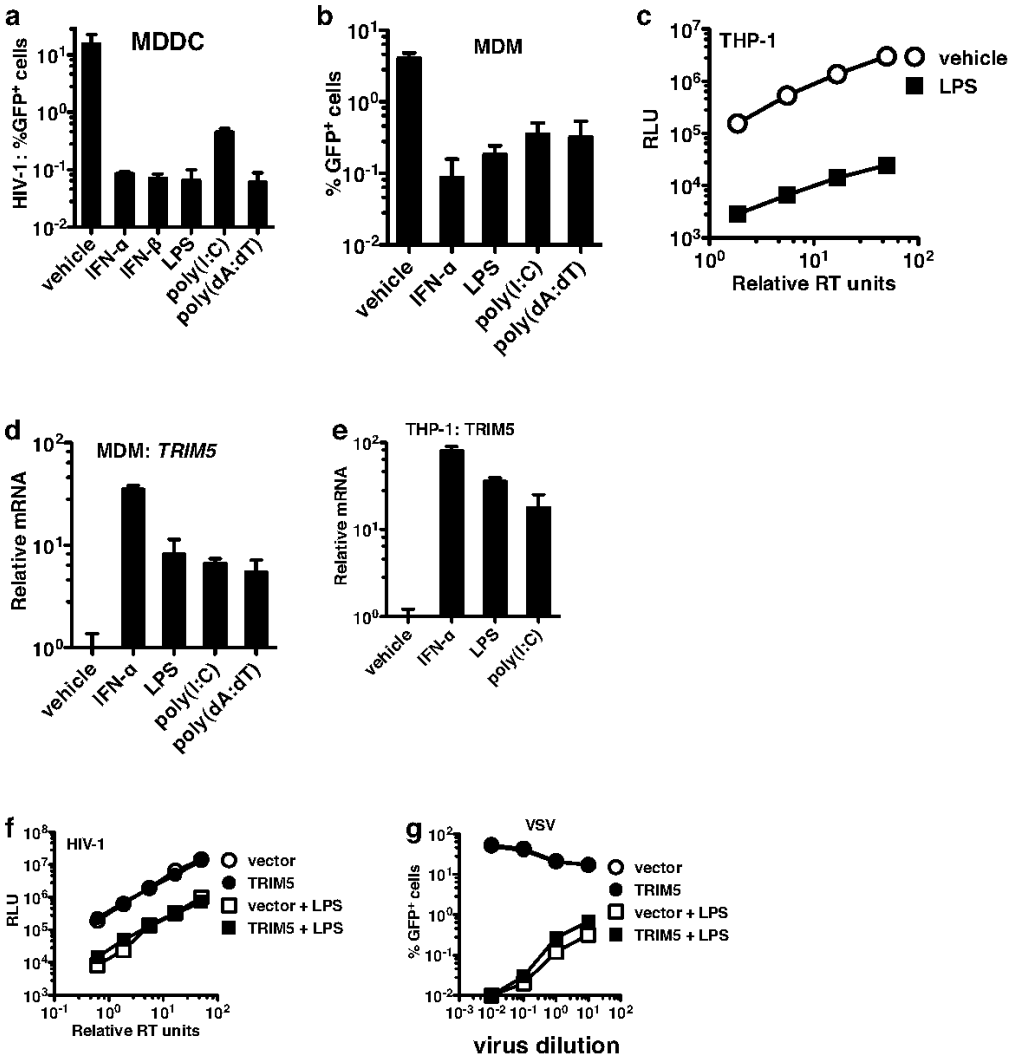

Supplementary Figure 3. MDDC (**a**) or MDM (**b**) were treated with the indicated compounds for 24 h, challenged with a VSV-G-pseudotyped HIV-1 GFP reporter minimal vector, and assayed by FACS 72 h post-transduction. TPA-differentiated THP-1 cells (**c**) were treated with ultrapure *E. coli* K12 LPS for 24 h and challenged with a VSV-G-pseudotyped HIV-1 luciferase reporter virus, and assayed by luciferase assay 72 h post-transduction. MDM (**d**) or TPA-differentiated THP-1 cells (**e**) were treated with the indicated compounds for 16 h, and qRT-PCR was performed for *TRIM5*. TPA-differentiated THP-1 cells stably expressing human TRIM5α, or empty vector control cells, were challenged with an HIV-1 luciferase reporter virus (**f**) or Vesicular Stomatitis Virus bearing a GFP reporter (**g**). HIV-1 was assayed by luciferase assay 72 h after challenge and VSV was assayed by FACS 20 h after challenge.

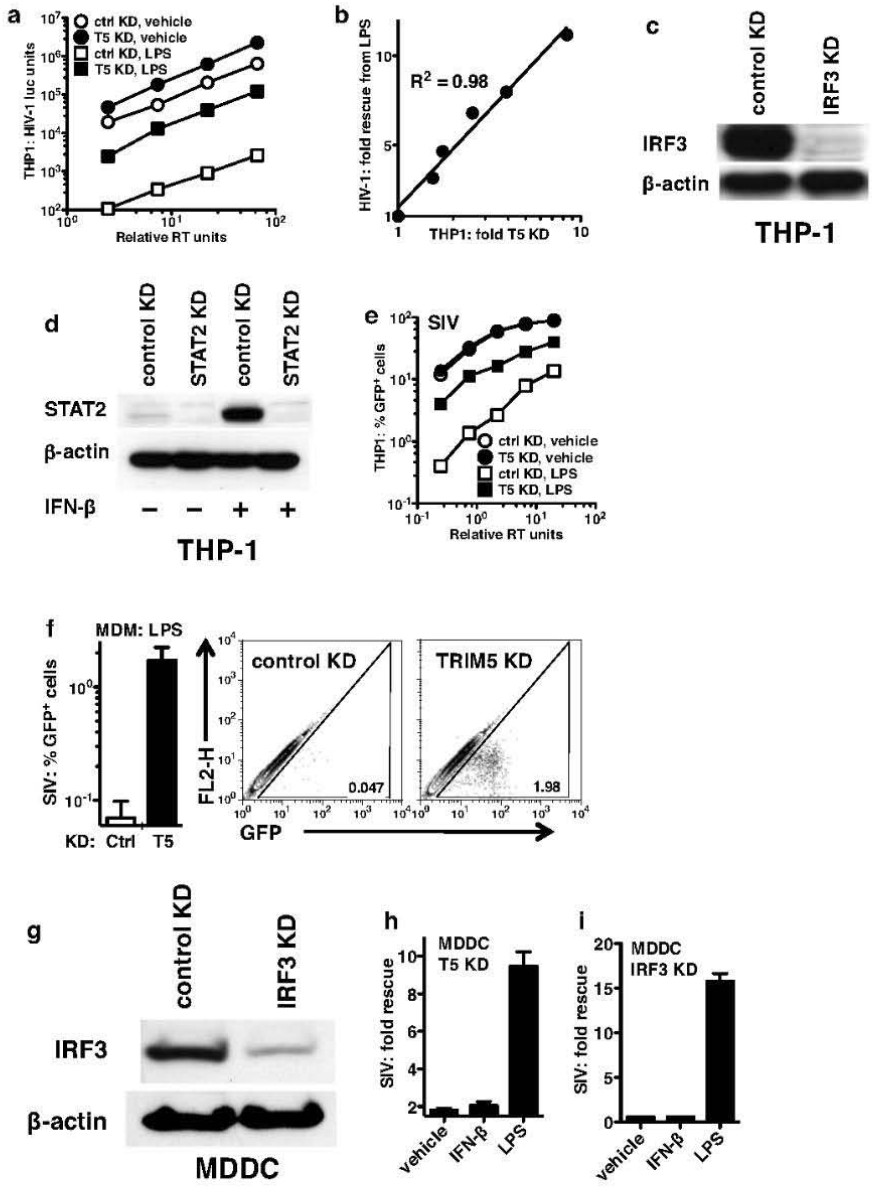

Supplementary Figure 4. a, CD4/CCR5-THP-1 macrophages transduced with lentiviral vectors expressing pol II-driven microRNA-based shRNAs targeting TRIM5 or control, were treated with LPS or vehicle, and challenged with CCR5-tropic HIV-1 luciferase reporter virus. **b**, Correlation between TRIM5 KD efficiency, as measured by qRT-PCR, and magnitude rescue of HIV-1 infectivity

from LPS. Immunoblot of whole-cell lysates from TPA-differentiated THP-1 cells transduced with pAPM expressing shRNA targeting IRF3 (**c**), STAT2 (**d**) or control shRNA. STAT2 KD and control KD cells were either treated with recombinant IFN-β for 16 h, or left untreated, prior to lysis. **e**, THP-1 macrophages were treated with LPS or vehicle and challenged with a VSV G-pseudotyped SIV_{MAC239}GFP reporter virus. MDM (**f**) or MDDCs (**g-i**), transduced with lentiviral KD vectors targeting TRIM5 (**f** and **h**) or IRF3 (**g and i**), were treated for 20 hrs with LPS (**f**) or as indicated (**h** and **i**), and then challenged with an SIV_{MAC239}GFP reporter virus. Results are reported as percent infected (**i**) or as fold-change compared to control (**h** and **i**). Lysates were probed with the indicated antibodies in (**g**).

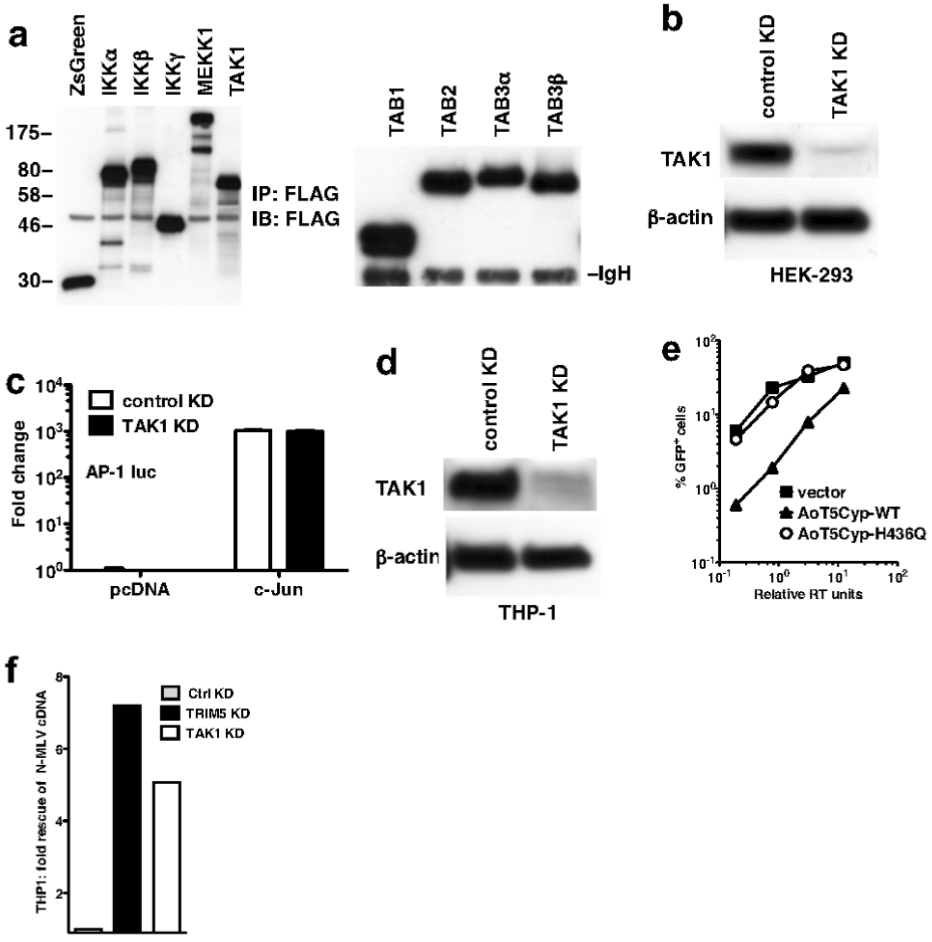

Supplementary Figure 5. a, Immunoblot of the indicated FLAG-tagged proteins immunopreciptated from transfected 293T cells. **b,** Immunoblot of TAK1 knockdown in HEK-293 cells. **c,** Luciferase assay of TAK1 or control KD HEK-293 cells transfected with an AP-1 luciferase reporter plasmid, and either empty pcDNA or a c-Jun expression plasmid. **d**, Immunoblot of TAK1 KD TPA-differentiated THP-1 cells. **e,** THP-1 cells expressing either wild type AtTRIM5Cyp or the H436Q mutant (or an empty vector control line) were challenged with a VSV-G-pseudotyped HIV-1 GFP reporter virus and analyzed by FACS 72 after transduction. **f,** PCR for full-length N-tropic MLV viral cDNA in TRIM5, TAK1, or control KD THP-1 cells.

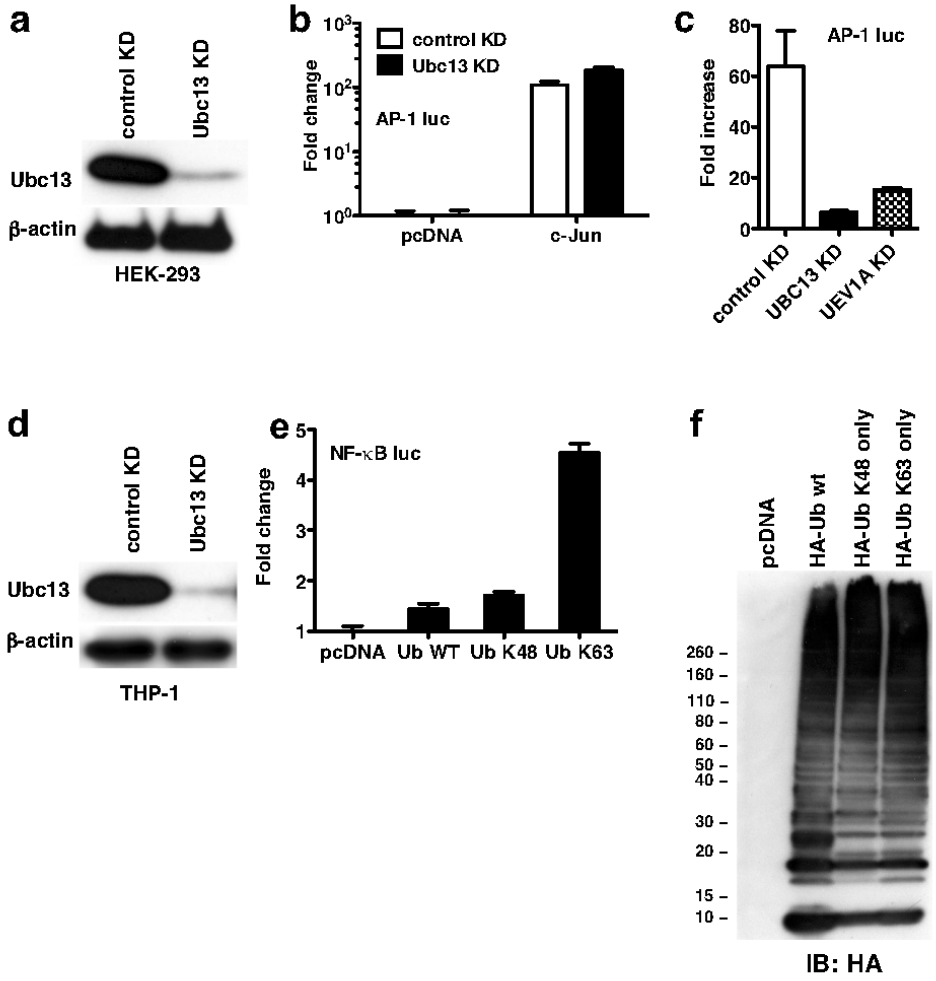

Supplementary Figure 6. a, Immunoblot of UBC13 KD in HEK-293 cells. **b,** Luciferase assay of UBC13 or control KD HEK-293 cells transfected with an AP-1 luciferase reporter plasmid, and either empty pcDNA or a c-Jun expression plasmid. **c,** Luciferase assay of control KD, UBC13 KD, or UEV1A KD HEK-293 cells transfected with an AP-1 luciferase reporter plasmid, and a human TRIM5α expression plasmid. **d**, Immunoblot of UBC13 KD in TPA-differentiated THP-1 cells. **e,** HEK-293 cells were transfected with the indicated plasmids, along with an NF-κB luciferase reporter. **f,** Immunoblot of whole cell lysates from HEK-293 cells transfected with the indicated plasmids.

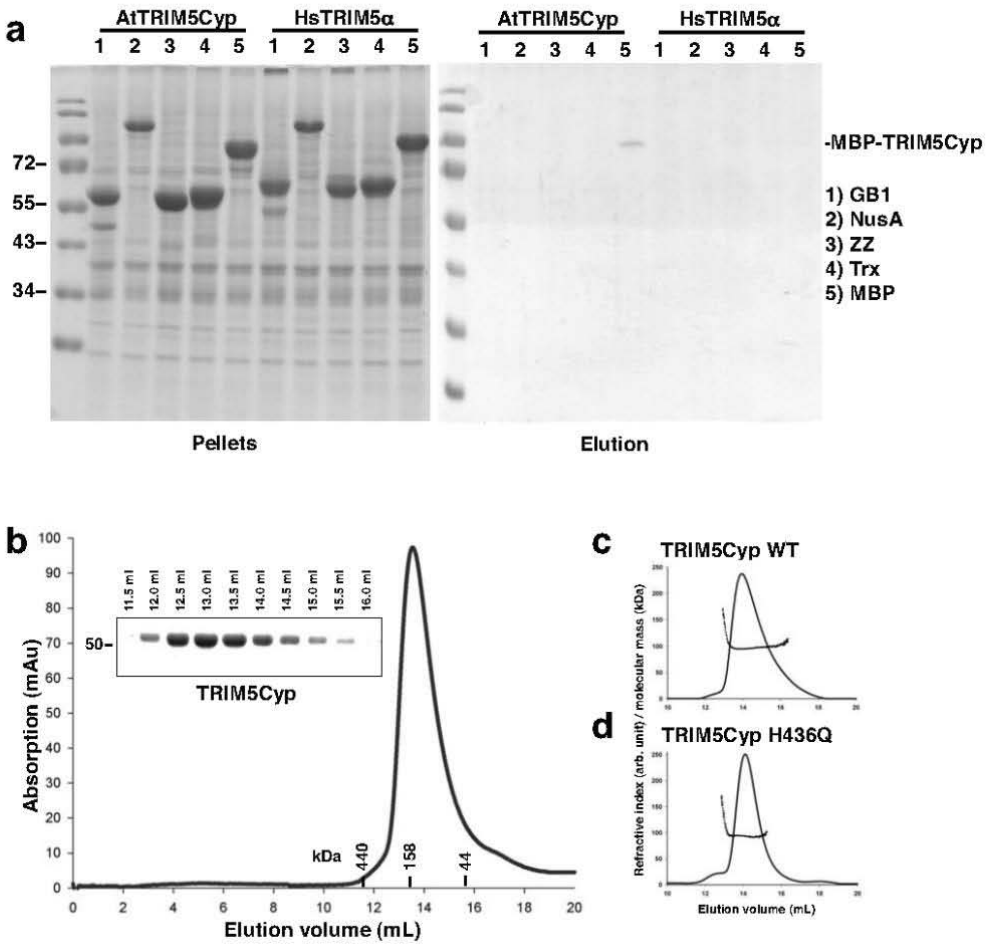

Supplementary Figure 7. a, Coomassie-stained SDS-PAGE gels showing insoluble (Pellets) or soluble (Elution) protein fractions. N-terminal tag fusions to Owl monkey TRIM5Cyp and human TRIM5α were screened for soluble expression in transfected Sf9 cells. The fusion constructs all carried an N-terminal His-tag. To detect soluble expressed constructs, fusion constructs were batch purified on Ni-NTA beads and analyzed by SDS-PAGE after elution with 250 mmol/L imidazole (Elution). Insoluble fractions were obtained by centrifugation of lysed cells (Pellets). **b,** Gel filtration chromatogram showing the elution profile of recombinant TRIM5Cyp protein on a Superdex 200 column, and a coomassie-stained SDS-PAGE gel of the indicated fractions (insert). The apparent molecular mass was estimated by comparison to standard molecular weight markers depicted in the chromatogram. **c, d,** SEC-MALS results. The elution profiles are depicted in refractive index detection and the calculated

molecular masses obtained from the light scattering data are shown as distributions across the peaks. Comparable molecular masses were obtained for TRIM5Cyp WT (**c**) and TRIM5Cyp H436Q (**d**) showing that both proteins behave the same in solution.

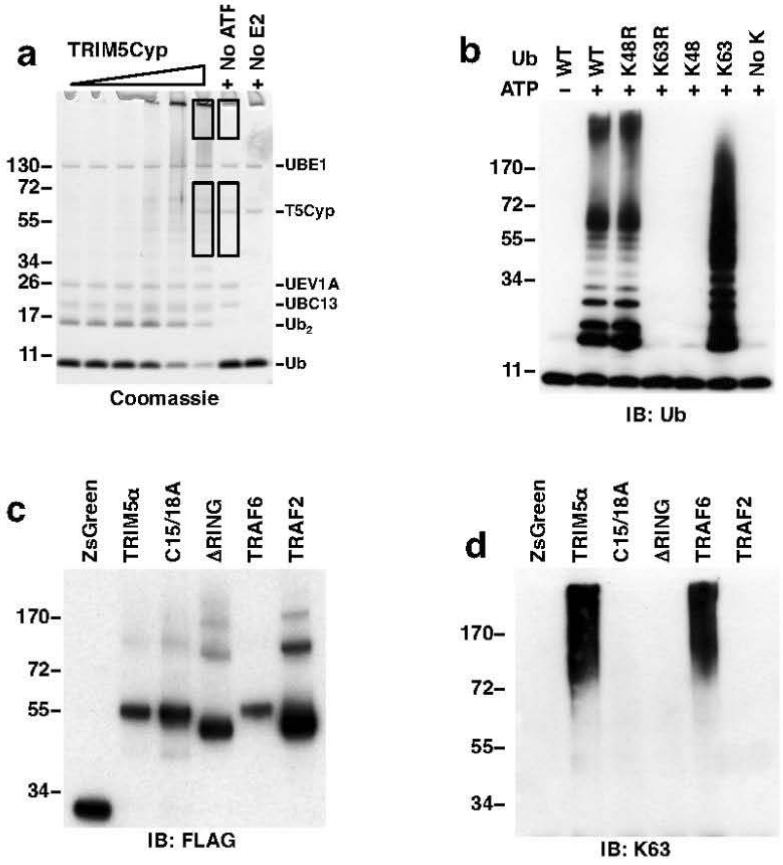

Supplementary Figure 8. a, Products of *in vitro* reactions with ATP, purified Ubiquitin, UBE1, the UBC13/UEV1A E2 complex, and increasing amounts of the E3 Ubiqutin Ligase AtTRIM5Cyp, revealed by Coomassie. Gel pieces in the higher molecular weight (> 170 kDa) and lower molecular weight (40 – 70 kDa) regions were cut out separately (black boxes) and analyzed by MALDI-MS/MS after in-gel tryptic digestion. **b,** Immunoblot of products from *in vitro* reactions with ATP, purified WT Ubiquitin, or the indicated Ubiquitin mutants, UBE1, the UBC13/UEV1A E2 complex, and AtTRIM5Cyp. **c,** Immunoblot of the indicated FLAG-tagged proteins immunoprecipitated from lysates of transfected HEK-293 cells. **d,** Immunoblot of products of *in vitro* reactions with ATP, purified Ubiquitin, UBE1, the UBC13/UEV1A E2 complex, and the indicated transfected FLAG-tagged proteins immunoprecipitated from HEK-293 lysates.

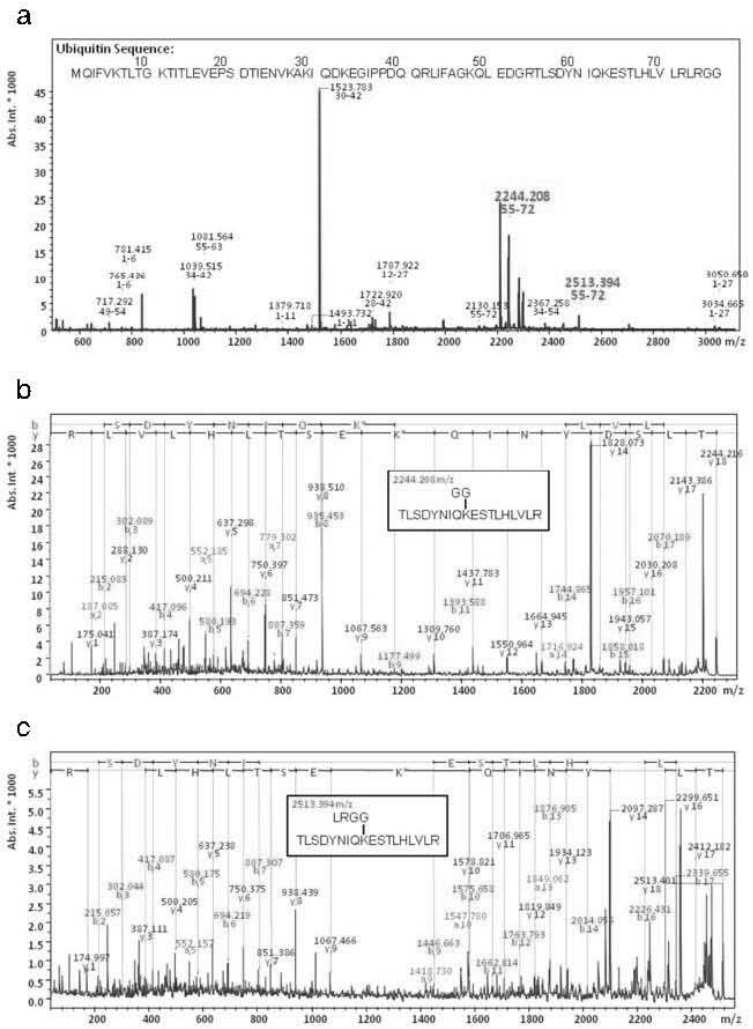

Supplementary Figure 9. Identification of K63-linked polyubiquitin chains formed by the E3-ligase activity of AtTRIM5Cyp: Gel pieces containing products from an *in vitro* ubiquitinylation assay are analyzed by MS after in-gel tryptic digestion. (**a**) MALDI spectrum of tryptically digested fragments: Mass over charge ratios (*m/z*) of signals matching theoretical peptide fragments of Ubiquitin are labeled in the spectrum. Numbers below the indicated *m/z* ratios correspond to residues in the Ubiquitin sequence (shown on top of the spectrum). Detected signals cover 94 % of the Ubiquitin sequence. Fragments with detected masses matching Ubiquitin peptides carrying a modified lysine are marked as red numbers in the spectrum and were further analyzed by MS/MS. MS/MS spectra of the peptides 2244.2 *m/z* (**b**) and 2513.4 *m/Z* (**c**)

show signals for fragment ions (a-, b-, and y-ions labelled in different colours) with mass differences corresponding to single amino acids in the peptide sequence (shown on top of the spectrum). The mass differences K* match a lysine modified with amino acids GG or LRGG. (**b**) MS/MS spectrum identifying fragment 2244.2 m/z as Ubiquitin peptide 55-72 with additional amino acids GG linked to K63 (see inset). (**c**) MS/MS spectrum identifying fragment 2513.4 m/z as Ubiquitin peptide 55-72 with additional amino acids LRGG linked to K63 (see inset).

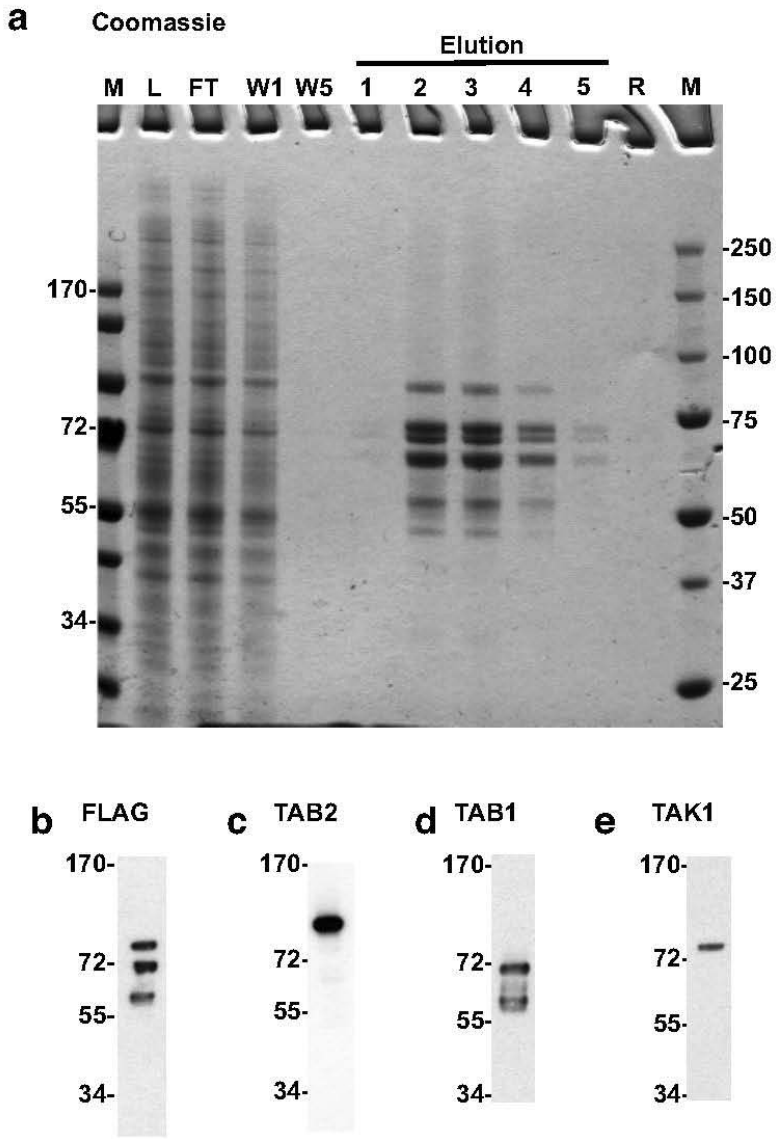

Supplementary Figure 10. Figure S10: Purification of recombinant TAK1 complex components. In panel a, FS-TAK1, FS-TAB1, and FS-TAB2 were produced in *293T* and purified by Streptactin Sepharose chromatography as described under Experimental Procedures. Aliquots (1 µL) of the soluble lysate (lane L), the Streptactin Sepharose flow-through (lane FT), and wash 1 (lane W1) fractions, and aliquots (10 µl) of the wash 5 (lane W5), and the 2.5 mM Desthiobiotin eluate fractions were analyzed by SDS−PAGE. The polypeptides were visualized by staining the gel with Coomassie Blue dye. The positions and sizes (kDa) of marker polypeptides are indicated. In panel b, c, d, and e, aliquots (10 µl) were analyzed by immunoblotting with the indicated antibodies.

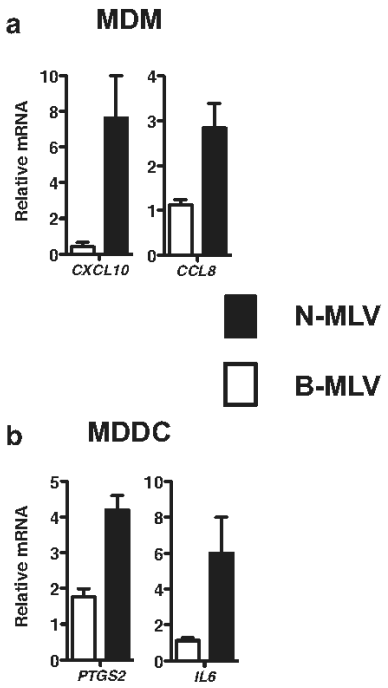

Supplementary Figure 11. qRT-PCR for the indicated mRNAs from MDM (**a**) or MDDC (**b**). mRNA was harvested 6 h after challenge with VSV-G-pseudotyped N-tropic or B-tropic MLV. Data are expressed as fold change versus media control.

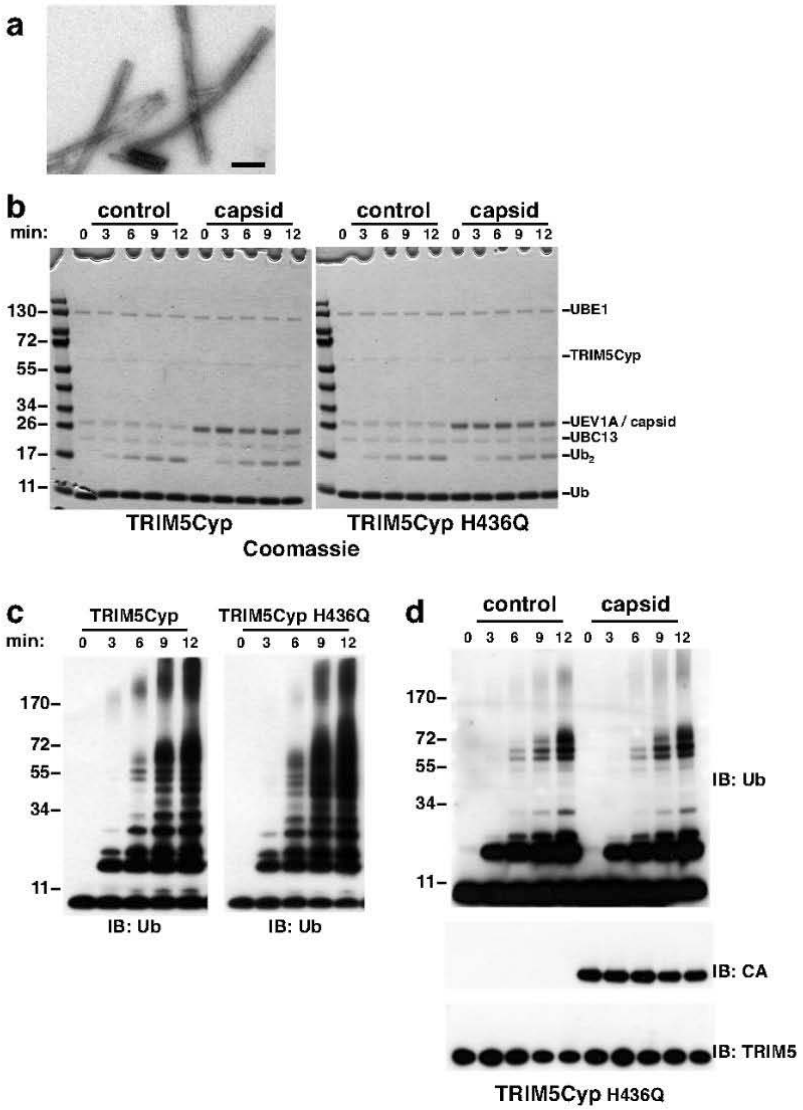

Supplementary Figure 12. a, Electron micrograph of HIV-1 capsid tubes made with oxidized A14C/E45C mutant in the absence of salt (magnification, 33,000x). **b,** Coomassie-stained SDS-PAGE gels of samples from the *in vitro* ubiquitylation time-course reactions using recombinant TRIM5Cyp WT or the H436Q mutant carried out in the presence of UBE1 and UBC13/UEV1A, with or without the addition of assembled HIV-1 capsid (CA A14C E45C). **c,** Immunoblot of samples from an *in vitro* ubiquitylation time-course reaction using recombinant TRIM5Cyp WT or the H436Q mutant, carried out in the presence of UBE1 and UBC13/UEV1A. **d,** Immunoblot of samples from an *in vitro* ubiquitylation time-course reaction using the recombinant TRIM5Cyp H436Q mutant, carried out in the presence of UBE1 and UBC13/UEV1A, with or without the addition of assembled HIV-1 capsid (CA A14C E45C).

2.2 Manuscript: Dissecting the HIV-1 capsid lattice into distinct TRIM5 binding units

Dissecting the HIV-1 Capsid Lattice into Distinct TRIM5 Binding Units

Title

Dissecting the HIV-1 Capsid Lattice into Distinct TRIM5 Binding Units

Autors
D. Morger[1], F. Zosel[1], S. Züger[1], M. Bühlmann[1], B. Schuler[1] and M.G. Grütter[1,2]

Affiliations
[1] Departement of Biochemistry, University of Zurich, Winterthurerstrasse 190, CH-8057 Zürich

[2] to whom correspondence should be addressed: gruetter@bioc.uzh.ch, Tel. +41-44-6355580,

Fax. +41-44-6356834

Keywords
TRIM, TRIM5, HIV, Capsid, Innate Immunity, Retrovirus, Restriction Factors

Abstract

TRIM5 proteins are bi-functional pattern recognition receptors: They restrict the infection by HIV-1 and other retroviruses by disrupting the viral capsid shell and induce an innate immune response.

TRIM5 binds to a complex epitope on the surface of the assembled retrovirion core. This epitope has to be composed of more than just one capsid molecule, because significant binding can only be observed to assembled capsids and only very weak interaction is detected with individual capsids.

To elucidate the arrangement of molecules recognized by TRIM5 we engineered a series of disulfide cross-linked HIV-1 capsid oligomers, which mimic interfaces in the hexagonal HIV-1 capsid lattice: We developed protocols for the production of soluble capsid (CA) oligomers that are either disulfide-linked over cysteine mutations P207C/T216C in the C-terminal trimer interface or cross-linked with the trifunctional maleimide TMEA via cysteine mutations along alpha helix 4 at the N-terminal threefold axis. These new constructs expand the repertoire of already known oligomers, which now include monomeric, dimeric, trimeric and hexameric HIV-1 capsids.

In an attempt to map the binding epitope of *rhesus* TRIM5α on the HIV-1 CA lattice we measured and compared the binding affinities of the TRIM5 B30.2 binding domain to the available CA oligomers. These measurements revealed that the rhesus B30.2 domain has an increased affinity for trimeric and hexameric CAs cross-linked via the N-terminal domains, compared to monomeric or *wild-type* dimeric CAs.

Introduction

The family of tripartite motif-containing (TRIM) proteins encompasses nearly 100 members, many of which have emerged to play important roles in innate immunity and have antiviral activity. Of the approximately 20 TRIMs identified to inhibit retroviral infectivity, TRIM5α

imposes the most potent block to retroviral entry [1]. The discovery of TRIM5α as the main restriction factor responsible for the HIV-1 resistance in rhesus macaques has unleashed an avalanche of publications, making TRIM5 one of the meanwhile best studied TRIMs [2]. In contrast to its primate ortholog, human TRIM5α only weakly inhibits HIV-1 infection but potently restricts N-MLV instead [3,4].

Many of the functional aspects on how TRIM5 acts to confer resistance to retroviruses have been unveiled and can be attributed to its multi-domain composition, characteristic of the tripartite/RBCC motif. TRIM5α is composed of an N-terminal RING, followed by a B-Box2 and a predicted coiled-coil domain, together forming the RBCC motif [5]. At the C-terminus, TRIM5α has an additional B30.2 domain. The RING domain functions as an E3 ubiquitin ligase [6], the B-Box2 mediates self-association important for higher-order oligomerization [7,8] and the coiled-coil mediates dimerization [9-11]. The C-terminal B30.2 domain binds to retroviral capsids (CA) and defines restriction specificity [12,13].

TRIM5α specifically recognizes and binds the viral CA lattice immediately upon exposure of the retrovirion core to the target cell cytoplasm at the early post-entry stage of retroviral infection [2,14]. CA binding is mediated by the B30.2 domain and is further potentiated through multiple avidity effects due to dimerization and higher oligomerization of TRIM5α [7,8,15]. Binding to the hexagonal CA lattice has been shown to trigger self-assembly of TRIM5α into a complementary hexagonal lattice requiring all of its domains [16]. Sensing of invading retrovirion cores by TRIM5α has several consequences: 1) TRIM5α fragmentizes the virus shell by disrupting the CA lattice at the inter-hexamer interfaces leading to a premature uncoating of the virion core [11,17]. 2) While remaining bound to virus associated CA fragments TRIM5α may recruit the proteasome and mediate virus degradation indirectly through UbcH5b mediated self-ubiquitination, thereby preventing reverse transcription [18-21]. 3) Binding to the retroviral CA lattice stimulates the E3 ligase activity of TRIM5α and enhances the Uev1a/Ubc13

mediated formation of K63 linked ubiquitin chains. Free K63-linked ubiquitin chains activate TAK1 to initiate downstream signaling leading to an innate immune response [10].

While much is known about the overall mechanism of TRIM5α restriction, the structural basis for CA recognition at the crucial step of binding remains elusive. The binding properties of TRIM5α are remarkable in the sense that it can recognize a broad range of retroviruses while remaining specific for the common lattice pattern of retroviral CAs. For example HIV-1, FIV and EIAV are all restricted by the same allele of rhesus TRIM5α [22-24]. And human TRIM5α restricts both the gammaretrovirus N-MLV and the distantly related lentivirus EIAV sharing as little as 25% sequence identity [3,4,22,25]. Furthermore, discrete variations in the variable loops of the B30.2 domain such as single nucleotide polymorphisms can change the restriction specificities of TRIM5α between different populations or species, further broadening the range of restricted retroviruses. For example a single amino acid substitution from arginine to proline at position 332 of human TRIM5α is sufficient to confer resistance to HIV-1 to a similar extent as for rhesus TRIM5α [24,26]. The row of retroviruses targeted by TRIM5α spans the families of spumaviruses, betaretroviruses, lentiviruses and gammaretroviruses [27].

Significant binding of TRIM5α is only detected with assembled retroviral CA lattices, as TRIM5α has been shown to co-sediment with detergent striped virions and in vitro assembled CA tubes [9,12]. In contrast, the interaction with soluble monomeric or dimeric CAs is very weak. The dissociation constant of the rhesus B30.2 domain to a monomeric HIV-1 CA has recently been estimated to be between 400 – 500 μM [28,29]. This specific sensing of a conserved lattice pattern is remarkable, as TRIM5α not only tolerates large variations in CA sequence but also large differences in the shape of the assembled CA: TRIM5α has been shown to bind both spherical (e.g. N-MLV) and conical virions (e.g. HIV-1), as well as in-vitro assemblies of CA or capsid-nucleocapsid (CA-NC) forming cylindrical tubes or even planar two-dimensional lattices [16]. The differences in surface curvature displayed in those CA structures are accommodated by changes in the inter-hexamer spacings of the CA lattice, while

the hexameric and pentameric building blocks remain rigid [30]. Therefore it appears rather surprising that no appreciable binding to isolated CA hexamers was reported and the finding that rhesus TRIM5α breaks the lattice at the trimeric inter-hexamer interfaces rather suggest that TRIM5α engages at the inter-hexamer interfaces [11,31]. This apparent discrepancy might be compensated by TRIM5α through the long flexible binding loops in the B30.2 domain that could adapt to differences in the inter-hexamer distances.

Although oligomerization through the B-Box and coiled-coil domains greatly contributes to the binding affinity of TRIM5α, the B30.2 domain alone is sufficient to significantly bind to assembled CA tubes [28]. The recently solved high-resolution structures of the TRIM5α B30.2 domain revealed that the predicted CA-binding surface based on sequence comparisons and mutational studies is larger than the surface presented by one CA subunit in the CA lattice [28,31]. This suggests that the B30.2 domain binds to an epitope composed of multiple CA subunits.

Here we describe the isolation of engineered trimeric HIV-1 CAs that mimic interfaces at the threefold symmetric axis of the HIV-1 CA lattice. In order to identify the binding epitope of rhesus TRIM5α on the HIV-1 CA lattice, we measured the binding affinities of the B30.2 domain to these trimeric CAs and compared them with the affinities to monomeric, dimeric and hexameric interface mimics of the HIV-1 CA lattice.

Results and Discussion

Design of HIV-1 CA mutants that allow cross-linking at trimeric lattice interfaces and soluble purification

As TRIM5 is known to detectably bind to assembled retroviral CAs and the interaction to unassembled CA's is difficult to detect, we aimed for the production of isolated CA oligomers that mimic the interfaces present in the hexagonal HIV-1 CA lattice (Figure 1A). Procedures for the isolation of the hexameric and pentameric building blocks of the HIV-1 CA lattice have been reported [32,33]. And the wild-type HIV-1 CA, which forms dimers in solution via its C-

terminal domain, mimics an interface between two neighboring hexamers [34]. To complete the collection of isolated lattice interfaces, we designed HIV-1 CA mutants that allow isolation of CAs cross-linked at the threefold symmetry axis of the lattice, reflecting the common interface between three adjacent hexamers. This interface is formed by six CA molecules, with three of them forming a trimeric contact via the C-terminal domains (CTDs) and the others coming into proximity at their N-terminal domains (NTDs) (Figure 1B).

CA oligomers cross-linked at the threefold inter-hexamer interface were produced by two independent approaches. In the first approach three CAs were linked via engineered cysteines in their NTDs and in the second approach three CAs were linked via engineered cysteines in their CTDs placing the NTDs distantly apart.

We inspected available HIV-1 CA models to identify residues of the CA NTD that come into proximity at the threefold axis. The most recent model of the mature HIV-1 capsid (pdb entry: 3J34) shows that only alpha helix 4 of the three CA NTDs is coming together at the trimer interface with the closest residues located roughly 20 Å apart (Figure S 1A), too far for chemical crosslinking with commercially available trifunctional crosslinkers [30]. TRIM5α is able to recognize a broad range of retroviruses harboring different capsid curvatures and binding to CA-NC mutants that form two-dimensional hexagonal crystals has previously been demonstrated *in vitro* [16]. Therefore we also considered the HIV-1 CA lattice structure derived from planar two-dimensional CA crystals as a valuable model to design potential TRIM5 binding CA oligomers (Figure 1A&B). An alignment of the high resolution CA NTD structure (pdb entry: 1AK4) onto the 9 Å lattice model derived from planar 2D-crystals of the HIV-1 CA (pdb entry: 3DIK) revealed that the NTDs come closer together at the trimer interface due to the lack of curvature in the 2D-lattice (Figure 2, Figure S 1B) [35,36]. This illustrates the importance of flexibility at the inter-hexameric interfaces to accommodate different capsid curvatures. The closest distances were estimated to about 10 Å for residues R82 and P85, making them reasonable candidates for crosslinking with the trifunctional crosslinker TMEA

(Figure 2C&D). Besides R82 and P85, also residues E75, A78 and E79 along alpha helix 4 were chosen for mutation to cysteines and crosslinking with TMEA (Figure 2A&B).

Cysteine mutations that allow crosslinking of the C-terminal trimer-interface in assembled virus-like CA particles have previously been described (Figure S 2A) [37].

Cysteine mutations were combined with either of two sets of destabilizing mutations in the CTD dimer interface (Figure S 2B), aiming to facilitate later disassembly of cross-linked CA assemblies. The first set of destabilizing mutations (W184A/P185A) was taken from the published procedure for the isolation of soluble CA hexamers described by Pornillos et al. [32]. Another set of dimer destabilizing mutations (E180D/V181A) was found in a presumably infectious virus variant isolated from the plasma of HIV-infected patients and has been characterized by del Alamo et al. [38,39]. A list with all CA mutants that were designed for the production of trimeric CAs is shown in Table 2.

Isolation of trimeric HIV-1 capsids and biophysical characterization

Purified recombinant HIV-1 capsid mutants bearing cysteine mutations in the NTD combined with or without destabilizing mutations in the C-terminal dimer interface were tested for their ability to assemble *in vitro*. All CA mutants, except for the ones bearing W184A/P185A mutations in the CTD region, turned turbid when dialysed against 1M NaCl at protein concentrations around 10 mg/ml, indicative for CA assembly. Further analysis of the assembly products by negative stained EM revealed that cysteine mutants without destabilizing mutations formed elongated tubes as observed for the wild type capsid (data not shown), while cysteine mutants with combined E180D/V181A mutations formed both elongated tubes and planar sheets (Figure 4A&B).

Initial cross-linking trials with a five-fold molar excess of trifunctional maleimide TMEA and long incubation times resulted in the production of covalently linked trimeric CA products for all the assembly-competent CA mutants as determined by SDS-PAGE (Figure S 3). The fact that all cysteine mutations along alpha helix 4, even the ones with predicted distances of 20 Å

(Figure 2B), were cross-linked by the 10.3 Å linker TMEA further points out the suggested flexibility at the threefold symmetry axis of the CA lattice. However long incubation times in presence of a 5-fold molar excess of TMEA also lead to nonspecific TMEA coupling to the native cysteines in the CTD, as reaction products with more than one molecule of TMEA coupled were detected by ESI-MS (data not shown). Therefore we had to optimize the procedure for obtaining trimers. Finally, short incubations in presence of equimolar concentrations of TMEA yielded CA oligomers coupled to only one TMEA molecule (Figure 4E). Under these more selective conditions, the R82C and P85C mutants with predicted distances of 10 Å crosslinked more efficiently to trimers than the other mutants with more distantly positioned cysteines (Figure 3A&C). To verify if these trimers were specific to the assembled capsid fraction containing the hexagonal lattice interfaces, we separated assembled from soluble CAs by centrifugation. Indeed, crosslinked trimers were only found in the pellet fraction when analyzed by SDS-PAGE (Figure 3B&C). Interestingly, destabilized E180D/V181D CA mutants that partially assembled to planar sheets formed trimers more efficiently than mutants without destabilizing mutations. Furthermore A78C and E79C mutants with predicted inter-trimer distances of 16 and 20.9 Å, respectively, only crosslinked notably to trimers when combined with the E180D/V181D mutation, indicating that the NTDs come closer together in the absence of lattice curvature (Figure 3A&C).

Out of the R82C and P85C mutants that cross-linked more efficiently to trimers, we focused on the R82C mutation for further purification and characterization, because mutation of P85 that is located in the exposed cyclophilin A binding loop may interfere with rhesus TRIM5α binding. TMEA cross-linked HIV-1 CA particles were disassembled by dialysis into 20 mM Tris, pH8 and purified by size exclusion chromatography to separate trimeric capsids from incompletely crosslinked dimers or monomers. Reinjection of the trimer containing fractions onto size exclusion yielded essentially pure CA NTD-trimers (Figure 4C). Surprisingly, N-terminally cross-linked CA tubes without destabilizing mutations in the C-terminal dimerization interface

could also be disassembled. Possible explanations could be the incomplete CA crosslinking by TMEA indicated by the large fraction of only two-fold cross-linked CAs (Figure 3) or that crosslinking of the NTDs induces conformational changes that destabilize the CA lattice.

The same procedure was applied to isolate E180D/V181A/P207C/T216C CA mutants linked via disulfides in the C-terminal trimer interface from CA assemblies that were oxidized in analogy to Zhao et al. [11]. EM analysis of the assembled E180D/V181A/P207C/T216C mutants revealed both tubular and sheet-like morphologies, characteristic for the E180D/V181A mutation (Figure 4B).

On size exclusion the suspected CTD- and NTD-linked CA trimers eluted at an apparent mass of 193 and 135 kDa, respectively (Figure 4C&D). Analysis by sedimentation velocity analytical ultracentrifugation revealed that both the CTD- and the NTD-linked capsids are indeed trimers in solution when combined with the destabilizing E180D/V181A mutation (Figure 4G&H). The NTD-linked capsids without destabilizing mutations formed higher oligomers when analysed by analytical ultracentrifugation (data not shown). The molecular mass of the CA trimers determined by ESI-MS corresponded to the mass of three CA monomers modified with one TMEA linker (Figure 4E&F).

Binding of TRIM5α B30.2 to distinct HIV-1 capsid interface mimics

Based on the hypothesis that TRIM5α recognizes retroviral capsids via the B30.2 binding to multiple CA epitopes, we tested if the B30.2 domain has a stronger affinity for a particular CA lattice interface. Therefore we produced the established disulfide linked hexameric and the wild type dimeric HIV-1 capsids alongside with the newly designed trimeric HIV-1 capsids to measure their binding affinities to TRIM5α B30.2. Each of these CA oligomers mimics a distinct symmetry interface present in the assembled CA lattice (Figure 1). TRIM5α binds to the outer surface of invading retroviral CA shells, formed by the capsid NTDs. While the NTDs in the NTD-linked trimers come together and form one potential multivalent epitope for TRIM5α, the NTDs in the CTD-linked trimer are placed distal apart (Figure 1C). Therefore we

considered the CTD-trimer as a negative control to rule out nonspecific contribution of CA oligomerisation to the TRIM5α binding affinity.

Low affinity binding of the rhesus TRIM5α B30.2 domain to the CA NTD of HIV-1 has previously been reported and the K_D was determined to be in the range of 410 ± 90 μM by NMR [28]. To measure such low affinities, one has to reach very high protein concentrations into the mM range. This makes affinity determinations by most conventional biochemical methods very difficult, as viscosity effects and other artifacts usually mask the actual affinity measurement. One method that requires relatively small sample volumes and is not affected by viscosity is microscale thermophoresis (MST), where migration of a fluorescently labeled protein is measured along a temperature gradient in the function of a titrated unlabeled binding partner. In our setup, the HIV-1 capsid constructs were taken as unlabeled titrants, because they can be produced in large amounts and can easily be concentrated to high concentrations, and the B30.2 domains from rhesus TRIM5α and its TRIM20 homolog were fluorescently labeled. Labeling reactions with the fluorophor NT-647(NHS) were performed at a pH of 8.5, where labeling of the N-terminal amine is favored to minimize the risk of modifying lysines near the binding interface. MS analysis of fluorescent tryptic digestion products of the labeled *rhesus* B30.2 that were isolated via reversed phase chromatography confirmed the N-terminus as the major site of labeling (data not shown). Initial MST measurements were carried out at 20 °C with wild-type HIV-1 CA and revealed an affinity of 338 ± 26 μM for the rhesus TRIM5α B30.2 domain (Figure S 4), suggesting that CA dimerization might slightly improve binding as compared to the reported 410 ± 90 μM for the CA NTD. Because the engineered trimeric CAs did not remain soluble to high concentrations at ambient temperatures, all binding experiments were carried out in a cold room (T = 7 °C). Furthermore, all CA constructs could be titrated to higher concentrations at low temperatures. The binding affinity of rhesus TRIM5α B30.2 for the wild-type HIV-1 CA measured at 7 °C was 327 ± 16 μM (Figure 5A), comparable to the dissociation constant measured at 20 °C. The B30.2 domain of TRIM20/pyrin, that has no restriction activity

against retroviruses, was taken as a negative control [1]. The measured K_D for the B30.2 domain of TRIM20 and wild-type HIV-1 capsid was 922 ± 57 μM (Figure 5E). Also no significant binding of rhesus TRIM5α B30.2 to Lysozyme was detected (Figure 5D). Surprisingly though, the K_D measured for human TRIM5α B30.3 was 232 ± 17 μM, a higher affinity than for the B30.2 domain of rhesus TRIM5α (Figure 5D). This suggests that the wild-type HIV-1 CA dimer alone does not form the multivalent epitope that defines retroviral specifity for rhesus TRIM5α. We also tested the HIV-1 CA hexamer and the NTD-trimer for binding to rhesus TRIM5α B30.2 by MST. However, the NTD-trimer could was not amenable to MST measurements due to convection effects induced by the temperature gradient. To assess at least partially if the NTD-trimer has an increased affinity towards rhesus TRIM5α we tested binding with an incompletely cross-linked R82C/E180D/V181A dimer instead, which was obtained as a side-product in the purification of the NTD-trimer (Figure 3). This CA dimer linked over the NTD-trimer interface could be measured by MST and had an affinity of 275 ± 12 μM for rhesus TRIM5α B30.2 (Figure 5B&F). The affinity determined for the CA hexamer and rhesus TRIM5α B30.2 was 258 ± 11 μM (Figure 5C&F). All K_Ds were determined under the assumption that the B30.2 domain interaction with the CA oligomers follows simple one-to-one binding kinetics. Unlike with the wild-type HIV-1 CA, titrations of the rhesus B30.2 domain with incompletely cross-linked R82C/E180D/V181A NTD-dimers or CA hexamers did not reach near saturation of binding and therefore fitting of this data did not allow to discriminate whether a one-to-one binding model is appropriate or not. These K_Ds have to be considered with caution, because the actual stoichiometry of B30.2 binding to HIV-1 CAs is unknown and may involve multiple overlapping epitopes.

Altogether, the CA wild-type dimer, the R28C connected dimer and the CA hexamer all have comparable affinities for rhesus TRIM5α B30.2, with the R28C connected dimer and the CA hexamer having a slightly increased affinity as compared to the monomeric CA NTD or the wild-type CA dimer. This suggests that the lattice surface sampled by the B30.2 domain of

TRIM5α could be more complex than the ones mimicked by the CA oligomers so far measured. One possibility would be that TRIM5 recognizes a lattice surface that is shared in common between the CA oligomers tested.

Another possibility would be that the B30.2 domain of TRIM5α binds three CA molecules at the threefold symmetric axis of the lattice as mimicked by the NTD-trimer. But since the NTD-trimer could not be measured by MST, we had to find another approach to measure this interaction. We finally used dual-focus fluorescence correlation spectroscopy (dual-focus FCS) to measure the affinity of rhesus TRIM5α B30.2 to the CA NTD-trimer. Binding affinities are determined by measuring the diffusion time of a fluorescently labeled protein in the function of the titrated unlabeled binding partner, resulting in an increased calculated Stokes radius upon binding. The fluorescently labeled protein is kept at low nanomolar concentrations, so a pseudo-first-order binding model can be used to evaluate the data. As the viscosity at high CA concentrations also leads to a significantly increased diffusion time, overlaying the actual change in Stokes radius caused by the binding event, we had to implicate an appropriate control. Human cyclophilin A (CypA) combines two properties that make it an ideal control to predict the contribution of viscosity to the measured binding curves: First, it has a similar molecular weight (19 kDa for flag-CypA) as compared to rhesus TRIM5α B30.2 (23 kDa) and both have an overall globular shape, therefore having similar expected diffusion rates. Second, it has a relatively high affinity for the HIV-1 capsid (K_D = 16 μM) [40]. This has the advantage that CypA is saturated with HIV-1 CA already at concentrations of 100 μM CA, before viscosity started to interfere with the binding measurements. Hereby we predicted the Stokes radius of a B30.2 bound CA NTD-trimer complex to be 5 nm and determined the affinity of this complex to be 168 ± 6.3 μM (Figure 6B).

To verify the affinities measured by MST and allow to a better comparison of the K_Ds we also measured binding of the rhesus B30.2 domain to the wild-type CA dimer and the CA hexamer using dual-focus FCS with the same approach (Figure 6A,C,E). The K_D determined by dual-

focus FCS for the rhesus B30.2 domain binding to the wild-type CA is 344 ± 14.4 μM and fits very well to the K_D of 327 ± 16 μM measured by MST (Figure 6A). This is in contrast to the dual-focus FCS measurements with the CA hexamer. Here, the K_D determined using a simple one-to-one binding model is 94 ± 9.3 μM, which differs considerably from the affinity measured by MST (K_D = 258 ± 11 μM). However, the curve obtained with the kinetic model for only one binding site does not fit the measured data suggesting that the CA hexamer does not follow simple one-to-one binding kinetics when interacting with the rhesus B30.2 domain (Figure 6C). Fitting of the same data using a two-binding-sites model yields a calculated curve that aligns very well with the measured data, with a K_{D1} = 21.5 ± 2.5 μM for the more affine binding site and a K_{D2} = 356.8 ± 35.7 μM for the less affine binding site. However, these K_Ds cannot be taken as absolute values because our K_D determination is based on the hypothesis that CypA binds to the CA hexamer with the same stoichiometry as the B30.2 domain, which may not be fulfilled anymore. Nevertheless, it can be concluded that the HIV-1 CA hexamer likely provides more than just one possible binding site for the rhesus B30.2 domain.

Our binding studies with the B30.2 domain of rhesus TRIM5α revealed an increased binding affinity both for the CA NTD-trimer and the CA hexamer compared to the wild-type CA dimer or the monomeric CA NTD. This suggests that the B30.2 domain may bind to an epitope on the CA lattice that spans CA interfaces that are represented both in the CA NTD-trimer and the CA hexamer. One such epitope is found at the inter-hexamer gap between two neighboring CA hexamers of the hexagonal HIV-1 CA lattice and encompasses two NTD subunits on one hexamer and one NTD subunit on the neighboring hexamer. This binding epitope would match the best to our binding data, because it would go in line with the two binding site model for the CA hexamer and would explain the increased affinity for the CA NTD-trimer because it encompasses two CA subunits represented on the CA NTD-trimer. Considering that our engineered CA NTD-trimer is artificial and probably very flexible, it is likely that the NTD

trimer as presented in the context of the HIV-1 CA lattice would have a higher affinity for rhesus TRIM5α than actually measured with the engineered R82C/E180D/V181A NTD-trimer.

Materials and Methods

Design and production of cross-linked CA trimers

HIV-1 capsid (CA) cDNA was amplified from psPAX2 [41] and cloned into the pET-20b vector (Invitrogen). Mutations were introduced by Quickchange mutagenesis (Invitrogen) and verified by DNA sequencing. Proteins were expressed and purified as previously described [42], with the addition of 100 mM β-mercaptoethanol (βME) to all buffers. CA proteins were assembled *in vitro* by overnight dialysis at 4 °C [43] into assembly buffer (20 mM Tris-HCl, pH8, 1 M NaCl) in the presence of 100mM βME.

In the case of assembled (E180D/V181A/P207C/T216C) CA tubes, the reducing agent was removed by dialysis into assembly buffer prior to cross-linking via the cysteines introduced into their C-terminal domains (CTD) as described in Zhao et al. [11]. Crosslinking products were analyzed by non-reducing SDS-PAGE.

For crosslinking of assembled CA tubes harboring mutations E75C, A78C, E79C, R82C or P85C in their N-terminal domains (NTD) combined with or without destabilizing E180D/V181A mutations in the CTDs, the initial assembly buffer was exchanged against crosslinking buffer (20mM HEPES-HCl, pH 7.2, 1M NaCl, 0.5 mM TCEP) by a two-step dialysis. Chemical crosslinking of neighboring NTDs via the introduced cysteines was performed by incubation with trifunctional maleimid cross-linker TMEA (Thermo Scientific) in a 1:1 molar ratio for 5 minutes on ice, followed by quenching with 10 mM DTT. Crosslinking products were analyzed by reducing SDS-PAGE.

Crosslinked CA trimers were prepared by dialysis of crosslinked CA assemblies into disassembly buffer (20mM Tris-HCl, pH 8) at 4 °C followed by size exclusion chromatography on a Hi-Load Superdex 200 26/60 column equilibrated with disassembly buffer. Main fractions

containing trimeric CA were pooled, concentrated using Amicon concentrators (Millipore) and re-injected onto Hi-Load Superdex 200 to yield purified CA trimers (>90%).

Transmission electron microscopy (TEM) analysis of CA assemblies

Aliquots from CA assemblies were diluted to 10-20 µM and 6 µL samples incubated on Formvar-coated copper-grids for 30 s. The grids were blotted, negatively stained 3 times on 20 µL drops of 2% uranyl acetate for 10 s, blotted and air dried. Samples were imaged on a Philips CM 100 transmission electron microscope at a magnification of…

Electrospray ionization mass spectrometry (ESI-MS) of cross-linked CA trimers

NanoESI-MS analysis of the samples was performed on a Q-TOF Ultima API mass spectrometer (Micromass, UK). The solutions were infused through a fused silica capillary (ID 75 µm) at a flow rate of 0.50 µL min^{-1}. Electrospray Pico Tips (ID 30 µm) were obtained from New Objective (Woburn, MA). Mass spectra were acquired by scanning an *m/z* range from 500 to 2500 with a scan duration of 1 s and an interscan delay of 0.1 s. Spray voltage was set to 2.1 kV, cone voltage to 35 V, RF lens 1 energy to 50 V, and collision to 10eV. Before injection, the samples were desalted using C_4-ZipTips (Millipore) from which they were eluted with 10 µL of 50:50:0.01 (v/v/v) CH_3OH:H_2O:HCOH (pH ~2).

Analytical ultracentrifugation

The oligomeric state of cross-linked CA proteins after purification was verified by sedimentation velocity analytical ultracentrifugation (SV-AUC) in 20 mM Tris-HCl, pH 8 at a concentration of 0.5 mg/ml. Sedimentation velocity measurements were conducted at 30000 rpm and 4°C using a ProteomeLab XL-1 (Beckman Coulter) ultracentrifuge. Data was analyzed with SEDFIT [44].

Production of fluorescently labeled TRIM B30.2 domains

cDNAs coding for the B30.2 domains of human and rhesus TRIM5α (residues 286-493 and 288-497, respectively) were cloned into the pFXGST vector using fragment exchange (FX) cloning [45]. The pFXGST vector was generated by modification of the MultiBac vector

pFBDM [46] multiple cloning site 1 (MCS1) to enable fragment exchange (FX) cloning. Briefly, the *Sap*I restriction site between the transposon element Tn7R and the Col-E1 origin of replication was removed and an *Nde*I restriction site was inserted into the MCS1 by Quikchange mutagenesis (Invitrogen). The FX-cassette of the pBXGST vector [45] was used as template (incl. coding region for N-terminal His_{10}-tag, followed by GST and 3C cleavage site) and cloned into the modified pFBDM vector using *Nde*I and *Xba*I restriction sites. The *Nde*I restriction site was later removed by Quikchange yielding the pFXGST vector.

Recombinant bacmid DNA was produced by transforming the resulting plasmids into E.coli DH10α (Invitrogen). The bacmid DNA was used to transfect Sf9 cells and isolate recombinant viruses. Sf-21 cells were grown to a density of 1.8 x 10^6 cells/ml in Sf-900 II media (Invitrogen) and infected with baculoviruses expressing human or rhesus B30.2 domain at a multiplicity of infection of 1. Cells were harvested after 65 h to 72 h of expression at 27 °C. Sf21 cells were lysed in lysis buffer (50 mM Tris-HCl, pH 8, 300 mM NaCl, 10 mM imidazole, DNAse I, RNase I, Benzoase, and EDTA-free complete inhibitor cocktail (Roche Diagnostics)) using a homogenizer (EmulsiFlex). Soluble proteins were purified over a 1ml Ni-NTA column followed by over night dialysis at 4 °C against cleavage buffer (50 mM Tris-HCl, pH 8.5, 150 mM NaCl, 0.2 mM TCEP) in the presence of a 1:20 (w/w) ratio of 3C-protease. Cleaved HisGST-tag and 3C-protease were removed by passing the sample twice over a 1ml Ni-NTA column. The flow-trough was collected and concentrated to 2 mg/ml.

The B30.2 domain of TRIM20 was prepared as described in Weinert et al. [47] and concentrated to 2 mg/ml.

Purified B30.2 domains were dialyzed in labeling buffer (25 mM sodium carbonate, pH 8.5, 100mM NaCl, 0.5 mM TCEP) over night at 4 °C. Labeling reactions were carried out on ice in the presence of 1.2 fold molar amounts of NT-647-NHS (Nanotemper) by overnight incubation in the dark. Proteins were separated from free dye by size exclusion chromatography on a Superdex 200 10/300 column. Coupling efficiency was calculated by measuring the absorptions

spectra at 280 nm and 650 nm. The average number of lysines labeled with NT-647 was estimated to be 0.43, 0.31 and 0.41 for human TRIM5α B30.2, rhesus TRIM5α B30.2 and human TRIM20 B30.2, respectively.

Microscale thermophoresis (MST)

25 nM of labeled B30.2 homologs were titrated with 2:1 dilution series of different CA constructs in a total volume of 12 µl to 20 µl. Due to the increased viscosities at high CA concentrations, extensive mixing by pipetting up and down at least 30 times was needed to obtain reproducible dilution series. The samples were loaded into standard capillaries (NanoTemper Technologies GmbH), sealed with soft wax and equilibrated by incubation at 4 °C for 3 to 4 hours before measurement. Thermophoresis measurements were carried out using the NanoTemper Monolith NT.115 instrument (NanoTemper Technologies GmbH) using 40% LED and 20% laser power with the laser on for 30 sec followed by an off period of 5 sec. 15 to 16 thermophoresis measurements were carried out from three independently prepared dilution series (triplicate). Samples from each dilution series were recorded twice (technical duplicate). The resulting raw data were analysed using the NanoTemper software to obtain binding curves and the Kds were calculated using Prism (GraphPad Software).

Dual-focus fluorescence correlation spectroscopy (dual-focus FCS)

For dual-focus FCS measurements [48], a CA dilution series as described for MST was prepared with Alexa Fluor 488-labeled Trim5α B30.2 and Cyclophilin A at a final protein concentration of 2 nM. The experiment was carried out at 7°C on a confocal single-molecule instrument (MT200, PicoQuant), equipped with a differential interference contrast prism (U-DICTHC, Olympus). The labeled proteins were excited alternatingly with two orthogonally polarized diode lasers at 485 nm (LDH-D-C-485, PicoQuant) with a repetition rate of 40 MHz and a laser power of 30 µW each. The distance d = 400 ± 10 nm between the two foci in aqueous solution was determined by measuring a series of reference samples of known diffusion coefficient [49]. A custom-built temperature-controlled sample holder was used to cool the

sample cell. The microscope objective was cooled as well to minimize the temperature gradient between sample cell and objective.

The fluorescence intensity cross- and autocorrelation curves obtained from the data of each focus were analyzed using C++ and Mathematica (Wolfram Research) to obtain diffusion coefficients D. These were converted into hydrodynamic radii R_H with the Stokes-Einstein relation $R_H = \frac{k_B T}{6\pi\eta D}$,

where k_B is the Boltzmann constant, T is the temperature and η is the viscosity of the sample. The increase in R_H of the labeled molecules upon binding to CA was analyzed with a simple stoichiometric binding model multiplied with a corrective term for the increased viscosity at high CA concentrations.

$$R_H = \left(R_{H_0} + \frac{(R_{H_{end}} - R_{H_0}) \cdot [CA]}{K_d + [CA]} \right) \cdot \eta_{[CA]}$$

In a first step, the hydrodynamic radius of the unbound molecule (R_{H_0}), the hydrodynamic radius of the CA complex ($R_{H_{end}}$), the dissociation constant K_d and the concentration-dependent viscosity contribution $\eta_{[CA]}$ were extracted from fitting the Cyclophilin A dataset, where the complex is fully formed before the viscosity starts to increase. The extracted parameters (with exemption of K_d) were used to fit the Trim5α B30.2 data, allowing the precise determination of a dissociation constant by controlling the viscosity effect.

Acknowledgments

References

1. Uchil PD, Quinlan BD, Chan WT, Luna JM, Mothes W (2008) TRIM E3 ligases interfere with early and late stages of the retroviral life cycle. PLoS Pathog 4: e16.

2. Stremlau M, Owens CM, Perron MJ, Kiessling M, Autissier P, et al. (2004) The cytoplasmic body component TRIM5alpha restricts HIV-1 infection in Old World monkeys. Nature 427: 848-853.
3. Perron MJ, Stremlau M, Song B, Ulm W, Mulligan RC, et al. (2004) TRIM5alpha mediates the postentry block to N-tropic murine leukemia viruses in human cells. Proc Natl Acad Sci U S A 101: 11827-11832.
4. Yap MW, Nisole S, Lynch C, Stoye JP (2004) Trim5alpha protein restricts both HIV-1 and murine leukemia virus. Proc Natl Acad Sci U S A 101: 10786-10791.
5. Nisole S, Stoye JP, Saib A (2005) TRIM family proteins: retroviral restriction and antiviral defence. Nature reviews Microbiology 3: 799-808.
6. Diaz-Griffero F, Li X, Javanbakht H, Song B, Welikala S, et al. (2006) Rapid turnover and polyubiquitylation of the retroviral restriction factor TRIM5. Virology 349: 300-315.
7. Li X, Sodroski J (2008) The TRIM5alpha B-box 2 domain promotes cooperative binding to the retroviral capsid by mediating higher-order self-association. J Virol 82: 11495-11502.
8. Diaz-Griffero F, Qin XR, Hayashi F, Kigawa T, Finzi A, et al. (2009) A B-box 2 surface patch important for TRIM5alpha self-association, capsid binding avidity, and retrovirus restriction. J Virol 83: 10737-10751.
9. Langelier CR, Sandrin V, Eckert DM, Christensen DE, Chandrasekaran V, et al. (2008) Biochemical characterization of a recombinant TRIM5alpha protein that restricts human immunodeficiency virus type 1 replication. J Virol 82: 11682-11694.
10. Pertel T, Hausmann S, Morger D, Züger S, Guerra J, et al. (2011) TRIM5 is an innate immune sensor for the retrovirus capsid lattice. Nature 472: 361-365.
11. Zhao G, Ke D, Vu T, Ahn J, Shah VB, et al. (2011) Rhesus TRIM5α Disrupts the HIV-1 Capsid at the Inter-Hexamer Interfaces. PLoS Pathog 7: e1002009.
12. Sebastian S, Luban J (2005) TRIM5alpha selectively binds a restriction-sensitive retroviral capsid. Retrovirology 2: 40.
13. Stremlau M, Perron M, Welikala S, Sodroski J (2005) Species-specific variation in the B30.2(SPRY) domain of TRIM5alpha determines the potency of human immunodeficiency virus restriction. J Virol 79: 3139-3145.
14. Sayah DM, Sokolskaja E, Berthoux L, Luban J (2004) Cyclophilin A retrotransposition into TRIM5 explains owl monkey resistance to HIV-1. Nature 430: 569-573.
15. Javanbakht H, Yuan W, Yeung DF, Song B, Diaz-Griffero F, et al. (2006) Characterization of TRIM5alpha trimerization and its contribution to human immunodeficiency virus capsid binding. Virology 353: 234-246.
16. Ganser-Pornillos BK, Chandrasekaran V, Pornillos O, Sodroski JG, Sundquist WI, et al. (2011) Hexagonal assembly of a restricting TRIM5alpha protein. Proc Natl Acad Sci U S A 108: 534-539.
17. Stremlau M, Perron M, Lee M, Li Y, Song B, et al. (2006) Specific recognition and accelerated uncoating of retroviral capsids by the TRIM5alpha restriction factor. Proc Natl Acad Sci U S A 103: 5514-5519.
18. Rold CJ, Aiken C (2008) Proteasomal degradation of TRIM5alpha during retrovirus restriction. PLoS Pathog 4: e1000074.

19. Lukic Z, Hausmann S, Sebastian S, Rucci J, Sastri J, et al. (2011) TRIM5alpha associates with proteasomal subunits in cells while in complex with HIV-1 virions. Retrovirology 8: 93.
20. Black LR, Aiken C (2010) TRIM5alpha disrupts the structure of assembled HIV-1 capsid complexes in vitro. Journal of virology 84: 6564-6569.
21. Yamauchi K, Wada K, Tanji K, Tanaka M, Kamitani T (2008) Ubiquitination of E3 ubiquitin ligase TRIM5 alpha and its potential role. FEBS J 275: 1540-1555.
22. Hatziioannou T, Cowan S, Goff SP, Bieniasz PD, Towers GJ (2003) Restriction of multiple divergent retroviruses by Lv1 and Ref1. The EMBO journal 22: 385-394.
23. Keckesova Z, Ylinen LM, Towers GJ (2004) The human and African green monkey TRIM5alpha genes encode Ref1 and Lv1 retroviral restriction factor activities. Proc Natl Acad Sci U S A 101: 10780-10785.
24. Wilson SJ, Webb BL, Maplanka C, Newman RM, Verschoor EJ, et al. (2008) Rhesus macaque TRIM5 alleles have divergent antiretroviral specificities. Journal of virology 82: 7243-7247.
25. Sastri J, Campbell EM (2011) Recent insights into the mechanism and consequences of TRIM5alpha retroviral restriction. AIDS research and human retroviruses 27: 231-238.
26. Newman RM, Hall L, Connole M, Chen GL, Sato S, et al. (2006) Balancing selection and the evolution of functional polymorphism in Old World monkey TRIM5alpha. Proc Natl Acad Sci U S A 103: 19134-19139.
27. Fletcher AJ, Towers GJ (2013) Inhibition of retroviral replication by members of the TRIM protein family. Current topics in microbiology and immunology 371: 29-66.
28. Biris N, Yang Y, Taylor AB, Tomashevski A, Guo M, et al. (2012) Structure of the rhesus monkey TRIM5alpha PRYSPRY domain, the HIV capsid recognition module. Proc Natl Acad Sci U S A 109: 13278-13283.
29. Biris N, Tomashevski A, Bhattacharya A, Diaz-Griffero F, Ivanov DN (2013) Rhesus monkey TRIM5alpha SPRY domain recognizes multiple epitopes that span several capsid monomers on the surface of the HIV-1 mature viral core. J Mol Biol 425: 5032-5044.
30. Zhao G, Perilla JR, Yufenyuy EL, Meng X, Chen B, et al. (2013) Mature HIV-1 capsid structure by cryo-electron microscopy and all-atom molecular dynamics. Nature 497: 643-646.
31. Yang H, Ji X, Zhao G, Ning J, Zhao Q, et al. (2012) Structural insight into HIV-1 capsid recognition by rhesus TRIM5alpha. Proc Natl Acad Sci U S A 109: 18372-18377.
32. Pornillos O, Ganser-Pornillos BK, Kelly BN, Hua Y, Whitby FG, et al. (2009) X-ray structures of the hexameric building block of the HIV capsid. Cell 137: 1282-1292.
33. Pornillos O, Ganser-Pornillos BK, Yeager M (2011) Atomic-level modelling of the HIV capsid. Nature 469: 424-427.
34. Gamble TR, Yoo S, Vajdos FF, von Schwedler UK, Worthylake DK, et al. (1997) Structure of the carboxyl-terminal dimerization domain of the HIV-1 capsid protein. Science 278: 849-853.

35. Ganser-Pornillos BK, Cheng A, Yeager M (2007) Structure of full-length HIV-1 CA: a model for the mature capsid lattice. Cell 131: 70-79.
36. Gamble TR, Vajdos FF, Yoo S, Worthylake DK, Houseweart M, et al. (1996) Crystal structure of human cyclophilin A bound to the amino-terminal domain of HIV-1 capsid. Cell 87: 1285-1294.
37. Byeon I-JL, Meng X, Jung J, Zhao G, Yang R, et al. (2009) Structural convergence between Cryo-EM and NMR reveals intersubunit interactions critical for HIV-1 capsid function. Cell 139: 780-790.
38. del Alamo M, Rivas G, Mateu MG (2005) Effect of macromolecular crowding agents on human immunodeficiency virus type 1 capsid protein assembly in vitro. Journal of virology 79: 14271-14281.
39. Yoshimura FK, Diem K, Learn GH, Jr., Riddell S, Corey L (1996) Intrapatient sequence variation of the gag gene of human immunodeficiency virus type 1 plasma virions. Journal of virology 70: 8879-8887.
40. Yoo S, Myszka DG, Yeh C, McMurray M, Hill CP, et al. (1997) Molecular recognition in the HIV-1 capsid/cyclophilin A complex. J Mol Biol 269: 780-795.
41. Salmon P, Trono D (2007) Production and titration of lentiviral vectors. Current protocols in human genetics / editorial board, Jonathan L Haines [et al] Chapter 12: Unit 12 10.
42. Byeon IJ, Meng X, Jung J, Zhao G, Yang R, et al. (2009) Structural convergence between Cryo-EM and NMR reveals intersubunit interactions critical for HIV-1 capsid function. Cell 139: 780-790.
43. Gross I, Hohenberg H, Krausslich HG (1997) In vitro assembly properties of purified bacterially expressed capsid proteins of human immunodeficiency virus. European journal of biochemistry / FEBS 249: 592-600.
44. Schuck P (2000) Size-distribution analysis of macromolecules by sedimentation velocity ultracentrifugation and lamm equation modeling. Biophysical journal 78: 1606-1619.
45. Geertsma ER, Dutzler R (2011) A versatile and efficient high-throughput cloning tool for structural biology. Biochemistry 50: 3272-3278.
46. Berger I, Fitzgerald DJ, Richmond TJ (2004) Baculovirus expression system for heterologous multiprotein complexes. Nature biotechnology 22: 1583-1587.
47. Weinert C, Grutter C, Roschitzki-Voser H, Mittl PR, Grutter MG (2009) The crystal structure of human pyrin b30.2 domain: implications for mutations associated with familial Mediterranean fever. J Mol Biol 394: 226-236.
48. Dertinger T, Pacheco V, von der Hocht I, Hartmann R, Gregor I, et al. (2007) Two-focus fluorescence correlation spectroscopy: a new tool for accurate and absolute diffusion measurements. Chemphyschem 8: 433-443.
49. Hofmann H, Soranno A, Borgia A, Gast K, Nettels D, et al. (2012) Polymer scaling laws of unfolded and intrinsically disordered proteins quantified with single-molecule spectroscopy. Proc Natl Acad Sci U S A 109: 16155-16160.

Figure legends

Figure 1. The HIV-1 CA lattice and models of isolated lattice interface mimics. (A) Excerpt from the low-resolution structure of the hexagonal HIV-1 CA lattice derived from planar two-

dimensional CA crystals (pdb entry: 3DIK), illustrating the twofold (ellipses), threefold (triangles) and sixfold (hexagons) symmetric lattice interfaces. (B) The threefold symmetric lattice interface is composed of six CA subunits: Three of them meet via their CTDs (orange) and the other three via their NTDs (dark green). (C) Models of isolated CA oligomers extracted from the HIV-1 CA lattice structure: The NTD-trimeric and the CTD-trimeric CAs are represented in dark/pale green and red/orange, respectively. The already known monomeric, wild-type dimeric and hexameric HIV-1 CAs are represented in gray.

Figure 2. High-resolution model of the trimeric lattice interface formed by the HIV-1 CA NTDs. The high-resolution structure of the HIV-1 CA NTD (cyan, pdb entry: 1AK4) was superimposed onto the cryoEM-based coordinate model of the planar HIV-1 CA lattice (pdb entry: 3DIK). Residues that appeared in close proximity between the NTDs at the threefold lattice interface were identified for mutagenesis to cysteines. (A&B) Side-view of two NTDs in the threefold lattice interface. (C&D) Top-view onto the threefold lattice interface formed by the CA NTDs. (A&C) Residues that appear in close proximity are colored in magenta and are located along alpha helix 4 and in the CypA binding loop of the CA NTD. (B&D) Measured interdomain-distances between cysteines (blue) introduced into the alpha helix 4 and the CypA binding loop. (E) The trifunctional maleimide TMEA with 10.3 Å spacer arms was used for chemical cross-linking of engineered cysteine residues.

Figure 3. Cross-linking of CA assemblies from engineered NTD-trimer interface mutants. In-vitro assembled HIV-1 CA cysteine mutants were chemically cross-linked by short incubations with equimolar amounts of TMEA. The soluble and assembled reaction products separated by centrifugation and analysed by SDS-PAGE. (A) Reaction products before centrifugation. (B) Supernatants after centrifugation corresponding to the soluble un-assembled CA fraction. (C) Pellets after centrifugation, containing assembled CA.

Figure 4. Biophysical characterization of NTD- and CTD-linked CA trimers. (A&B) Negative-stained EM of the in-vitro assembled (R82C/E180D/V181A) HIV-1 CA mutant after TMEA cross-linking (A) and oxidized assemblies of the (E180D/V181A/P207C/T216C) HIV-1 CA mutant (B). (C&D) Size exclusion chromatographic profiles of the isolated NTD-linked (R82C/E180D/V181A) (C) and the isolated CTD-linked (E180D/V181A/P207C/T216C) CA trimers (D). Elution volumes of protein standards are indicated on top. (E&F) ESI-MS spectra of the purified TMEA cross-linked (R82C/E180D/V181A) NTD-trimer (E) and the oxidized (E180D/V181A/P207C/T216C) CTD-trimer (F). (G&H) Sedimentation velocity analytical ultracentrifugation of the (R82C/E180D/V181A) NTD-trimer (G) and the oxidized (E180D/V181A/P207C/T216C) CTD-trimer (H).

Figure 5. Determination of CA-binding affinities by Microscale Thermophoresis (MST). Kinetic fitting of the binding curves measured for TRIM B30.2 domains and engineered oligomeric HIV-1 CA constructs at 7 °C. Fitting of the binding data of rhesus TRIM5α B30.2 with the wild-type dimeric HIV-1 CA (K_D = 327.4 μM) (A), the incompletely TMEA-linked dimeric (R82C/E180D/V181A) HIV-1 CA, obtained as a side-product from the NTD-trimer purification (K_D = 275.5 μM) (B), the hexameric HIV-1 CA (K_D = 258.4 μM) (C) and the Lysozyme control (K_D = 2588 μM) (D) are shown. (E) Comparison of rhesus TRIM5, human TRIM5 and human TRIM20 B30.2 domains binding to wild-type HIV-1 CA. (F) Comparison of rhesus TRIM5 binding to different HIV-1 CA constructs and the Lysozyme control.

Figures

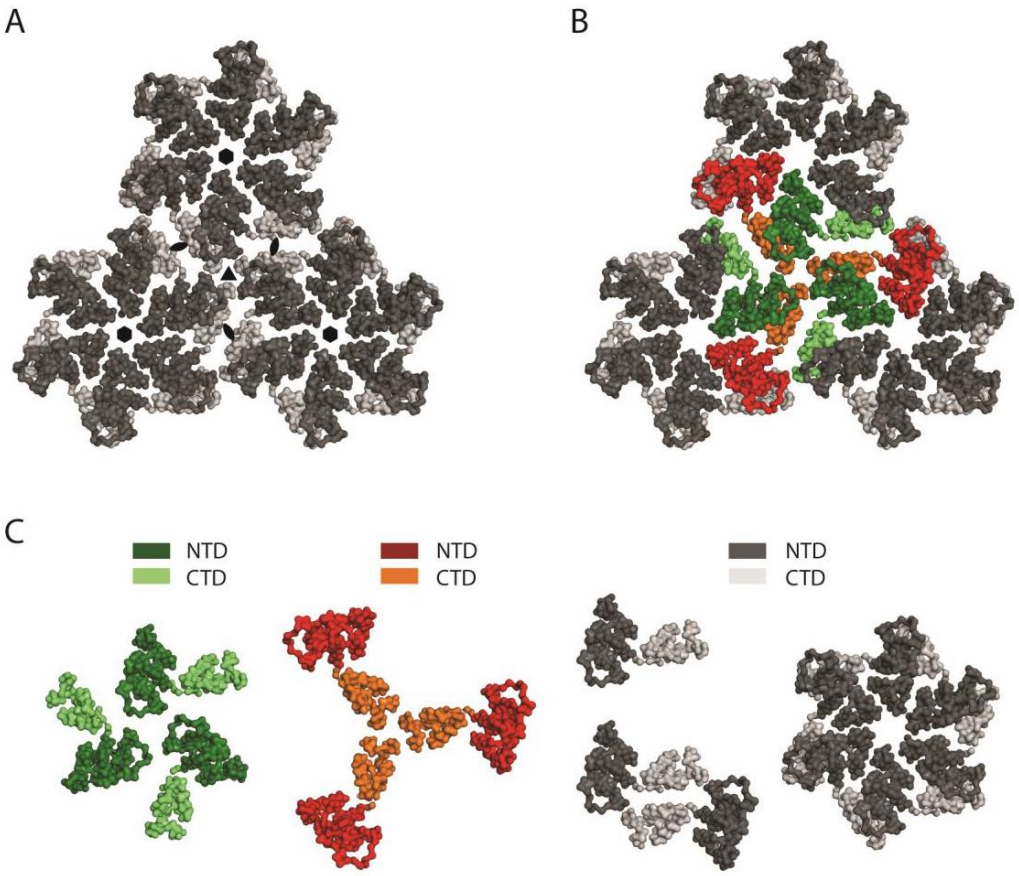

Figure 1

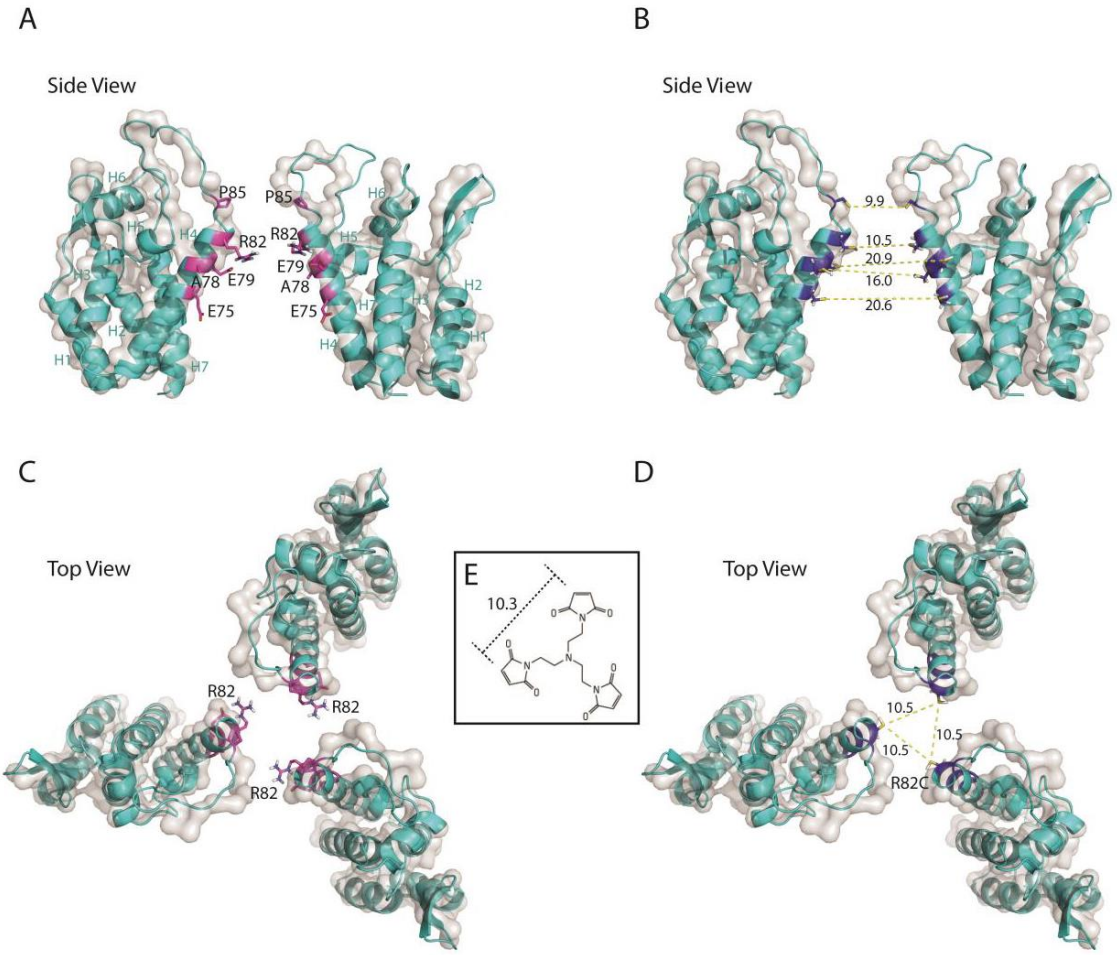
A
Side View
P85
R82
E79
A78
E75
H6
H5
H4
H3
H2
H1
H7
B
Side View
9.9
10.5
20.9
16.0
20.6
C
Top View
R82
D
Top View
10.5
10.5
10.5
R82
E
10.3

1

2 **Figure 2**

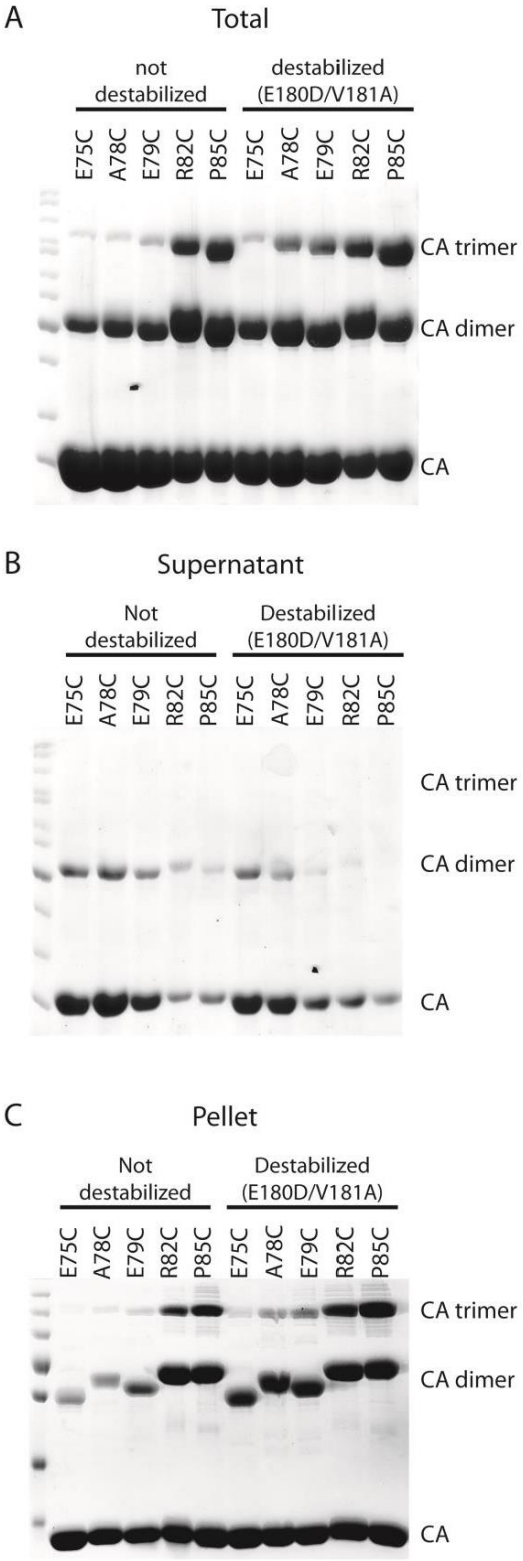
A
Total
not destabilized
destabilized (E180D/V181A)
E75C
A78C
E79C
R82C
P85C
E75C
A78C
E79C
R82C
P85C
CA trimer
CA dimer
CA
B
Supernatant
Not destabilized
Destabilized (E180D/V181A)
E75C
A78C
E79C
R82C
P85C
E75C
A78C
E79C
R82C
P85C
CA trimer
CA dimer
CA
C
Pellet
Not destabilized
Destabilized (E180D/V181A)
E75C
A78C
E79C
R82C
P85C
E75C
A78C
E79C
R82C
P85C
CA trimer
CA dimer
CA

1

2 **Figure 3**

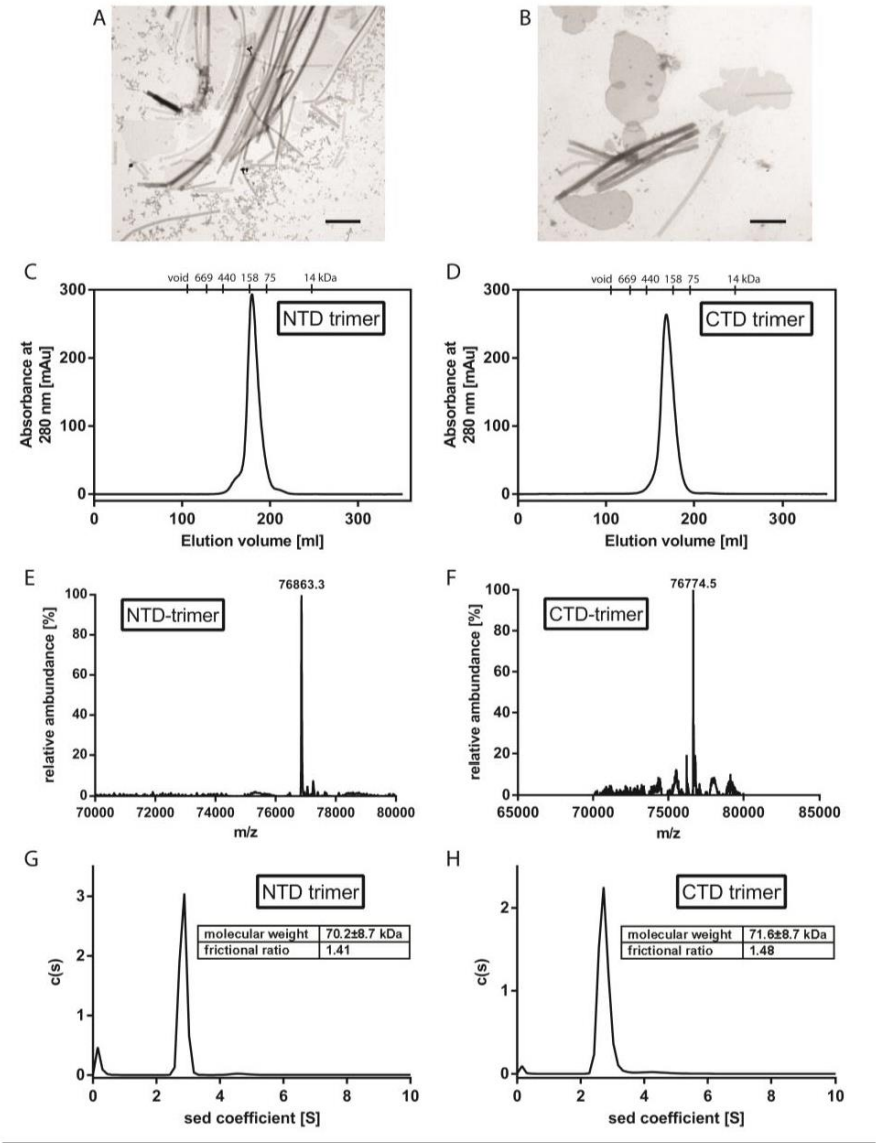
A
B
C
void 669 440 158 75 14 kDa
NTD trimer
Absorbance at 280 nm [mAu]
Elution volume [ml]
D
void 669 440 158 75 14 kDa
CTD trimer
Absorbance at 280 nm [mAu]
Elution volume [ml]
E
76863.3
NTD-trimer
relative ambundance [%]
m/z
F
76774.5
CTD-trimer
relative ambundance [%]
m/z
G
NTD trimer
molecular weight 70.2±8.7 kDa
frictional ratio 1.41
c(s)
sed coefficient [S]
H
CTD trimer
molecular weight 71.6±8.7 kDa
frictional ratio 1.48
c(s)
sed coefficient [S]

Figure 4

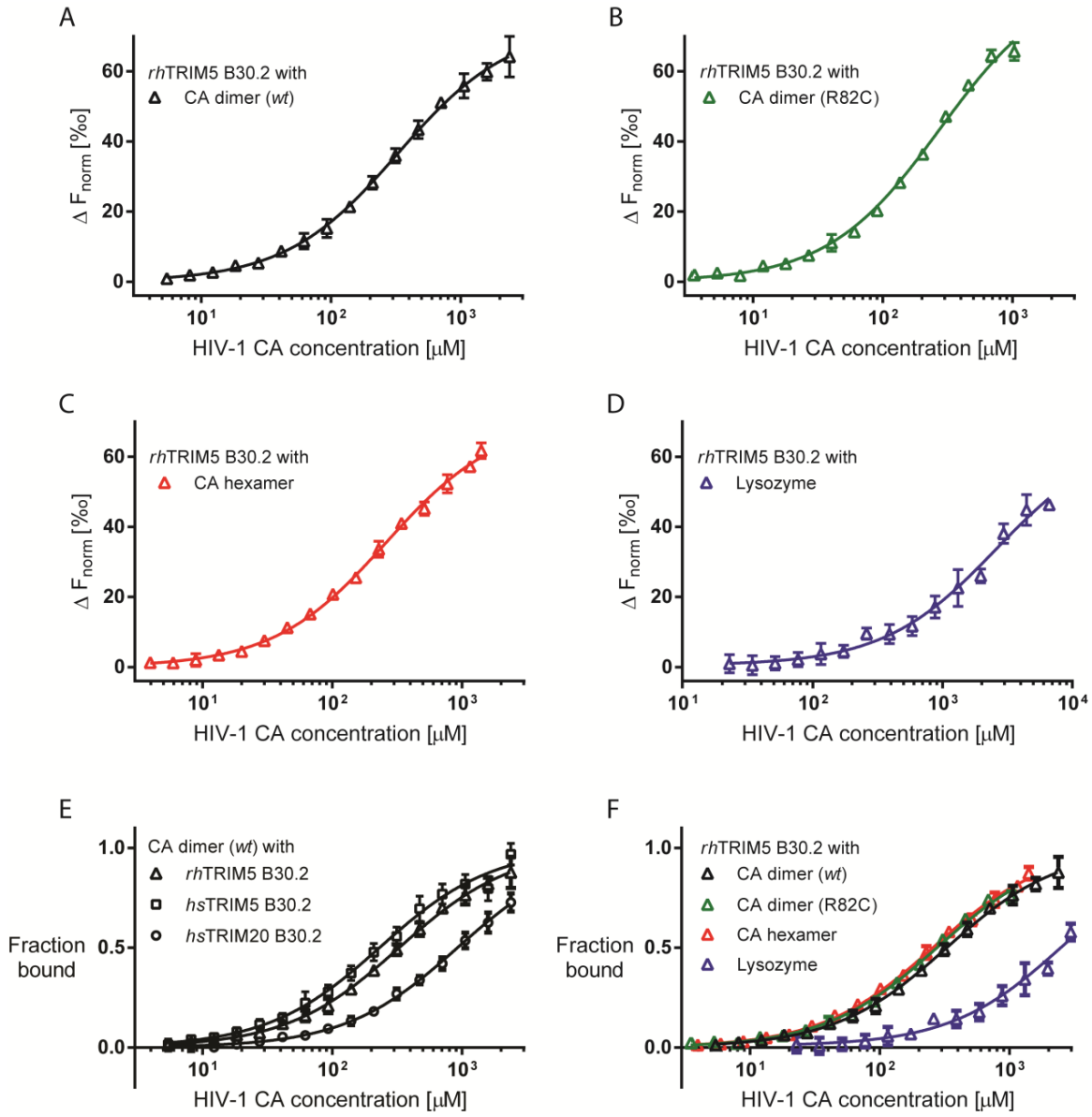
A
rhTRIM5 B30.2 with
CA dimer (wt)
Δ F norm [‰]
HIV-1 CA concentration [μM]
B
rhTRIM5 B30.2 with
CA dimer (R82C)
C
rhTRIM5 B30.2 with
CA hexamer
D
rhTRIM5 B30.2 with
Lysozyme
E
CA dimer (wt) with
rhTRIM5 B30.2
hsTRIM5 B30.2
hsTRIM20 B30.2
Fraction bound
F
rhTRIM5 B30.2 with
CA dimer (wt)
CA dimer (R82C)
CA hexamer
Lysozyme

Figure 5

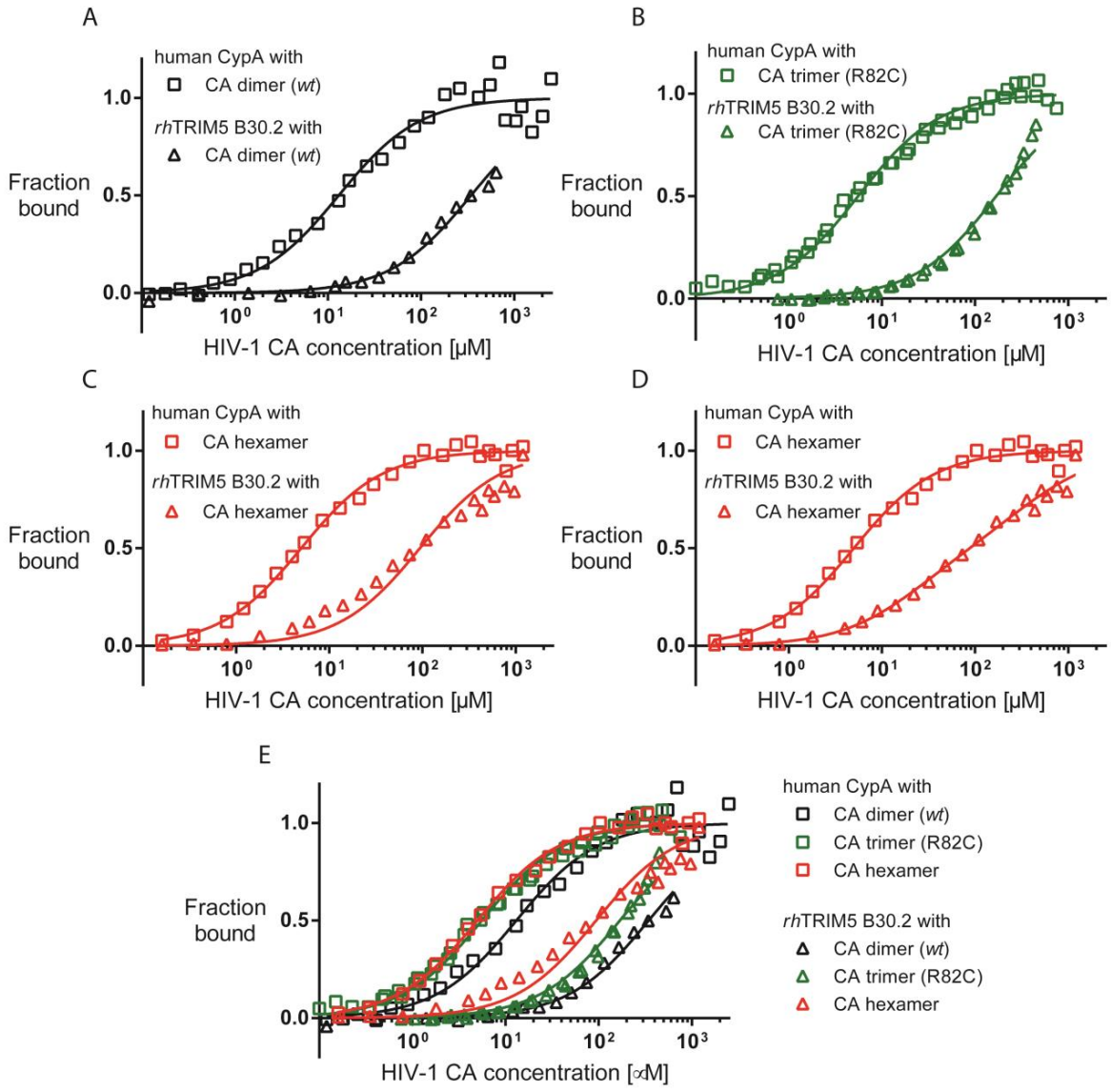
A
human CypA with
CA dimer (wt)
rhTRIM5 B30.2 with
CA dimer (wt)
Fraction bound
HIV-1 CA concentration [μM]
B
human CypA with
CA trimer (R82C)
rhTRIM5 B30.2 with
CA trimer (R82C)
Fraction bound
HIV-1 CA concentration [μM]
C
human CypA with
CA hexamer
rhTRIM5 B30.2 with
CA hexamer
Fraction bound
HIV-1 CA concentration [μM]
D
human CypA with
CA hexamer
rhTRIM5 B30.2 with
CA hexamer
Fraction bound
HIV-1 CA concentration [μM]
E
Fraction bound
HIV-1 CA concentration [∝M]
human CypA with
CA dimer (wt)
CA trimer (R82C)
CA hexamer
rhTRIM5 B30.2 with
CA dimer (wt)
CA trimer (R82C)
CA hexamer

Figure 6

Tables

CA domain cross-linked	Destabilizing mutations in the CTD	Mutants
NTD	-	E75C
NTD	-	A78C
NTD	-	E79C
NTD	-	R82C
NTD	-	P85C
NTD	W184A/P185A	E75C/W184A/P185A
NTD	W184A/P185A	A78C/W184A/P185A
NTD	W184A/P185A	E79C/W184A/P185A
NTD	W184A/P185A	R82C/W184A/P185A
NTD	W184A/P185A	P85C/W184A/P185A
NTD	E180D/V181A	E75C/E180D/V181A
NTD	E180D/V181A	A78C/E180D/V181A
NTD	E180D/V181A	E79C/E180D/V181A
NTD	E180D/V181A	R82C/E180D/V181A
NTD	E180D/V181A	P85C/E180D/V181A
CTD	-	P207C/T216C
CTD	W184A/P185A	W184A/P185A/P207C/T216C
CTD	E180D/V181A	E180D/V181A/P207C/T216C

Table 1

1

	Rhesus TRIM5α B30.2			Human TRIM5α B30.2			Human TRIM20 B30.2		
	MST w jump	MST w/o jump	FCS	MST w jump	MST w/o jump	FCS	MST w jump	MST w/o jump	FCS
CA dimer (wt)	327.4 ± 16	312.4 ± 19	343.7 ± 14.4	232.6 ± 17		-	922.4 ± 57		-
CA dimer (R82C/E180D/V181A)	275.5 ± 12		-	243.2 ± 12		-	-	-	-
CA trimer (R82C/E180D/V181A)	-	-	168.8 ± 6.3	-	-	-	-	-	-
CA trimer (E180D/V181A/P207C/T216C)	-	-	-	-	-	-	-	-	-
CA 6mer (A14C/E45C/W184A/M185A)	258.4 ± 11		93.8 ± 9.3	195.5 ± 12		-	-	-	-
Lysozyme	2588 ± 357		-	14036 ± 6420		-	-	-	-

2 **Table 2**

3

Supplementary figures

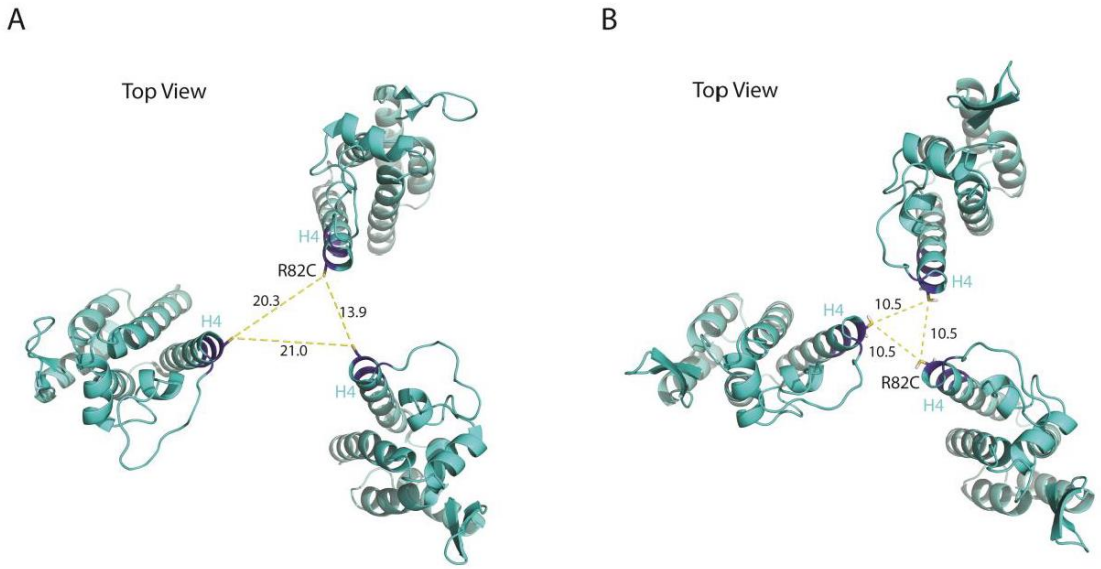

Figure S 1

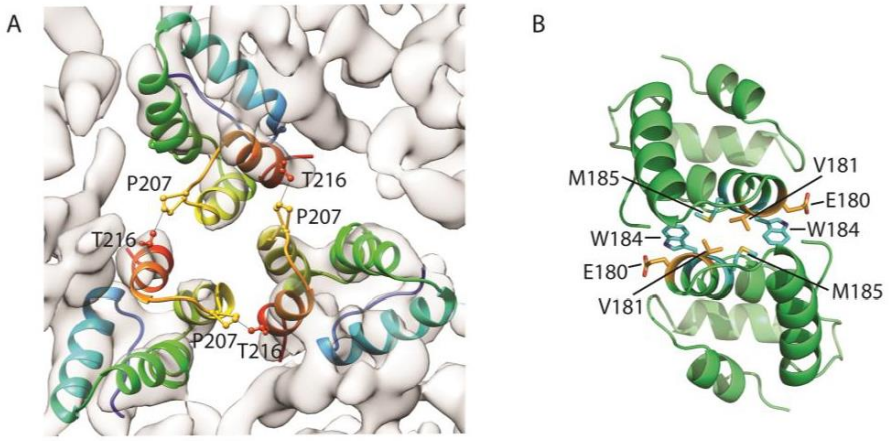

Figure S 2

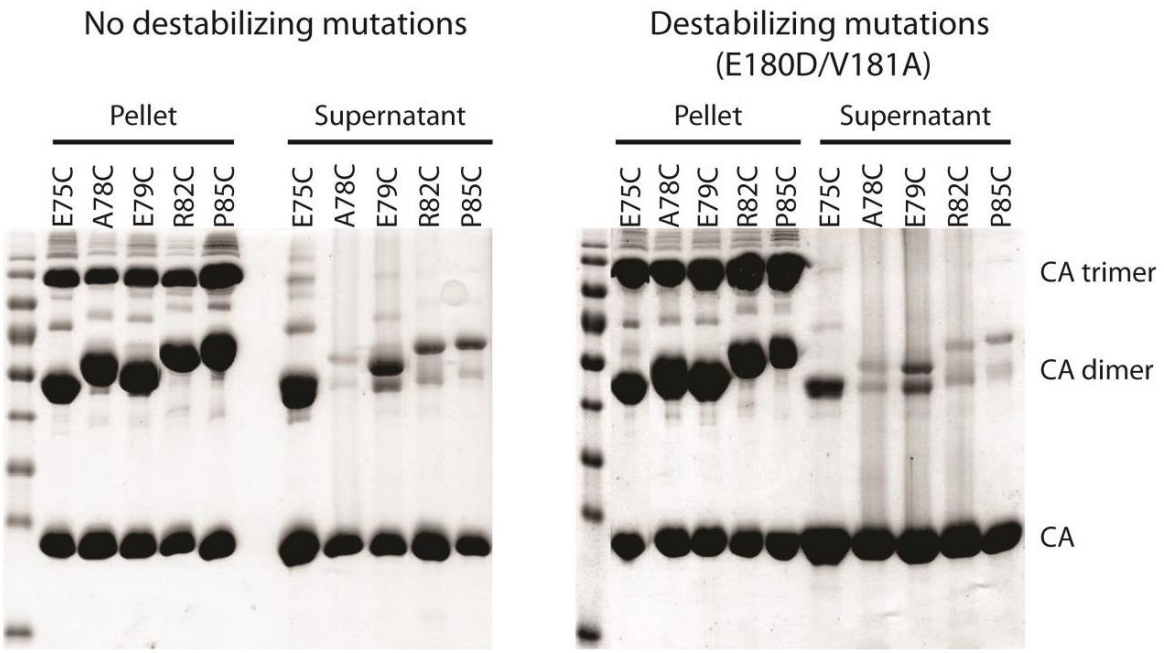

1

2 **Figure S 3**

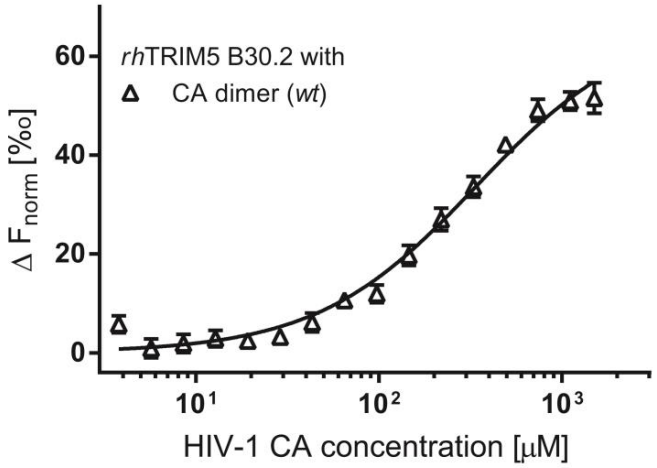

3

4 **Figure S 4**
5

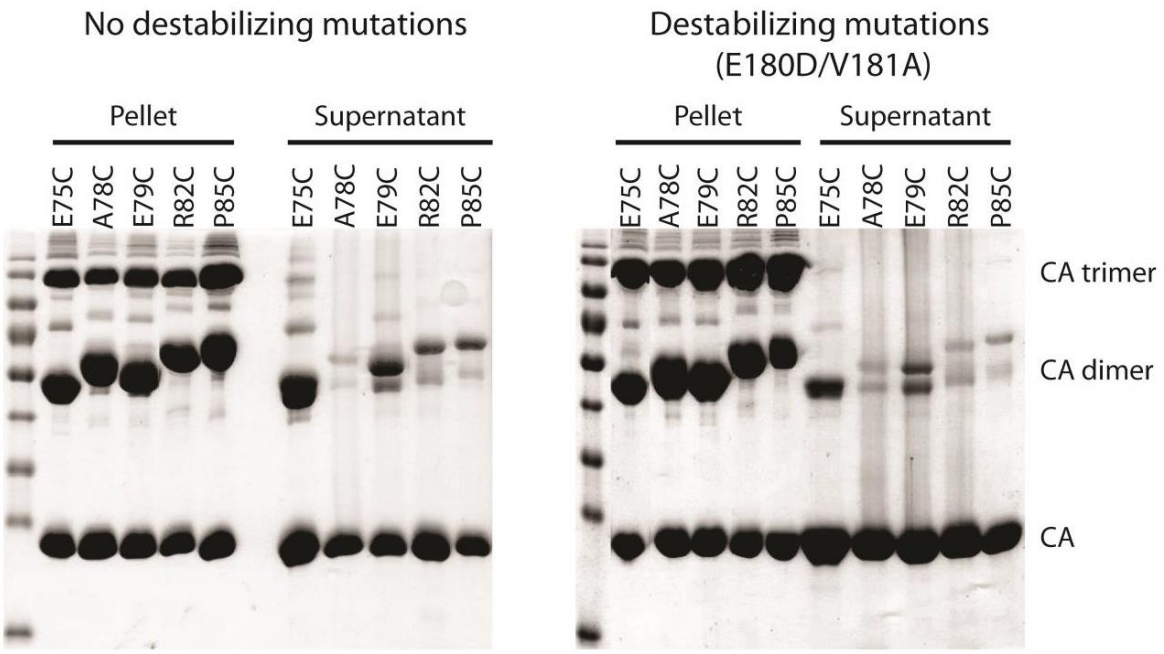

1

2 **Figure S 3**

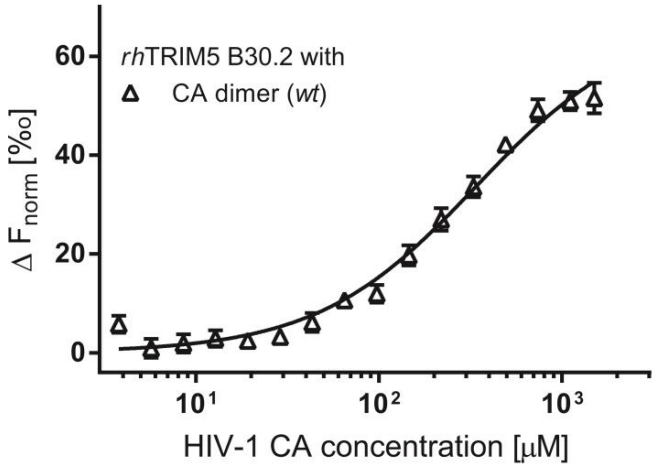

3

4 **Figure S 4**
5

2.3 Manuscript: Overall architecture and mode of dimerization of TRIM proteins revealed by the TRIM20 structure

Overall architecture and mode of dimerization of TRIM proteins revealed by the TRIM20 structure

Christopher Weinert[1], Damien Morger[1], Aleksandra Djekic[1], Peer R E Mittl[1] and Markus G Grütter[1,2]

[1] Department of Biochemistry, University of Zurich, Winterthurerstrasse 190, CH-8057 Zürich, Switzerland [2] to whom correspondence should be addressed: gruetter@bioc.uzh.ch, Tel. +41-44-6355580, Fax. +41-44-6356834

Submitted to Proceedings of the National Academy of Sciences of the United States of America

Tripartite motif-containing (TRIM) proteins comprise a RING finger, a B-Box, a predicted coiled coil here termed central helical scaffold (CHS) domain and in most cases a C-terminal B30.2 domain. So far the overall architecture of TRIM proteins is unknown since only structures of individual domains are available. Here we present the 2.4 Å crystal structure of a functional portion of TRIM20 consisting of the CHS and B30.2 domains. In contrast to the previously assumed parallel arrangement, two CHS domains arrange in antiparallel manner thereby forming elongated dimers with centrally positioned B30.2 domains and B-Boxes placed distal 170 Å apart. Interdimeric contacts between B30.2 and CHS domains construct a yet unknown TRIM tetramer and unveil the mechanism of higher order self assembly. Together with the full length model, our data provides unprecedented insights into the structural and functional modularity of these proteins.

TRIM20 | pyrin | pro-IL-1β | TRIM | coiled coil

“”

Introduction

Tripartite motif-containing (TRIM) proteins represent a large family of proteins comprising approximately 100 human members, linked to diverse cellular functions including regulation of the innate immune system, retroviral restriction, cell proliferation and differentiation (1, 2). They share a conserved domain architecture consisting of an N-terminal RING domain, one or two B-Box domains followed by a predicted coiled coil motif here called central helical scaffold (CHS) domain (3). The RING and B-Box domains are zinc fingers that confer E3-ligase activity and protein-protein interactions to form higher order oligomers (HO), respectively (2, 4-6). The B-Box is followed by the CHS domain, which is responsible for low order oligomerization (3). C-terminal of the CHS domain about half of the TRIMs contain a B30.2 domain that mediates ligand binding (7-9).

TRIM20, also named pyrin, has an N-terminal pyrin domain (PYD) and a linker region of unknown structure, preceding a degenerated RING sequence (10). The PYD belongs to the death domain superfamily enabling homotypic interactions with other PYD containing proteins (11, 12). TRIM20 is involved in the modulation of the pro-inflammatory cytokine pro-Interleukin-1β (pro-IL-1β) and is associated to the auto-inflammatory disease Familial Mediterranean Fever (FMF) (13, 14). Through a direct interaction to pro-IL-1β, TRIM20 is considered to inhibit the inflammasome mediated maturation of the cytokine (15). However, TRIM20 can also potently induce the maturation of pro-IL-1β (6, 16-18). The exact mechanism of regulation between these two contrary functions is not known.

Several structures of isolated RING, B-Box and C-terminal domains of TRIM proteins are known to date (5, 19, 20). With respect to the TRIM tripartite motif (RING, B-Box and CHS domain), the CHS is the only domain where no structural information exists so far. This domain is of particular interest as it defines the spatial arrangement of the adjacent domains and thus the overall architecture of TRIM proteins.

Within the CHS sequence a coiled coil (CC) motif and an L2 linker to the B30.2 domain is predicted (21). The CC motif is prognosticated within the first 100-120 amino acids C-terminal of the B-Box and the adjacent L2 linker is between 50 to 70 amino acids in length (22). For the retroviral restriction factor TRIM5α and the intracellular Fc-receptor TRIM21, the CHS domain is responsible for dimerization (23-25). This formation of low order oligomers is essential for function as in both TRIM20 and TRIM5α a deletion of the CHS results in a monomeric and inactive protein (6, 26). However, dimerization does not seem to be the only function of the CHS. In addition, residues have been identified in the CHS domain of TRIM5α that do not interfere with dimerization, but lead to a loss of restriction (27).

Here we present the crystal structure of a functional part of TRIM proteins, the TRIM20 CHS-B30.2 C-terminal portion, providing insight into the overall structure of TRIM proteins. Using small angle X-ray scattering (SAXS) we revealed the flexibility between the CHS and the B30.2 domains mediated by a short hinge. In addition, we characterized the binding of the CHS-B30.2 fragment to pro-IL-1β *in vitro*.

Results

Crystal Structure of TRIM20Δ413. To investigate the mode of oligomerization and the relative arrangement of the B30.2 domain in TRIM proteins we designed a construct that comprises the CHS and the B30.2 domains. Secondary structure prediction for TRIM20 suggests that the bipartite CC motif of the CHS starts shortly after the B-Box domain (Fig. S1). We therefore engineered a construct that starts with the conserved glutamate 414 yielding a fragment called TRIM20Δ413 (Fig. 1*A*). Analytical

Significance

TRIM proteins are involved in various processes that include regulation of the innate immune response. Despite their functional diversity they share a common domain architecture. A striking feature is their ability to form higher order self-assemblies that in case of TRIM5 creates a hexagonal lattice. However, due to the lack of high resolution structures, the connectivity of the domains as well as a precise model of higher order assemblies remained unknown. We present the first crystal structure of a functional TRIM20 C-terminal fragment that reveals the antiparallel mode of dimerization as well as how two dimers form a tetramer. The presented structure not only allows modeling a full length TRIM protein, but also a precise model of a TRIM lattice.

Reserved for Publication Footnotes

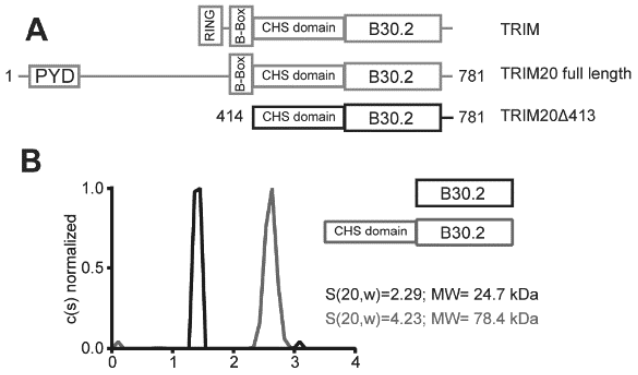

Fig. 1. Central position of the CHS domain in TRIM proteins and its importance in dimerization. (*A*) Schematic representation of the domains of TRIM proteins comprising a RING, B-Box, and CHS domain. In the literature the CHS domain is referred to as coiled coiled domain with a L2 linker that connects to the C-terminal B30.2 domain. TRIM20 is a RING-less TRIM member and has a long N-terminal insertion composed of a PYD domain and a long linker region. For crystallization a construct starting at position 414 was designed. (*B*) Sedimentation velocity analytical ultracentrifugation of the B30.2 domain and the CHS-B30.2 fragment of TRIM20 show a monomer and a dimer, respectively. The calculated monomeric masses are 23.305 kDa and 42.737 kDa for the B30.2 domain and the TRIM20Δ413 construct, respectively.

ultracentrifugation at 4 °C shows that this C-terminal fragment is a dimer in solution (Fig. 1*B*).

TRIM20Δ413 crystallized in space group $P2_1$ with 3 dimers in the asymmetric unit (Table S1 and Fig. S2*A*). The protein has an elongated structure formed by the CHS dimer (E414-N586) that is connected to the globular B30.2 domains (E589-G776) through a short hinge region (Fig. 2*A*).

The monomeric CHS domain folds into 4 helices (α1-α4). The first α-helix that harbors the predicted CC motif consists of 106 residues (E414-E520) and spans a length of approximately 155 Å (Fig. 2*A*). The designated L2 linker consists of two short helices α2 and α3 (E524-T539) followed by an 11 amino acid extended stretch and helix α4 (N551-Q586). A short linker of 2 amino acids (V587 and P588) connects the C-terminus of α4 to the B30.2 domain. The extended stretch and α4 are oriented antiparallel to the helix α1 whereas helix α2 and α3 are in the peripheral turn forming a hairpin.

The two protomers arrange in an antiparallel fashion along helix α1 with a shared interface of over 4700 Å^2 that is created by all four helices including the extended stretch. As a result, the adjacent domains are distinctly placed where the N-termini of both monomers and consequently also the B-Box domains are positioned 167 Å apart from each other, while the B30.2 domains are in proximity close to the central 2-fold axis of the dimer.

The predicted two CC regions localize on the N- and C-terminal part of helix α1 that due to the antiparallel dimerization structurally align and form a 2-helical coiled coil (2-CC; Fig. 2*B*). In case of TRIM20, residues L427 and L430 coil with residues L513' and L516' (the prime indicates residues from the other protomer). Additionally, an antiparallel 3-helical coiled coil is formed between residues in α1, α4, and α1' (L484, V487, and V491; L560, and I557, I553; L458', T455' and F451', Fig. 2B). Whereas the residues involved in the 2-CC are highly conserved in TRIM proteins, the 3-CC seems to be TRIM20 specific as these residues show no sequence conservation (Fig. S1). Nevertheless, compared to the length of helix α-1 and the size of the entire CHS domain, the CC character of the fold, i.e. the supercoiling of the helices, is small. In addition, the predicted CC motif and the designated L2 linker form one helical domain that is centrally located in TRIM proteins and provides the molecular scaffold for the placement of the adjacent domains (Fig. 2*A* and *C*). Therefore, we suggest the term CHS domain.

In the central core around the 2-fold axis, helices α1 and α4 of both subunits form an antiparallel four helix bundle. This bundle is slightly bent, which leads to a curvature of the entire CHS domain, reminiscent of a coat hanger. Due to the crystal packing, the overall curvature found in the three dimers of the asymmetric unit varies (Fig. S2*B*). The changes in the curvature appear in the bundle while the rest remains identical suggesting the bundle of the CHS domain to be a flexible structural element.

The B30.2 domain, connected through a short linker, point upwards along the 2-fold axis of the dimer, just like the hook on the coat hanger. Its orientation relative to the CHS domain differs slightly in the six monomers suggesting a certain degree of flexibility for the linker by acting as a hinge (Fig. S2*C*). The lack of interactions between the CHS and B30.2 domain within a dimer supports the assumption of a flexible connectivity between the two domains.

An interesting feature of the X-ray structure is the crystal contact between two neighboring dimers. Two B30.2 domains, one of each dimer, interact with the extended stretch between α3 and α4 of the CHS domain of the other dimer and share an additional small interface via their N-terminal helices (Fig. 3*A*). The interface formed between the B30.2 and CHS domains is formed by hydrogen bonds whereas the interaction between the two B30.2 domains involves hydrophobic residues (Fig. 3*B*). Papin et al. have shown by *in-vivo* co-immunoprecipitation experiments that the isolated B30.2 domain can interact with an isolated B-Box-CHS construct (15). They suggested a model, in which TRIM20 can be present in an open and a closed conformation. In the latter the B30.2 domain binds intramolecular to the B-Box-CHS segment. The presented crystal contact could resemble this intramolecular epitope. In this case the B30.2 domain would have to rotate 180° compared to the conformation found in the crystal structure to bind to its own extended stretch.

Another consequence of the binding of the B30.2 domain to the CHS could be the formation of TRIM20 tetramers as found in the crystal structure.

Solution structure of TRIM20Δ413. The dimeric TRIM20Δ413 forms HOs in solution, which can be observed by an increasing radius of gyration (R_G) in a concentration dependent manner revealed by SAXS measurements (Fig. S3*A* and *B*, Table S2). The R_G for an infinitely diluted sample is 4.15 nm, which is in perfect agreement with the calculated R_G using the dimeric crystal structure (4.29 nm; Fig. S3*C*). However, the crystal structure does not fit perfectly to the experimental data (χ^2=3.62) in the scattering range s (nm^{-1})=0.8-1.8 (Fig. 4*A* and *B*). Because the Kratky plot suggests an interdomain flexibility (Fig. S3*D*), we generated a rigid body model by introducing flexibility between the CHS and the B30.2 domains, which significantly improves the fit to the experimentally determined scattering profile (χ^2=2.01). In the obtained model, one of the two B30.2 domains is arranged as in the crystal structure whereas the second B30.2 domain is rotated perpendicular to the dimeric 2-fold axis placing it sideways the CHS domain (Fig. 4*A* and *C*). Fitting an ensemble of structures to the scattering data resulted in the best agreement (χ^2=1.31) and reveals the conformational space available for the B30.2 domain (Fig. 4*A*, *D* and *E*). The conformation seen in the crystal structure defines one populated state but in solution the B30.2 domains are also positioned sideways the CHS domain thereby increasing the possible radius for an interaction of the B30.2 domain with its ligand. In the crystal structure the distance between the B30.2 center of masses is about 47 Å. Movement of the B30.2 domain sideways can increase the distance by almost 2-fold (85 Å). Notably, a conformation of the B30.2 domain that would resemble an intramolecular binding to the extended stretch of

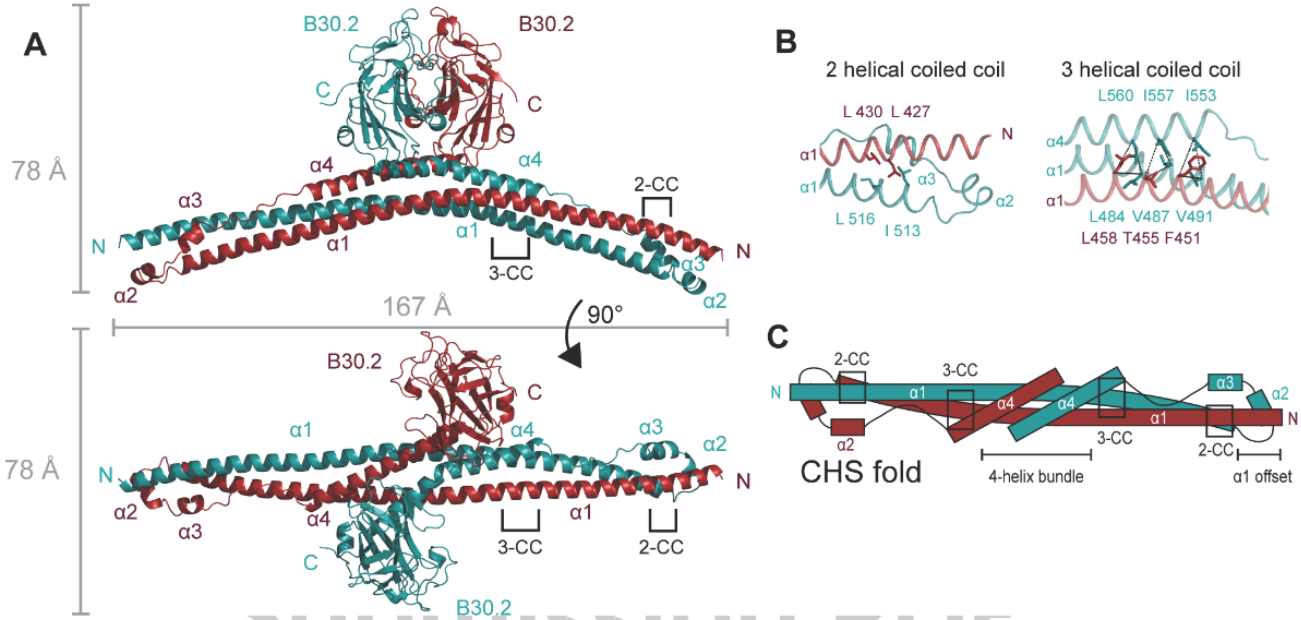

Fig. 2. Crystal structure of TRIM20Δ413. The crystal structure of one of the three dimers (chain A and B) in the asymmetric unit is presented. The chains of monomer A and B are colored in blue and red, respectively. The helices of each CHS monomer are numbered α-1 to α-4. The parts of the CHS domain that show a 2 helical (2-CC) or 3 helical coiled coil (3-CC) are indicated and depicted in more detail in *B*. (*A*) The dimer is shown from a side and a top view and its dimensions indicated. (*B*) Residues involved in the 2-CC (top) and 3-CC (bottom) are shown as sticks and labeled in the corresponding color of the helix. (*C*) Topology of the CHS domain including its structural motifs are shown schematically.

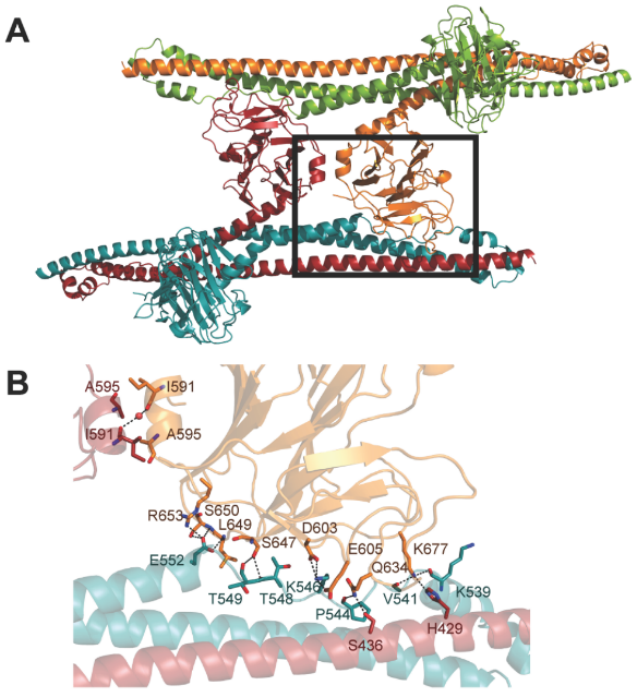

Fig. 3. Tetramer interface. (*A*) The crystal contact between two dimers is shown in a cartoon representation. Chain A and B are colored as in Fig. 2. The second dimer made of chain C and D is colored in orange and green, respectively. The black box indicates the display detail shown in *B*. (*B*) Detailed view of half of the tetramer interface. Residues involved in the interface are depicted in sticks and hydrogen bonds are indicated by black dashed lines. The coordinated water between the B30.2 domains is shows as a red sphere.

the CHS domain has not been observed in any model obtained from the SAXS data.

A flexibility of the CHS domain, as it is suggested by the differences in curvature of the three dimers in the crystal structure, was not modeled. Nevertheless, conformational flexibility of the CHS domain is also suggested from SAXS data as the average diameter found in solution is around 160 Å, which is a little less than in the crystal structure (173 Å).

Binding to pro-IL-1β. To elucidate the TRIM20Δ413 functionality, we investigated the reported binding to pro-IL-1β (15). Co-immunoprecipitation experiments revealed a direct interaction *in-vitro* between the purified proteins. The interaction required the presence of both the CHS and B30.2 domain as the individual domains could not be precipitated with pro-IL-1β (Fig. 5*A*). Surface Plasmon Resonance (SPR) experiments between TRIM20Δ413 and pro-IL-1β revealed a heterogeneous ligand behavior of TRIM20, suggesting that it is present in two states with measured affinities of 0.70 μM and 13.7 μM (Table S3 and Fig. S4*A*). A complex formation of the TRIM20Δ413 and pro-IL-1β in solution was detected by size exclusion chromatography (SEC). Stable complex formation however was only observed after incubating the proteins at room temperature whereas no complex was observed after incubation at 4 °C (Fig. 5*B* and Fig. S4*B*). The complex shows a large peak shift towards lower retention volumes corresponding to a molecular weight of approximately 400 kDa. This suggests a complex of more than one TRIM20Δ413 dimer (85.7 kDa) binding two pro-IL-1β (31.9 kDa) molecules but rather a higher oligomeric species. Longer incubation times yield the complex to form even higher oligomers. Nevertheless, the complex formation is reversible, as equilibrium between the individual proteins and the complex is observed upon reinjection (Fig.S4*C*). Incubation of TRIM20Δ413 or pro-IL-1β alone does not show signs of higher oligomerization upon incubation at room temperature (Fig. 5*C*). The formation of an apparent higher oligomeric complex in solution could explain the heterogeneous ligand behavior of TRIM20 in the SPR experiments, where presumably the dimer binds with a low affinity, and oligomers of the

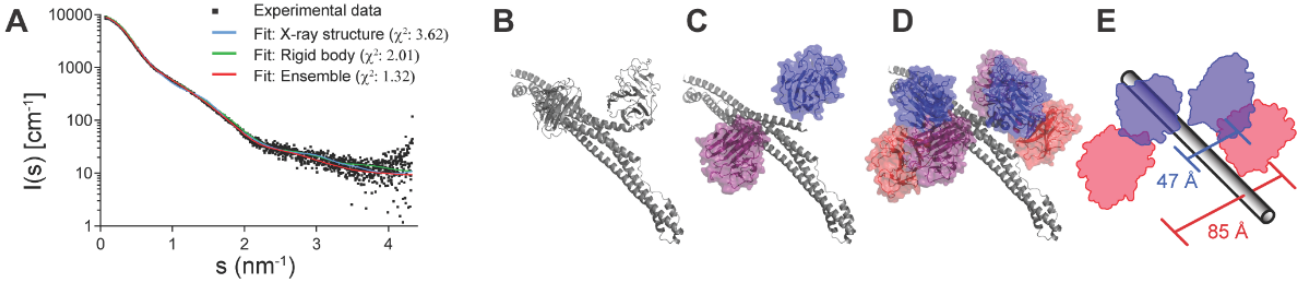

Fig. 4. Solution structure of TRIM20Δ413. (*A*) Data extrapolated to infinite dilution is shown together with the fits of the crystal structure, rigid body modeling and ensemble optimization method with the indicated χ^2 values. (*B*) The crystal structure is shown in a cartoon representation next to the (*C*) rigid body model, (*D*) three representatives of the ensemble fit, and a (*E*) schematic illustration of the distance between the B30.2 domains found in the crystal structure and the widest arrangement found in the ensemble. The orientation found to be most similar to the crystal structure is shown in a blue surface representation. Other orientations of the B30.2 domain found in the rigid body and ensemble fit are colored violet and red.

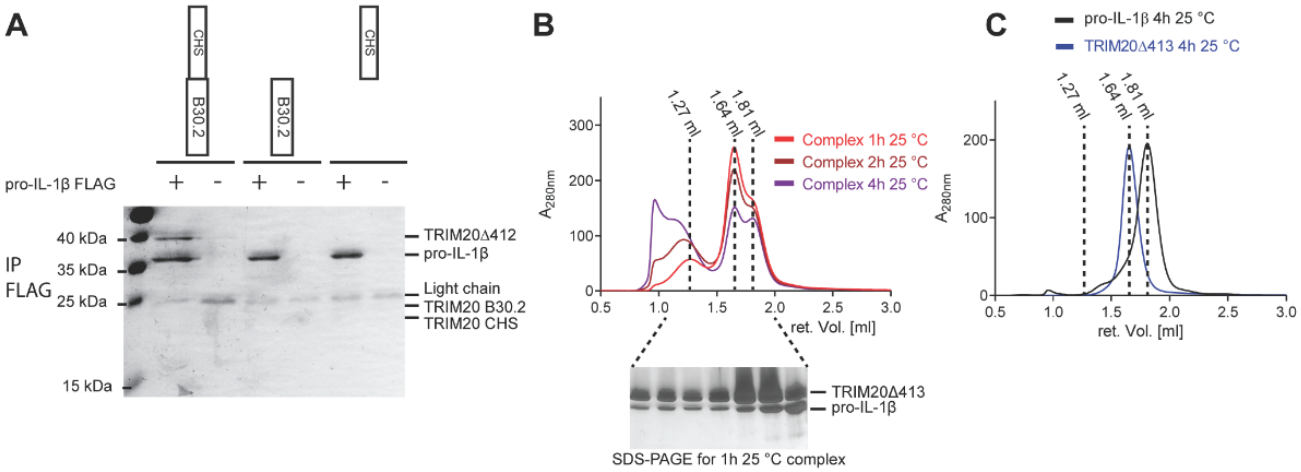

Fig. 5. Interaction between TRIM20 and pro-IL-1β. (A) 10 µM the indicated TRIM20 constructs were incubated with 10 µg FLAG-tagged pro-IL-1β in a total volume on 100 µl. Complex was co-immunoprecipitated using ANTI-FLAG® M2 Affinity Gel (Sigma-Aldrich) and subjected to SDS-PAGE analysis. (B) TRIM20Δ413 and pro-IL-1β were incubated as indicated and their SEC elution profiles shown with the corresponding retention volumes of 1.27 ml, 1.64 ml, and 1.81 ml for the complex after 1 h, TRIM20Δ413 and pro-IL-1β, respectively. Co-elution of both proteins in the appearing complex peak was verified by SDS-PAGE of the indicated fractions. (C) Elution profiles of the individual proteins incubated for 4h at 25 °C show no signs of peak shifts.

dimer (e.g. tetramer) have a significantly increased affinity to pro-IL-1β.

TRIM20Δ413 itself forms HOs as seen in SAXS experiments, however, they are presumably not stable enough to be detected by SEC. An interaction to pro-IL-1β seems to bind and stabilize TRIM20 HOs. A similar behavior of stabilized HOs upon ligand binding has been reported for TRIM5α when binding to the HIV-1 capsid lattice (28).

Stereotype TRIM model. Between the N-terminal PYD domain and the CHS domain, TRIM20 has a 318 amino acid region of mostly unknown structure, which makes a prediction of the TRIM20 full length structure impossible. However, the TRIM20Δ413 structure reveals around 75% of a TRIM full length molecule missing only the N-terminal RING and B-Box domains (Fig. 1*A*). A linkage between the B-Box and the CHS domain can be observed in the NMR structure of the TRIM29 B-Box domain as its C-terminal eight residues form an α-helix that aligns with α1 residues of the TRIM20 CHS domain (Fig. S5*A*) (29). As B-Box and RING domains share a common fold (30), a template for the connectivity between RING and B-Box domain is given by TRIM18 tandem B-Box (B-Box1/2) structure. It features an interaction surface between the two adjacent B-Box domains and based on the hypothesis that there is an equivalent RING/B-Box interface, this TRIM18 B-Box1/2 structure was used to generate a RING/B-Box model that was annealed to the CHS domain structure via the proposed domain linkage of TRIM29 (Fig. 6*A* and Fig. S5*B*). The overall model illustrates convincingly that the entire TRIM protein structure is dominated by the CHS domain which not only acts as the dimerization domain but also as a framework for the other domains.

Discussion

TRIM proteins share a common domain architecture, of which structures of isolated domains have been determined. Due to the lack of structural information on the relative spatial arrangement of the domains in a full length TRIM context, detailed molecular mechanisms for ligand binding, self-assembly and signal transduction remained elusive.

Here, the first high resolution structure of a TRIM CHS-B30.2 fragment at 2.4 Å resolution is presented. The predicted CC of the tripartite motif and the designated L2 linker to the B30.2 domain form one domain that we termed CHS domain. The elongated and helical CHS domain dimerizes over a large interface in an antiparallel fashion creating a coat hanger like structure and reveals the overall architecture of TRIM proteins. Furthermore, a crystal contact between two dimers provides a structural template for a B30.2 domain dependent formation of HOs.

The necessity for dimerization for correct function has been shown for several TRIM proteins. In TRIM20, a deletion of the CHS domain leads to a monomeric and inactive protein (6). The same is true for the TRIM20 homologue TRIM5α,

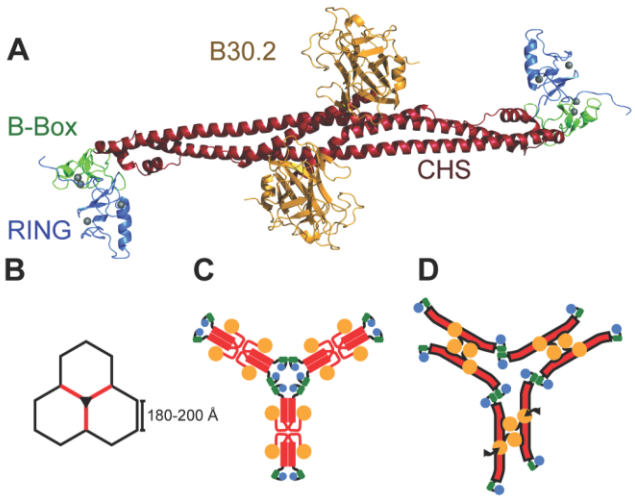

Fig. 6. Models of TRIM full length and lattice formation. (*A*) The modeled TRIM full length structure is shown in a cartoon representation with the B30.2 domain, CHS, B-Box2, and RING domain colored in orange, red, green, and blue, respectively. The coordinated Zn^{2+} atoms are shown in grey spheres. (*B*) Schematic drawing showing the dimensions of the reported hexagonal lattice formed by a TRIM21/TRIM5α chimera (28). Part of the lattice that is shown in detail in *D-E* is indicated in red with the central 3-fold axis depicted by the black triangle. (*C*) The currently proposed model suggests parallel arranged TRIM dimers that form tetramers via a L2/L2 contact. The tetramers assemble via B-Box/B-Box interactions into the hexagonal lattice. (*D*) Lattice formation using the B30.2 dependent tetramer as observed in the TRIM20 crystal. The revealed flexibility of the B30.2 domains is indicated by the arrows.

for which extensive mutational studies of the CHS domain have revealed insights into the precise contribution of this domain to the protein's function. The fact that the CHS domain of TRIM20 can be functionally exchanged with the corresponding region of TRIM5α suggests a structural conservation and allows comparison (6). Rhesus TRIM5α that potently restricts HIV-1 by binding to the capsid surface of the virion core, self-assembles into HOs (31). This oligomerization is dependent on the RING, B-Box as well as the CHS domain. Whereas dimerization is mediated by the CHS domain, the B-Box is thought to connect two dimers through a B-Box/B-Box interaction (4). However, several residues in the CHS domain of TRIM5α have been identified that are crucial for HO association and retroviral restriction activity regardless of dimerization (21, 27, 32). Based on these findings a CHS/CHS interaction was proposed to contribute to the self-assembly.

The CHS-B30.2 structure of TRIM20 provides a model to understand the structure function behavior of the CHS domain in TRIM proteins. Using this crystal structure as a model, two features are mediated by the CHS domain that are beyond dimerization, namely acting as a elongated scaffold domain and mediating tetramerization by a new mechanism.

As the B-Box directly precedes the α1 helix of the CHS domain without an appreciable linker, the peripheral edge of the CHS domain is a critical factor for the correct orientation of the B-Box. This region is created by the N- and C-terminus of the α1 and α1' helix, respectively, and by helix α2 and α3. Sequence comparison between several TRIM proteins shows that residues of these structural elements are conserved and mutations in the α2 helix of TRIM5α have been shown to interfere with the ability of the protein to self-assemble (Fig. S1; (32)). The TRIM20 structure suggests that this effect is due to alterations in the relative positioning of the B-Box relative to the CHS domain. From the modeled stereotype TRIM protein, even a direct interaction between the α2 helix and the B-Box domain can be imagined (Fig. 6*A*).

The 3-dimensional shape of a TRIM self-assembly has been shown by Ganser-Pornillos and colleagues (28). They have revealed that a TRIM21-TRIM5α chimera spontaneously forms hexagonal lattices with a length between 180 and 205 Å of each hexagonal side (Fig. 6*B*). Together with the modeled RING finger and B-Box domain the elongated CHS fold is roughly 200 Å in diameter. This reveals that the elongated fold of the CHS is providing the dimensions for a putative TRIM lattice and one could assume a single dimer to be sufficient to match the length of the hexagonal lattice. However, this leads to only 3 B-Box domains at each hexagon edge due to the antiparallel dimer arrangement. As the B-Box connects two dimers via a complementary surface, it introduces a two-fold symmetry (4). Therefore having only three B-Box domains connecting three dimers imposes a symmetry problem. Based on the suggested CHS/CHS interaction, Ganser-Pornillos and colleagues have proposed that each side of the hexagonal lattice is made of a tetramer, placing six B-Box domains at each hexagon edge (Fig. 6*C*). The structure determined here also implies the formation of tetramers, however with a different contribution of its domains. Instead of the proposed CHS/CHS interaction that connects two neighboring dimers, the tetramer is formed by the CHS/B30.2 interaction (Fig. 3*B* and Fig. 6*D*). This suggests a new mechanism for TRIM lattice formation where all symmetry axis' arising from oligomerization are parallel to each other and perpendicular to the created surface. As a consequence, all B30.2 domains are presented to the same side of the lattice, an essential feature missing in the previously suggested model. Our model is further supported by the observation that TRIM21-TRIM5α lattice formation was less efficient and less ordered, when the B30.2 domain was deleted (28). However, the general ability to form a lattice was retained. Remarkably, mutations of residues in TRIM5α that align with the extended stretch of the CHS domain cause a loss of restriction capability (27). Those TRIM5α mutants were stable dimers, but unable to form cytoplasmic bodies. As this stretch is distant from the outer conserved edge, one can assume that such mutations do not interfere with correct arrangement and connectivity to the B-Box and but rather lead to the inability to bind to the B30.2 domain of another dimer.

The ability of TRIM20Δ413 to form higher oligomers in solution was seen in the SAXS experiments. Our data on the TRIM20Δ413/pro-IL-1β interaction also supports the physiological relevance of higher oligomers as the complex formed between the two proteins indicates an oligomerization of TRIM20Δ413 dimers. Additionally, SPR experiments suggest two states for TRIM20 with different affinities to pro-IL-1β that could be explained by a dimer binding with low affinity (13.7 μM) and a higher oligomer binding more affine (0.7 μM). The binding of pro-IL-1β to TRIM20 is thought to inhibit the caspase-1 dependent maturation of the cytokine. This inhibition might be disrupted in case of FMF mutations (15). Interestingly, several FMF associated residues are located within the tetramer interface, these include I591, A595, L649 and R653 (33). Mutations could lower the affinity of dimers to assemble into tetramers, therefore preventing TRIM20 to effectively bind pro-IL-1β and inhibit its maturation. Mutational studies have to address the particular role of TRIM20 HO's and the involved tetramer interface in the binding to pro-IL-1β and the putative inhibition of is maturation.

As the designated L2 linker is fully structured and forms together with the CC motif the CHS domain, the flexible connection to the B30.2 domain is only mediated by a short hinge region that allows the B30.2 domain to adopt different orientations relative to the CHS domain. Together with the flexibility of the CHS domain, this feature adds to the structural and functional flexibility of TRIM proteins. For instance, various antibody coated surfaces, such as bacteria, non-coated viruses or latex beads are recognized by the intracellular Fc-receptor TRIM21 and induce downstream

signaling (34). TRIM5α can adapt to different capsid curvatures and restricts various retroviruses. The presented structure reveals how TRIM proteins can adopt their modular structure to adapt to differently presented ligands.

When comparing different TRIM proteins in sequence N-terminal of the B30.2 domain, namely the extended stretch and helix α4, it is noteworthy that conservation in length and sequence identity is low (Fig. S1). For instance, TRIM27 has a similar length of the α4 helix as TRIM20, while TRIM5α, 21 and 22 are shorter in sequence. This suggests that helix α4 and the extended stretch act as a ruler to specifically define the position the B30.2 domains, accommodating for ligand specificity of TRIM proteins.

Overall, the TRIM20Δ413 structure fits very well to the functional data on TRIM5α with respect to the overall architecture and the domain contributions for lattice formation. As the ability to form HOs has also been shown for other TRIM proteins suggests that higher order self-assembly or even lattice formation could be a common feature of TRIM proteins, where a tetramer as presented is the general building block[3,34]. However, it has to be shown if TRIM20 also associates into HO in a B-Box dependent manner. An alternative could be that TRIM20 forms HO purely via presented tetramer interface, as this is suggested by the interactions studies with pro-IL-1β.

Experimental Procedure

Cloning, expression and purification, SAXS experiments, Co-IP experiment, surface Plasmon resonance analysis, size exclusion experiments and model building are described in the *SI Methods*.

Crystallisation and structure determination

First crystals were found in 0.1 M Tris-AcOH, pH 8-8.5, 0.2-0.4% (w/v) Cystamine, 0.2 M $LiSO_4$, 8% (w/v) PEG 20'000, 8% (w/v) PEG 550 MME using sitting drop vapor diffusion at 20 °C. TRIM20Δ413 (7.5 mg/ml) was mixed in a 1:1 ratio with mother liquor. The obtained crystals were used for micro-seeding in 0.1 M Tris-AcOH, pH 7.4-8.0, 0.26% (w/v) Cystamine, 0.2 M $LiSO_4$, 8% (w/v) PEG 20'000, 8% (w/v) PEG 550 MME using sitting drop vapor diffusion at 20 °C. The protein sample was concentrated to 5 mg/ml and mixed in a 1:1 ratio. Crystals grew within 24 h and were fished within 18 days. Prior to flash freezing in liquid nitrogen, crystals were soaked in the mother liquor supplemented with 20% (v/v) ethylene glycol. A native data set of a TRIM20Δ413 crystal was recorded at the X06SA beam line of the Swiss Light Source (Paul-Scherrer Institut, Villigen, Switzerland). The protein crystallized in $P2_1$ with 6 molecules in the asymmetric unit forming 3 dimers. Data was indexed, integrated and scaled with XDS(35) to a resolution of 2.4 Å. Molecular replacement was done with Phaser (36) using the B30.2 domain of TRIM20 as search model (pdb entry: 2WL1). Model building and manual fitting was done in Coot (37). Refinement was performed with Phenix (38). In the final model, 98% of all residues are in the favored ramachandran area and no outliers. The accession code is 4cg4.

Acknowledgements.

We would like to thank the late Prof. J. Tschopp (University of Lausanne, Switzerland) for providing us with the DNA for the *MEFV* gene. We also thank Beat Blattmann and Celine Stutz-Ducommun of the NCCR crystallization facility and the staff of the Swiss Light Source (PSI, Villigen, Switzerland). Thilo Schroeder provided us the plasmid for pro-IL-1β. Stefan Schauer and Manfred Rössle are thanked for the support in surface plasmon resonance and SAXS experiments, respectively. Andreas Flütsch is thanked for carefully reviewing the manuscript. CW was participant of the Biomolecular Structure and Function PhD program of the NCCR Structural Biology. This work was financially supported by a Swiss National Science Foundation grant (No. 31-1022181 to M.G.G.).

1. Han K, Lou DI, & Sawyer SL (2011) Identification of a genomic reservoir for new TRIM genes in primate genomes. *PLoS Genet* 7(12):e1002388.
2. Ozato K, Shin DM, Chang TH, & Morse HC, 3rd (2008) TRIM family proteins and their emerging roles in innate immunity. *Nat Rev Immunol* 8(11):849-860.
3. Reymond A, *et al.* (2001) The tripartite motif family identifies cell compartments. *Embo J* 20(9):2140-2151.
4. Diaz-Griffero F, *et al.* (2009) A B-box 2 surface patch important for TRIM5alpha self-association, capsid binding avidity, and retrovirus restriction. *J Virol* 83(20):10737-10751.
5. Mrosek M, *et al.* (2008) Structural analysis of B-Box2 from MuRF1: identification of a novel self-association pattern in a RING-like fold. *Biochemistry* 47(40):10722-10730.
6. Yu JW, *et al.* (2007) Pyrin activates the ASC pyroptosome in response to engagement by autoinflammatory PSTPIP1 mutants. *Mol Cell* 28(2):214-227.
7. Grutter C, *et al.* (2006) Structure of the PRYSPRY-domain: implications for autoinflammatory diseases. *FEBS Lett* 580(1):99-106.
8. Rhodes DA & Trowsdale J (2007) TRIM21 is a trimeric protein that binds IgG Fc via the B30.2 domain. *Mol Immunol* 44(9):2406-2414.
9. Stremlau M, Perron M, Welikala S, & Sodroski J (2005) Species-specific variation in the B30.2(SPRY) domain of TRIM5alpha determines the potency of human immunodeficiency virus restriction. *J Virol* 79(5):3139-3145.
10. Chae JJ, Aksentijevich I, & Kastner DL (2009) Advances in the understanding of familial Mediterranean fever and possibilities for targeted therapy. *Br J Haematol* 146(5):467-478.
11. Martinon F, Hofmann K, & Tschopp J (2001) The pyrin domain: a possible member of the death domain-fold family implicated in apoptosis and inflammation. *Curr Biol* 11(4):R118-120.
12. Kohl A & Grutter MG (2004) Fire and death: the pyrin domain joins the death-domain superfamily. *C R Biol* 327(12):1077-1086.
13. Anonymous (1997) A candidate gene for familial Mediterranean fever. *Nat Genet* 17(1):25-31.
14. Anonymous (1997) Ancient missense mutations in a new member of the RoRet gene family are likely to cause familial Mediterranean fever. The International FMF Consortium. *Cell* 90(4):797-807.
15. Papin S, *et al.* (2007) The SPRY domain of Pyrin, mutated in familial Mediterranean fever patients, interacts with inflammasome components and inhibits proIL-1beta processing. *Cell Death Differ* 14(8):1457-1466.
16. Yu JW, *et al.* (2006) Cryopyrin and pyrin activate caspase-1, but not NF-kappaB, via ASC oligomerization. *Cell Death Differ* 13(2):236-249.
17. Gavrilin MA, *et al.* (2012) Activation of the pyrin inflammasome by intracellular Burkholderia cenocepacia. *J Immunol* 188(7):3469-3477.
18. Yu JW, Farias A, Hwang I, Fernandes-Alnemri T, & Alnemri ES (2013) Ribotoxic Stress through p38 Mitogen-activated Protein Kinase Activates in Vitro the Human Pyrin Inflammasome. *J Biol Chem* 288(16):11378-11383.
19. Roa A, *et al.* (2012) RING domain mutations uncouple TRIM5alpha restriction of HIV-1 from inhibition of reverse transcription and acceleration of uncoating. *J Virol* 86(3):1717-1727.
20. Perfetto L, *et al.* (2013) Exploring the diversity of SPRY/B30.2-mediated interactions. *Trends Biochem Sci* 38(1):38-46.
21. Javanbakht H, *et al.* (2006) Characterization of TRIM5alpha trimerization and its contribution to human immunodeficiency virus capsid binding. *Virology* 353(1):234-246.
22. Sardiello M, Cairo S, Fontanella B, Ballabio A, & Meroni G (2008) Genomic analysis of the TRIM family reveals two groups of genes with distinct evolutionary properties. *BMC Evol Biol* 8:225.
23. Langelier CR, *et al.* (2008) Biochemical characterization of a recombinant TRIM5alpha protein that restricts human immunodeficiency virus type 1 replication. *J Virol* 82(23):11682-11694.
24. Mallery DL, *et al.* (2010) Antibodies mediate intracellular immunity through tripartite motif-containing 21 (TRIM21). *Proc Natl Acad Sci U S A* 107(46):19985-19990.
25. Pertel T, *et al.* (2011) TRIM5 is an innate immune sensor for the retrovirus capsid lattice. *Nature* 472(7343):361-365.
26. Stremlau M, *et al.* (2006) Specific recognition and accelerated uncoating of retroviral capsids by the TRIM5alpha restriction factor. *Proc Natl Acad Sci U S A* 103(14):5514-5519.
27. Sastri J, *et al.* (2010) Identification of residues within the L2 region of rhesus TRIM5alpha that are required for retroviral restriction and cytoplasmic body localization. *Virology* 405(1):259-266.
28. Ganser-Pornillos BK, *et al.* (2011) Hexagonal assembly of a restricting TRIM5alpha protein. *Proc Natl Acad Sci U S A* 108(2):534-539.
29. Tao H, *et al.* (2008) Structure of the MID1 tandem B-boxes reveals an interaction reminiscent of intermolecular ring heterodimers. *Biochemistry* 47(8):2450-2457.
30. Lienlaf M, *et al.* (2011) Contribution of E3-ubiquitin ligase activity to HIV-1 restriction by TRIM5alpha(rh): structure of the RING domain of TRIM5alpha. *J Virol* 85(17):8725-8737.
31. Sebastian S & Luban J (2005) TRIM5alpha selectively binds a restriction-sensitive retroviral capsid. *Retrovirology* 2:40.
32. Li X, Yeung DF, Fiegen AM, & Sodroski J (2011) Determinants of the higher order association of the restriction factor TRIM5alpha and other tripartite motif (TRIM) proteins. *J Biol Chem* 286(32):27959-27970.
33. Milhavet F, *et al.* (2008) The infevers autoinflammatory mutation online registry: update with new genes and functions. *Hum Mutat* 29(6):803-808.
34. McEwan WA, *et al.* (2013) Intracellular antibody-bound pathogens stimulate immune signaling via the Fc receptor TRIM21. *Nat Immunol* 14(4):327-336.
35. Kabsch W (2010) Xds. *Acta Crystallogr D Biol Crystallogr* 66(Pt 2):125-132.
36. McCoy AJ, *et al.* (2007) Phaser crystallographic software. *J Appl Crystallogr* 40(Pt 4):658-674.
37. Emsley P, Lohkamp B, Scott WG, & Cowtan K (2010) Features and development of Coot. *Acta Crystallogr D Biol Crystallogr* 66(Pt 4):486-501.
38. Adams PD, *et al.* (2010) PHENIX: a comprehensive Python-based system for macromolecular structure solution. *Acta Crystallogr D Biol Crystallogr* 66(Pt 2):213-221.

Supporting Information

SI Methods

Construction of Expression Plasmids

The multiple cloning site 1 (MCS1) of the transfer vector pFBDM (1) was modified to enable fragment exchange (FX) cloning (2). The *Sap*I restriction site between the transposon element Tn7R and the Col-E1 origin of replication was removed using Quikchange mutagenesis (Invitrogen). A *Nde*I restriction site was inserted into the MCS1 by Quikchange. The FX-cassette of the pBXC3H vector (2) was used as template (incl. coding region for C-terminal His_{10}-tag and 3C cleavage site) and cloned into the modified pFBDM vector using *Nde*I and *Xba*I restriction sites yielding a pFX3CH vector. The *Nde*I restriction site was later removed. All TRIM20 constructs were cloned into the pFX3CH template vector. Primers and coding regions are stated in Table S4.

A similar procedure as for pFX3CH was applied to modify a pET28 (Novagen) vector. The *Sap*I site near the BR322 origin of replication was removed with Quikchange. The FX-cassette of pBXH3C (incl. coding region for N-terminal His_{10}-tag and 3C-cleavage site) was inserted using the *NdeI* and *XhoI* restriction yielding a pET28-FXH3C vector. Pro-IL-1β (codon optimized for *E.coli* expression) was cloned into the pET28-FXH3C vector using primers as stated in Table S4.

Expression and Purification

All TRIM constructs were expressed in *Sf*9 cells using the manufactures protocol (Invitrogen). Cells were harvested after 48-72 h expression at 27 °C. *Sf*9 cells expressing TRIM20Δ413 were lysed in lysis buffer (50 mM Tris-HCl, pH 8, 300 mM NaCl, 20 mM imidazole, DNAse I, RNase I, Benzoase, and EDTA-free complete inhibitor cocktail (Roche Diagnostics)) using an Emulsi-

Flex C3 homogenizer (Avestin, Canada). Cell debris was centrifuged (1 h, 4 °C, 20'000 rpm) and supernatant applied to Protino Ni-NTA agarose (Machery Nagel). His-tag was cleaved by His-3C Protease, the sample dialysed in 50 mM Tris-HCl, pH 8, 150 mM NaCl, 10 mM imidazole, 0.5 mM TCEP, and reapplied to Ni-NTA agarose. Cleaved TRIM20Δ413 was dialyzed in low salt buffer (20 mM Tris-HCl, pH 8, 50 mM NaCl, 0.5 mM TCEP) and applied on a RESOURCE Q anion exchange column (GE Healthcare). The protein was eluted with 7.5% high salt buffer (20 mM Tris-HCl, pH 8, 1 M NaCl, 0.5 mM TCEP) and dialysed in 20 mM Tris-HCl, pH 8, 100 mM NaCl, 0.5 mM TCEP. The protein could be stored at 4 °C for up to two weeks, or it was frozen in liquid nitrogen and stored at -80 °C until further use.

All other TRIM constructs were lysed using 0.5% CHAPS in lysis buffer, and purified as described above. After His-tag removal the proteins were applied on a Superdex 200 (10/300 GL; GE Healthcare; 50 mM Tris-HCl, pH 8, 150 mM NaCl, 0.5 mM TCEP). Proteins were frozen in liquid nitrogen after addition of glycerol to a final concentration of 8.7% (v/v). For TRIM20-CHS 300 mM NaCl was used throughout the purification.

Pro-IL-1β was expressed in *E.coli* BL21 (DE3) strain. Cells were grown in LB-media at 30 °C to an OD_{600nm} of 0.8, cooled down at 4°C for 30 min and expression induced with 0.1 mM IPTG (OD_{600nm} of 1.0). After 15 h expression at 18 °C, cells were harvested (4°C, 20 min, 4000 rpm) and lysed in 50 mM Tris-HCl, pH 8, 150 mM NaCl, 10 mM imidazole, DNAse I, RNase I, lysozyme, 0.5 mM PMSF, EDTA-free complete inhibitor cocktail (Roche Diagnostics) using an Emulsi-Flex C3 homogenizer (Avestin, Canada). Lysate was cleared and supernatant applied to Ni-NTA agarose. His-tag was cleaved by His-3C Protease, the sample dialysed in 50 mM Tris-HCl, pH 8, 50 mM NaCl, 0.25 mM TCEP) and reapplied to Ni-NTA agarose. As a final purification step the sample was applied on a Superdex 200 in 50 mM Tris-HCl, pH 8, 50 mM

NaCl, 0.5 mM TCEP). Fractions corresponding to monomeric pro-IL-1β were pooled and either used directly or frozen in liquid nitrogen after the addition of 8.7% glycerol and stored at -80 °C.

Co-IP experiments

10 µg of FLAG-pro-IL-1β were incubated with 10 µM TRIM20Δ412, TRIM20-B30.2 or TRIM20-CHS in a total volume of 100 µl (50 mM Tris-HCl, pH 7.4, 50 mM NaCl, 0.05% Tween 20). The mixture was incubated for 30 min at room temperature (RT) to allow complex formation. Putative complexes were co-immunoprecipitated using 20 µl ANTI-FLAG® M2 Affinity Gel (Sigma-Aldrich) for 10 min at RT. Beads were washed 3 times, and proteins eluted with 45 µl 2x SDS loading buffer. Eluted samples were analyzed by SDS-PAGE and visualized using silver staining (3).

Surface Plasmon Resonance

The interaction between TRIM20Δ412 and pro-IL-1β was measured on a ProteOn™ XPR 36 using a ProteOn™ GCL sensor chip (Bio Rad) equilibrated with running buffer (PBS, pH 7.5, 0.02% Tween 20). Monoclonal Anti-c-Myc IgG1 (20 µg/ml in 10 mM acetate, pH 5; Roche Diagnostics) was immobilized using amine coupling chemistry until the chip was saturated (6000-6400 RU). TRIM20Δ412 (1 µM) was applied to the immobilized antibody in running buffer and equilibrated until a stable baseline was reached (550-600 RU TRIM20Δ412; $\Delta RU <$ 0.2 RU/min). In total 5 lanes were immobilized with TRIM20Δ412. The sixth lane was coated with antibody only and used as a reference for unspecific binding. Single shot kinetic was applied using a two-fold dilution series of pro-IL-1β in running buffer (1.56, 3.125, 6.25, 12.5, 25 µM). For each lane two single shot experiments were performed. Data was double referenced against buffer and the antibody control lane. Binding affinity (K_D) was determined kinetically for each experiment using the heterogenous ligand model implemented in the ProteOn™-Software (Bio

Rad). The mean and standard deviation of the measured K_Ds was determined using GraphPad Prism6 (GraphPad Software).

Size exclusion chromatography analysis of complex formation

TRIM20Δ413 was mixed with freshly prepared pro-IL-1β. 3 mg of each protein were mixed and concentrated to a final concentration of 19 mg/ml. The buffer was exchanged to 20 mM Tris-HCl, pH 8, 100 mM NaCl, 0.5 mM TCEP while concentrating. Individual proteins were concentrated to 8 mg/ml and buffer was exchanged as for the complex. Samples were incubated for 1, 2 and 4 h at room temperature or 20 h at 4 °C, centrifuged (14'000 g, 10 min, 4 °C) and 5 µl injected onto a Superdex 200 (5/150 GL, GE Healthcare) in 20 mM Tris-HCl, pH 8, 100 mM NaCl, 0.5 mM TCEP at 4 °C. 50 µl fractions were collected, analyzed by SDS-PAGE and visualized using silver staining.

Small-angle X-ray scattering

SAXS data were collected at the Petra III (P62) beam line at the Deutsches Elektronen Synchroton (DESY), Hamburg. The incident wavelength was 1.24 Å. Data was recorded on a 2M Pilatus detector for the angular range of s between 0.0668-4.336 nm^{-1} ($s=4\pi \sin(\theta)/\lambda$, where 2θ is the diffraction angle and λ the wavelength of the incident beam). TRIM20Δ413 was measured at 10 °C in PBS and 5 mM DTT at several concentrations (1.7, 2.88, 4.6, 8.75, 13.3 mg/ml). Data was processed with PRIMUS (4) and a scattering curve extrapolated to infinite dilution was created using ALMERGE (5). The pair distribution function (P (r)) was calculated with GNOM (6). Radius of gyration R_G was estimated from the Guinier plot using PRIMUS and the P (r) function using GNOM. Rigid body modeling was carried out in CORAL(7) defining residues 586-590 as a flexible linker. Modeling various conformations simultaneously was performed with the ensemble optimization method (EOM; (8)) using residues 588-589 as flexible linker between the domains. Nine different conformations of the B30.2 domain relative to the CHS domain were

found by EOM analysis. Model with similar orientations of the B30.2 domain were combined in case their center of mass was within 6Å. Comparison with the crystal structure and the experimental scattering profile was done with CRYSOL(9).

Sequence alignment

Sequences used correspond to the UniProt entries O15553, Q9C035, P19474, Q8IYM9, P14373 for TRIM20, TRIM5α, TRIM21, TRIM22, TRIM27, respectively. Alignments were generated using T-coffee (10) and Jalview (11). Coiled coil predictions are taken from secondary structure predictions using Jpred 3 (12).

Modeling

The TRIM full-length model was generated using the MODELLER software (version 9.12) (13). Homology modeling was performed according to the Advanced Tutorial on the MODELLER homepage (http://salilab.org/modeller/tutorial/advanced.html) with a few modifications. The templates for the modeled RING and for the modeled B-Box were aligned separately using the SALIGN function and were subsequently merged manually to yield one multiple structure alignment for all the templates. TRIM5 RING (pdb entry 2ECV, residues 8-69 (14)) and B-Box1 of the TRIM18 tandem B-Boxes (pdb entry 2JUN, residues 114-173 (15)) served as templates for the modeled RING. TRIM5 B-Box (pdb entry 2YRG, residues 8-51 (16)), TRIM29 B-Box (pdb entry 2CSV, residues 16-63) and B-Box2 of the TRIM18 tandem B-Boxes (pdb entry 2JUN, residues 171-214) were taken as templates for the modeled B-Box. The target sequence, corresponding to residues 1-131 of human TRIM5α followed by residues 413-419 of TRIM20, was aligned to the pre-aligned template structures using the SALIGN function. To incorporate the zinc atoms into the modeling process, following lines were added to the alignment and modeling scripts: Env.io.atom_files_directory = ['.', '../atom_files'] and env.io.hetatm = True. The final multiple sequence alignment of template structures and target sequence is shown in

Supplementary Fig. 4. A tandem model of RING and BBox domains was built using the automodel class of MODELLER and structurally aligned onto the TRIM20Δ413 structure via the shared pyrin residues 413-419 yielding the TRIM full-length model.

Analytical ultracentrifugation

The B30.2 domain, expressed and purified as described (17), and TRIM20Δ413 were measured in PBS (pH 7.4) 10 mM β-Mercaptoethanol at a concentration of 0.6 mg/ml and 0.8 mg/ml, respectively. The sedimentation velocity measurements were carried out at 4°C on a ProteomeLab XL-1 (Beckman Coulter) ultracentrifuge at a speed of 30000 rpm. Data was analyzed with SEDFIT (18).

References

1. Berger I, Fitzgerald DJ, & Richmond TJ (2004) Baculovirus expression system for heterologous multiprotein complexes. *Nat Biotechnol* 22(12):1583-1587.
2. Geertsma ER & Dutzler R (2011) A versatile and efficient high-throughput cloning tool for structural biology. *Biochemistry* 50(15):3272-3278.
3. Nesterenko MV, Tilley M, & Upton SJ (1994) A simple modification of Blum's silver stain method allows for 30 minute detection of proteins in polyacrylamide gels. *J Biochem Biophys Methods* 28(3):239-242.
4. Konarev PV, Volkov VV, Sokolova AV, Koch MHJ, & Svergun DI (2003) PRIMUS: a Windows PC-based system for small-angle scattering data analysis. *J Appl Crystallogr* 36(5):1277-1282.
5. Franke D, Kikhney AG, & Svergun DI (2012) Automated acquisition and analysis of small angle X-ray scattering data. *Nuclear Instruments and Methods in Physics Research Section A: Accelerators, Spectrometers, Detectors and Associated Equipment* 689(0):52-59.
6. Svergun D (1992) Determination of the regularization parameter in indirect-transform methods using perceptual criteria. *J Appl Crystallogr* 25(4):495-503.
7. Petoukhov MV, *et al.* (2012) New developments in the ATSAS program package for small-angle scattering data analysis. *J Appl Crystallogr* 45(2):342-350.
8. Bernadó P, Mylonas E, Petoukhov MV, Blackledge M, & Svergun DI (2007) Structural Characterization of Flexible Proteins Using Small-Angle X-ray Scattering. *Journal of the American Chemical Society* 129(17):5656-5664.
9. Svergun D, Barberato C, & Koch MHJ (1995) CRYSOL– a Program to Evaluate X-ray Solution Scattering of Biological Macromolecules from Atomic Coordinates. *J Appl Crystallogr* 28(6):768-773.

10. Keller O, Kollmar M, Stanke M, & Waack S (2011) A novel hybrid gene prediction method employing protein multiple sequence alignments. *Bioinformatics* 27(6):757-763.
11. Waterhouse AM, Procter JB, Martin DM, Clamp M, & Barton GJ (2009) Jalview Version 2--a multiple sequence alignment editor and analysis workbench. *Bioinformatics* 25(9):1189-1191.
12. Cole C, Barber JD, & Barton GJ (2008) The Jpred 3 secondary structure prediction server. *Nucleic Acids Res* 36(Web Server issue):W197-201.
13. Eswar N, *et al.* (2007) Comparative protein structure modeling using MODELLER. *Curr Protoc Protein Sci* Chapter 2:Unit 2 9.
14. Lienlaf M, *et al.* (2011) Contribution of E3-ubiquitin ligase activity to HIV-1 restriction by TRIM5alpha(rh): structure of the RING domain of TRIM5alpha. *J Virol* 85(17):8725-8737.
15. Tao H, *et al.* (2008) Structure of the MID1 tandem B-boxes reveals an interaction reminiscent of intermolecular ring heterodimers. *Biochemistry* 47(8):2450-2457.
16. Diaz-Griffero F, *et al.* (2009) A B-box 2 surface patch important for TRIM5alpha self-association, capsid binding avidity, and retrovirus restriction. *J Virol* 83(20):10737-10751.
17. Weinert C, Grutter C, Roschitzki-Voser H, Mittl PR, & Grutter MG (2009) The crystal structure of human pyrin b30.2 domain: implications for mutations associated with familial Mediterranean fever. *J Mol Biol* 394(2):226-236.
18. Schuck P (2000) Size-distribution analysis of macromolecules by sedimentation velocity ultracentrifugation and lamm equation modeling. *Biophys J* 78(3):1606-1619.
19. Krissinel E & Henrick K (2004) Secondary-structure matching (SSM), a new tool for fast protein structure alignment in three dimensions. *Acta Crystallogr D Biol Crystallogr* 60(Pt 12 Pt 1):2256-2268.

Figure legends

Figure S1. Sequence alignment of the CHS domain of several TRIM20 homologues. Identical and similar residues are depicted by black and grey boxes, respectively. The predicted bipartite coiled coils for every TRIM are indicated by lines on top of the sequences and colored as indicated next to the protein names. The predicted L2 linker is marked by the grey line. Secondary structure elements as seen in the TRIM20 structure are indicated below the sequences. Residues that form the 2 helical coiled coil (2-CC) and 3 helical coil coiled (3-CC) are connected by black lines.

Figure S2. Different dimers in the asymmetric unit. Three dimers are found in the asymmetric unit (chains A&B, C&D, and E&F). For visualization only dimer of chain A&B and C&D were

used. (*A*) Superposition of the TRIM20 dimers are shown in a top and side view. The chains are colored in blue, red, orange and green for monomer A, B, C and D, respectively. (*B*) For a better visualization of the differences between the CHS monomers residues 486-560 of each monomer were superposed using Superpose (19). For each monomer the corresponding second protomer is shown in transparent black. (*C*) The hinge region between the helix α4 and the B30.2 domain is visualized by superposing the first N-terminal helix of each B30.2 domain (residues 590-595, shown in black). Helix α4 of each monomer is colored as in *A* and *B*.

Figure S3. SAXS data. (*A*) and (*B*) Overlay of experimental scattering curves are shown for all measured concentrations as indicated. For structural modeling a dataset was created corresponding to an infinite dilution. In (*A*) and (*B*) the data is plotted as X-log Y and log X-log Y, respectively, with the error bars depicted as lines in the corresponding color. (*C*) For the dataset extrapolated to infinite dilution (black dots) the guinier plot (black line) shows linearity without signs of interparticle attraction. (*D*) The Krakty-plot (black dots) shows a typical curve for a two domain protein with interdomain flexibility. The errors are depicted by grey lines. (*E*) The P(r) curve approaches zero for r = rmax. For r = 0, P(r) does not fully approach zero suggesting a minimal mismatch of the buffers in the sample and in the buffer control. (*F*) R_G distribution for the pool used in the ensemble optimization method and the selected ensemble is shown in. The vertical dashed line indicates the average R_G for the selected ensemble.

Figure S4. Binding of TRIM20 to pro-IL-1β. (*A*) Typical sensogram of the SPR measurements is shown. Myc-TRIM20Δ412 was immobilized and a dilution series of pro-IL-1β, as indicated, was subjected (black lines). The obtained fit for every concentration using the heterogeneous ligand

model is shown by the grey lines and the resulting K_Ds and their standard deviations (s.d.) are stated. (*B*) SEC profile for pro-IL-1β, TRIM20Δ413 and both proteins incubated for 20 h at 4 °C (complex) are shown in the corresponding color. The dotted lines indicate the retention volumes for the individual proteins and the complex as seen in Fig. 1*B*. (*C*) SEC profile of a mixture of both proteins incubated as stated (Complex) is shown (left y-axis). The black box indicates the fraction that was reinjected (Reinject complex; right y-axis).

Figure S5. Modeling a stereotype TRIM full length protein. (*A*) The periphery of the TRIM20 CHS domain and the NMR structure of the TRIM29 B-Box (pdb code: 2CSV) are shown in a cartoon representation. A sequence alignment of the structural overlap between the two structures is shown in the middle. Residues of the B-Box are colored in green. Residues that overlap in both structures are colored solid black while the rest of the CHS domain is colored transparent red. (*B*) The structure of the TRIM18 B-Box1/2 tandem motif (pdb code: 2JUN (15)), the TRIM5α RING (pdb code: 2ECV (14)), and the TRIM5α B-Box2 (pdb code: 2YRG (16)) are shown in a cartoon representation. (*C*) Multiple sequence alignment of the template structures TRIM5 RING, TRIM5 B-Box, TRIM29 B-Box and TRIM18 tandem B-Boxes (pdb entries 2ECV, 2YRG, 2CSV and 2JUN, respectively) and the target sequence used for homology modeling. Numbering of residues correspond to the pdb entries including the zinc atoms (z). Residues of the RING, B-Box and CHS domains are framed in blue, green and red, respectively.

Supplementary figure 1

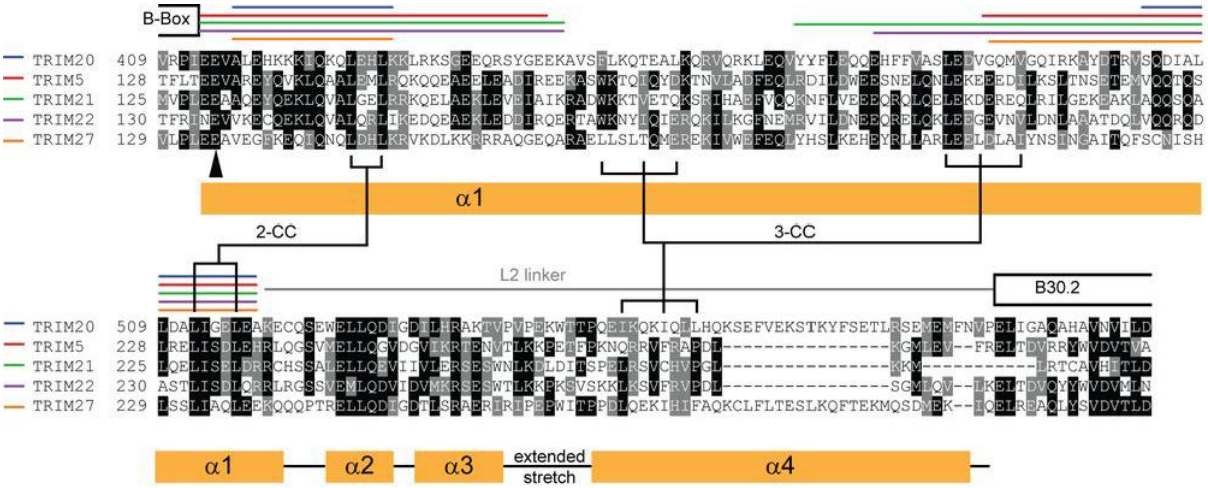

Supplementary figure 2

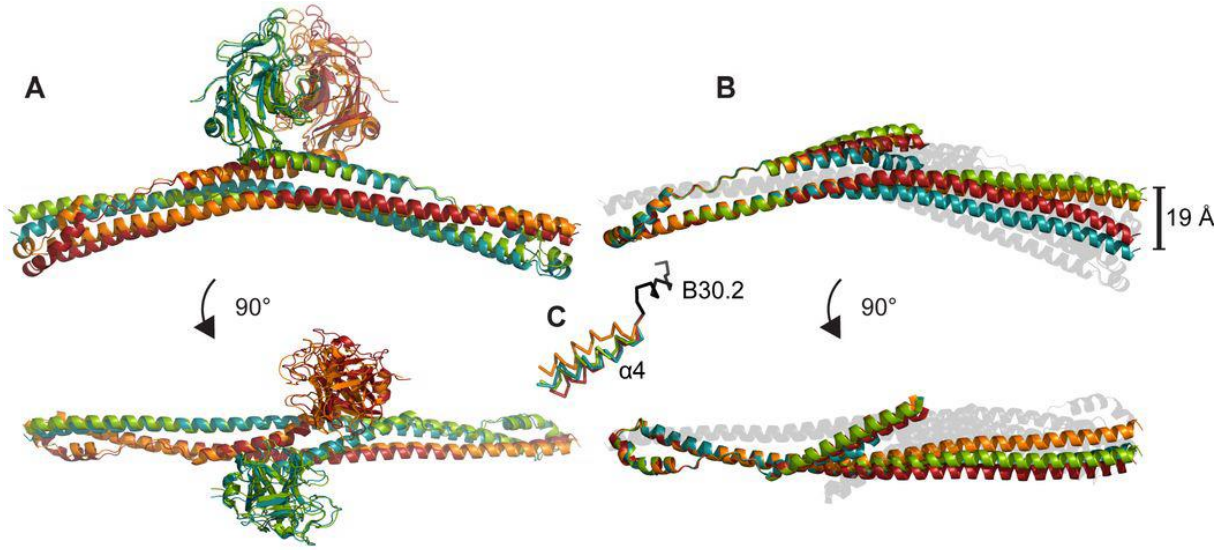

Supplementary figure 3

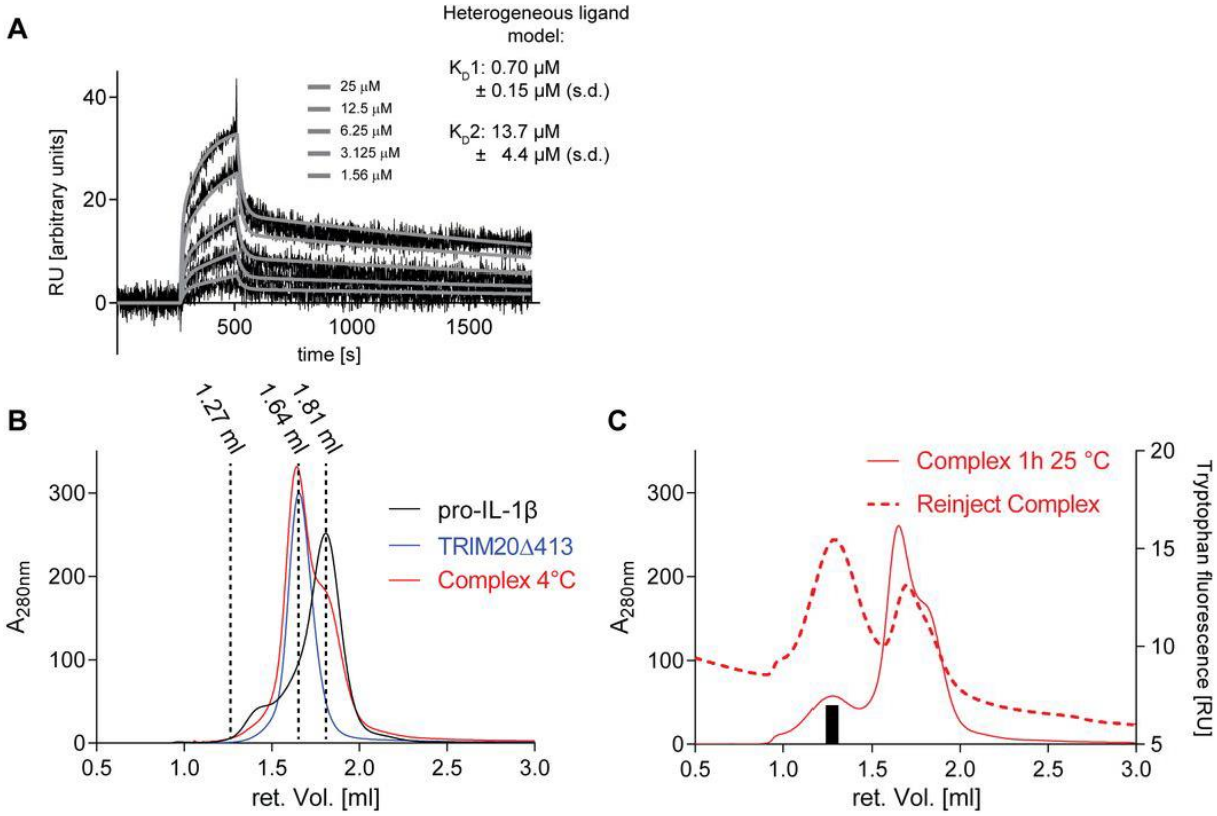

Supplementary figure 4

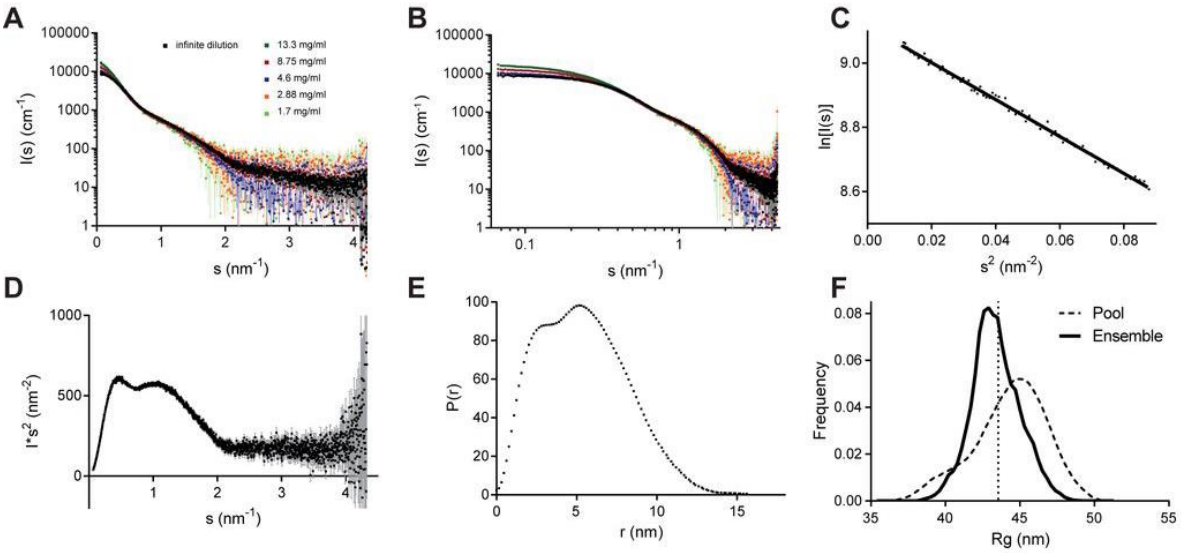

Supplementary figure 5

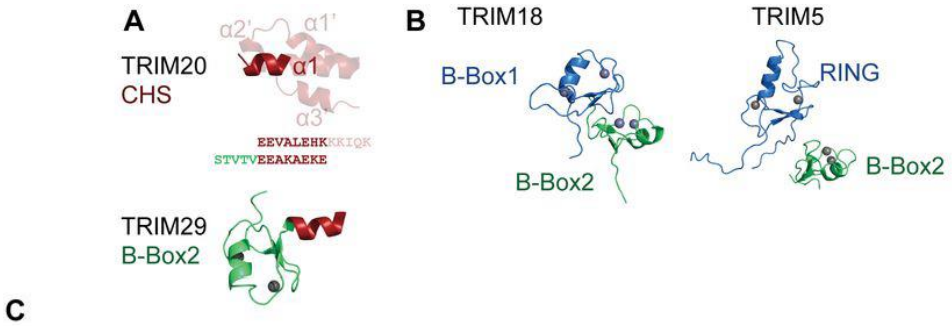

C

```
TRIM5_RING        8  MASGILVNVK EEVTCPICL- --ELLTQPLS LDCGHSFCQA CLTANHKKSM   54
TRIM5_BBox        0  ---------- ---------- ---------- ---------- ----------    0
TRIM29_BBox       0  ---------- ---------- ---------- ---------- ----------    0
TRIM18_tandem   114  ---------A EKVLCQFCDQ DPAQDAVKTC VTCEVSYCDE CLKATHP---  151
Target_seq.       1  MASGILVNVK EEVTCPICL- --ELLTQPLS LDCGHSFCQA CLTANHKKSM   47

TRIM5_RING       55  LDKGESSCPV CRISY----- ---------- ---------- ----------   69
TRIM5_BBox        8  ---------- ---------- ---------- -------SP EGQKVDHCAR   19
TRIM29_BBox      16  ---------- ---------- ---------- ---------- --FEARKCPV   23
TRIM18_tandem   152  ---------- -----NKKPF TGHRLIEPIP ----DSHI-- ---RGLMCLE  177
Target_seq.      48  LDKGESSCPV CRISYQPENI RPNRHVANIV EKLREVKLSP EGQKVDHCAR   97

TRIM5_RING       69  ---------- ---------- ---------- ---------- --zz--      71
TRIM5_BBox       20  HG-EKLLLFC QEDGKVICWL CERSQEHRGH HTF------- --zz--      53
TRIM29_BBox      24  HG-KTMELFC QTDQTCICYL CMFQ-EHKNH STVTVEEAKA EKzz--      65
TRIM18_tandem   178  HEDEKVNMYC VTDDQLICAL CKLVGRHRDH QVAALSE--- --zzzz     218
Target_seq.      98  HG-EKLLLFC QEDGKVICWL CERSQEHRGH HTFLTEEVAL EHzzzz     142
```

Table S1. X-ray data collection and refinement statistics

	TRIM20Δ413
Data collection	
Space group	$P2_1$
Cell dimensions	
a, *b*, *c* (Å)	69.82 388.21 70.88
α, β, γ (°)	90 116.52 90
Resolution (Å)	48.53 - 2.4 (2.486 - 2.4)*
R_{merge}	0.1724 (1.857)*
$I / \sigma I$	9.77 (0.88)*
Completeness (%)	98.96 (93.07)*
Redundancy	7.4 (6.6)*
$CC_{1/2}$	99.6 (51.3)*
Refinement	
Resolution (Å)	48.53 – 2.4
No. reflections	129414
R_{work} / R_{free} (%)	21.15 / 26.07
No. atoms	
Protein	17943
Ligand/ion	68
Water	33
B-factors	
Protein	54.8
Ligand/ion	67.7
Water	33.6
R.m.s. deviations	
Bond lengths (Å)	0.012
Bond angles (°)	1.37

The dataset was recorded from a single crystal.
*Values in parentheses are for highest-resolution shell.

Table S2: SAXS data collection and processing

	TRIM20Δ413
Data collection	
Instrument	Petra 12; Pilatus 2M
Beam geometry	0.2x0.12 mm2
Wavelength (Å)	1.24
s range (nm^{-1})	0.0668-4.336
Exposure time (s)	0.05
Concentration range [mg/ml]	1.7-13.3
Temperature	283
Structural parameters	
I(0) (cm-1) [from P(r)]	9184 (± 8.47)
Rg (nm) [from P(r)]	4.27 (± 0.056)
I(0) (cm-1) (from guinier)	9100.84 (±20.24)
Rg (nm) (from guinier)	4.15 (± 0.023)
Dmax [nm]	15.9
Porod volume estimate (Å3)	131.72
Dry volume calculated from structure (Å3)	100.5
Molecular mass determination	
Partial specific volume (cm3g-1)	1.37
Molecular mass Mr [kDa]	90.0
Molecular mass Mr [kDa; analytical ultracentrifugation]	78.4
Monomeric Mr from MS analysis [kDa]	42.737
Software employed	
Primary data reduction	*PRIMUS*
Data processing	*PRIMUS / GNOM*
Extrapolation to infinite dilution	*ALMERGE*
Ab initio analysis	*DAMMIN*
Validation and averaging	*DAMAVER*
Rigid-body modelling	*SASREF*
Multiple conformation modelling	*EOM*
Computation of model intensities	*CRYSOL*
3D graphics representation R.m.s. deviations	*PyMOL*

Table S3. Kinetic data of SPR experiment

k_{on}**1 [1/Ms]**	k_{off}**1 [1/s]**	K_D**1 [µM]**	R_{max}**1 [RU]**	k_{on}**2 [1/Ms]**	k_{off}**2 [1/s]**	K_D**2 [µM]**	R_{max}**2 [RU]**	χ^2 **[RU]**
$4.17*10^2$ $\pm 1.4*10^2$	$2.83*10^{-4}$ $\pm 0.59*10^{-4}$	0.70 ± 0.15	20.3 ± 3.88	$3.96*10^3$ $\pm 1.32*10^3$	$5.10*10^{-2}$ $\pm 1.38*10^{-2}$	13.7 ± 4.4	25 ± 3.27	2.55 ±0.54

Table S4. Construct design

Construct	Coding region	Tag	Forward primer	Reverse primer	Template vector
TRIM20Δ413	414-781	-	atatatgctcttctagtgaggtcgccctggaac	tatatagctcttcttgcgtcaggcccctgacc	pFX3CH
TRIM20Δ412	413-781	N-terminal c-Myc (EQGKLISEEDL)	atatatgctcttctagtgagcagaaactcatctct gaagaggatctggaggaggttgccc	tatatagctcttcttgcgtcaggcccctgacc	pFX3CH
TRIM20-CHS	413-577	N-terminal c-Myc (EQGKLISEEDL)	atatatgctcttctagtgagcagaaactcatctct gaagaggatctggaggaggttgccc	tatatagctcttcatgcggtttctgagaagtac	pFX3CH
TRIM20-B30.2	577-781	C-terminal c-Myc (EQGKLISEEDL)	atatatgctcttctagtctgcgttcagaaatgg	tatatagctcttcatgccagatcctcttcagagat gagtttctgctcgtcaggccctgacc	pFX3CH
Pro-IL-1β	Full length	C-terminal FLAG (DYKDDDDK)	atatatgctcttctagtgcggaagtgccggaac	tatatagctcttcatgc cttatcgtcgtcatccttgta atcgctgctcacaaactgc	pET28-FXH3C

3 Final Discussion

Establishing protocols for the production of purified full-length TRIM5 proteins, which are unprecedented in harboring the wild-type RING domain, has opened the door to in-vitro characterization of the TRIM5 E3 ubiquitin-ligase activity. Using ubiquitin assays in a collaborative work with Pertel and colleagues, we demonstrated that TRIM5 cooperates with the heterodimeric E2 ubiquitin-conjugating enzyme Ubc13/Uev1a to catalyze the formation of unanchored K-63 linked ubiquitin-chains, which trigger TAK1 activation by autophosphorylation in-vitro. In the cell, TAK1 activation leads to the induction of innate immune signaling pathways. The link to retroviral restriction was made by showing that binding of owl monkey TRIMCyp to in-vitro assembled HIV-1 CA tubes stimulates the formation of K-63 ubiquitin chains in the ubiquitin assay. This was not the case when the interaction of TRIMCyp with the HIV-1 CA was disrupted by mutation or the inhibitor cyclosporine A (CsA). Thus TRIM5 proteins act as PAMP (pathogen associated molecular pattern) receptors by recognizing a pattern on the retroviral CA lattice.

A first structural hint on how binding of the TRIM5 C-terminal domain to the viral CA may lead to an enhanced E3-ligase activity mediated by the N-terminal RING domain has been found by Ganser-Pornillos *et al.* [136]. They reported that binding of chimeric TRIM5-21R proteins to planar hexagonal HIV-1 CA-NC arrays stimulates TRIM5-21R self-assembly into a complementary hexagonal lattice. It transpires that TRIM5 lattice formation may be coupled to E3 ligase activity via conformational changes or proximity effects, as both activities are stimulated when interacting with the retroviral CA lattice. A comparable mechanism where formation of supramolecular complexes by self-association improves RING E3-ubiquitin ligase activity is known for Mdm2, a negative regulator of the p53 tumor suppressor. Compared to monomeric Mdm2, these supramolecular complexes have an increased ubiquitination activity in the presence of limiting Ubc5Hc amounts, suggesting that oligomerization of RING E3s may induce ubiquitin polymerization by providing a scaffold for the efficient recruitment of E2 enzymes.

To elucidate whether the RING domains are brought into proximity in hexagonal TRIM5 arrays, the relative positioning of the TRIM5 domains in the lattice needs to be known. However, the resolution of the electron density map derived from TRIM5 paracrystalline arrays is not sufficient to determine the position of individual domains in the lattice [136]. To gain structural insight into the relative domain organization of TRIM5 proteins, we have taken extensive efforts to crystallize either full-length or N-terminally truncated TRIM5 proteins. But no diffracting crystals were obtained for any of these TRIM5 constructs. Instead, the atomic structure of a homologous TRIM20/pyrin C-terminal fragment encompassing the CC-L2, here termed CHS (central helical scaffold), and B30.2 domains could be solved independently. This structure reveals an antiparallel dimerization mode mediated by the elongated CHS domain with the B30.2 domains centrally positioned on top of the CHS. To verify whether TRIM5 shares the same fold, we have performed SAXS measurements with a homologous human TRIM5 construct and have determined its low resolution shape. Measured SAXS curves are shown in the appendix of this thesis (Figure 22). Indeed, the TRIM20/pyrin crystal structure

fits relatively well into the SAXS envelope corresponding to the filtered average of ab-initio models (Figure 18 A). This suggests that TRIM5 and TRIM20/pyrin share the same overall domain organization. While the dimeric CHS domain matches only into the region spanning the maximal diameter of the SAXS envelope, the remaining volume in the probability map leaves conformational space for different orientations of the TRIM5 B30.2 domains (Figure 18). Interdomain flexibility was also observed in SAXS measurements of the TRIM20/pyrin C-terminal fragment and rigid body modelling based on the scattering curve revealed a large conformational space for different B30.2 domain orientations relative to the CHS.

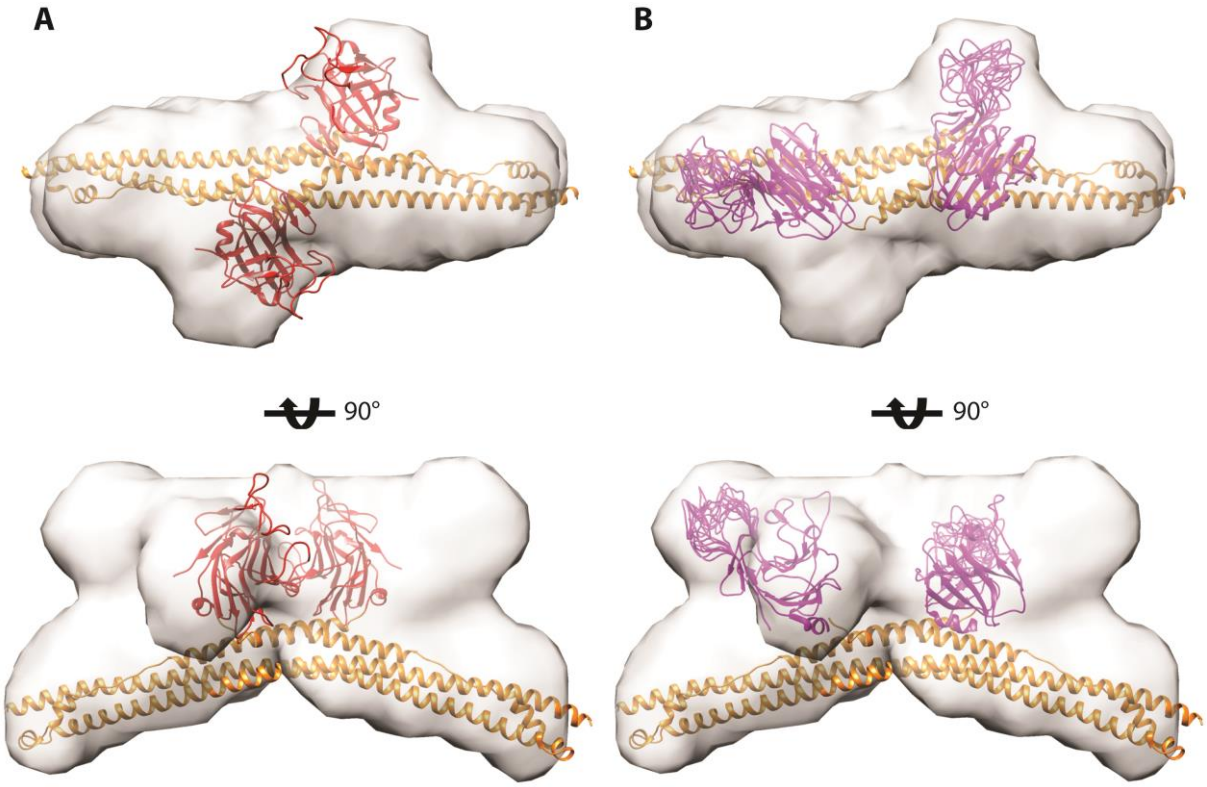

Figure 18. Docking of atomic structures into the averaged SAXS envelope of a human TRIM5α CHS-B30.2 fragment. The depicted SAXS envelope is the filtered average of Dammin refined ab-initio models generated from a pre-calculated Damaver probability map of the human TRIM5α CHS-B30.2 domains. **(A)** Docking of the TRIM20/pyrin CHS-B30.2 structure into the TRIM5α SAXS envelope. The TRIM20/pyrin CHS and B30.2 domains are shown in orange and red ribbons, respectively. **(B)** The rhesus TRIM5α B30.2 structure (magenta ribbon, pdb entry: 2LM3) fitted into the TRIM5α SAXS envelope on top of the TRIM20/pyrin CHS domain (orange ribbon). Two possible orientations of the rhesus TRIM5α B30.2 domains are shown.

Due to the antiparallel fold of the CHS domain, the preceding N-terminal RING and B-Box domains in TRIM proteins are placed distal apart at the extreme ends of the CHS. The availability of overlapping RING and B-Box domain structures from several TRIM proteins has allowed us to generate a stereotype full-length model for TRIM proteins containing the RING and B-Box domains from human TRIM5α (Figure 19). To evaluate whether the TRIM full-length model applies to published data on TRIM5, we inspected the model for accessibility of known functional patches expected to be surface exposed (Figure 19 B). Both cluster 1 on

the B-Box domain and the putative E2 interaction patch on the RING domain remain surface exposed in our full-length TRIM model. Cluster 1 is implicated in higher-order oligomerization and lattice formation by mediating homodimerization of B-Box domains. The E2-patch is expected to interact with the E2 ubiquitin-conjugating enzyme as mutations in this region impair E3-ligase activity without affecting higher-order self-assembly and maps with residues of the E2 interaction site in homologous RING domains. A large fraction of the residues in the designated RING-RING interaction region map into the modelled interface between the RING and B-Box domains. This region was named RING-RING by Lienlaf and colleagues because of the structural similarity to the RING-RING interaction region between BRCA-1 and BARD1. The interface between BRCA-1 and BARD1 also corresponds to the binding interface between B- Box1 and B-Box2 in the tandem structure of the MID1 B-Boxes, which was taken as a template for modelling of the TRIM5 RING and B-Box domains. This explains why the RING-RING patch maps into the interface between RING and B-Box in our TRIM model and the existence of such a RING/B-Box contact in TRIM5 remains to be proven. Mutation of residues in RING-RING surface of TRIM5 have been shown to impair higher-order self-assembly and therefore restriction activity [84]. Another surface patch that forms an interface in our TRIM model is cluster 2 on the B-Box domain, which is formed by hydrophobic residues. In our model, these residues are buried between the B-Box and helix 2 on the outer edge of the CHS domain. Although mutational studies on cluster 2 are sparse, mutation of residues mapping to CHS helix 2 on the opposite side have been shown to impair TRIM5 restriction activity and could be important for the proper orientation of the B-Box domains.

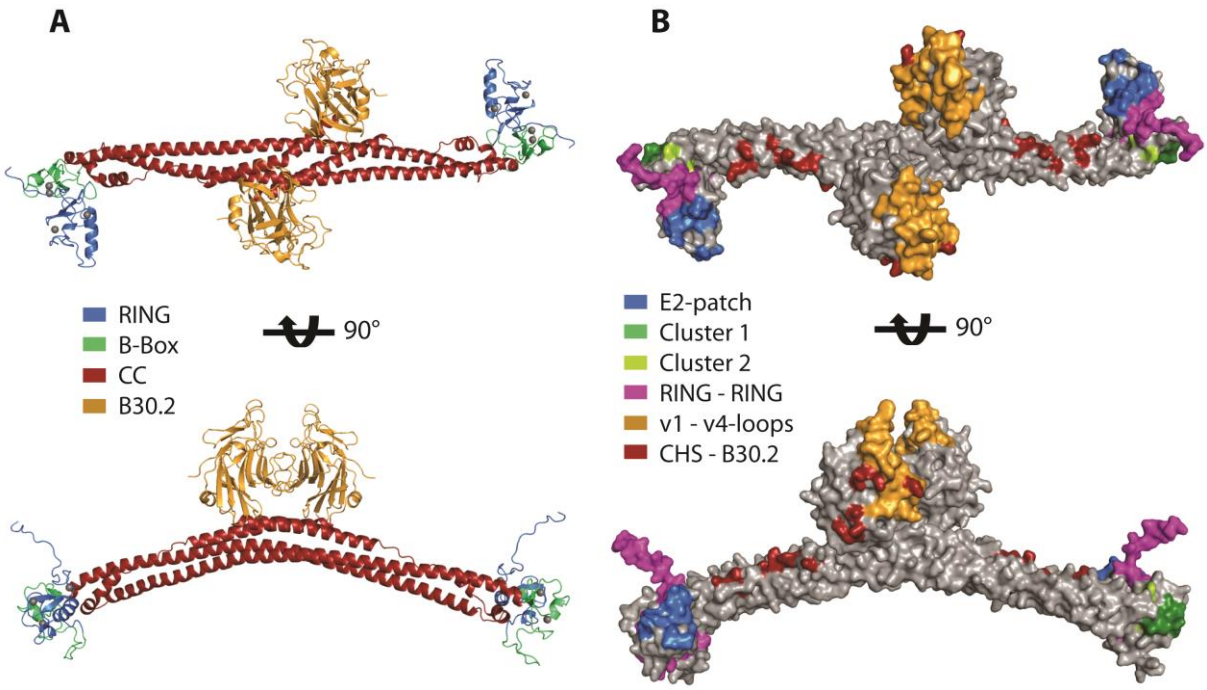

Figure 19. Stereotype full-length TRIM model. The model is shown in top and side view. **(A)** Cartoon representation of the full-length TRIM model obtained by docking the modelled RING/B-Box domains of human TRIM5α docked onto the crystal structure of the TRIM20/pyrin CHS-B30.2 domains. The individual TRIM domains are colored according to the depicted color code. **(B)** Full-length TRIM model in surface representation with known functional patches highlighted according to the depicted color code. The CHS – B30.2 patch mediates tetramerization by forming contacts between the CHS and B30.2 domain of two TRIM20/pyrin dimers.

The contacts in the crystal-packing of the TRIM20/pyrin C-terminal fragment suggest the existence of TRIM tetramers. These tetramers are formed by binding of the B30.2 domain into the elongated stretch between helix 3 and helix 4 of the CHS of a neighboring dimer. The functional relevance of the tetramer interface is further supported by mutations in the corresponding CHS - B30.2 patch of TRIM5α that abolish restriction activity [122,199] (Figure 19 B). Our full-length TRIM model also allows the construction of tetramers without clashing of the modelled domains (Figure 20 A,B) and reveals the domain organization of TRIM5 in the hexagonal lattice (Figure 20 C). The inter-ring spacing in the hexagonal TRIM5-21R arrays reported by Ganser-Pornillos *et al.* amounts to 315-355 Å, which is significantly larger than the HIV-1 CA lattice spacing of 90 Å [136]. Therefore each hexagon side of the TRIM5-21R lattice is approximately 180-200 Å in length and fits well to the maximal diameter in the TRIM full-length model (Figure 20 C). Placing of TRIM tetramers into the hexagon sides and connecting them to each other via homodimeric B-Box contacts allows the construction of a hexagonal lattice. The arrangement of the TRIM5 domains in this lattice suggests that enhancement of the E3 ligase activity upon CA binding and TRIM5 self-assembly may be induced by proximity effects as the RING domains join at the threefold lattice interfaces. As the TRIM5 RING is known to contribute to higher-order self-assembly, it may additionally involve rearrangements of the RING domains that would allow inter-dimer contacts in the lattice.

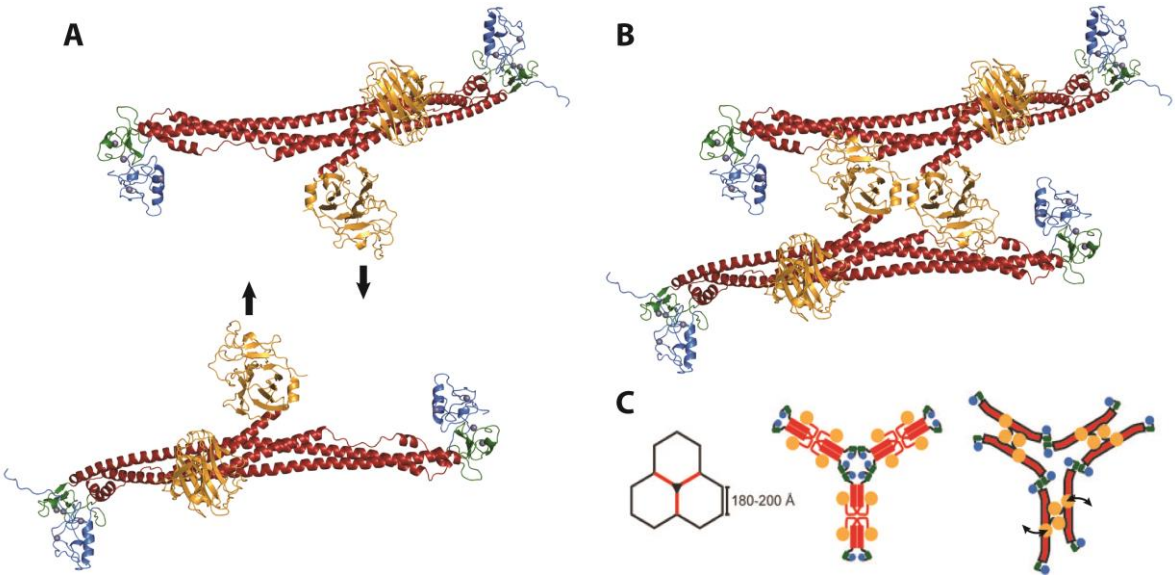

Figure 20. Model of the full-length TRIM tetramer revealing the domain arrangement in the TRIM5 lattice. (A) Two separated TRIM dimers are shown in the relative orientation as found in TRIM20/pyrin tetramers. The arrows indicate how the B30.2 domains bind to the extended stretch in the CHS domain of a neighboring dimer to form a tetramer. **(B)** Full-length TRIM tetramer as observed in the TRIM20/pyrin crystal packing. **(C)** A schematic drawing showing the dimensions of the reported hexagonal lattice formed by the TRIM5-21R chimera is depicted on the left and the currently proposed lattice model by Ganser-Pornillos *et al.* with tetramers of parallel arranged TRIM dimers placed at the hexagon sides is shown in the middle [136]. Shown on the right is the lattice model using the B30.2 dependent tetramer as observed in the TRIM20/pyrin crystal. The arrows indicate the flexibility of the B30.2 domains revealed by SAXS measurements of the TRIM20/pyrin C-terminal fragment.

TRIM5α binds with a considerable affinity exclusively to the assembled CA core of restricted retroviruses and binding to isolated monomeric of dimeric CAs is very weak. Furthermore, both the E3 ligase activity and the efficiency of TRIM5-21R lattice formation are only stimulated upon presentation of an assembled retroviral CA lattice. Together with the discovery that TRIM5 proteins act as pattern recognition receptors by inducing an innate immune response upon recognition of a retroviral CA lattice, it transpires that TRIM5α binds to a complex epitope that is only presented in the context of an assembled CA lattice. Considering the size of the predicted binding surface in the atomic structures of the rhesus TRIM5α B30.2 domain, it becomes evident that this surface must cover multiple CA subunits in the hexagonal CA lattice. To elucidate which arrangement of CA molecules, and therefore which symmetric interface, is bound by TRIM5α in the HIV-1 CA lattice, we have generated a series of HIV-1 CA oligomers that mimic symmetric interfaces of the HIV-1 CA lattice. Together with newly engineered trimeric CAs, the gallery of available CA oligomers now includes mono-, di-, tri-, and hexameric CAs. The measurement of the binding affinities of the rhesus TRIM5α B30.2 domain to these building blocks of the HIV-1 CA lattice revealed that the NTD-linked trimeric CAs and hexameric CAs have an increased affinity compared to monomeric or wild-type dimeric CAs. Furthermore, the binding data from dual-focus FCS measurements of the interaction with the CA hexamer could not be fitted using a single binding site model, but fitted well using a

two binding site model instead. Based on these findings, we concluded that the inter-hexamer gap spanning two neighboring hexamers would constitute the most promising epitope on the HIV-1 CA lattice. This epitope involves two NTD subunits on one CA hexamer and one NTD subunit on the neighboring CA hexamer. With two of these three NTD subunits participating at the N-terminal trimer interface, this potential TRIM5α binding epitope is supported the best by our interaction data, as it would both explain the increased affinity for the NTD-trimer and the two binding sites on the CA hexamer suggested by the binding kinetics.

The binding avidity of the TRIM5α B30.2 domains for the retroviral CA lattice is greatly enhanced upon lower-order and higher-order oligomerization of TRIM5α. Therefore it is important to consider the relative arrangement of the B30.2 domains in the context of TRIM5 oligomers to gain an overall picture of how TRIM5 may bind to retroviral lattices. With the crystal structure of a TRIM20/pyrin in hands and the provided evidence that TRIM5α shares the same fold, we can estimate geometrical constrains imposed to the relative orientation of the B30.2 domains in dimers and tetramers of TRIM5. Placing the TRIM20/pyrin tetramer structure on top of the HIV-1 CA lattice provides a fist idea on the dimensions and distribution of the B30.2 binding epitopes on the HIV-1 CA lattice (Figure 21A). Due to the antiparallel dimerization of the CHS, the B30.2 domains are oriented in an antiparallel fashion relative to each other in the dimer as well as in the tetramer of TRIM20/pyrin. Interestingly, neighboring NTD-trimer interfaces as well as the inter-hexamer gaps in the HIV-1 CA lattice, which are suggested as potential TRIM5α binding epitopes in our CA interaction study, are oriented antiparallel relative to each other. Based on the geometrical restrains of a hypothetical TRIM5α tetramer, conceptual models on how TRIM5 may bind to the HIV-1 CA lattice are shown in Figure 21 B, C and D.

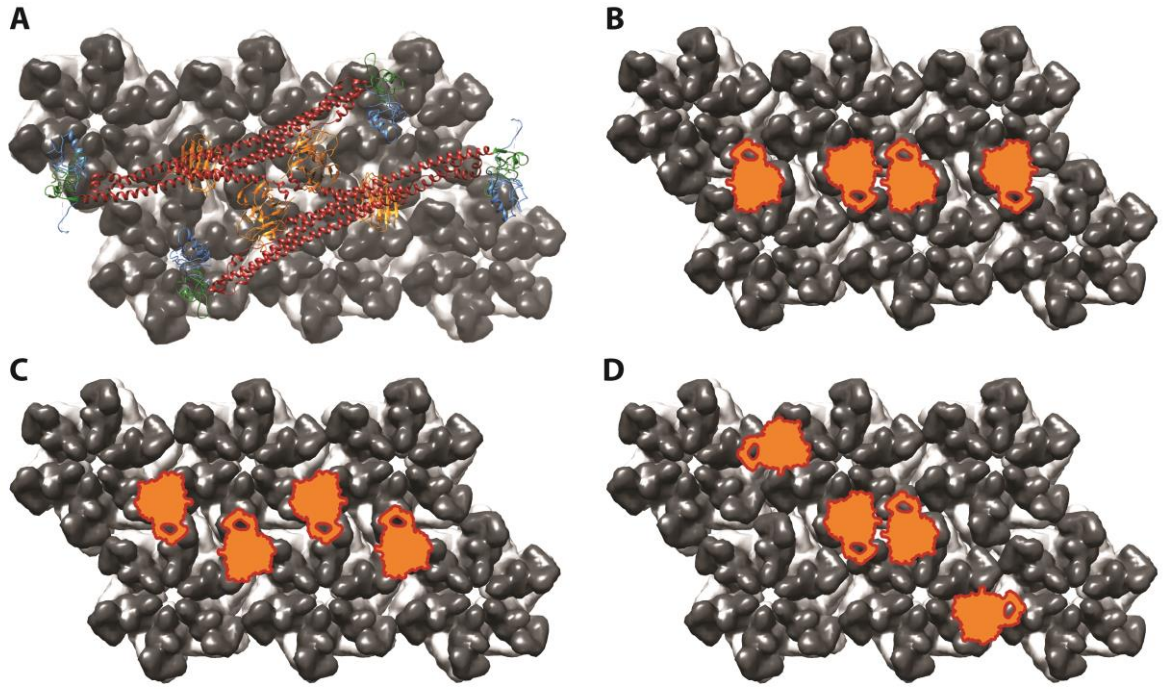

Figure 21. Conceptual models for binding of the B30.2 domains onto the HIV-1 CA lattice in the context of a TRIM5α tetramer. (A) Placing of the full-length TRIM tetramer model on top of the HIV-1 CA lattice (pdb entry: 3DIK). **(B)** Binding of the rhesus B30.2 domain (pdb entry: 2LM3) at the inter-hexamer gaps. The B30.2 domains are oriented antiparallel to each other as observed in TRIM20/pyrin tetramers. **(C)** Binding of the rhesus B30.2 domain (pdb entry: 2LM3) at the NTD-trimer interfaces. The B30.2 domains are oriented antiparallel to each other as observed in TRIM20/pyrin tetramers. **(D)** Binding of the rhesus B30.2 domain (pdb entry: 2LM3) at the inter-hexamer gaps with two B30.2 domains being fixed in an antiparallel fashion as the B30.2 domains in the TRIM20/pyrin tetramer interface. Compared to (B), the other two B30.2 domains are allowed to swing out as suggested by the SAXS measurements of TRIM20/pyrin and bind to an inter-hexamer gap of a different orentation.

4 Appendix

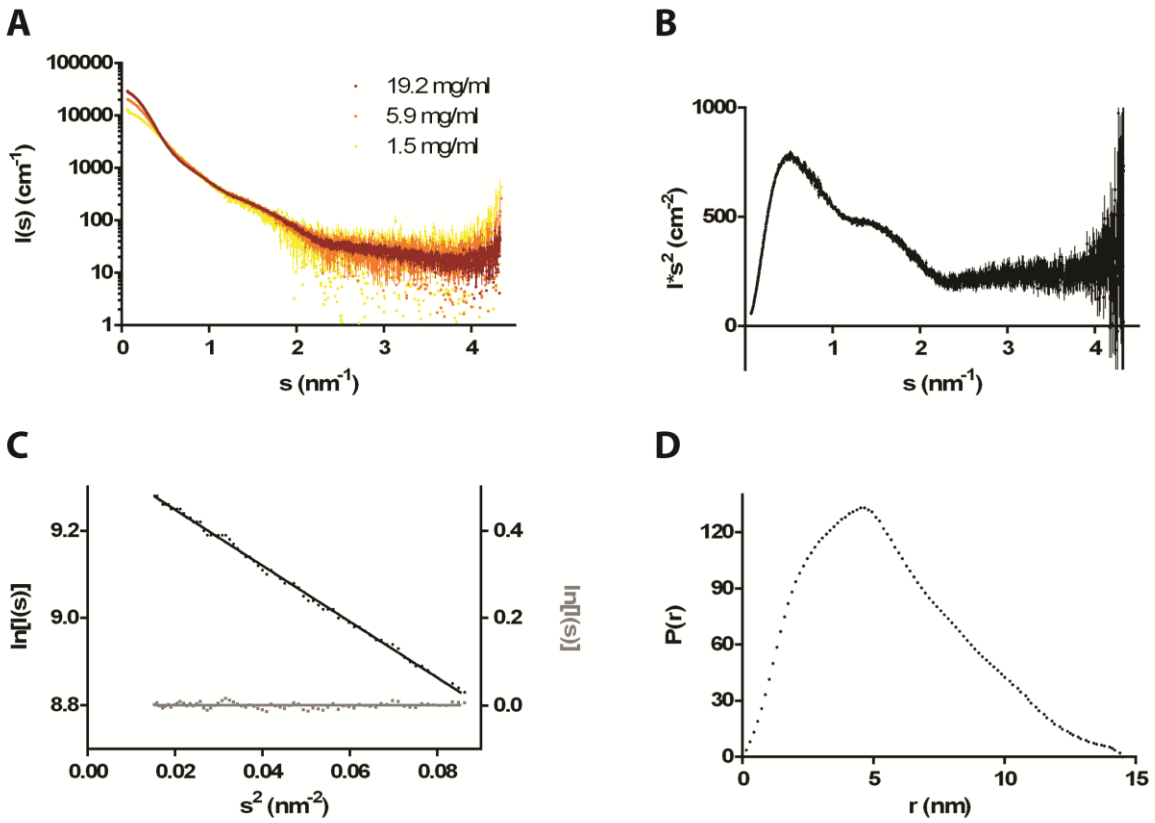

Figure 22. SAXS data for the CHS-B30.2 fragment of human TRIM5α. (A) Experimental scattering curves taken for calculation of the SAXS envelope. The sample shows a tendency for interparticle attraction at higher protein concentrations. The sample at 1.5 mg/ml was collected freshly from size exclusion prior to SAXS measurement. **(B)** The Kratky-plot of the merged SAXS data set shows a typical curve for a two domain protein with interdomain flexibility, comparable to the corresponding plot for the SAXS data of the TRIM20/pyrin C-terminal fragment. **(C)** The guinier plot of the merged data set shows linearity without signs of interparticle attraction. **(D)** Pair distribution function P(r) showing the distance distribution in the measured TRIM5α molecule.

5 References

1. Centers for Disease C (1981) Kaposi's sarcoma and Pneumocystis pneumonia among homosexual men--New York City and California. MMWR Morb Mortal Wkly Rep 30: 305-308.
2. Barre-Sinoussi F, Chermann JC, Rey F, Nugeyre MT, Chamaret S, et al. (1983) Isolation of a T-lymphotropic retrovirus from a patient at risk for acquired immune deficiency syndrome (AIDS). Science 220: 868-871.
3. Gallo RC, Salahuddin SZ, Popovic M, Shearer GM, Kaplan M, et al. (1984) Frequent detection and isolation of cytopathic retroviruses (HTLV-III) from patients with AIDS and at risk for AIDS. Science 224: 500-503.
4. (2013) UNAIDS report on the global AIDS epidemic 2013.
5. (2013) UNAIDS Fact Sheet 2013.
6. Chakrabarti L, Guyader M, Alizon M, Daniel MD, Desrosiers RC, et al. (1987) Sequence of simian immunodeficiency virus from macaque and its relationship to other human and simian retroviruses. Nature 328: 543-547.
7. Guyader M, Emerman M, Sonigo P, Clavel F, Montagnier L, et al. (1987) Genome organization and transactivation of the human immunodeficiency virus type 2. Nature 326: 662-669.
8. Huet T, Cheynier R, Meyerhans A, Roelants G, Wain-Hobson S (1990) Genetic organization of a chimpanzee lentivirus related to HIV-1. Nature 345: 356-359.
9. Hirsch VM, Olmsted RA, Murphey-Corb M, Purcell RH, Johnson PR (1989) An African primate lentivirus (SIVsm) closely related to HIV-2. Nature 339: 389-392.
10. Apetrei C, Kaur A, Lerche NW, Metzger M, Pandrea I, et al. (2005) Molecular epidemiology of simian immunodeficiency virus SIVsm in U.S. primate centers unravels the origin of SIVmac and SIVstm. J Virol 79: 8991-9005.
11. Apetrei C, Lerche NW, Pandrea I, Gormus B, Silvestri G, et al. (2006) Kuru experiments triggered the emergence of pathogenic SIVmac. AIDS 20: 317-321.
12. Santiago ML, Lukasik M, Kamenya S, Li Y, Bibollet-Ruche F, et al. (2003) Foci of endemic simian immunodeficiency virus infection in wild-living eastern chimpanzees (Pan troglodytes schweinfurthii). J Virol 77: 7545-7562.
13. Keele BF, Van Heuverswyn F, Li Y, Bailes E, Takehisa J, et al. (2006) Chimpanzee reservoirs of pandemic and nonpandemic HIV-1. Science 313: 523-526.
14. Van Heuverswyn F, Li Y, Bailes E, Neel C, Lafay B, et al. (2007) Genetic diversity and phylogeographic clustering of SIVcpzPtt in wild chimpanzees in Cameroon. Virology 368: 155-171.
15. Neel C, Etienne L, Li Y, Takehisa J, Rudicell RS, et al. (2010) Molecular epidemiology of simian immunodeficiency virus infection in wild-living gorillas. J Virol 84: 1464-1476.
16. Keele BF, Jones JH, Terio KA, Estes JD, Rudicell RS, et al. (2009) Increased mortality and AIDS-like immunopathology in wild chimpanzees infected with SIVcpz. Nature 460: 515-519.

17. Bailes E, Gao F, Bibollet-Ruche F, Courgnaud V, Peeters M, et al. (2003) Hybrid origin of SIV in chimpanzees. Science 300: 1713.
18. Peeters M, Courgnaud V, Abela B, Auzel P, Pourrut X, et al. (2002) Risk to human health from a plethora of simian immunodeficiency viruses in primate bushmeat. Emerg Infect Dis 8: 451-457.
19. Sharp PM, Hahn BH (2011) Origins of HIV and the AIDS pandemic. Cold Spring Harb Perspect Med 1: a006841.
20. Kirchhoff F (2010) Immune evasion and counteraction of restriction factors by HIV-1 and other primate lentiviruses. Cell Host Microbe 8: 55-67.
21. Sauter D, Schindler M, Specht A, Landford WN, Munch J, et al. (2009) Tetherin-driven adaptation of Vpu and Nef function and the evolution of pandemic and nonpandemic HIV-1 strains. Cell Host Microbe 6: 409-421.
22. Balzarini J, De Clercq E, Uberla K (1997) SIV/HIV-1 hybrid virus expressing the reverse transcriptase gene of HIV-1 remains sensitive to HIV-1-specific reverse transcriptase inhibitors after passage in rhesus macaques. J Acquir Immune Defic Syndr Hum Retrovirol 15: 1-4.
23. Besnier C, Takeuchi Y, Towers G (2002) Restriction of lentivirus in monkeys. Proc Natl Acad Sci U S A 99: 11920-11925.
24. Cowan S, Hatziioannou T, Cunningham T, Muesing MA, Gottlinger HG, et al. (2002) Cellular inhibitors with Fv1-like activity restrict human and simian immunodeficiency virus tropism. Proc Natl Acad Sci U S A 99: 11914-11919.
25. Himathongkham S, Luciw PA (1996) Restriction of HIV-1 (subtype B) replication at the entry step in rhesus macaque cells. Virology 219: 485-488.
26. Hofmann W, Schubert D, LaBonte J, Munson L, Gibson S, et al. (1999) Species-specific, postentry barriers to primate immunodeficiency virus infection. J Virol 73: 10020-10028.
27. Li J, Lord CI, Haseltine W, Letvin NL, Sodroski J (1992) Infection of cynomolgus monkeys with a chimeric HIV-1/SIVmac virus that expresses the HIV-1 envelope glycoproteins. J Acquir Immune Defic Syndr 5: 639-646.
28. Munk C, Brandt SM, Lucero G, Landau NR (2002) A dominant block to HIV-1 replication at reverse transcription in simian cells. Proc Natl Acad Sci U S A 99: 13843-13848.
29. Towers GJ, Hatziioannou T, Cowan S, Goff SP, Luban J, et al. (2003) Cyclophilin A modulates the sensitivity of HIV-1 to host restriction factors. Nat Med 9: 1138-1143.
30. Stremlau M, Owens CM, Perron MJ, Kiessling M, Autissier P, et al. (2004) The cytoplasmic body component TRIM5alpha restricts HIV-1 infection in Old World monkeys. Nature 427: 848-853.
31. Sayah DM, Sokolskaja E, Berthoux L, Luban J (2004) Cyclophilin A retrotransposition into TRIM5 explains owl monkey resistance to HIV-1. Nature 430: 569-573.
32. Yap MW, Nisole S, Lynch C, Stoye JP (2004) Trim5alpha protein restricts both HIV-1 and murine leukemia virus. Proc Natl Acad Sci U S A 101: 10786-10791.
33. Engelman A, Cherepanov P (2012) The structural biology of HIV-1: mechanistic and therapeutic insights. Nat Rev Microbiol 10: 279-290.

34. Coiras M, Lopez-Huertas MR, Perez-Olmeda M, Alcami J (2009) Understanding HIV-1 latency provides clues for the eradication of long-term reservoirs. Nat Rev Microbiol 7: 798-812.
35. Karlsson Hedestam GB, Fouchier RA, Phogat S, Burton DR, Sodroski J, et al. (2008) The challenges of eliciting neutralizing antibodies to HIV-1 and to influenza virus. Nat Rev Microbiol 6: 143-155.
36. Zhu P, Liu J, Bess J, Jr., Chertova E, Lifson JD, et al. (2006) Distribution and three-dimensional structure of AIDS virus envelope spikes. Nature 441: 847-852.
37. Zanetti G, Briggs JA, Grunewald K, Sattentau QJ, Fuller SD (2006) Cryo-electron tomographic structure of an immunodeficiency virus envelope complex in situ. PLoS Pathog 2: e83.
38. Liu J, Bartesaghi A, Borgnia MJ, Sapiro G, Subramaniam S (2008) Molecular architecture of native HIV-1 gp120 trimers. Nature 455: 109-113.
39. Kwong PD, Wyatt R, Robinson J, Sweet RW, Sodroski J, et al. (1998) Structure of an HIV gp120 envelope glycoprotein in complex with the CD4 receptor and a neutralizing human antibody. Nature 393: 648-659.
40. Rizzuto CD, Wyatt R, Hernandez-Ramos N, Sun Y, Kwong PD, et al. (1998) A conserved HIV gp120 glycoprotein structure involved in chemokine receptor binding. Science 280: 1949-1953.
41. Chan DC, Fass D, Berger JM, Kim PS (1997) Core structure of gp41 from the HIV envelope glycoprotein. Cell 89: 263-273.
42. Weissenhorn W, Dessen A, Harrison SC, Skehel JJ, Wiley DC (1997) Atomic structure of the ectodomain from HIV-1 gp41. Nature 387: 426-430.
43. Buzon V, Natrajan G, Schibli D, Campelo F, Kozlov MM, et al. (2010) Crystal structure of HIV-1 gp41 including both fusion peptide and membrane proximal external regions. PLoS Pathog 6: e1000880.
44. McDonald D, Vodicka MA, Lucero G, Svitkina TM, Borisy GG, et al. (2002) Visualization of the intracellular behavior of HIV in living cells. J Cell Biol 159: 441-452.
45. Piller SC, Caly L, Jans DA (2003) Nuclear import of the pre-integration complex (PIC): the Achilles heel of HIV? Curr Drug Targets 4: 409-429.
46. Arhel NJ, Souquere-Besse S, Munier S, Souque P, Guadagnini S, et al. (2007) HIV-1 DNA Flap formation promotes uncoating of the pre-integration complex at the nuclear pore. EMBO J 26: 3025-3037.
47. Forshey BM, von Schwedler U, Sundquist WI, Aiken C (2002) Formation of a human immunodeficiency virus type 1 core of optimal stability is crucial for viral replication. J Virol 76: 5667-5677.
48. Guntaka RV (1993) Transcription termination and polyadenylation in retroviruses. Microbiol Rev 57: 511-521.
49. Sakai H, Kawamura M, Sakuragi J, Sakuragi S, Shibata R, et al. (1993) Integration is essential for efficient gene expression of human immunodeficiency virus type 1. J Virol 67: 1169-1174.
50. Kelly J, Beddall MH, Yu D, Iyer SR, Marsh JW, et al. (2008) Human macrophages support persistent transcription from unintegrated HIV-1 DNA. Virology 372: 300-312.

51. Swingler S, Brichacek B, Jacque JM, Ulich C, Zhou J, et al. (2003) HIV-1 Nef intersects the macrophage CD40L signalling pathway to promote resting-cell infection. Nature 424: 213-219.
52. Wu Y, Marsh JW (2001) Selective transcription and modulation of resting T cell activity by preintegrated HIV DNA. Science 293: 1503-1506.
53. Engelman A, Cherepanov P (2008) The lentiviral integrase binding protein LEDGF/p75 and HIV-1 replication. PLoS Pathog 4: e1000046.
54. Stevenson M (2003) HIV-1 pathogenesis. Nat Med 9: 853-860.
55. Pomerantz RJ (2002) Reservoirs of human immunodeficiency virus type 1: the main obstacles to viral eradication. Clin Infect Dis 34: 91-97.
56. Shen L, Siliciano RF (2008) Viral reservoirs, residual viremia, and the potential of highly active antiretroviral therapy to eradicate HIV infection. J Allergy Clin Immunol 122: 22-28.
57. Nabel G, Baltimore D (1987) An inducible transcription factor activates expression of human immunodeficiency virus in T cells. Nature 326: 711-713.
58. Jeang KT, Xiao H, Rich EA (1999) Multifaceted activities of the HIV-1 transactivator of transcription, Tat. J Biol Chem 274: 28837-28840.
59. Greene WC, Peterlin BM (2002) Charting HIV's remarkable voyage through the cell: Basic science as a passport to future therapy. Nat Med 8: 673-680.
60. Daugherty MD, Liu B, Frankel AD (2010) Structural basis for cooperative RNA binding and export complex assembly by HIV Rev. Nat Struct Mol Biol 17: 1337-1342.
61. DiMattia MA, Watts NR, Stahl SJ, Rader C, Wingfield PT, et al. (2010) Implications of the HIV-1 Rev dimer structure at 3.2 A resolution for multimeric binding to the Rev response element. Proc Natl Acad Sci U S A 107: 5810-5814.
62. Gheysen D, Jacobs E, de Foresta F, Thiriart C, Francotte M, et al. (1989) Assembly and release of HIV-1 precursor Pr55gag virus-like particles from recombinant baculovirus-infected insect cells. Cell 59: 103-112.
63. Gottlinger HG, Sodroski JG, Haseltine WA (1989) Role of capsid precursor processing and myristoylation in morphogenesis and infectivity of human immunodeficiency virus type 1. Proc Natl Acad Sci U S A 86: 5781-5785.
64. Bryant M, Ratner L (1990) Myristoylation-dependent replication and assembly of human immunodeficiency virus 1. Proc Natl Acad Sci U S A 87: 523-527.
65. Saad JS, Miller J, Tai J, Kim A, Ghanam RH, et al. (2006) Structural basis for targeting HIV-1 Gag proteins to the plasma membrane for virus assembly. Proc Natl Acad Sci U S A 103: 11364-11369.
66. Ono A, Ablan SD, Lockett SJ, Nagashima K, Freed EO (2004) Phosphatidylinositol (4,5) bisphosphate regulates HIV-1 Gag targeting to the plasma membrane. Proc Natl Acad Sci U S A 101: 14889-14894.
67. Freed GE, Martin MA (2001) HIVs and their replication. Fields Virology: 1971–1204.
68. Carlton JG, Martin-Serrano J (2007) Parallels between cytokinesis and retroviral budding: a role for the ESCRT machinery. Science 316: 1908-1912.
69. Morita E, Sandrin V, Chung HY, Morham SG, Gygi SP, et al. (2007) Human ESCRT and ALIX proteins interact with proteins of the midbody and function in cytokinesis. EMBO J 26: 4215-4227.

70. Pettit SC, Moody MD, Wehbie RS, Kaplan AH, Nantermet PV, et al. (1994) The p2 domain of human immunodeficiency virus type 1 Gag regulates sequential proteolytic processing and is required to produce fully infectious virions. J Virol 68: 8017-8027.
71. von Schwedler UK, Stemmler TL, Klishko VY, Li S, Albertine KH, et al. (1998) Proteolytic refolding of the HIV-1 capsid protein amino-terminus facilitates viral core assembly. EMBO J 17: 1555-1568.
72. Newman RM, Johnson WE (2007) A brief history of TRIM5alpha. AIDS Rev 9: 114-125.
73. Towers G, Bock M, Martin S, Takeuchi Y, Stoye JP, et al. (2000) A conserved mechanism of retrovirus restriction in mammals. Proc Natl Acad Sci U S A 97: 12295-12299.
74. Dorfman T, Gottlinger HG (1996) The human immunodeficiency virus type 1 capsid p2 domain confers sensitivity to the cyclophilin-binding drug SDZ NIM 811. J Virol 70: 5751-5757.
75. Hatziioannou T, Cowan S, Goff SP, Bieniasz PD, Towers GJ (2003) Restriction of multiple divergent retroviruses by Lv1 and Ref1. The EMBO journal 22: 385-394.
76. Owens CM, Yang PC, Gottlinger H, Sodroski J (2003) Human and simian immunodeficiency virus capsid proteins are major viral determinants of early, postentry replication blocks in simian cells. J Virol 77: 726-731.
77. Stremlau M, Perron M, Lee M, Li Y, Song B, et al. (2006) Specific recognition and accelerated uncoating of retroviral capsids by the TRIM5alpha restriction factor. Proc Natl Acad Sci U S A 103: 5514-5519.
78. Fletcher AJ, Towers GJ (2013) Inhibition of retroviral replication by members of the TRIM protein family. Current topics in microbiology and immunology 371: 29-66.
79. Ozato K, Shin DM, Chang TH, Morse HC, 3rd (2008) TRIM family proteins and their emerging roles in innate immunity. Nat Rev Immunol 8: 849-860.
80. Xu L, Yang L, Moitra PK, Hashimoto K, Rallabhandi P, et al. (2003) BTBD1 and BTBD2 colocalize to cytoplasmic bodies with the RBCC/tripartite motif protein, TRIM5delta. Exp Cell Res 288: 84-93.
81. Liu F, Walters KJ (2010) Multitasking with ubiquitin through multivalent interactions. Trends Biochem Sci 35: 352-360.
82. Deshaies RJ, Joazeiro CA (2009) RING domain E3 ubiquitin ligases. Annu Rev Biochem 78: 399-434.
83. Huang DT, Hunt HW, Zhuang M, Ohi MD, Holton JM, et al. (2007) Basis for a ubiquitin-like protein thioester switch toggling E1-E2 affinity. Nature 445: 394-398.
84. Lienlaf M, Hayashi F, Di Nunzio F, Tochio N, Kigawa T, et al. (2011) Contribution of E3-ubiquitin ligase activity to HIV-1 restriction by TRIM5alpha(rh): structure of the RING domain of TRIM5alpha. J Virol 85: 8725-8737.
85. Brzovic PS, Rajagopal P, Hoyt DW, King MC, Klevit RE (2001) Structure of a BRCA1-BARD1 heterodimeric RING-RING complex. Nat Struct Mol Biol 8: 833-837.

86. Borden KL (2000) RING domains: master builders of molecular scaffolds? J Mol Biol 295: 1103-1112.
87. Kentsis A, Borden KL (2004) Physical mechanisms and biological significance of supramolecular protein self-assembly. Curr Protein Pept Sci 5: 125-134.
88. Kentsis A, Gordon RE, Borden KL (2002) Control of biochemical reactions through supramolecular RING domain self-assembly. Proc Natl Acad Sci U S A 99: 15404-15409.
89. Poyurovsky MV, Priest C, Kentsis A, Borden KL, Pan ZQ, et al. (2007) The Mdm2 RING domain C-terminus is required for supramolecular assembly and ubiquitin ligase activity. EMBO J 26: 90-101.
90. Yamauchi K, Wada K, Tanji K, Tanaka M, Kamitani T (2008) Ubiquitination of E3 ubiquitin ligase TRIM5 alpha and its potential role. FEBS J 275: 1540-1555.
91. Diaz-Griffero F, Li X, Javanbakht H, Song B, Welikala S, et al. (2006) Rapid turnover and polyubiquitylation of the retroviral restriction factor TRIM5. Virology 349: 300-315.
92. Rold CJ, Aiken C (2008) Proteasomal degradation of TRIM5alpha during retrovirus restriction. PLoS Pathog 4: e1000074.
93. Lukic Z, Hausmann S, Sebastian S, Rucci J, Sastri J, et al. (2011) TRIM5alpha associates with proteasomal subunits in cells while in complex with HIV-1 virions. Retrovirology 8: 93.
94. O'Connor C, Pertel T, Gray S, Robia SL, Bakowska JC, et al. (2010) p62/sequestosome-1 associates with and sustains the expression of retroviral restriction factor TRIM5alpha. J Virol 84: 5997-6006.
95. Yap MW, Mortuza GB, Taylor IA, Stoye JP (2007) The design of artificial retroviral restriction factors. Virology 365: 302-314.
96. Diaz-Griffero F, Kar A, Lee M, Stremlau M, Poeschla E, et al. (2007) Comparative requirements for the restriction of retrovirus infection by TRIM5alpha and TRIMCyp. Virology 369: 400-410.
97. Anderson JL, Campbell EM, Wu X, Vandegraaff N, Engelman A, et al. (2006) Proteasome inhibition reveals that a functional preintegration complex intermediate can be generated during restriction by diverse TRIM5 proteins. J Virol 80: 9754-9760.
98. Wu X, Anderson JL, Campbell EM, Joseph AM, Hope TJ (2006) Proteasome inhibitors uncouple rhesus TRIM5alpha restriction of HIV-1 reverse transcription and infection. Proc Natl Acad Sci U S A 103: 7465-7470.
99. Li X, Yeung DF, Fiegen AM, Sodroski J (2011) Determinants of the higher order association of the restriction factor TRIM5alpha and other tripartite motif (TRIM) proteins. J Biol Chem 286: 27959-27970.
100. Roa A, Hayashi F, Yang Y, Lienlaf M, Zhou J, et al. (2012) RING domain mutations uncouple TRIM5alpha restriction of HIV-1 from inhibition of reverse transcription and acceleration of uncoating. J Virol 86: 1717-1727.
101. Mrosek M, Meier S, Ucurum-Fotiadis Z, von Castelmur E, Hedbom E, et al. (2008) Structural analysis of B-Box 2 from MuRF1: identification of a novel self-association pattern in a RING-like fold. Biochemistry 47: 10722-10730.

102. Diaz-Griffero F, Qin XR, Hayashi F, Kigawa T, Finzi A, et al. (2009) A B-box 2 surface patch important for TRIM5alpha self-association, capsid binding avidity, and retrovirus restriction. J Virol 83: 10737-10751.
103. Massiah MA, Simmons BN, Short KM, Cox TC (2006) Solution structure of the RBCC/TRIM B-box1 domain of human MID1: B-box with a RING. J Mol Biol 358: 532-545.
104. Massiah MA, Matts JA, Short KM, Simmons BN, Singireddy S, et al. (2007) Solution structure of the MID1 B-box2 CHC(D/C)C(2)H(2) zinc-binding domain: insights into an evolutionarily conserved RING fold. J Mol Biol 369: 1-10.
105. Tao H, Simmons BN, Singireddy S, Jakkidi M, Short KM, et al. (2008) Structure of the MID1 tandem B-boxes reveals an interaction reminiscent of intermolecular ring heterodimers. Biochemistry 47: 2450-2457.
106. Sardiello M, Cairo S, Fontanella B, Ballabio A, Meroni G (2008) Genomic analysis of the TRIM family reveals two groups of genes with distinct evolutionary properties. BMC Evol Biol 8: 225.
107. Mason JM, Arndt KM (2004) Coiled coil domains: stability, specificity, and biological implications. Chembiochem 5: 170-176.
108. Landschulz WH, Johnson PF, McKnight SL (1988) The leucine zipper: a hypothetical structure common to a new class of DNA binding proteins. Science 240: 1759-1764.
109. Lupas A (1996) Coiled coils: new structures and new functions. Trends Biochem Sci 21: 375-382.
110. Arndt KM, Pelletier JN, Muller KM, Pluckthun A, Alber T (2002) Comparison of in vivo selection and rational design of heterodimeric coiled coils. Structure 10: 1235-1248.
111. Crick FH (1952) Is alpha-keratin a coiled coil? Nature 170: 882-883.
112. Harbury PB, Plecs JJ, Tidor B, Alber T, Kim PS (1998) High-resolution protein design with backbone freedom. Science 282: 1462-1467.
113. Stetefeld J, Jenny M, Schulthess T, Landwehr R, Engel J, et al. (2000) Crystal structure of a naturally occurring parallel right-handed coiled coil tetramer. Nat Struct Mol Biol 7: 772-776.
114. Zhao G, Ke D, Vu T, Ahn J, Shah VB, et al. (2011) Rhesus TRIM5α Disrupts the HIV-1 Capsid at the Inter-Hexamer Interfaces. PLoS Pathog 7: e1002009.
115. Langelier CR, Sandrin V, Eckert DM, Christensen DE, Chandrasekaran V, et al. (2008) Biochemical characterization of a recombinant TRIM5alpha protein that restricts human immunodeficiency virus type 1 replication. J Virol 82: 11682-11694.
116. Reymond A, Meroni G, Fantozzi A, Merla G, Cairo S, et al. (2001) The tripartite motif family identifies cell compartments. EMBO J 20: 2140-2151.
117. Berthoux L, Sebastian S, Sayah DM, Luban J (2005) Disruption of human TRIM5alpha antiviral activity by nonhuman primate orthologues. J Virol 79: 7883-7888.
118. Mische CC, Javanbakht H, Song B, Diaz-Griffero F, Stremlau M, et al. (2005) Retroviral restriction factor TRIM5alpha is a trimer. J Virol 79: 14446-14450.

119. Javanbakht H, Yuan W, Yeung DF, Song B, Diaz-Griffero F, et al. (2006) Characterization of TRIM5alpha trimerization and its contribution to human immunodeficiency virus capsid binding. Virology 353: 234-246.
120. Javanbakht H, Diaz-Griffero F, Stremlau M, Si Z, Sodroski J (2005) The contribution of RING and B-box 2 domains to retroviral restriction mediated by monkey TRIM5alpha. J Biol Chem 280: 26933-26940.
121. Perez-Caballero D, Hatziioannou T, Yang A, Cowan S, Bieniasz PD (2005) Human tripartite motif 5alpha domains responsible for retrovirus restriction activity and specificity. J Virol 79: 8969-8978.
122. Sastri J, O'Connor C, Danielson CM, McRaven M, Perez P, et al. (2010) Identification of residues within the L2 region of rhesus TRIM5alpha that are required for retroviral restriction and cytoplasmic body localization. Virology 405: 259-266.
123. Vernet C, Boretto J, Mattei MG, Takahashi M, Jack LJ, et al. (1993) Evolutionary study of multigenic families mapping close to the human MHC class I region. J Mol Evol 37: 600-612.
124. Ponting C, Schultz J, Bork P (1997) SPRY domains in ryanodine receptors (Ca(2+)-release channels). Trends Biochem Sci 22: 193-194.
125. Rhodes DA, de Bono B, Trowsdale J (2005) Relationship between SPRY and B30.2 protein domains. Evolution of a component of immune defence? Immunology 116: 411-417.
126. Grutter C, Briand C, Capitani G, Mittl PR, Papin S, et al. (2006) Structure of the PRYSPRY-domain: implications for autoinflammatory diseases. FEBS Lett 580: 99-106.
127. Grutter MG, Luban J (2012) TRIM5 structure, HIV-1 capsid recognition, and innate immune signaling. Curr Opin Virol 2: 142-150.
128. James LC, Keeble AH, Khan Z, Rhodes DA, Trowsdale J (2007) Structural basis for PRYSPRY-mediated tripartite motif (TRIM) protein function. Proc Natl Acad Sci U S A 104: 6200-6205.
129. Biris N, Yang Y, Taylor AB, Tomashevski A, Guo M, et al. (2012) Structure of the rhesus monkey TRIM5alpha PRYSPRY domain, the HIV capsid recognition module. Proc Natl Acad Sci U S A 109: 13278-13283.
130. Yang H, Ji X, Zhao G, Ning J, Zhao Q, et al. (2012) Structural insight into HIV-1 capsid recognition by rhesus TRIM5alpha. Proc Natl Acad Sci U S A 109: 18372-18377.
131. Weinert C, Grutter C, Roschitzki-Voser H, Mittl PR, Grutter MG (2009) The crystal structure of human pyrin b30.2 domain: implications for mutations associated with familial Mediterranean fever. J Mol Biol 394: 226-236.
132. D'Cruz AA, Kershaw NJ, Chiang JJ, Wang MK, Nicola NA, et al. (2013) Crystal structure of the TRIM25 B30.2 (PRYSPRY) domain: a key component of antiviral signalling. Biochem J 456: 231-240.
133. Park EY, Kwon OB, Jeong BC, Yi JS, Lee CS, et al. (2010) Crystal structure of PRY-SPRY domain of human TRIM72. Proteins 78: 790-795.
134. Luban J (2010) Retroviral Restriction Factors. Retroviruses: Molecular Biology, Genomics and Pathogenesis: 285-307.

135. Sebastian S, Luban J (2005) TRIM5alpha selectively binds a restriction-sensitive retroviral capsid. Retrovirology 2: 40.
136. Ganser-Pornillos BK, Chandrasekaran V, Pornillos O, Sodroski JG, Sundquist WI, et al. (2011) Hexagonal assembly of a restricting TRIM5alpha protein. Proc Natl Acad Sci U S A 108: 534-539.
137. Hatziioannou T, Perez-Caballero D, Yang A, Cowan S, Bieniasz PD (2004) Retrovirus resistance factors Ref1 and Lv1 are species-specific variants of TRIM5alpha. Proc Natl Acad Sci U S A 101: 10774-10779.
138. Keckesova Z, Ylinen LM, Towers GJ (2004) The human and African green monkey TRIM5alpha genes encode Ref1 and Lv1 retroviral restriction factor activities. Proc Natl Acad Sci U S A 101: 10780-10785.
139. Nakayama EE, Miyoshi H, Nagai Y, Shioda T (2005) A specific region of 37 amino acid residues in the SPRY (B30.2) domain of African green monkey TRIM5alpha determines species-specific restriction of simian immunodeficiency virus SIVmac infection. J Virol 79: 8870-8877.
140. Owens CM, Song B, Perron MJ, Yang PC, Stremlau M, et al. (2004) Binding and susceptibility to postentry restriction factors in monkey cells are specified by distinct regions of the human immunodeficiency virus type 1 capsid. J Virol 78: 5423-5437.
141. Perron MJ, Stremlau M, Song B, Ulm W, Mulligan RC, et al. (2004) TRIM5alpha mediates the postentry block to N-tropic murine leukemia viruses in human cells. Proc Natl Acad Sci U S A 101: 11827-11832.
142. Sawyer SL, Wu LI, Emerman M, Malik HS (2005) Positive selection of primate TRIM5alpha identifies a critical species-specific retroviral restriction domain. Proc Natl Acad Sci U S A 102: 2832-2837.
143. Song B, Gold B, O'Huigin C, Javanbakht H, Li X, et al. (2005) The B30.2(SPRY) domain of the retroviral restriction factor TRIM5alpha exhibits lineage-specific length and sequence variation in primates. J Virol 79: 6111-6121.
144. Song B, Javanbakht H, Perron M, Park DH, Stremlau M, et al. (2005) Retrovirus restriction by TRIM5alpha variants from Old World and New World primates. J Virol 79: 3930-3937.
145. Stremlau M, Perron M, Welikala S, Sodroski J (2005) Species-specific variation in the B30.2(SPRY) domain of TRIM5alpha determines the potency of human immunodeficiency virus restriction. J Virol 79: 3139-3145.
146. Yap MW, Nisole S, Stoye JP (2005) A single amino acid change in the SPRY domain of human Trim5alpha leads to HIV-1 restriction. Curr Biol 15: 73-78.
147. Fischer G, Tradler T, Zarnt T (1998) The mode of action of peptidyl prolyl cis/trans isomerases in vivo: binding vs. catalysis. FEBS Lett 426: 17-20.
148. Gamble TR, Vajdos FF, Yoo S, Worthylake DK, Houseweart M, et al. (1996) Crystal structure of human cyclophilin A bound to the amino-terminal domain of HIV-1 capsid. Cell 87: 1285-1294.
149. Franke EK, Yuan HE, Luban J (1994) Specific incorporation of cyclophilin A into HIV-1 virions. Nature 372: 359-362.
150. Thali M, Bukovsky A, Kondo E, Rosenwirth B, Walsh CT, et al. (1994) Functional association of cyclophilin A with HIV-1 virions. Nature 372: 363-365.

151. Braaten D, Aberham C, Franke EK, Yin L, Phares W, et al. (1996) Cyclosporine A-resistant human immunodeficiency virus type 1 mutants demonstrate that Gag encodes the functional target of cyclophilin A. J Virol 70: 5170-5176.
152. Braaten D, Franke EK, Luban J (1996) Cyclophilin A is required for an early step in the life cycle of human immunodeficiency virus type 1 before the initiation of reverse transcription. J Virol 70: 3551-3560.
153. Franke EK, Luban J (1996) Inhibition of HIV-1 replication by cyclosporine A or related compounds correlates with the ability to disrupt the Gag-cyclophilin A interaction. Virology 222: 279-282.
154. Braaten D, Luban J (2001) Cyclophilin A regulates HIV-1 infectivity, as demonstrated by gene targeting in human T cells. EMBO J 20: 1300-1309.
155. Sokolskaja E, Sayah DM, Luban J (2004) Target cell cyclophilin A modulates human immunodeficiency virus type 1 infectivity. J Virol 78: 12800-12808.
156. Hatziioannou T, Perez-Caballero D, Cowan S, Bieniasz PD (2005) Cyclophilin interactions with incoming human immunodeficiency virus type 1 capsids with opposing effects on infectivity in human cells. J Virol 79: 176-183.
157. Yoo S, Myszka DG, Yeh C, McMurray M, Hill CP, et al. (1997) Molecular recognition in the HIV-1 capsid/cyclophilin A complex. J Mol Biol 269: 780-795.
158. Nisole S, Lynch C, Stoye JP, Yap MW (2004) A Trim5-cyclophilin A fusion protein found in owl monkey kidney cells can restrict HIV-1. Proc Natl Acad Sci U S A 101: 13324-13328.
159. Ribeiro IP, Menezes AN, Moreira MA, Bonvicino CR, Seuanez HN, et al. (2005) Evolution of cyclophilin A and TRIMCyp retrotransposition in New World primates. J Virol 79: 14998-15003.
160. Brennan G, Kozyrev Y, Hu SL (2008) TRIMCyp expression in Old World primates Macaca nemestrina and Macaca fascicularis. Proc Natl Acad Sci U S A 105: 3569-3574.
161. Newman RM, Hall L, Kirmaier A, Pozzi LA, Pery E, et al. (2008) Evolution of a TRIM5-CypA splice isoform in old world monkeys. PLoS Pathog 4: e1000003.
162. Virgen CA, Kratovac Z, Bieniasz PD, Hatziioannou T (2008) Independent genesis of chimeric TRIM5-cyclophilin proteins in two primate species. Proc Natl Acad Sci U S A 105: 3563-3568.
163. Wilson SJ, Webb BL, Ylinen LM, Verschoor E, Heeney JL, et al. (2008) Independent evolution of an antiviral TRIMCyp in rhesus macaques. Proc Natl Acad Sci U S A 105: 3557-3562.
164. Nakayama EE, Shioda T (2012) Role of Human TRIM5alpha in Intrinsic Immunity. Front Microbiol 3: 97.
165. Neagu MR, Ziegler P, Pertel T, Strambio-De-Castillia C, Grutter C, et al. (2009) Potent inhibition of HIV-1 by TRIM5-cyclophilin fusion proteins engineered from human components. J Clin Invest 119: 3035-3047.
166. Saenz DT, Teo W, Olsen JC, Poeschla EM (2005) Restriction of feline immunodeficiency virus by Ref1, Lv1, and primate TRIM5alpha proteins. J Virol 79: 15175-15188.

167. Sokolskaja E, Berthoux L, Luban J (2006) Cyclophilin A and TRIM5alpha independently regulate human immunodeficiency virus type 1 infectivity in human cells. J Virol 80: 2855-2862.
168. Diaz-Griffero F, Vandegraaff N, Li Y, McGee-Estrada K, Stremlau M, et al. (2006) Requirements for capsid-binding and an effector function in TRIMCyp-mediated restriction of HIV-1. Virology 351: 404-419.
169. Price AJ, Marzetta F, Lammers M, Ylinen LM, Schaller T, et al. (2009) Active site remodeling switches HIV specificity of antiretroviral TRIMCyp. Nat Struct Mol Biol 16: 1036-1042.
170. Ylinen LM, Price AJ, Rasaiyaah J, Hue S, Rose NJ, et al. (2010) Conformational adaptation of Asian macaque TRIMCyp directs lineage specific antiviral activity. PLoS Pathog 6: e1001062.
171. Liu HL, Wang YQ, Liao CH, Kuang YQ, Zheng YT, et al. (2005) Adaptive evolution of primate TRIM5alpha, a gene restricting HIV-1 infection. Gene 362: 109-116.
172. Newman RM, Hall L, Connole M, Chen GL, Sato S, et al. (2006) Balancing selection and the evolution of functional polymorphism in Old World monkey TRIM5alpha. Proc Natl Acad Sci U S A 103: 19134-19139.
173. Ortiz M, Bleiber G, Martinez R, Kaessmann H, Telenti A (2006) Patterns of evolution of host proteins involved in retroviral pathogenesis. Retrovirology 3: 11.
174. Sawyer SL, Wu LI, Akey JM, Emerman M, Malik HS (2006) High-frequency persistence of an impaired allele of the retroviral defense gene TRIM5alpha in humans. Curr Biol 16: 95-100.
175. Maillard PV, Reynard S, Serhan F, Turelli P, Trono D (2007) Interfering residues narrow the spectrum of MLV restriction by human TRIM5alpha. PLoS Pathog 3: e200.
176. Ohkura S, Yap MW, Sheldon T, Stoye JP (2006) All three variable regions of the TRIM5alpha B30.2 domain can contribute to the specificity of retrovirus restriction. J Virol 80: 8554-8565.
177. Perron MJ, Stremlau M, Sodroski J (2006) Two surface-exposed elements of the B30.2/SPRY domain as potency determinants of N-tropic murine leukemia virus restriction by human TRIM5alpha. J Virol 80: 5631-5636.
178. Woo JS, Suh HY, Park SY, Oh BH (2006) Structural basis for protein recognition by B30.2/SPRY domains. Mol Cell 24: 967-976.
179. Luban J, Bossolt KL, Franke EK, Kalpana GV, Goff SP (1993) Human immunodeficiency virus type 1 Gag protein binds to cyclophilins A and B. Cell 73: 1067-1078.
180. Lin TY, Emerman M (2006) Cyclophilin A interacts with diverse lentiviral capsids. Retrovirology 3: 70.
181. Caines ME, Bichel K, Price AJ, McEwan WA, Towers GJ, et al. (2012) Diverse HIV viruses are targeted by a conformationally dynamic antiviral. Nat Struct Mol Biol 19: 411-416.
182. Ohkura S, Goldstone DC, Yap MW, Holden-Dye K, Taylor IA, et al. (2011) Novel escape mutants suggest an extensive TRIM5alpha binding site spanning the

entire outer surface of the murine leukemia virus capsid protein. PLoS Pathog 7: e1002011.
183. Ganser-Pornillos BK, Yeager M, Sundquist WI (2008) The structural biology of HIV assembly. Curr Opin Struct Biol 18: 203-217.
184. Li S, Hill CP, Sundquist WI, Finch JT (2000) Image reconstructions of helical assemblies of the HIV-1 CA protein. Nature 407: 409-413.
185. Kozak CA, Chakraborti A (1996) Single amino acid changes in the murine leukemia virus capsid protein gene define the target of Fv1 resistance. Virology 225: 300-305.
186. Maillard PV, Zoete V, Michielin O, Trono D (2011) Homology-based identification of capsid determinants that protect HIV1 from human TRIM5alpha restriction. J Biol Chem 286: 8128-8140.
187. Nomaguchi M, Yokoyama M, Kono K, Nakayama EE, Shioda T, et al. (2013) Generation of rhesus macaque-tropic HIV-1 clones that are resistant to major anti-HIV-1 restriction factors. J Virol 87: 11447-11461.
188. Papin S, Cuenin S, Agostini L, Martinon F, Werner S, et al. (2007) The SPRY domain of Pyrin, mutated in familial Mediterranean fever patients, interacts with inflammasome components and inhibits proIL-1beta processing. Cell Death Differ 14: 1457-1466.
189. Pornillos O, Ganser-Pornillos BK, Kelly BN, Hua Y, Whitby FG, et al. (2009) X-ray structures of the hexameric building block of the HIV capsid. Cell 137: 1282-1292.
190. Pornillos O, Ganser-Pornillos BK, Yeager M (2011) Atomic-level modelling of the HIV capsid. Nature 469: 424-427.
191. Zhao G, Perilla JR, Yufenyuy EL, Meng X, Chen B, et al. (2013) Mature HIV-1 capsid structure by cryo-electron microscopy and all-atom molecular dynamics. Nature 497: 643-646.
192. Ganser BK, Li S, Klishko VY, Finch JT, Sundquist WI (1999) Assembly and analysis of conical models for the HIV-1 core. Science 283: 80-83.
193. Jin Z, Jin L, Peterson DL, Lawson CL (1999) Model for lentivirus capsid core assembly based on crystal dimers of EIAV p26. J Mol Biol 286: 83-93.
194. Heymann JB, Butan C, Winkler DC, Craven RC, Steven AC (2008) Irregular and Semi-Regular Polyhedral Models for Rous Sarcoma Virus Cores. Comput Math Methods Med 9: 197-210.
195. Chen B, Tycko R (2011) Simulated self-assembly of the HIV-1 capsid: protein shape and native contacts are sufficient for two-dimensional lattice formation. Biophys J 100: 3035-3044.
196. Meng X, Zhao G, Yufenyuy E, Ke D, Ning J, et al. (2012) Protease cleavage leads to formation of mature trimer interface in HIV-1 capsid. PLoS Pathog 8: e1002886.
197. Ganser-Pornillos BK, Cheng A, Yeager M (2007) Structure of full-length HIV-1 CA: a model for the mature capsid lattice. Cell 131: 70-79.
198. Li X, Sodroski J (2008) The TRIM5alpha B-box 2 domain promotes cooperative binding to the retroviral capsid by mediating higher-order self-association. J Virol 82: 11495-11502.

199. Sebastian S, Grutter C, Strambio de Castillia C, Pertel T, Olivari S, et al. (2009) An invariant surface patch on the TRIM5alpha PRYSPRY domain is required for retroviral restriction but dispensable for capsid binding. J Virol 83: 3365-3373.

6 Acknowledgement

This thesis would not have been possible without the help of many people. Therefore, I would like to express my gratitude for their contribution and support during the last years.
First, I would like to thank Prof. M.G. Grütter for giving me the opportunity to work on such a fascinating project in the challenging field of HIV and for the freedom he provided throughout my time in his lab.
I further would like to thank Prof. Jeremy Luban and Prof. Ohad Medalia for being in my thesis committee. I am especially grateful to Prof. Jeremy Luban for the collaboration on TRIM5 projects and his contagious enthusiasm for science.
I would like to thank Prof. Leonardo Scapozza from the University in Geneva and Dr. Timothy Sharpe from the Biozentrum Basel for giving me the opportunity to perform MST measurements in their Laboratories.
I am very thankful to Dr. Sara Züger, who introduced me into the TRIM5 project and performed preceding work on which this thesis could build on.
I especially thank Dr. Christopher Weinert for the work we have performed together, for the many scientific discussions on TRIM proteins and beyond, and for sharing the fortune of being the last members of the Grütter lab. I thank Tim Knehans for helpful inputs on homology modelling. For their support with Mass Spectrometry I thank Serge Chesnov and Peter Hunziker. For their valuable advises on the measurement of protein-protein interactions I would like to thank Dr. Stefan Schauer and Dr. Nikolas Stefan.
I am very grateful to Franziska Zosel, who helped gaining crucial data on the interaction of TRIM5 with the HIV-1 capsid using dual-focus FCS.
A special thank goes out to Martin Bühlmann who assisted me with the production of TRIM5 and HIV-1 capsids, and implemented his own creativity to help improving the purification processes.
Moreover, I had the fortune to supervise the bachelor work of Maximilian Mittelviefhaus and the internship of Mauro Pellanda, who helped progressing with the challenging TRIM5 studies and allowed me to collect valuable experiences on managing projects.
I would like to thank the staff of the Institute of Biochemistry, namely our secretary Salome Rittmeyer, Adrian Schmid and Sascha Weidner of the workshop, and Steve Rast and Stefan Klauser from the IT service. I also want to thank Beat Blattmann and Céline Stutz-Ducommun of the NCCR crystallization facility.
Many thanks to all the former members of the Grütter group for the great lab atmosphere and their support.
Last but not least I would like to thank my family and friends for the good time outside the lab, especially Judith for being very supportive and sharing such a charming daughter.

7 Curriculum Vitae

Damien Pierre Morger

Date of Birth	12.01.1981
Nationality	Swiss
Adress	Erlachstr. 19, 8003 Zürich
Phone	079 702 56 26
E-Mail	d.morger@bioc.uzh.ch

Education

03/2008 – now **PhD in Biochemistry,** Department of Biochemistry, University of Zürich, Laboratory of Prof. Dr. Markus Grütter, Zürich, Switzerland

03/2007 **Diploma in Natural Sciences (Master of Science ETH)**

10/2001– 03/2007 Biology studies at the ETH-Zurich, chemical track
Specialization: **Microbiology**

Research experience

03/2008 – now **Graduate Researcher, University of Zurich**
Group of Prof. Dr. Markus Grütter, Department of Biochemistry

Thesis: *Structural and Functional Studies on the Antiretroviral Host Factor TRIM5 and its Interaction with the HIV-1 Capsid Lattice*

- Published the first protocol for expression and purification of full-length TRIM5 proteins, providing enough material for biochemical characterization and *in-vitro* ubiquitin assays.
- Designed HIV-1 capsid mutants, allowing cross-linking of lattice interfaces and soluble purification.
- Performed interaction assays with TRIM5 and HIV-1 capsid constructs.
- Generated a TRIM5 model structure based on SAXS data and the X-ray structure of a homologous protein.

03/2007 – 06/2007 **Scientific assistance, ETH Zurich**
Group of Prof. Dr. Peter Dimroth, Department of Microbiology

- Purified ATP-syntase mutants and reconstituted into proteo-liposomes for kinetic measurements of ATP synthesis.

04/2006 – 06/2006 **Scientific assistance, ETH Zurich**
Group of Prof. Dr. Peter Dimroth, Department of Microbiology

- Performed crystallization trials with the rotor-C subunit of *M. kandleri* ATP-synthase.

10/2005 – 04/2006 **Diploma student** (equiv. to master thesis), **ETH Zurich**
Group of Prof. Dr. Peter Dimroth, Department of Microbiology

Thesis: *The A-Type ATP-Synthase of the Hyperthermophile Archaeon Methanopyrus kandleri: Biochemical Characterization, Heterologous Expression and Purification of the Rotor-C Subunit.*

- Established an expression and purification protocol for the rotor-C subunit of *M. kandleri* ATP-synthase.

07/2005 – 10/2005 **Semester student** (equiv. to bachelor thesis), **ETH Zurich**
Group of Prof. Dr. Peter Dimroth, Department of Microbiology

Thesis: *Design and Synthesis of new Detergents for the Solubilisation of Membrane Proteins out of Hyperthermophilic Archeons.*

- Synthesized detergents containing unsaturated and methylated aliphatic chains and tested them for solubilisation of *M. kandleri* membranes.

Conferences and Meetings

Talks

08/2010 **3rd BSM PhD Program Retreat,** Ligerz, Switzerland
Morger D., Sara Z., Studer V., Hausamann S., Luban J., Markus M.G.
Towards Structural and Functional Characterization of TRIM5 Proteins

Posters

08/2012 **5th BSM PhD Program Retreat**, Einsiedeln, Switzerland
Pertel T., Hausmann S., **Morger D.**, Züger S., Guerra J., Lascano J., Reinhard C., Santoni F.A., Uchil P.D., Chatel L., Bisiaux A., Albert M.L., Strambio-De-Castillia C., Mothes W., Pizzato M., Grütter M.G., Luban J. TRIM5 is an innate immune sensor for the retrovirus capsid lattice.

06/2011 **10th Day of Clinical Research 2011,** Zürich, Switzerland
Pertel T., Hausmann S., **Morger D.**, Züger S., Guerra J., Lascano J., Reinhard C., Santoni F.A., Uchil P.D., Chatel L., Bisiaux A., Albert M.L., Strambio-De-Castillia C., Mothes W., Pizzato M., Grütter M.G., Luban J. TRIM5 is an innate immune sensor for the retrovirus capsid lattice.

05/2013 **37th Cold Spring Harbor Retroviruses Meeting,** New York, U.S.A.
Morger D., Bühlmann M., Grütter M.G. Dissecting the HIV-1 Capsid Lattice into Potential TRIM5 Binding Units.

Awards

08/2012 **Poster Award,** 5th BSM PhD Program Retreat, Einsiedeln, Switzerland

08/2010 **1st Place Presentation Award,** 3rd BSM PhD Program Retreat, Ligerz, Switzerland

05/2013 **SSB Travelgrant,** 37th Cold Spring Harbor Retroviruses Meeting, New York, U.S.A.

Publications

Morger D., Zosel F., Bühlmann M., Sara Z., Schuler B., Luban J., Grütter M.G. Dissecting the HIV-1 Capsid Lattice into Potential TRIM5 Binding Units. Manuscript in preparation.

Weinert C., **Morger D.**, Djekic A., Mittl P.R.E. and Grütter M.G. Overall architecture and mode of dimerization of TRIM proteins revealed by the TRIM20 structure. Manuscript in revision at PNAS.

Pertel T., Hausmann S., **Morger D.**, Züger S., Guerra J., Lascano J., Reinhard C., Santoni F.A., Uchil P.D., Chatel L., Bisiaux A., Albert M.L., Strambio-De-Castillia C., Mothes W., Pizzato M., Grütter M.G., Luban J. TRIM5 is an innate immune sensor for the retrovirus capsid lattice. *Nature* 472, 361-365 (2011)

Vorburger T., Zingg Ebneter J., Wiedenmann A., **Morger D.**, Weber G., Diederichs K., Dimroth P., von Ballmoos C. Arginine-induced conformational change in the c-ring/a-subunit interface of ATP synthase. *FEBS J* 275, 2137-50 (2008)